NANO - ZINC OXIDE:
A Novel Modifier for Thermoplastics

Thesis submitted to the

Cochin University of Science and Technology

In partial fulfillment of the requirements for the award of the degree of

Doctor of Philosophy

Under the Faculty of Technology

by

ASWATHY K.V.

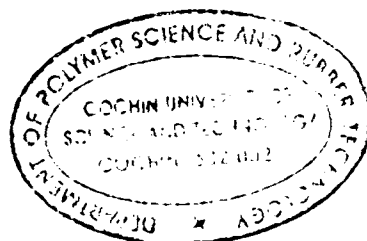**Department of Polymer Science and Rubber Technology**

Cochin University of Science and Technology

Kochi- 682 022, Kerala, India.

http://cusat.ac.in/

September 2007

Department of Polymer Science and Rubber Technology
Cochin University of Science and Technology
Kochi 22, Kerala, India

Dr. Rani Joseph
Professor
E mail : rani@cusat.ac.in
Phone : 0484-2575723(Off)
            0484-2577850(Res)

Certificate

This is to certify that the thesis entitled "NANO - ZINC OXIDE: A Novel Modifier for Thermoplastics" which is being submitted by Mrs. Aswathy K.V. in partial fulfillment of the requirements for the award of the degree of Doctor of Philosophy, to the Cochin University of Science and Technology, Kochi - 22 is a record of the bonafide research work carried out by her under my guidance and supervision, in the Department of Polymer Science and Rubber Technology, Kochi - 22 and no part of the work reported in the thesis has been presented for the award of any degree from any other institution.

Kochi -22,
05-09-2007.

Dr. RANI JOSEPH
(Supervising Teacher)

Declaration

I hereby declare that, the work presented in this thesis entitled **"NANO - ZINC OXIDE: A Novel Modifier for Thermoplastics"** is based on the original research work carried out by me under the guidance and supervision of Dr. Rani Joseph, Professor, Department of Polymer Science and Rubber Technology, Cochin University of Science and Technology, Kochi 22 and no part of the work reported in this thesis has been presented for the award of any degree from any other institution.

Kochi - 22,
05-09-2007

Aswathy K.V.

Acknowledgements

I have been extremely fortunate in the boons that I am bestowed with. I had the opportunity to get excellent teachers, loving friends, and cooperative office staff. I know that it a tedious task to thank all of them by name and I think it is not appropriate to express my gratitude by saying mere thanks and that may undervalue the great concern and encouragement showered upon me. With the utmost respect and politeness I tell you with all my heart, I bear you always in my mind even though I haven't mentioned all your names here.

I express my hearty thanks and indebtedness primarily to my guide Dr. Rani Joseph, Professor and former H.O.D for her invaluable help, sincere guidance, timely suggestions and constant encouragement which paved way for the successful completion of this research work. I wish to express my deep sense of gratitude to Prof. Dr. K.E. George, for the competent advices, professional guidance and extensive support provided to me throughout my research endeavor.

I wish to record my deep appreciation and gratitude to other faculty members of PSRT: Dr. Thomas Kurian (Head of the Dept.), Dr. Eby Thomas, Dr. Philip Kurian, Dr. Sunil Narayanankutty and Ms. Jayalatha Gopalakrishnan for the keen interest in my work and for the whole hearted cooperation throughout my research work.

I am extremely thankful to Dr.Ushamani, Dr.Honey, Dr. Soney, Dr. Thomas, Dr. Lovely Mathew, Dr. Nisha V.S. Dr. Rinku, Dr. Anoop Anand K and Miss.Lity Alen whose sound advice, co-operation and friendship are greatly valued and appreciated. I am also grateful to all FIP teachers (Maya K.S, Joshy M.K, Jude Martin, Raju P, Sreenivasan P.V, Parameswaran, Mary Alexander, Bhuvaneswari, Prema, Saboora and Suma) and young researchers (Ansu Jacob, Bipinpal, Sinto, Saritha, Dhanya, Priya, Abhilash, Vijayalekshmi and Sreekanth) in the Polymer Science Department for their selfless co-operation and who made my course of study a delightful experience.

Also I offer special thanks to Dr. Vipin Rajan, Mr. Gurulinga IISc, Banglore, for the support in analytical studies. I remember with gratitude the help rendered by the librarian and staff of the following institutions in providing access to relevant literature; IISc

PREFACE

Nano zinc oxide is a multifunctional inorganic nanoparticle, has drawn increasing attention in recent years due to its many significant physical and chemical properties such as high chemical stability, low dielectric constant, large elecromechanical coupling coefficient, high luminous transmittance, high catalysis activity, intensive ultraviolet and infrared absorption. The addition of nano scale fillers to polymers can have a dramatic effect on the properties of polymers as compared to micro scale fillers. Large part of this effect is due to the small size and the large surface area of nano scale fillers. The control of particle size, morphology and crystallinity of the particles during the preparation is essential to achieve the key properties.

The current research aims at preparing nano ZnO powder by polymer induced crystallization in chitosan solution and the possibility of using nano ZnO as a modifier in thermoplastics to impart several properties to the matrix polymer.

It has been undertaken to explore the potential of nano ZnO as reinforcement in engineering as well as commodity thermoplastics to widen their application spectra.

Content of the thesis:

This thesis is divided into six chapters:

Chapter 1 presents a concise introduction and literature survey of nanocomposites, nanomaterials and ZnO based nanocomposites. The scope and objectives of the present investigation is summarized.

Chapter 2 discusses various materials and methods used for the preparation and characterization of the nanocomposites.

Chapter 3 includes the method of preparation of nano zinc oxide from zinc chloride and sodium hydroxide in chitosan solution by polymer induced

crystallization. Characterization of nano zinc oxide using different analytical techniques is presented in this chapter.

Chapter 4 includes the modification of engineering thermoplastics using nano ZnO. This chapter is divided into three parts. Part a deals with the preparation and characterization of polyethylene terephthalate–ZnO nanocomposites. Part b comprises the preparation and characterization of polyamide 6–ZnO nanocomposites and part c includes the preparation and characterization of polycarbonate–ZnO nanocomposites. The composites have been prepared by simple melt compounding technique and their crystallization (both isothermal and non-isothermal); mechanical, dynamic mechanical, thermal and rheological properties are studied. A comparison of properties with commercial ZnO is also presented.

Chapter 5 deals with the modification of commodity thermoplastics using nano ZnO. This chapter is divided into three parts. Part a deals with the preparation and characterization of polypropylene–ZnO nanocomposites. Part b comprises the preparation and characterization of high density polyethylene–ZnO nanocomposites and part c includes the preparation and characterization of polystyrene–ZnO nanocomposites. The composites have been prepared by simple melt compounding technique and their crystallization (both isothermal and non-isothermal), mechanical, dynamic mechanical, thermal and rheological properties are studied. A comparison of properties with commercial ZnO is also presented.

Chapter 6 consists of summary and conclusions of the investigations.

At the end of each chapter a list of pertinent references is given. A list of abbreviations used in this thesis is also cited.

Contents

Part c
Modification of polystyrene using nano zinc oxide

Chapter 6

List of publications and conference papers
List of abbreviations and symbols
Curriculum Vitae

GENERAL INTRODUCTION

Man's insatiable appetite for invention of new things is unquenchable. Since ancient times, his voraciousness brought him many new tools and discoveries. For new things, he interacted well with nature, and it responded well. However, he was unsatisfied with it and expanded his thought to produce synthetic materials. Polymer is the one of such materials. He was familiar to so many natural polymers such as cellulose, natural rubber, lignin, starch etc. Man introduced polymers successfully in many areas to simplify his life. This age is also referred as "polymer era" while speaking about materials. Presently we can find polymers finding their application in every field like in structural engineering, automobile engineering, aeronautic engineering, film and packaging industries, food packaging, high performance applications, paint and dyes industry, drug synthesis, home appliances and many more areas. Polymer finds such a large number of applications because of their important properties. They are easy to handle, process, maintain, have excellent heat and chemical resistance, corrosion resistant and most importantly they show efficient productivity and cost reduction. Because of this, they are replacing wood, metal, ceramic and other structural elements.

1.1 Composites

Materials engineering is being used for developing new high tech materials for variety of applications ranging from opto electronics to space vehicles. Combining and orienting materials to achieve superior properties are old and well-proven concepts; examples of this synergism are bound in nature.[1] Wood contains an oriented hard phase for toughness. Other natural composites are found in teeth, bones, plant leaves etc. Synthetic composites are found in artifacts and in recorded history. The use of chopped straw by Israelites to

control the residual cracking in bricks is an example.[2] More representative of the modern structural composites are Mongolian bowls, which were laminates of wood, animal tendons, and silk and Japanese Samurai woods formed by repeated folding of a steel bar back upon itself. The resulting structure contains as many as 215 alternating layers of hard oxide and tough, ductile steel.

A polymer can alone not provide all the superior properties like strength, less thermal coefficients, resistance to shock loads, resistance to thermal or chemical degradation etc. Fillers have important roles in modifying properties of various polymers. Mineral fillers, metals and fibres have been added to thermoplastics (TP) and thermosets (TS) for decades to form composites. The effect of fillers on properties of the composites depends on their concentration, their particle size and shape as well on their interaction with the matrix. A composite material can be defined as a macroscopic combination of two or more distinct materials, having a recognizable interface between them. Composites are made up of continuous and discontinuous medium. The discontinuous medium that is stiffer and stronger than the continuous phase is called the reinforcement and the so called continuous phase is referred to as the matrix.[3,4,5] The constituents retain their identity; they do not dissolve or merge completely into one another. Composite provides the design fabricator, equipment manufacturers and consumers with sufficient flexibility to meet the demands presented by different environments and special requirements.

1.1.1 Classification of composites

Composites can be classified in different ways-

- Depending on the size of the constituents-
    - Macro composites- these composites consist of macro sized particles like galvanized steel, helicopter blades etc.
    - Micro composites- comprising of metallic alloys, reinforced plastics etc.
    - Nanocomposites- polymers/particles ranging in nano size.

- Depending on the occurrence of composites-

    - Natural composites- for e.g., jute, silk, wood, bamboo

    - Manmade composites- for e.g., glass reinforced fibre

- Depending on the matrix system-

    - Polymer matrix composites (PMC)

    - Ceramic matrix composites (CMC)

    - Metal matrix composites (MMC)

    - Rubber matrix composites (RMC)

- Depending on structural components-

    - Fibrous composites (composed of fibrous filler in matrix)

    - Laminar composites (composed of layers of materials)

    - Particulate composites (composed of particulate fillers in matrix)

    - Skeletal composites (composed of continuous skeletal matrix filled by a second matrix)

Another classification of particulate composites is based on the particle size of the dispersed phase. More recently, with advances in synthetic techniques and the ability to readily characterize materials on an atomic scale has lead to interest in nanometer size materials. Nanometer size grains, fibres and plates have dramatically increased surface area compared to their conventional-size materials. The chemistry of these nanosized materials is altered compared to conventional materials. This can be micro composites, nanocomposites and molecular composites.

1.2 Nanotechnology

A revolution is occurring in science and technology, based on the recently developed ability to measure, manipulate and organize matter on the nanoscale -1 to 100 billionths of a meter.[6] At the nanoscale, physics, chemistry, biology, materials science, and engineering converge towards the same principles and tools. As a result, progress in nanoscience will have very far-reaching impact. As knowledge in nanoscience increases worldwide, there will likely be fundamental

scientific advances. In turn, this will lead to dramatic changes in the ways materials, devices, and systems are understood and created. Innovative nanoscale properties and functions will be achieved through the control of matter at its building blocks: atom-by-atom, molecule-by-molecule, and nanostructure-by-nanostructure. Nanotechnology will include the integration of these nanoscale structures into larger material components, systems, and architectures. However, within these larger scale systems the control and construction will remain at the nanoscale. Today, nanotechnology is still in its infancy, because only rudimentary nanostructures can be created with some control. However, among the envisioned breakthroughs are orders-of-magnitude increase in computer efficiency, human organ restoration using engineered tissue, "designer" materials created from directed assembly of atoms and molecules, as well as emergence of entirely new phenomena in chemistry and physics.

The term "nanotechnology" has evolved over the years via terminology drift to mean "anything smaller than microtechnology," such as nano powders, and other things that are nanoscale in size, but not referring to mechanisms that have been purposefully built from nanoscale components. It has been said that a nanometer is "a magical point on the length scale, for this is the point where the smallest man-made devices meet the atoms and molecules of the natural world." (Eugene Wong, quoted by Boyd RS. Knight Rider Newspapers, Kansas City Star, Monday, November 8, 1999.)

Many materials, once they are individually reduced below 100 nanometers begin displaying a set of unique characteristics based on quantum mechanical forces that are exhibited at the level. Due to these quantum mechanical effects, materials may become more conducting, be able to transfer heat better or have modified mechanical properties.

Nanotechnology covers many field of science such as:

1. Nano crystals: The solid materials that can be reversibly switch between conductor and insulator at room temperature and pressure without change in chemical nature.

2. Nano laser: Here ground breaking experiments are done to cool and trap atoms with laser light.

3. Nano coat: A coating will allow miniature sensors to detect dangerous, even lethal, air or water molecules much more quickly. This is used for nano detection of dangerous materials.

4. Nano computer: The use of DNA molecule in computing offers an advantage over desktop PCs. Recent progress in this field includes the development of DNA computing algorithms to solve mathematical challenges.

5. Nano scan: Accelerator that will map structures, biological molecules in 3- dimensional.

6. Nano traps: Cesium atoms were allowed to fall downwards on to a prism. When the atoms strike the prism they are reflected upwards. After several bounces the atoms collect in the chilled cloud.

7. Nano devices: The parts of scientific instruments, which includes gears, wheels etc. which are in the nano level.

8. Nanocomposites: A combination of a polymer matrix and an inorganic particle, which have at least one dimension (i.e. length, width or thickness) in the nanometer range (one billionth of a meter or 10^{-9} m)

Recently, nanoprticles have attracted a great deal of attention in both fundamental and industry studies.[7,8] Because of their unique morphologies and properties endow them with potential applications.

1.3 Nanocomposites

Polymer nanocomposites are generally defined as the combination of a polymer matrix and an inorganic particle, which have at least one dimension (i.e., length, width or thickness) in the nanometer range (one billionth of a meter or 10^{-9} m).[9-13]

Polymer nanocomposites were first developed in the late 1980's, which is polyamide 6 (PA 6) (from caprolactum), which has dispersed ion exchanged

montmorillonite as the reinforcement. This material is commercially available and has been used to mould engine covers on some models of Toyota vehicles. The recent scientific discoveries and technical breakthroughs have enabled simple commodity plastics to be turned into hi tech materials featuring much improved properties.[14-16] Nanocomposite technology offers advantages such as increased tensile strength, modulus and heat distortion, improved fire retardance and UV stability, reduced permeability to gases and can even be used to impart electrical conductivity to the raw polymer. In many cases, these improvements can even be made without loss of clarity.[17-18] Numerous commercial applications are now emerging including structural materials, packaging, medical and biomedical products and electronic and photonic devices.

Materials with features on the scale of nanometer often have properties dramatically different from that of their bulk scale counterparts. For e.g., nanocrystal Cu is five times harder than ordinary Cu with its micrometer sized crystal structure.

Important among these nanoscale materials are nanocomposites; in which the constituents are mixed on a nanometer length scale. They often have properties that are superior to conventional micro scale composites[19-23] and can be synthesized using surprisingly simple and inexpensive technique.

A nanoscale dispersion of sheet like inorganic silicate particles in a polymer matrix is superior in properties such as optical clarity, strength, stiffness, thermal stability, reduced permeability and flame retardance.[24-28] The key to the synthesis of nanocomposites is how the silicate is made to disperse in the polymer.

1.3.1 Properties of nanocomposites

Nanocomposites have revealed clearly the property advantage that nanomaterial additives can provide in comparison to both their conventional filler counterparts and base polymer.[29-30] Properties, which have been shown to undergo substantial improvements, include:

- Improvements in physical and mechanical properties such as strength and modulus

- Thermal stability

- Decreased permeability to liquids and gases

- Beneficial flame retardancy with reduced smoke emissions

- Electrical conductivity

- Chemical resistance

- Optical clarity

- Aesthetic improvements.

Tensile strength, tensile modulus and heat distortion temperature (HDT) characteristics are improved with the use of nanotechnology.[31-33] Cloisite®, a nylon nanocomposite produced by Southern Clay Products with a clay loading of 5 %, exemplifies these increased mechanical properties. Nanoclays in nylon increase tensile strength in this example by 23 %. The tensile modulus is increased by 69 % and the flexural modulus is increased by 56 %. In addition, HDT is raised by 68 %. The amount of change in mechanical properties is directly related to the quantity of nanofiller used in the particular nanocomposite. For example, by adding 2 % nanoclay to nylon 6 nanocomposite increases tensile strength by 49 %. However, adding 6 % nanoclay dramatically increases the tensile strength by 98 % (Ling, et. al.).[34] This pattern also applies to the HDT and flexural modulus characteristics (table 1.1). Other nylon nanocomposite polymers have increased mechanical properties similar to Cloisite®.

Table 1.1 Mechanical properties of nylon 6 nanocomposites

	Nylon 6	**Cloisite® nanocomposite (5 %)**
Tensile strength (MPa)	82	101
Tensile modulus (MPa)	2756	4657
Flexural modulus (MPa)	2431	3780
HDT, °C	57	96

Source: Southern Clay Products, 2005

In addition to the observed improvements in performance, a lower loading level of nano filler is required.[35-37] Polymer based nanocomposites are also being developed for electronic application such as thin film capacitors in integrated circuits and solid polymer electrolytes for batteries. It is a field of broad scientific interest with impressive technological promise.[38-41]

The gaseous barrier property improvement that can result from incorporation of relatively small quantities of nano fillers is shown to be substantial.[42-43] The presence of filler incorporation at nano levels has also shown to have significant effects on the transparency and haze characteristics of films. Thermoplastic based composites; with nano filler has shown modification in crystallization behaviour in smaller spherilitic domain dimensions. As new space material candidate, nano reinforced polymers have shown a dramatic improvement over existing polymer and composite technologies.[44-47] Polymeric materials offer many advantages for space applications including ease of processing and reduced payload-to-orbit costs derived from a reduction in weight.[48-50]

Studies show that "Nylon-6 nanocomposites can achieve an OTR (oxygen transmission rate) almost four times lower than unfilled nylon-6" (Brody, 2003, p53).[51] In the case of Honeywell Aegis™ OX, the nanoclay layers act as a trap to retain the active oxygen scavengers in the polymer while reducing OTR 100-fold (Leaversuch, 2001)[52] (figure 1.1).

(Source: Plastics Technology. 2001)
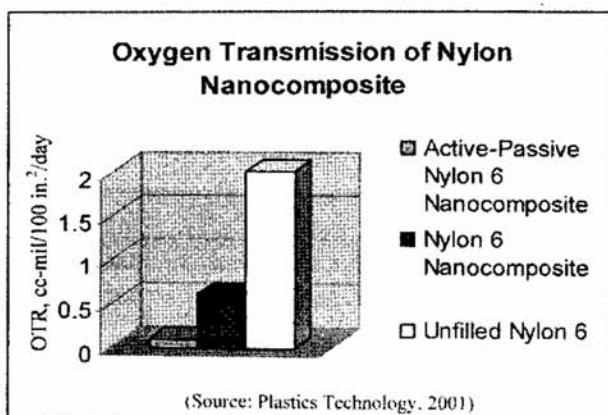
Figure 1.1 Oxygen transmission rates of nylon 6 nanocomposites

1.3.2 Classification of nanocomposites

Polymer composites are widely used in the areas of electronics, transportation, construction and consumer products, as they offer unusual combinations of properties that are difficult to obtain from individual components.[53]

Fillers are generally in the form of fibres or platelets. The nature of the fillers, including their composition, dimensions, homogeneity of dispersion and adhesion level in a polymeric matrix, is important for the bulk properties of the composites. In the last years nanoparticles have become of interest as fillers for polymeric matrices. Because of the nanoscale dimensions, nanocomposites possess superior physical and mechanical properties compared to the more conventional microcomposites, and therefore offer new technology opportunities. Three types of nanocomposites can be distinguished, depending on the number of dimensions of the dispersed particles that are in the nanometer range. When the fillers are nanosized in the three dimensions, they are practically isodimensional, such as spherical silica nanoparticles obtained by in situ sol-gel methods[54] or by polymerization promoted directly from their surface.[55] When two dimensions of the fillers are in the nanometer scale and the third is larger, forming an elongated structure, the reinforcing particles are generally named nanotubes or whiskers, such as carbon nanotubes[56] or cellulose whiskers.[57-58] Finally, nanocomposites of the third type contain reinforcing particles that have only one lateral dimension in the nanometer range: the fillers have the shape of sheets that are a few nanometers thick with a length of the order of microns.[59-60]

They can be classified based on the filler into three viz., clay (silica) based, inorganic-polymer layered and inorganic-polymer hybrids.

1.3.3 Methods of nanocomposite preparation

Nanocomposites can be prepared by the following processes:

- In situ polymerization
- Sol-gel process

- In situ intercalative polymerization

- Solution polymerization

- Emulsion polymerization

- Melt intercalation process

- Mechanical mixing.

1.3.3.1 In situ polymerization

The degree of homogeneity or phase separation between the organic and inorganic components can be controlled using in situ polymerization method.[61-62] One approach utilizes organic polymers functionalized with trialkoxy silane moieties to facilitate cross linking between the polymer and the growing organic oxide network. Cross reaction of the organic and inorganic components retard the phase separation, producing homogeneous hybrid materials. Alternatively, it is possible to produce homogeneous transparent organic inorganic composites with highly dispersed organic oxide phases using organic polymers without trialkoxy silane functionality if appropriate polymer bones are used. This approach relies on specific interaction such as hydrogen between the organic and inorganic components to retard phase separation.

1.3.3.2 Sol-gel process

Sol-gel process has been investigated for many years and has been employed for improving or modifying the process[63-64] of making inorganic glasses. E.g., acid catalyzed hydrolysis and polycondensation of tetraethyl orthosilicate (TEOS) yield a silicate glass temperature much lower than conventional fusion process. Many researches have demonstrated the successful combination of various polymers and copolymers with inorganic structures like silica at molecular level to form inorganic-organic hybrid materials through the sol- gel process. A significant feature of these new materials is the formation of covalent bonding and elimination of macroscopic interfaces, as existing in the conventional composites materials, between the polymer and inorganic components. Thus the physical properties of these hybrid materials could be

designed and controlled by varying nature and composition of both polymer and inorganic components. A number of polymers have been incorporated into SiO_2 and or /TiO_2 glass networks.

The sol-gel process provides a method for the preparation of inorganic metal oxides under mild conditions starting from organic metal oxides. This permits the structural variation without compositional alteration.

The process includes two approaches:

a   Hydrolysis of metal oxides

b   Followed by the polycondensation of hydrolysed intermediates.

Interest is mostly concerned on metal organic alkoxides, especially silicon oxide since they can form an oxide network in organic matrices.

1.3.3.3 In situ intercalative polymerizaion

This method[65] is an effective method to prepare clay-polymer composites that can provide high performance at relatively low cost, but this method adapts only to clay minerals, which is also a significant disadvantage for its application. In this process, the polymer chains are sandwiched between ultra thin layers of the clay silicates. These multi-layered sandwiches like materials are promising candidate for engineering applications

Work from the Toyota research laboratories sparked a large interest in PA 6 based silicate nanocomposites. Their papers describe PA 6 nanocomposites made by an in situ polymerization process with superior strength, modulus, heat distortion temperature, and water and gas barrier properties with respect to pure PA 6.[66-69]

The chemistry and crystal structure, in each layer in the multilayer can be quite different from those a few atoms away due to incorporation of polymer into the nano sized gaps that exists between clay's layers. Intercalated polymers do not undergo the transitions of amorphous and crystalline polymers, because the molecular confinement hinders their translational and rotational motions. Thus, the confinement of interacted polymers in layered silicates gives thermal and

oxidative stability. This concept allows designing of materials that combines the high strength and high thermal stability of clay with processability and crack-defecting properties of frequent periodic interlayer boundaries.

A way of achieving intercalation of polymers is by cation exchange grafting of the polymer through chemical bonds of layered clays to produce nano-phase organic inorganic hybrids. The principles are:

a   Intercalation of suitable monomer to the surface of the clay interlayer to produce organophilic clays followed by subsequent polymerization of the monomers to grow the polymeric chains in the interlayer spaces

b   Direct intercalation of the positively charged polymer chains from solution to anionic clay-layers.

1.3.3.4 Solution polymerization

In the solution radical polymerization technique, the grafting of polymers into clay interlayer depends on the swelling of the organophilic-modified clay promoted by a solvent. Swelling is manifested due to solvation of interlayer cations thus; inclusion of the vinyl monomer between the layers of the clays can be maximized by the use of appropriate solvent. The interlayer distance can be increased remarkably in the solvent, which have strong attractive forces between the intercalated monomer of clay and solvent molecules. Nanocomposites based on high density polyethylene, polyimide and nematic liquid crystal polymers have been synthesized by this method. The major advantage of this method is that it offers the possibility to synthesize intercalated nanocomposites based on polymers with low or even no polarity.[70-71]

1.3.3.5 Emulsion polymerization

The emulsion polymerization is recently introduced technique for nanocomposite synthesis.[72-75] The disadvantage of intercalation process is the lack of affinity between hydrophilic silicate interlayer and hydrophobic polymer and they can be applied only to pretreated silicate layer swellable with organic ions by ion exchange between organic onium ions salt and interlayer cation of clay.[76-78]

Emulsion polymerization is a heterogeneous reaction system. In this process, reacting monomer is dispersed in a water phase and polymerized with a water soluble radical initiator in presence of Na^+ montmorillonite. E.g., nanocomposites of PMMA/clay can be obtained by adding MMA monomer in continuous water phase with the aid of sodium lauryl sulfate and polymerized with potassium per sulphate in presence of Na+ montmorillonite at 70 °C for 12 hours. Formation of self induced dipole forces leads strong fixation of polymer chain into the interlayer of organic surfaces. An exfoliated composite can be obtained by using this simple technique.[79]

1.3.3.6 Melt intercalation

Polymer melt intercalation is a more efficient and environmentally being alternative to traditional intercalation process for synthesis of nanophase polymer silicate hybrids. Nanocomposites via polymer melt intercalation process involve annealing, statically under shear, a polymer and layered silicate above the softening point of the polymer. During heating, polymer chains diffuse from the bulk and polymer melt into the interlayer or galleries between the silicate layers. Depending on the degree of penetration of polymer into the layered clay hybrid is obtained with structure ranging from intercalated to exfoliate.

The melt intercalation process has become increasingly popular because[80-81] of its great potential for application with rapid processing methods such as injection moulding. A wide range of thermoplastics, from strongly polar polyamide 6 to styrene have been intercalated or exfoliated between silicate layers. However, polyolefines, which represent the biggest volume of polymers produced, have been successfully intercalated only to a limited extent.

1.3.3.7 Mechanical mixing

Melt compounding – or processing – of the nanofillers into a polymer is done simultaneously when the polymer is being processed through an extruder, injection moulder, or other processing machine. The polymer pellets and filler are pressed together using shear forces to help dispersion.[82-83]

1.3.4 Applications of nanocomposites

The nanocomposites have widely used in the various fields of injection moulding, e.g., engine cover, timing belt cover, oil reservoir tank and fuel hose in automobile industries.[84] Nanocomposites of nylon 6 –clay hybrid (NCH) shows a high modulus and high distortion temperature. The timing belt covers made from NCH by injection moulding was the first example of industrialized use of polymer-clay nanocomposites.[85-86]

Nanocomposites find applications in the following areas:

- For interior and exterior body parts resulting from improved dimensional stability
- In barrier packaging to reduce permeability of oxygen and other gases and liquids
- For use in multi layer PET (polyethylene terephthalate) bottles
- Tyre cords for radial wires
- Food grade drinking containers
- Electric component
- Sensors
- Sensitive areas like high corrosive environment, artificial bio implants etc.

Polymer-ceramic composites have been of great interest[87] as embedded capacitor material because they combine the processability of polymers with the high dielectric constant of ceramics. At present a wide range of polymer based devices such as light emitting diodes, photodiodes, solar cells, gas sensors, field electric transmitters etc., exists which have been developed and intensely studied all over the world, some of which are even produced commercially in pilot scale series. Polymer nanocomposites are being extensively studied as high capacity magnetic storage media. The magnetic behaviour of $PVA-Fe_3O_4$ nanocomposites has been studied in detail. Table 1.2 lists recent polymeric-based nanocomposite systems prepared via the sol–gel technique, in situ intercalative polymerization, and in situ polymerization.

1.3.5 Advantages of nanocomposites [88-90]

- They possess excellent stiffness and strength
- High heat distortion temperature value than base polymer
- Enhancement of property without compromising impact strength, toughness and clarity of base polymer
- Require very less quantity of fillers (5 wt%) to obtain good properties
- Enhance barrier properties and permeability property of base material
- Possess excellent flame retardant and oxidative properties
- Possess excellent optical properties such as transparency, high gloss
- Excellent corrosion resistance etc.

Table 1.2 Recent polymeric-based nanocomposite systems prepared via the sol–gel technique, in situ intercalative polymerization and in situ polymerization[91]

Systems	Uses
Sol–gel technique Polycaprolactone (PCL)/silica (TEOS)	Bone–bioerodible polymer composites for skeletal tissue repair
Polyimide/silica (TEOS)	Micro-electronics
PMMA/silica	Dental application, optical devices
Polyethylacrylate(PEA)/silica	Catalysis support, stationary phase for chromatography
Polyethyleneoxide (PEO)/silica (TEOS)	Electrolyte and highly conductive polymer
Poly(p-phenylene vinylene)(PPV)/silica (TMOS)	Non-linear optical material for optical wave guides
Poly(amide–imide)/TiO_2 composite membranes	Gas-separation applications
Polycarbonate/silica (TEOS)	Abrassion-resistant coating
In situ intercalative polymerization PCL/Cr^{3+} fluorohectorite and montmorillonite	Biodegradable/biocompatible materials, packaging (enhanced barrier-properties)
Epoxy/organo-modified montmorillonite	Improved properties (aeronautics, …)

Systems	Uses
Polyimide/organo-modified montmorillonite	Materials for microelectronics with reduced thermal expansion coefficient and moisture absorption
Polystyrene/organo-modified montmorillonite	Improved properties
Copolymer butadiene/acrylonitrile/organo-modified montmorillonite	Rubber with enhanced barrier properties (H_2, H_2O)
iPP/organo clay	Improved properties
Starch/organo-modified montmorillonite	Enhanced barrier properties
Nylon/organo-modified montmorillonite	Improvement of structural, mechanical, thermal and barrier characteristics without significant loss in clarity or strength
In situ polymerization **Polyimide/AlN**	Materials for microelectronics with reduced thermal expansion coefficient and moisture absorption
PET/SiC	Improved properties
PMMA/CaCO$_3$	Biocompatible materials and optical devices
Polystyrene–polyvinylbenzene/Fe$_2$O$_3$	Optical transparency and superparamagnetism (colour imaging and printing)

1.3.6 Nanocomposite structure

Depending on the strength of interfacial interactions between the polymer matrix and the silicate layers, three types of polymer composites may be formed as shown in figure 1.2. In conventional composites, the clay tactoids exist in their original aggregated state with nanolayers stacked face to face and without any polymer intercalation, which results in poor mechanical properties. In the

case of intercalated polymer-clay nanocomposite few molecular layers of polymer penetrate the clay host galleries increasing the d spacing. And finally, exfoliated polymer-clay nanocomposites contain individual nanolayers separated in a continuous polymer matrix by an average distance which depends on the clay loading. Usually, the clay content of an exfoliated nanocomposite is lower than that of an intercalated nanocomposite. Exfoliation is more appealing for enhancement of certain properties of the material because of the high degree of dispersion and maximum interfacial area between polymer and clay (figure 1.2).
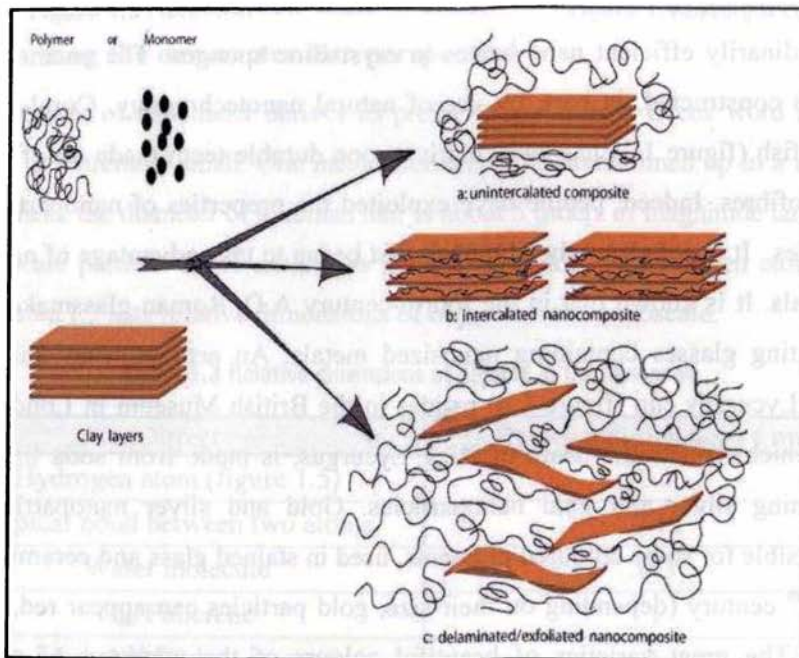
Figure 1.2 Nanocomposite structure

1.4 Nanomaterials

Nanomaterials have generated tremendous interest because they present an opportunity to deliver unprecedented material performance.[92-95] This opportunity is based on the unique properties (*e.g.*, magnetic, optical, mechanical, electronic) that vary continuously or abruptly with changes in the size of the material at the nanoscale (1 to100 nanometers). These step-like changes in nanoscale properties suggest both enormous potential and challenges. The term nanoparticle covers a diverse range of chemical and other

entities. They can be metallic, mineral, polymer-based or a combination of materials. Nanoparticles include metal (Au, Pt, Pd, Cu etc.), semiconductor (CdS, CdSe, ZnS etc.), metal and semiconductor oxide (Fe_2O_3, Al_2O_3, SiO_x, ZnO etc.). They have multiple uses: as catalysts, drug delivery mechanisms, dyes, sunscreens, filters and much more.

1.4.1 Historical approach

Nanoparticles are not new: they have existed widely in the natural world, for millions of years, created by living things or volcanic activity. Nano-effects are astonishingly common in nature – from non reflective moths' eyes to extraordinarily efficient nano-lenses in crystalline sponges. The enamel of our teeth is constructed, in part, by use of natural nanotechnology. Coral- grazing parrot fish (figure 1.3) has particularly strong durable teeth made up of bundles of nanofibres. Indeed, people have exploited the properties of nanoparticles for centuries. It is not clear when humans first began to take advantage of nanosized materials. It is known that in the fourth-century A.D. Roman glassmakers were fabricating glasses containing nanosized metals. An artifact from this period called Lycurgus cup (figure 1.4) resides in the British Museum in London. The cup, which depicts the death of King Lycurgus, is made from soda lime glass containing silver and gold nanoparticles. Gold and silver nanoparticles are responsible for some coloured pigments, used in stained glass and ceramics since the 10th century (depending on their size, gold particles can appear red, blue or gold). The great varieties of beautiful colours of the windows of medieval cathedrals are due to the presence of metal nanoparticles in the glass. Photography is an advanced and mature technology developed in the eighteenth and nineteenth centuries, which depends on production of silver nanoparticles sensitive to light. Computer chips have been made using nanotechnologies for the last 20 years, and chemists have been making polymers – large molecules made up of nanoscale subunits – for decades.
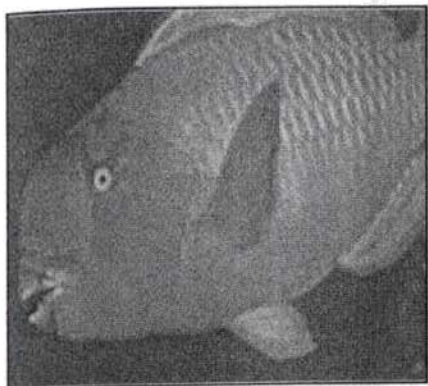
Figure 1.3 Parrot fish

Figure 1.4 Lycurgus cup

1.4.2 Putting the nanometer into perspective

The unit of nanometer derives its prefix 'nano' from a Greek word meaning 'dwarf' or extremely small. One nanometer spans 3-5 atoms lined up in a row. For comparison, the diameter of a human hair is about 5 orders of magnitude larger than a nanoscale particle. DNA molecules are 2.5 nm wide, 10 hydrogen atoms span 1nm. Table 1.3 lists relative dimensions of objects in the nanoscale.

Table 1.3 Relative dimensions of objects in the nanoscale

Object	Relative dimensions (nm)
Hydrogen atom (figure 1.5)	0.1
Typical bond between two atoms	0.15
Water molecule	0.3
C_{60} Fullerene	1
6 bonded Carbon atoms	1
Helix of DNA (figure 1.6)	2.5
Quantum dots of CdSe	8
Cell membranes	8
Dendrimers	10
Virus	100
Red Blood Cell (figure 1.7)	7,000
Human hair	80,000
Dust mite	200,000
Head of pin	1,000,000
Human height	2,000,000,000
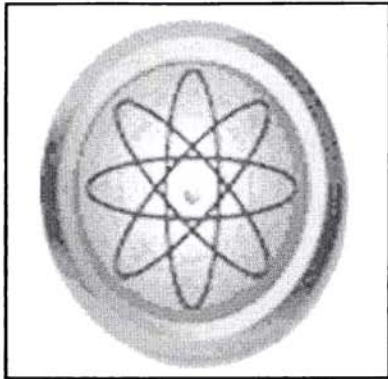
Figure 1.5 Hydrogen atom
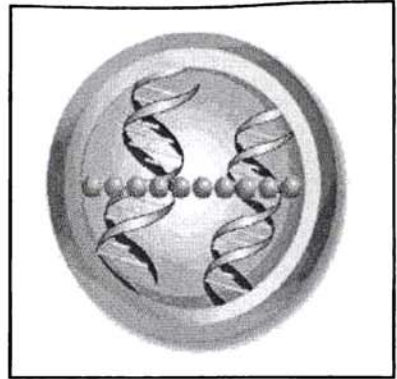
Figure 1.6 DNA molecules
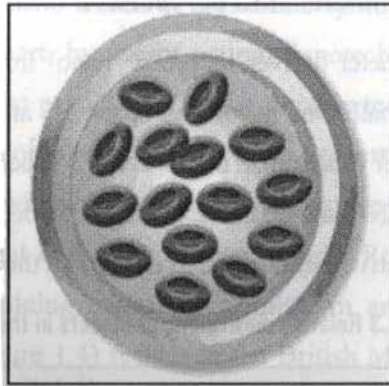
Figure 1.7 Biological cells are thousands of nanometers

1.4.3 Properties of nanomaterials

Nanomaterials fall into one of three general categories depending upon their defining nanometer dimension. Thin (nano) films or surface coatings used in computer chips and emerging catalyst and fuel cell applications represent one-dimensional nanomaterials. Carbon nanotubules (which are extended tubes of single or multiwalled rolled graphene sheets), inorganic nanotubes (*i.e.*, oxide-based nanotubes), nanowires (made of silicone, gallium nitride, and indium phosphide) and biopolymers (such as DNA) represent two-dimensional nanomaterials. Nanoparticles exist in three dimensions having diameters of less than 100 nm. They include naturally occurring particles like those resulting from the combustion of organic material, as well as engineered

particles such as the fullerenes and quantum dots. Engineered nanomaterials are not a uniform group of substances, as they differ in size, shape, surface area, chemical composition (*e.g.*, cadmium, carbon, cobalt, copper, gold, iron, platinum, silicon, silver, titanium dioxide, zinc, and others), biopersistence, and possible environmental and human health impact. Concerns are that these new and unique properties result in different behaviours that may present unforeseen or unintended risks.

In the mid- 1980s a new class of material-hollow carbon spheres was discovered. These spheres were called buckyballs or fullerenes. The C_{60} (60 carbon atoms chemically bonded together in a ball shaped molecule) buckyballs (figure 1.8) inspired research that led to fabrication of carbon nanofibres, with diameters under 100 nm. In 1991 S. Iijima of NEC in Japan reported the first observation of carbon nanotubes, (figure 1.9) which are now produced by a number of companies in commercial quantities.[96] Figure 1.9 shows the structure of a tube formed by rolling the graphite sheet about an axis parallel to C-C bonds. Nanoparticles of carbon-rods, fibres, tubes with single walls or double walls, open or closed ends and straight or spiral forms have been synthesized. They are reported to be thermally stable in vacuum upto 2800 °C, to have a capacity to carry an electric current a thousand times better than copper wires, and to have twice the thermal conductivity of diamond. They are used as reinforcing particles in nanocomposites.
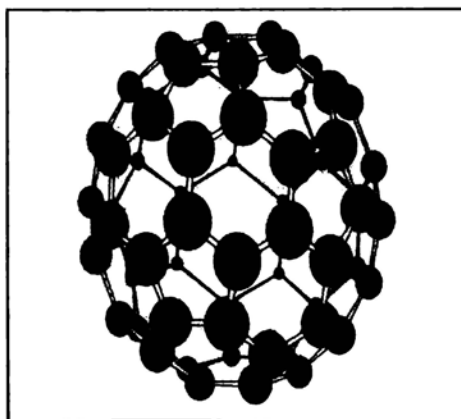
Figure 1.8 Structure of fullerenes
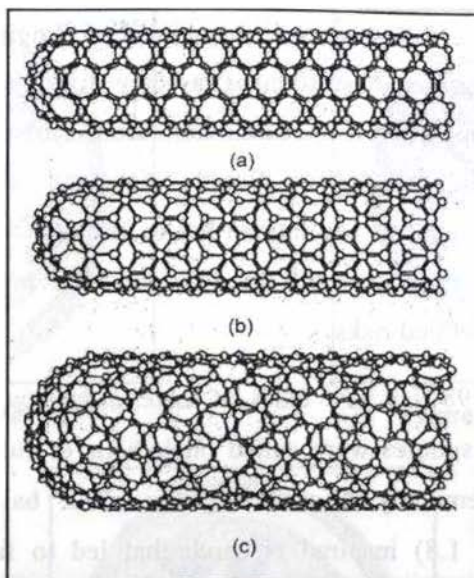
Figure 1.9 Illustration of some possible structures of carbon nanotubes, depending on how graphite sheets are rolled: (a) armchair structure; (b) zigzag structure; (c) chiral structure

1.4.4 Classification of nanomaterials

Nanomaterial serve as a bridge between the molecular and condensed phase.[97-98] The thousands of substances that are solids under normal temperatures and pressures can be subdivided into metals, ceramics, semiconductors, composites, and polymers. These can be further subdivided into biomaterials, catalytic materials, coatings, glasses, and magnetic and electronic materials. All of these solid substances, with their widely variable properties take on another subset of new properties when produced in nanoparticle form.

The classification of nanomaterials is the following:[99]

Cluster A collection of units of upto about 50 units.

Colloid A stable liquid phase containing particles in the 1-1000 nm range

Nanoparticle A solid particle in the 1-1000 nm range that could be noncrystalline, an aggregate of crystallites or a single crystallite.

Nanocrystal A solid particle that is single crystal in the nanometer size range.

Nanostructured or nanoscale material Any solid material that has a nanometer dimension; three dimensions-particles; two dimensions-thin films; one dimensions-thin wire. Metals, semiconductors, ceramics belongs to this class.

Nanophase material The same as nanostructured material.

Quantum dot A particle that exhibits a size quantization effect in at least one dimension.

1.4.5 Preparation of nanomaterials

There are two general ways available to produce nanomaterials. The first way is to start with a bulk material and then break it into smaller pieces using mechanical, chemical or other form of energy (top-down). An opposite approach is to synthesize the material from atomic or molecular species via chemical reactions, allowing for the precursor particles to grow in size (bottom-up). Both approaches can be done in either gas, liquid, supercritical fluids, solid states, or in vacuum.[100-104] Most of the manufacturers are interested in the ability to control: a) particle size b) particle shape c) size distribution d) particle composition e) degree of particle agglomeration.[105-107]

1.4.5.1 What processes are used for bottom-up manufacturing? [108]

Methods to produce nanoparticles from atoms are chemical processes based on transformations in solution. E.g., sol-gel processing, chemical vapour deposition (CVD), plasma or flame spraying synthesis (figure 1.10), laser pyrolysis (figure 1.11),[109] atomic or molecular condensation. These chemical processes rely on the availability of appropriate "metal-organic" molecules as precursors. Sol-gel processing differs from other chemical processes due to its relatively low processing temperature. This makes the sol-gel process cost-effective and versatile. In spraying processes the flow of reactants (gas, liquid in form of aerosols or mixtures of both) is introduced to high-energy flame produced, for example by plasma spraying equipment or carbon dioxide laser. The reactants decompose and particles are formed in a flame by homogeneous nucleation and growth. Rapid cooling results in the formation of nanoscale particles.

These are chemical processes[110] to materials based on transformations in solution such as sol-gel processing, hydro or solvo thermal synthesis, metal organic decomposition (MOD), or in the vapour phase chemical vapour deposition (CVD). Most chemical routes rely on the availability of appropriate "metal-organic" molecules as precursors. Among the various precursors of metal oxides, namely metal β-diketonates and metal carboxylates, metal alkoxides are the most versatile. They are available for nearly all elements and cost-effective synthesis from cheap feedstock has been developed for some.[111]

1.4.5.2 How to control the construction and growth of the nanoparticles

Two general ways are available to control the formation and growth of the nanoparticles. One is called arrested precipitation (figure 1.12) which depends either on exhaustion of one of the reactants or on the introduction of the chemical that would block the reaction. Another method relies on a physical restriction of the volume available for the growth of the individual nanoparticles by using templates.

$$TiCl_4 + 2H_2O = TiO_2\downarrow + 4HCl$$

Formation of TiO_2 nanoparticles via above reaction is shown schematically in figure 1.12.
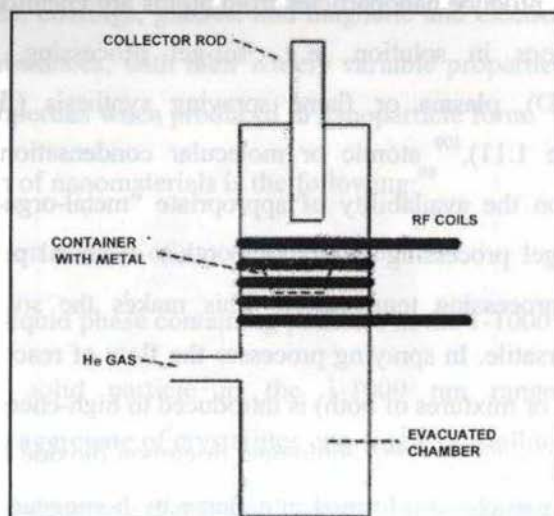
Figure 1.10 Illustration of apparatus for the synthesis of nanoparticle using an RF produced plasma (from reference 111)·
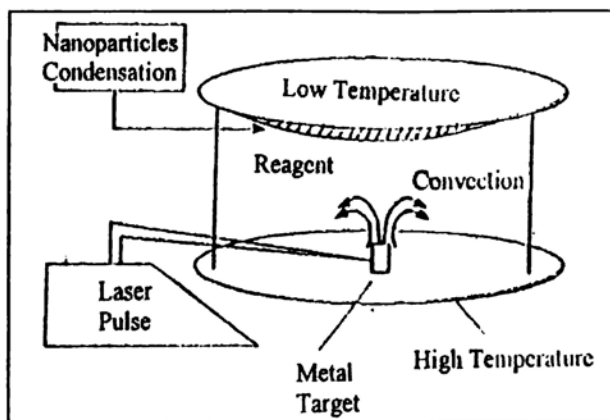
Figure 1.11 Schematic view of the installation for the synthesis of nanoparticles by laser vapourization of metals (from reference 111)
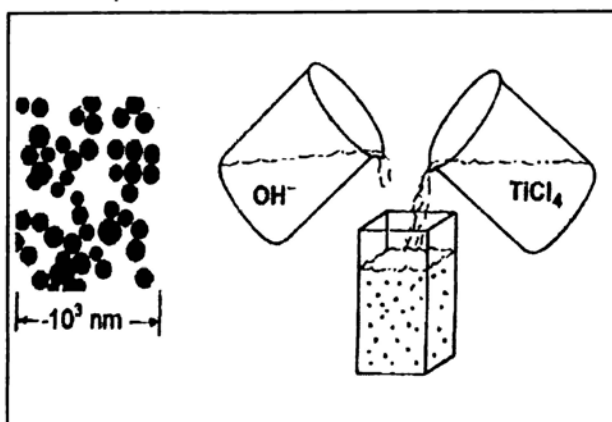
Figure 1.12 Scheme of TiO₂ nanoparticles formation by the method of arrested precipitation TEM picture of TiO₂ nanoparticles is shown on the left (from reference 111)

1.4.5.3 Sol-gel process

The sol gel technique is a long-established industrial process for the generation of colloidal nanoparticles from liquid phase, which has been further developed in last years for the production of advanced nanomaterials and coatings.[112] Sol-gel-processes are well adapted for oxide nanoparticles and composites nanopowder synthesis. The main advantages of sol-gel techniques for the preparation of materials are low temperature of processing, versatility, and flexible rheology allowing easy shaping and embedding. They offer unique opportunities for access to organic-inorganic materials.[113-115] The most commonly used precursors of oxides are alkoxides, due to their commercial availability and to

the high liability of the M-OR bond allowing *facile tailoring in situ* during processing.

1.4.5.4 Aerosol-based processes

Aerosol-based processes are a common method for the industrial production of nanoparticles. Aerosols can be defined as solid or liquid particles in a gas phase, where the particles can range from molecules up to 100 μm in size. Aerosols were used in industrial manufacturing long before the basic science and engineering of the aerosols were understood. For example, carbon black particles used in pigments and reinforced car tyres are produced by hydrocarbon combustion; titania pigment for use in paints and plastics is made by oxidation of titanium tetrachloride; fumed silica and titania formed from respective tetrachlorides by flame pyrolysis; optical fibres are manufactured by similar process.

Traditionally, spraying is used either to dry wet materials or to deposit coatings. Spraying of the precursor chemicals onto a heated surface or into the hot atmosphere results in precursor pyrolysis and formation of the particles. For example, a room temperature electro-spraying process was developed at Oxford University to produce nanoparticles of compound semiconductors and some metals. In particular, CdS nanoparticles were produced by generating aerosol micro-droplets containing Cd salt in the atmosphere containing hydrogen sulphide.

1.4.5.5 Chemical vapour deposition (CVD)

CVD consists in activating a chemical reaction between the substrate surface and a gaseous precursor. Activation can be achieved either with temperature (Thermal CVD) or with a plasma[116] (PECVD: Plasma Enhanced Chemical Vapour Deposition). The main advantage is the nondirective aspect of this technology. Plasma allows decreasing significantly the process temperature compared to the thermal CVD process. CVD is widely used to produce carbon nanotube (figure 1.13).
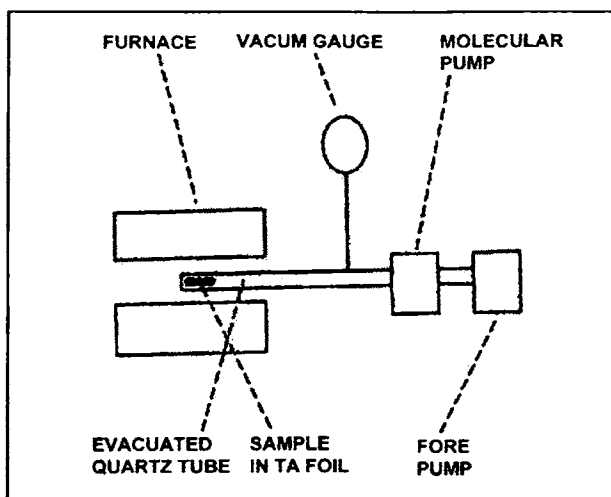
Figure 1.13 Apparatus used to make metal nanoparticle by thermally decomposing solids consisting of metal cations and molecular anions, or metal organic solids

1.4.5.6 Atomic or molecular condensation

This method is used mainly for metal containing nanoparticles. A bulk material is heated in vacuum to produce a stream of vapourized and atomized matter, which is directed to a chamber containing either inert or reactive gas atmosphere. Rapid cooling of the metal atoms due to their collision with the gas molecules results in the condensation and formation of nanoparticles. If a reactive gas like oxygen is used then metal oxide nanoparticles are produced.

1.4.5.7 Using gas-phase condensation to produce metal nanopowders

The theory of gas-phase condensation for the production of metal nanopowders is well known, having been first reported in 1930. Gas-phase condensation uses a vacuum chamber that consists of a heating element, the metal to be made into nano-powder, powder collection equipment and vacuum hardware. The process utilises a gas, which is typically inert, at pressures high enough to promote particle formation, but low enough to allow the production of spherical particles. Metal is introduced onto a heated element and is rapidly melted. The metal is quickly taken to temperatures far above the melting point, but less than the boiling point, so that an adequate vapour pressure is achieved. Gas is continuously introduced into the chamber

and removed by the pumps, so the gas flow moves the evaporated metal away from the hot element. As the gas cools the metal vapour, nanometer-sized particles form. These particles are liquid since they are still too hot to be solid. The liquid particles collide and coalesce in a controlled environment so that the particles grow to specification, remaining spherical and with smooth surfaces. As the liquid particles are further cooled under control, they become solid and grow no longer. At this point the nanoparticles are very reactive, so they are coated with a material that prevents further interaction with other particles (agglomeration) or with other materials.

1.4.5.8 Supercritical fluid synthesis

Methods using supercritical fluids are also powerful for the synthesis of nanoparticles. For these methods, the properties of a supercritical fluid (fluid forced into supercritical state by regulating its temperature and its pressure) are used to form nanoparticles by a rapid expansion of a supercritical solution. Supercritical fluid method is currently developed at the pilot scale in a continuous process.

1.4.5.9 Spinning to make thin polymer fibres

An emerging technology for the manufacture of thin polymer fibres is based on the principle of spinning dilute polymer solutions in a high voltage electric field. Electro spinning is a process by which a suspended drop of polymer is charged with thousands of volts. At a characteristic voltage the droplet forms a Taylor cone and a fine jet of polymer releases from the surface in response to the tensile forces generated by interaction of an applied electric field, with the electrical charge carried by the jet. This produces a bundle of polymer fibres. The jet can be directed to a grounded surface and collected as a continuous web of fibres ranging in size from a few μm's to less than 100 nm.

1.4.5.10 Mechanical processes

These include grinding, milling, and mechanical alloying techniques. Provided that one can produce a coarse powder as a feedstock, these processes utilize the age-old technique of physically pounding coarse powders into finer

and finer ones, similar to flour mills. Today, the most common processes are either planetary or rotating ball mills. The advantages of these techniques are that they are simple, require low-cost equipment and, provided that a coarse feedstock powder can be made, the powder can be processed. However, there can be difficulties such as agglomeration of the powders, broad particle size distributions, contamination from the process equipment itself, and often difficulty in getting the very fine particle sizes with viable yields. It is commonly used for inorganic and metals, but not organic materials.

1.4.5.11 Using templates to form nanoparticles

Any material containing regular nano-sized pores or voids can be used as a template to form nanoparticles. Examples of such templates include porous alumina, zeolites, di-block co-polymers, dendrimers, proteins and other molecules. The template does not have to be a 3D object. Artificial templates can be created on a plane surface or a gas-liquid interface by forming self-assembled monolayers.

1.4.6 Characterization techniques

It is very important to adapt and develop a range of techniques that can characterize the optical, structural, electronic and magnetic properties of nanostructured systems.[117-120] The different techniques are high resolution transmission electron microscopy (HRTEM), scanning probe microscopies (scanning tunneling microscopy; atomic force microscopy), X-ray diffraction (XRD), X-ray photoelectron spectroscopy (XPS), X-ray absorption fine structure spectroscopy (EXAFS), infra red spectroscopy (IR). Nuclear magnetic resonance (NMR), scanning electron microscope (SEM), transmission electron microscope (TEM) etc. are some of the techniques used.[121-122]

1.4.7 Novel applications of nanomaterials[123]

Since nanomaterials possess unique, beneficial chemical, physical, and mechanical properties, they can be used for a wide variety of applications. These applications include, but are not limited to, the following:

1.4.7.1 Next-generation computer chips

The microelectronics industry has been emphasizing miniaturization, whereby the circuits, such as transistors, resistors, and capacitors, are reduced in size. By achieving a significant reduction in their size, the microprocessors, which contain these components, can run much faster, thereby enabling computations at far greater speeds. However, there are several technological impediments to these advancements, including lack of the ultrafine precursors to manufacture these components; poor dissipation of tremendous amount of heat generated by these microprocessors due to faster speeds; short mean time to failures (poor reliability) etc. Nanomaterials help the industry break these barriers down by providing the manufacturers with nanocrystalline starting materials, ultra-high purity materials, materials with better thermal conductivity, and longer-lasting, durable interconnections (connections between various components in the microprocessors).

1.4.7.2 Kinetic energy (KE) penetrators with enhanced lethality

The Department of Defense (DoD) is currently using depleted-uranium (DU) projectiles (penetrators) for its lethality against hardened targets and enemy armored vehicles. However, DU has residual radioactivity, and hence, is toxic (carcinogenic), explosive, and lethal to the personnel who use them. However, some of the important reasons for the continued use of DU penetrators are that they possess a unique self-sharpening mechanism on impact with a target, and the lack of suitable non-explosive, non-hazardous replacement for DU. Nanocrystalline tungsten heavy alloys lend themselves to such a self-sharpening mechanism because of their unique deformation characteristics, such as grain-boundary sliding. Hence, nanocrystalline tungsten heavy alloys and composites are being evaluated as potential candidates to replace DU penetrators.

1.4.7.3 Better insulation materials

Nanocrystalline materials synthesized by the sol-gel technique results in foam like structure called an "aerogel." These aerogels are porous and extremely

lightweight; yet, they can withstand 100 times their weight. Aerogels are composed of three-dimensional, continuous networks of particles with air (or any other fluid, such as a gas) trapped at their interstices. Since they are porous and air is trapped at the interstices, aerogels are currently being used for insulation in offices, homes etc. By using aerogels for insulation, heating and cooling bills are drastically reduced, thereby saving power and reducing the attendant environmental pollution. They are also being used as materials for "smart" windows, which darken when the sun is too bright (just as in changeable lenses in prescription spectacles and sunglasses) and they lighten themselves, when the sun is not shining too brightly.

1.4.7.4 Phosphorus for high-definition TV

The resolution of a television, or a monitor, depends greatly on the size of the pixel. These pixels are essentially made of materials called "phosphorus," which glow when struck by a stream of electrons inside the cathode ray tube (CRT). The resolution improves with a reduction in the size of the pixel, or the phosphorus. Nanocrystalline zinc selenide, zinc sulfide, cadmium sulfide, and lead telluride synthesized by the sol-gel technique are candidates for improving the resolution of monitors. The use of nanophosphorus is envisioned to reduce the cost of these displays so as to render high-definition televisions (HDTVs) and personal computers affordable to be purchased by an average household in the U. S.

1.4.7.5 Low-cost flat panel displays

Flat-panel displays represent a huge market in the laptop (portable) computers industry. However, Japan is leading this market, primarily because of its research and development efforts on the materials for such displays. By synthesizing nanocrystalline phosphorus, the resolution of these display devices can be greatly enhanced, and the manufacturing costs can be significantly reduced. Also, the flat-panel displays constructed out of nanomaterials possess much higher brightness and contrast than the conventional ones owing to their enhanced electrical and magnetic properties.

1.4.7.6 Tougher and harder cutting tools

Cutting tools made of nanocrystalline materials, such as tungsten carbide, tantalum carbide, and titanium carbide, are much harder, much more wear-resistant, erosion-resistant, and last longer than their conventional (large-grained) counterparts. They also enable the manufacturer to machine various materials much faster, thereby increasing productivity and significantly reducing manufacturing costs. Also, for the miniaturization of microelectronic circuits, the industry needs microdrills (drill bits with diameter less than the thickness of an average human hair or 100 μm) with enhanced edge retention and far better wear resistance. Since nanocrystalline carbides are much stronger, harder, and wear-resistant, they are currently being used in these microdrills.

1.4.7.7 Elimination of pollutants

Nanocrystalline materials possess extremely large grain boundaries relative to their grain size. Hence, nanomaterials are very active in terms of their chemical, physical, and mechanical properties. Due to their enhanced chemical activity, nanomaterials can be used as catalysts to react with such noxious and toxic gases as carbon monoxide and nitrogen oxide in automobile catalytic converters and power generation equipment to prevent environmental pollution arising from burning gasoline and coal.

1.4.7.8 High-power magnets

The strength of a magnet is measured in terms of coercivity and saturation magnetization values. These values increase with a decrease in the grain size and an increase in the specific surface area (surface area per unit volume of the grains) of the grains. It has been shown that magnets made of nanocrystalline yttrium-samarium-cobalt grains possess very unusual magnetic properties due to their extremely large surface area. Typical applications for these high-power rare-earth magnets include quieter submarines, automobile alternators, land-based power generators, motors for ships, ultra-sensitive analytical instruments, and magnetic resonance imaging (MRI) in medical diagnostics.

From the above examples, it is quite evident that nanocrystalline materials, synthesized by the sol-gel technique, can be used in a wide variety of new, unique and existing applications. It is also very evident that nanomaterials outperform their conventional counterparts because of their superior chemical, physical, and mechanical properties and of their exceptional formability. Table 1.4 lists primary types of nanomaterials and their applications.

Table 1.4 Primary types of nanomaterials and their applications

Type	Market
Nanoparticles (dots, bars, dendrimers, or colloids)	Chemicals (*e.g.*, cosmetics, sunscreens)
Quantum dots (molecular tags)	Medical/pharmaceutical (*e.g.*, drug delivery, controlled release, drug targeting, increased bioavailability, cancer detection)
Fullerenes	Information/communication (*e.g.*, computer chips, semiconductors)
Nanoporous materials	Energy
Nanotubes (single or multiwalled)	Automotive (*e.g.*, lighter, stronger, and safer components/composites; fog and crack resistant coatings for windshields; self-cleaning windows; batteries; lubricants; catalytic converters; fuel cells; suspension fluids; paints; more adherent and longer running tyres; electronics.
Nanostructured materials	Aerospace
Nanofibres	Textiles (*e.g.*, stain and wrinkle resistant; stronger)
Nanocapsules	Agriculture (*e.g.*, flavour and nutrient storage; food quality sensors)
Nanowires	Consumer goods (*e.g.*, disinfectant sprays, dyes, paints)
Other	Environmental (*e.g.*, nanosponges to strip contaminants from waste streams or for remediation and drinking water purposes; air quality monitoring)

1.5 Filler

The term filler is usually applied to solid additives incorporated into the polymer to modify its physical (usually mechanical) properties.[124-125] Air and other gases, which could be considered as filler in cellular polymers, are dealt with separately. A number of types of filler are generally recognized in polymer technology and there are summarized in figure (1.14).
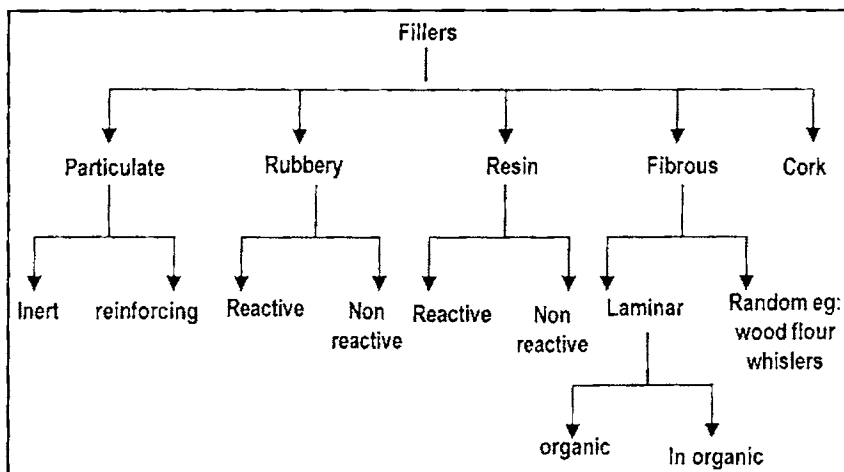
Figure 1.14 Classification of filler in polymer compounds

Fillers or extruders as they are called in the industry are finely divided solids are added to polymer system to improve properties or reduce cost.[126-132] Fillers can be classified as inactive, semi-active or active. Although the difference between the various classes cannot be rigidly defined, the designation normally relates to the influence of the filler in the compound on viscosity, crystallization, and mechanical properties etc. It is generally assumed that the degrees of activity depend on interaction forces between the polymer and filler. In plastics, fillers increase stiffness, affect electrical properties, improve chemical resistance and reduce cost.[133-134]

1.5.1 Polymer-filler interface[135]

Interfaces may arise in polymer systems for two reasons. On the one hand they may be the surfaces between two mutually insoluble and chemically distinct phases, which are at equilibrium with respect to each other. On the other hand

they may exist between two essentially miscible components, which have not yet reached equilibrium.

The mechanical behaviour of the composite reflects the interaction between the various phases. In short if there is no binding between the two, whether chemical or physical, as from secondary valence forces, the material response, for small strains at least, will be as if the matrix contained holes of shape identical to that of the filler. At higher strain the deforming matrix may impress itself on the more rigid filler, thereby producing a mechanical friction or related effect, which will permit the filler to generate some growing influence on sample response. If there is adhesion between the two phases then even at low strains stress transfer can take place across the interface, thus allowing the filler to share the stress and by so doing, provide a reinforcing effect. If the interface is very rigid because of very strong interaction, a possibility arises of deterioration in some properties, which require some interface flexibility in order perhaps to dissipate excess energy.

1.6 Polymer crystallization and nucleating agents

Nucleation mechanisms for semicrystalline polymers have a significant influence on the morphology of the crystalline phase. The number and size distribution of nucleation sites affect product performance. In many cases, when there is a deliberate attempt to control polymer properties by manipulating morphology, nucleating agents are used. There are a few hundred publications in the research literature that focus on polymer crystallization via organic[136] and inorganic[137] nucleating agents. However, there are only 10–15 investigations based on nanoscale-size nucleating agents for polymers, in general, and even fewer that employ nanoparticles of zinc oxide.[138] The most common polymers whose crystallization kinetics have been enhanced by nucleating agents are (i) isotactic polypropylene (iPP), (ii) poly (ethylene terephthalate) (PET), and (iii) nylon 6. Several hundred publications discuss nucleation in polypropylene, but there are more than order-of magnitude fewer that employ inorganic nucleating agents.

The use of inorganic nanoparticle nucleating agents for iPP is extremely rare.[139] Zhang et al.[140] studied the mechanical properties and crystallization behaviour of isotactic polypropylene composites with crosslinked styrene-butadiene nanoparticles that contain sodium benzoate. The stiffness of these nanocomposites is enhanced because the nucleation density is higher and the crystallization kinetics of iPP proceed faster in the presence of ultrafine elastomeric particles with length scales below 100 nm. Gui et al.[141] report that 0.8 wt% of an organic phosphorus nucleating agent dispersed in iPP increases the calculated nucleation density by six orders of magnitude, and the crystallization temperature is enhanced by 12 $^\circ$C. Hydrophobic nano-silicates with good wettability and dispersion characteristics enhance thermal stability, reinforce mechanical properties and increase the crystallization temperature of poly(ethylene terephthalate).[142] However, hydrophilic nano-silicates in PET, which also increase its crystallization temperature, induce shear-thinning behaviour at very low frequencies in dynamic rheometry and function as viscosity-reducers.[142]

Nucleating agents can be classified as natural[143] or synthetic.[144] In most cases, dibenzylidene sorbitol and 3,4- dimethyldibenzylidene sorbitol, at concentrations between 0.5 and 1.5 wt%, increase the rate of polymer crystallization and the temperature at which the maximum rate of crystallization occurs upon cooling from the molten state. Organocarboxylic acids function as nucleating agents for polyolefins because their polar groups make them insoluble in the molten polymer, and their organic groups provide the necessary wetting characteristics that are required when a foreign surface is implanted in the molten polymer. Molecular interactions between the polymer and the surface of the nucleating agent must be operative to increase the rate of crystallization and the temperature at which the maximum rate occurs upon cooling from the molten state.[145-147] These polymer-surface interactions reduce the interfacial free energy barrier for spontaneous nucleation and growth of a birefringent dendritic phase in the molten

polymer. When the nucleation induction period is shorter and the number of primary nucleation sites increases, the overall rate of crystallization increases. Heterogeneous nucleating agents have been used industrially to reduce process cycle times, induce crystallization at smaller degrees of supercooling (i.e., T_{melt} to $T_{crystallization}$), and produce translucent materials with smaller crystallite sizes.[148] Several classes of inorganic compounds can be employed as nucleating agents[149-150], but the oxides of aluminum (Al_2O_3), calcium (CaO), silicon (SiO_2), titanium (TiO_2), and zinc (ZnO) are most useful. Both micro- and nanoscale-size zinc oxides function as inorganic supports for organic nucleating agents. Typical organic nucleating agents for semicrystalline polymers are based on the modification of sorbitol.[144,] Shepard et al.[151] found that dibenzylidene sorbitol (DBS) undergoes self-assembly and promotes the formation of spherulites in commercially important polyolefins, such as polypropylene. Feng et al.[152] investigated isothermal and nonisothermal crystallization kinetics of virgin and DBS-nucleated isotactic polypropylene.

1.7 Chitin and chitosan

Nature has chosen two different but related polysaccharides to provide structure and integrity to plants and animals like crustaceans and insects. Plants have cellulose in their walls while insects and crustaceans have chitin in their shells. Cellulose molecules are large chains of glucose units while chitin molecules are large chains of N-acetyl glucosamine units. Cellulose and chitin are two kinds of the most abundant biopolymers on earth. Chitin is a highly insoluble material resembling cellulose in its solubility and chemical reactivity. It may be regarded as cellulose with hydroxyl at position C-2 replaced by acetamido groups. The principle derivative of chitin is chitosan.[153] It is formed through N-deacetylation of the chitin molecule. The structure of chitin, chitosan and cellulose are shown in figure 1.15.
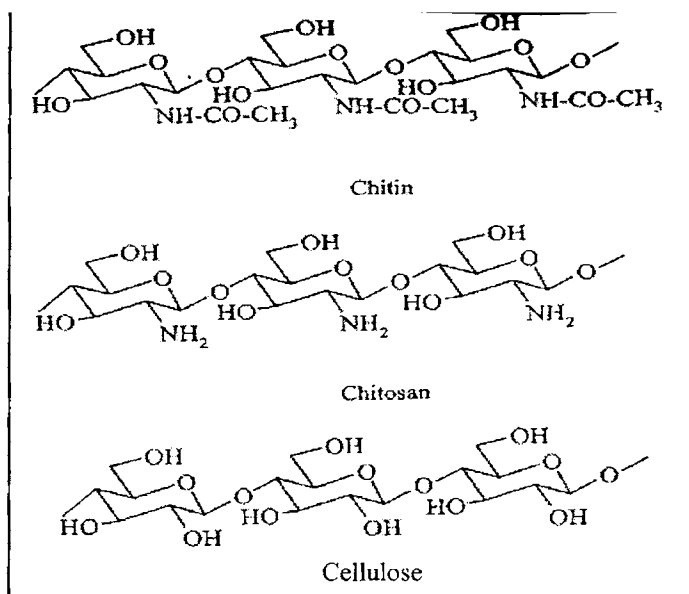
Figure 1.15 Structure of chitin, chitosan and cellulose

Thus chitin is a nitrogenous polysaccharide, which is white, hard and inelastic. It is found in the outer skeleton of insects, crab, shrimp and lobsters and in the internal structure of other vertebrate.[154]

Chitin has a crystalline structure and it constitutes a network of organized fibres. Chitosan also occurs naturally in some fungi but its occurrence is much less widespread than that of chitin.[155]

1.7.1 Physiochemical characteristics of chitosan

Most of the naturally occurring polysaccharides such as cellulose, dextran, pectin, agar etc. are neutral or acidic in nature, while chitin and chitosan are highly basic polysaccharides. Their unique properties include polyoxysalt formation, ability to form films, chelate metal ions and optical structural characteristics.

1.7.1.1 Degree of N-acetylation

Chitosan is characterized by either the degree of acetylation (DA), which corresponds to the N-acetylamine groups or the degree of deacetylation DDA (DDA = 100-DA), D-glucosamine groups. The degree of acetylation has an

influence on all the physicochemical properties (molecular weight, viscosity, solubility etc.). Many techniques have been tried to determine the degree of acetylation more precisely, which include IR spectroscopy, pyrolysis gas chromatography, gel permeation chromatography and UV spectrophotometry. The most appropriate technique for rapid characterization seems to be IR spectroscopy.

1.7.1.2 Molecular weight

The knowledge of average molecular weight of chitin and chitosan is very important for industrial uses and for critical applications fields. Although the primary structure of chitosan comprises a backbone of (1-4)-β-D-glucosamine residues randomly acetylated to various extents, the name chitosan is in fact a collective term for deacetylated chitin differing in terms of crystallinity, optical characteristics, degree of deacetylation, impurity content and average molecular weight. Chitosan molecular weight distribution has been obtained using HPLC. Viscosity measurements are widely used. More recently gel permeation chromatography (GPC) or gel filtration chromatography (GFC) has been applied to study the molecular weight.

1.7.1.3 Solubility

Chitin is highly hydrophobic in nature and is insoluble in common organic solvents as well. It is soluble in hexafluoroisoproponol, hexaflouroacetone, chloroalcohol in conjugation with aqueous solution of mineral acids and dimethyl acetamide containing 5 % lithium chloride. Chitosan, the deacetylated product of chitin, is soluble in dilute acids like acetic acid, formic acids etc. Hydrolysis of chitin with concentrated acids produces relatively pure amino sugars, D-glucosamine. The nitrogen content in chitin varies from 5 to 8 % depending on the extent of deacetylation.

In fact, chitosan is soluble in dilute acids on account of protonation of free amino groups. As in all polyelectrolytes, the dissociation constant of chitosan is not constant but depends on the degree of dissociation at which it is determined. The solubility of chitosan depends on its degree of dissociation.

1.7.1.4 Crystallinity

On the basis of the crystalline structures, chitin is classified into three forms: α, β and γ -chitins (hydrated, anhydrous crystal, and non-crystal). These forms can be examined easily by measuring the X-ray powder diffraction pattern of a chitosan sample. The modified forms of chitosan are less crystalline than pure deacetylated chitosan.

1.7.2 Application areas of chitin and chitosan

The driving force for much of the excitement surrounding chitin and chitosan are the potential applications that the material can be used for. Table 1.5 lists potential applications for chitin, chitosan and their derivatives.

Table 1.5 Potential applications for chitin, chitosan and their derivatives

| Application	Specific use
Water treatment	Coagulating agents for polluted water, removal of metal ions
Agriculture	Plant elicitor, antimicrobial agents, plant seed coating
Textile, paper industry	Fibres for textile and woven fabrics, paper and film industry
Biotechnology	Chromatography, packing, enzyme immobilizing material
Food/health supplements	Natural thickeners, food additives, filtration and clarification, hypocholesteromic agents (slimming agents)
Cosmetics	Ingredients for hair and skin care
Biomedical	Wound dressings, absorbable sutures, anticoagulant or antithrombogenic materials, homeostatic agents, drug delivery, gene delivery

1.8 Thermoplastic nanocomposites
1.8.1 PET nanocomposites

Poly (ethylene terephthalate) (PET) is one of the most extensively used thermoplastic polyesters, which has assumed a role of primacy in fibres, films, packaging and moulding materials.[156-158] Due to its performance characteristics

such as hardness, clarity, wear-resistance, dimensional stability, resistance to chemicals etc. PET has worldwide consumption next only to polyolefines. As compared to poly (butylene terephthalate) (PBT), the slower crystallization of PET limits its usage in engineering applications which require fast crystallization for low cycle time for injection moulding. Enhancement of crystallization rate of PET is generally achieved through the addition of minerals such as talc or organic acid salts such as sodium benzoate. Other nucleating agents that have been mentioned in the literature include metal oxides and hydrides, residual catalysts and diamide segments.[159-161] Several workers have reported the use of nanoparticles, such as organically modified nanoclays as crystallization promoters for a variety of polymers.[162-163]This has prompted the evaluation of nanoclays for crystallization enhancement in PET also.[164] Non isothermal crystallization behaviour of PET on adding SWNTs is shown in figure 1.16.[165]
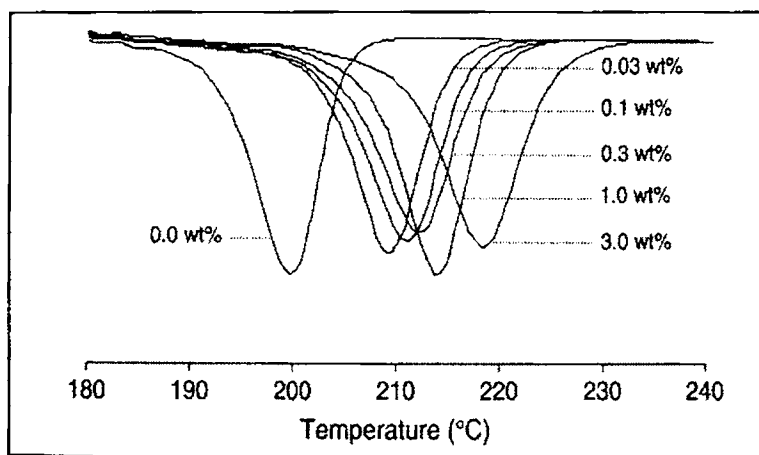
Figure 1.16 Non isothermal crystallization behaviour of PET/SWNTs nanocomposites (taken from ref. 165)

Barium sulphate, silica, clay etc. are used for reinforcement for PET matrix.[166-168]

1.8.2 PA 6 nanocomposites

Among the thermoplastic polymers, nylon 6 is one of the few that has met with commercial success and thus many investigators reported on clay-based nanocomposites with nylon 6.[66,67, 169-171] The main applications of PA 6 are in fibres, films and as injection-moulded engineering plastic.[172-175] The mechanical

properties and the crystallization rate can be modified by the addition of inorganic fillers.[176] Fillers widely used are calcium carbonate, talc, silica, clay, glass fibre etc. that play an important role in the plastics filler market.[177-181] The influence of these fillers on the polyamide strongly depends on their shape, particle size, distribution and surface characteristics. Structure-property relationship of PA 6/attapulgite nanocomposite was reported by Shen et al.[182]

1.8.3 PC nanocomposites

Amorphous polycarbonate (PC) is one of the most important engineering thermoplastics used in a wide variety of applications, distinguished by its versatile combination of toughness, transparency, heat resistance.[183] PC was modified in many different ways, particularly by blending with polyolefin resin such as polyethylene (PE), polypropylene (PP) for use in demanding applications when its outstanding notched impact strength is important.[184-186] Unfortunately, the enhancement of the toughness is obtained at the expense of the strength and thermal resistance. In principle, addition of well-dispersed nanofillers of layered silicate clay to PC could improve stiffness, modulus, and heat resistance, which makes a compelling case for exploring PC nanocomposites, particularly if toughness is needed to be preserved.[187] PC-ZnO nanocomposites containing 0.1, 0.5, 1 or 5 wt% nanoparticles have been prepared by milling and injection moulding.[188] PC + 0.5 % ZnO presents a higher modulus and similar tensile strength compared to neat PC, with a 74 % reduction in the elongation at break. A ZnO concentration of 1 wt% dramatically reduces both the tensile strength and the elongation at break of PC. A 0.5 wt% proportion of ZnO nanoparticles increases hardness and reduces the wear rate with respect to neat PC.

1.8.4 PP nanocomposites

Filled polypropylenes are important commercial materials; widely used in large quantities in different application segments.[189] The most common reinforcements that are used in polypropylene are wollastonite, talc, mica, silica, and calcium carbonate, in amounts of 10–40 % by weight. Experimental work on polymer composites indicates large improvements in mechanical properties, such as tensile

and flexural modulus, impact resistance, as well as outstanding barrier properties, flame retardancy, resistance to heat deformation or distortion.[190-198] In addition, large influences on crystallization process, degree of crystallinity, and nucleation have been reported: ceramic reinforcements can increase the starting crystallization temperature of a thermoplastic polymer,[199-203] inducing shorter processing times in injection moulding,[204] as well as higher crystallinity levels.[199-201,205] As a radical alternative to conventional micro- filled polymers, new materials based on nanometer sized filler particles in polymeric matrices have been proposed.[206-212] As well known, composite properties are strongly influenced by the nature and extent of the interface, hence, having nanoparticles a high surface to volume ratio, nanofillers allow to largely improve material properties, compared to conventional microdimensioned fillers.[213] The properties of nanocomposites can be also affected by the shape of the reinforcement, as well as by the coupling agent used.[214-215] The use of either spherical or elongated nanoparticles, that have different aspect ratio, is expected to differently influence many physical properties of the final material, such as permeability to gases, thermal and mechanical behaviour etc. Preliminary analysis revealed that, in isotactic polypropylene/calcium carbonate nanocomposites, the addition of $CaCO_3$ nanoparticles coated with a polypropylene-g-maleic anhydride copolymer causes an increase in the glass transition temperature and a better thermal stability of the material. The presence of the nanofiller also induces crystallization to start at higher temperatures when at least 3 % $CaCO_3$ is added to iPP, the effect being slightly dependent on the aspect ratio of $CaCO_3$ nanoparticles.[216] The most commonly used fillers for PP are calcium carbonate or clay.[217-224] Nanosilica provided effective reinforcement to PP matrix.[225]

1.8.5 HDPE nanocomposites

High-density polyethylene (HDPE) is considered a primary material in the materials substitution chain because of availability and recyclability. The performance criterion to encourage the application of HDPE requires superior modulus and yield strength in conjunction with high-impact strength. A substantial enhancement in mechanical properties (modulus, yield strength, and toughness) of thermoplastic

materials can be realized by reinforcement with inorganic minerals including talc,[226-227], mica,[228] wollastonite,[229-231] glass bead [232] and calcium carbonate. [233-242] In polymer (polyethylene)–clay nanocomposite the clay particles are about the same size as the polymer molecules themselves, which enables them to be intimately mixed and chemically bonded to each other. The improvement in mechanical properties such as tensile strength, tensile modulus,[243-249] decreased thermal expansion coefficient, increased solvent resistance, outstanding diffusion barrier properties and flame retardant capability [250-251] are a few selected examples of the advantages provided by this new class of materials. The presence of nanoparticles generally improves the elastic modulus, and does not significantly influence the rheological and processing behaviour and the optical properties of the polymer matrix.[252-253]

1.8.6 PS nanocomposites

There are a number of studies in which polystyrene (PS) was used as nanocomposite matrix. Most of these investigations concerned organoclays.[254-259] However, metals[260-261] metal sulfides (CdS),[262-263] a metal oxide,[264] nanotubes,[265] SiO_2,[266] and graphite[267] are also mentioned. The common conclusion that can be drawn from these studies is that the polymer matrix is significantly affected by the presence of nanofillers. Nevertheless, depending on the particle dimensions, shape and chemical structure different properties will arise.

1.9 Importance of ZnO[268]

Perhaps the most common use of zinc is for healing and protecting the skin. Zinc oxide has been used for generations to soothe diaper rash and relieve itching. Zinc oxide is a natural sunscreen, protecting chapped lips and skin from the sun's UV rays. Zinc sulfate can be taken orally to effectively treat acne, while it also comes in a topical form to improve healing of wounds caused by surgical incisions, burns or other skin irritations. Zinc alleviates sunburn and blisters and can also be used as an anti-inflammatory.

1.9.1 Rubber

The rubber industry, in its development over the past one hundred years, has utilized an increasing number of the many optical, physical and chemical

properties of ZnO. ZnO proved the most effective activator to speed up the rate of cure with the new accelerators. Heavy-duty pneumatic tyres carry high loadings of ZnO for heat conductivity as well as reinforcement since heat-buildup is critical at their higher operating speeds compared with their solid-rubber counterparts.

1.9.1.1 Activation

In the curing process for natural rubber and most types of synthetic rubbers, the chemical reactivity of ZnO is utilized to activate the organic accelerator.

The unreacted portion of the ZnO remains available as a basic reserve to neutralize the sulfur-bearing acidic decomposition products formed during vulcanization. Adequate levels of ZnO contribute markedly to chemical reinforcement; scorch control, and resistance to heat-ageing and compression fatigue.

1.9.1.2 Acceleration

Zinc oxide serves as the accelerator with some types of elastomer and the crosslinking, which it induces, takes several forms. With some systems, ZnO is an effective co-accelerator in the vulcanization process.

1.9.1.3 Biochemical activity

ZnO is useful in the preservation of plantation latex as it reacts with the enzyme responsible for the decomposition. The oxide is also a fungistat, inhibiting the growth of such fungi as mold and mildew.

1.9.1.4 Dielectric strength

In high-voltage wire and cable insulation, ZnO improves the resistance to corona effects by its dielectric strength, and at elevated operating temperatures it contributes to maintenance of the physical properties of the rubber compound by neutralization of acidic decomposition product.

1.9.1.5 Heat stabilization

ZnO similarly retards devulcanization of many types of rubber compounds operating at elevated temperatures.

1.9.1.6 Latex gelation

In the production of latex foam rubber products, ZnO is particularly effective in gelation of the foam with sufficient stability.

1.9.1.7 Light stabilization

ZnO is outstanding among white pigments and extenders for its absorption of ultraviolet rays. Thus, it serves as an effective stabilizer of white and tinted rubber compounds under prolonged exposure to the destructive rays of the sun.

1.9.1.8 Pigmentation

Through its high brightness, refractive index, and optimum particle size, ZnO provides a high degree of whiteness and tinting strength for such rubber products as tyre sidewalls, sheeting and surgical gloves.

1.9.1.9 Reinforcement

ZnO provides reinforcement in natural rubber, and in some synthetic elastomers such as polysulfides and chloroprenes. The degree of reinforcement appears to depend upon a combination of the particle size of the oxide, the finest size being the most effective, and the reactivity of the oxide with the rubber.

Under such service condition involving rapid flexing or compression, ZnO also provides heat conduction to more rapidly dissipate the heat and thereby provides lower operating temperatures. In addition, it imparts heat stabilization by reacting with acidic decomposition products.

1.9.1.10 Rubber - metal bonding

In the bonding of rubber to brass, ZnO reacts with copper oxide on the brass surface to form a tightly adhering zinc-copper salt.

1.9.1.11 Tack retention

One of the unique properties of ZnO is its ability to retain over many months of shelf –storage the tack of uncured rubber compounds for adhesive tapes.

French process ZnO impart heat-ageing resistance superior to that of American-process ZnO. The former type, being sulfur-free, has a higher pH and, thus, can neutralize more effectively the acidic decomposition products formed during ageing. Moreover, the finer French-process ZnO prove superior to coarser grades in heat-ageing resistance.

1.9.2 Plastics

Zinc compounds can provide a variety of properties in the plastics field. Heat resistance and mechanical strength are imparted to acrylic composites by ZnO. ZnO contributes to the formation and cure of epoxide resin. Addition of ZnO to epoxy resins cured with aliphatic polyamines imparts higher tensile strength and water resistance. ZnO imparts fire-resistant properties to nylon fibres and mouldings. ZnO is also useful in the preparation of nylon polymers and in increasing their resistance. The formation of polyesters in the presence of ZnO imparts higher viscosity and other improvements. ZnO reacts with unsaturated polyesters to form higher viscosity and a thixotropic body. The dyeability of polyester fibres is improved by ZnO. ZnO mixtures stabilize polyethylene against ageing and ultraviolet radiation. ZnO increases the transparency of poly (chlorofluoroethylene) moulding resin. Polyolefin's are improved in colour, tensile strength, and vulcanization properties by addition of ZnO. Thermal stabilization of PVC is effected by ZnO. Antistatic, fungistatic and emulsion stability are additional properties imparted to vinyl polymers by ZnO.

Applications in development for ZnO-stabilized polypropylene and high-density polyethylene include safety helmets, stadium seating, insulation, pallets, bags, fibre and filament, agricultural and recreational equipment.

1.9.3 Ceramics

The properties imparted by ZnO to some of the newer applications are as electronic glass, low-melting glass for metal-to-glass seals, thermistors for use as lighting arresters and devitrified glasses of low thermal expansion.

ZnO imparts a unique combination of properties when used in glass. ZnO reduces the coefficient of thermal expansion, imparts high brilliance and luster and high stability against deformation under stress. As a replacement flux for the more soluble constituents, it provides a viscosity curve of lower slope. The specific heat is decreased and the conductivity increased by the substitution of ZnO for BaO and PbO.

1.9.4 Pharmaceutical industry

ZnO is mainly used in zinc soap, ointment, dental inlays, food powders etc. ZnO forms an indispensable element of the production process of this industry.

1.9.5 Cosmetics

The optical and biochemical properties of ZnO and its derivatives impart special features to a variety of cosmetic preparations for care of the hair and skin. In powders and creams it protects the skin by absorbing the ultraviolet sunburn rays; in burn ointments it aids healing.

Simple salts of zinc provide astringent and skin-conditioning properties to creams, while more complex salts furnish fungistatic properties which contribute to the effectiveness of deodorants, soaps, and antidandruff preparations.

1.9.6 Adhesives, mastics, sealants

ZnO has long been a major constituent of surgical and industrial tapes based on natural or synthetic rubber as it is outstanding in retention of tack during shelf–ageing.

Neoprene adhesives are improved by the addition of both Phenolic resins and zinc compounds (including ZnO), the reaction products imparting special

properties such as high heat resistance, high bond strength, improved peel and shear – stress resistance, and stability to settling of neoprene solution adhesives.

1.9.7 Photocopying

Some of the unique electronic properties of ZnO are distinctively utilized in the photocopying process. For use in that process, ZnO is increased in photoconductivity and semiconductor properties by special heat and/or doping treatments (addition of foreign elements). Also, ZnO is greatly modified in optical properties to increase its absorption of light rays in the visible region. This process known as sensitization is generally carried out by addition to certain dyes, which are absorbed on the surface of the ZnO.

Commercial ZnO for photocopying is generally produced from metallic zinc, rather than ore, to obtain a product of higher purity.

1.9.8 Lubricants

In the research and development of improved lubricants over the past two decades, ZnO and its derivatives have been intently studied. zinc dithiophosphates which are prepared by reacting ZnO with organic phosphates, are used in substantial quantities as additives to lubricating oils for automotive engines, to reduce oxidation corrosion and wear. ZnO has been found to contribute special properties in many types of lubricants, such as extreme-pressure lubricants, seizure-resistant lubricants, and greases. Improved adhesion is another feature which ZnO contributes.

ZnO imparts special properties to greases and other variety of lubricants. Such greases are useful in the lubrication of food–processing equipment.

1.9.9 Paints

Zinc oxide in organic coatings provides a broad spectrum of properties: optical, chemical, biochemical and physical. Over the past century the paint industry, in its constant development of improved products, has utilized various aspects of those properties to high degree.

Manufacturers discovered that they could produce coatings of brushing consistency and good suspension properties by incorporation of ZnO into their pastes. Painters noted that they furnished better hiding power, whiteness, cleaner tints, tint retention, and durability as well as nondarkening in the presence of sulfur fumes. French-process ZnO has been proved superior to American-process type in fungus resistance and less sulfide staining.

1.9.9.1 Metal-protective coatings

Zinc metal powder (zinc dust) and zinc compounds have long been utilized for their anticorrosive properties in metal-protective coatings, and today they are the basis of such important especially metal primers as zinc chromate primers.

Zinc dust- ZnO paints are especially useful as primers for new or weathered galvanised iron. Such surfaces are difficult to protect because their reactivity with organic coatings leads to brittleness and lack of adhesion. Zinc dust- ZnO paints however, retain their flexibility and adherence on such surfaces for many years. Zinc dust- ZnO paints also provide excellent protection to steel structures under normal atmospheric conditions, as well as to steel surfaces in such under-water conditions as dam faces and the interior of fresh water tanks.

1.9.10 Cigarette filters

ZnO as a constituent of cigarette filters is effective in removal of selected ingredients from tobacco smoke. A filter consisting of charcoal impregnated with ZnO and iron oxide removes significant amounts of HCN and H_2S from tobacco smoke without affecting its flavour.

1.9.11 Sulfur removal

ZnO is effective in removal of sulfur and sulfur compounds from a variety of fluids and gases, particularly industrial flue gases. Zinc is also effective in removal of H_2S from hydrocarbon gases and for desulfurization of H_2S and certain other sulfur-containing compounds.

1.9.12 Foods and food packaging materials

ZnO and its derivatives contributing special fungi-static and chemical properties to the processing and packaging of various animal and vegetable products.

In the packaging of meat, fish, corn and peas, for examples, ZnO has long been incorporated into the varnish linings of the metal containers to prevent formation of black sulfides which discolour the food.

1.9.13 Fire retardants

ZnO and its derivatives were used extensively in fire retardants for the military in World War II and those zinc compounds have since been the subject of extensive research and development for preparation of fire-retardant compositions for a variety of substances.

Solutions for fireproofing textiles contain ZnO, boric acid, and ammonia in various proportions. It deposits water-insoluble zinc borate on the fibres.

1.9.14 Ferrites

ZnO continues as an essential ingredient in the "soft" type of ferromagnetic materials for television, radio, and tele-communication applications. In these fields ferrites based on magnetite, nickel oxide and ZnO are used as elements in many types of electronic devices.

Numerous electronic instruments for the consumer market utilize ferrites to impart specific functions. In portable and car radios, the antenna cores are ferrites designed to provide highly selective tuning. Television picture tubes constitute a major market for ferrites, particularly for use in fly back transformers and deflection yokes. In the communications area, ferrites are extensively used in the filter inductors of telephone circuits to permit precise inductance adjustment for the purpose of separating channels. Magnetic tape for recorders is improved by use of a magnetite precipitated in the presence of ZnO.

1.9.15 Batteries, fuel cells, photocells

ZnO is used in zinc-carbon dry cells, zinc-silver oxide batteries, nickel oxide-cadmium batteries and even in secondary batteries. In fuel cells, ZnO is used as electrode material, cathodic material and as a fuel element. And in solar energy cells, it can act as a photocatalyst. Purification of motor car exhaust gases is currently the subject of extensive research, and zinc oxide is already demonstrating its catalytic properties in some of those programs.

1.9.16 Thermoelements

ZnO plays an important role in semiconductor ceramic elements for operation at elevated temperatures or high voltages. Such thermoelements can be produced to cover a broad range of thermal and electrical properties.

Varistors are composed of semiconductor ZnO modified by other oxides. Developed for use as lightning arrestors and high-voltage surge arrestors in electric transmission lines, they are based on a unique electronic property of semiconductor ZnO, nonlinear resistance. ZnO varistors have high-temperature stability and resistance to humidity, electrical load, and current shocks.

1.9.17 Silicate compositions

ZnO reacts with aqueous solutions of silicates, such as sodium silicate solutions (commonly known as water glass) to form zinc silicate, a waterproof, fireproof refractory material, which is useful as a binder in paints. Such refractory adhesives are used in bonding asbestos-cement moulded products to building structures.

1.9.18 Fungicides

ZnO and its derivatives contribute effectively to the control of fungi in many different types of applications. ZnO is not a fungicide; rather it is a fungistat, that is, it inhibits the growth of fungi, such as mildew on the surface of exterior house paints. This property is also used to particular advantage in the fortifying of fungicides; ZnO is added to fungicides to increase their effectiveness in specific applications.

1.9.19 Portland cement

The beneficial effects of ZnO additions to portland cement have long been known-retardation of setting and hardening (to reduce the rate of heat evolution), improvement in whiteness and final strength.

1.10 Zinc oxide based nanocomposites

There are limited publications in the research literature that focus on the zinc oxide based nanocomposites. Owing to the recent commercial availability of nanoparticles, the outlook for composite materials with new or modified physical properties became even brighter. Nanoscale fillers are different from bulk materials and conventional micron-size fillers due to their small size and corresponding increase in surface area. It is expected that the addition of nanoparticles into polymers would lead to unprecedented ability to control the electrical properties of filled polymers.[269-270] Hong et al. prepared ZnO/LDPE nanocomposites and studied the dielectric properties.[271] SEM images of the ZnO/LDPE nanocomposites are shown in figure 1.17. Good dispersion of nanoparticles in the LDPE matrix is confirmed from no observation of nanoparticle agglomeration.
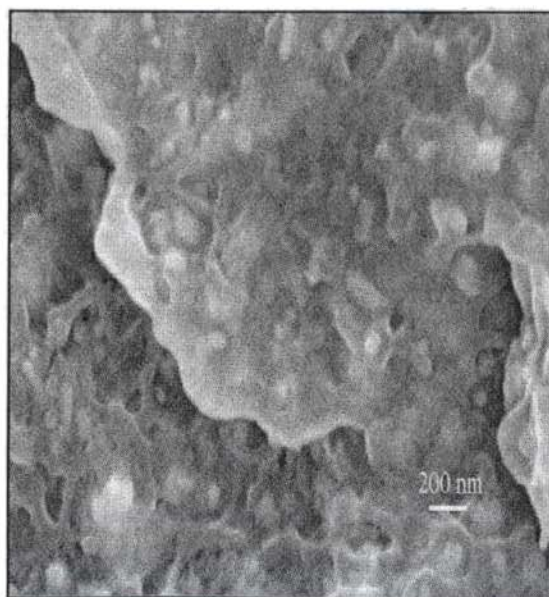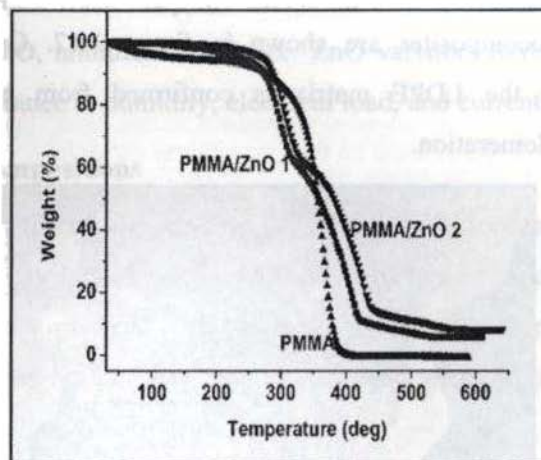

Figure 1.17 SEM image of ZnO/LDPE nanocomposite (taken from reference 271)

PMMA/ZnO nanocomposites via in-situ polymerization method were reported by Peng Liu et al.[272] TEM image of ZnO nanoparticles in PMMA is shown in figure 1.18.
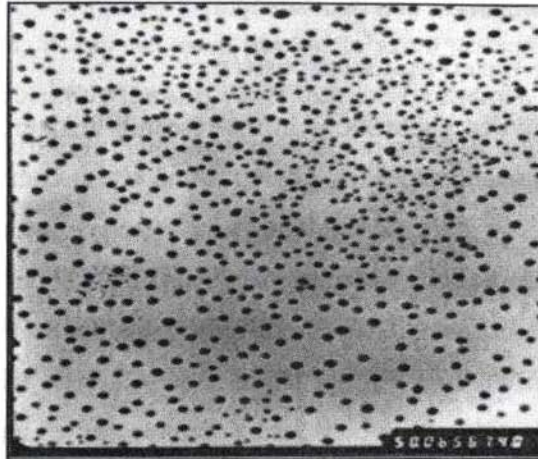
Figure 1.18 TEM image of ZnO nanoparticles in PMMA

Figure 1.19 TGA curves

The TGA curves of the pure PMMA, PMMA/ZnO (1) (5.0 % weight ZnO added), and PMMA/ZnO (2) (10.0 % weight ZnO added) are shown in figure 1.19. The pure PMMA decomposed completely at about 400 °C. However, PMMA/ZnO (1) and PMMA/ZnO (2) remained more than 30 % and 50 % at this temperature, respectively. It could be concluded that the addition of the

nanoparticles had improved the thermal properties of the nanocomposites obtained and the improvement depends on the amounts of nanoparticles added.

The bulk polymerization of MMA in the presence of up to 11 wt% of nanosized ZnO particles give access to composite materials, which showed an improved resistance to thermal degradation in comparison to the blends of PMMA with the same ZnO particles.[273] A study on photodegradation of ZnO filled polypropylene was done by Zhao et al.[274] They reported an improvement in crystallization, mechanical and dynamic mechanical characteristics of PP/ZnO nanocomposites. Electrical properties of LDPE/ZnO nanocomposites were studied and the results showed that dielectric constant of the composites reinforced with micro- and nanoparticles increased almost linearly with increasing ZnO volume content.[275] The effect of thermal treatment on electrical properties of LDPE/ ZnO nanocomposites were analyzed and the results showed that thermal treatments exerted a pronounced effect.[276] The effect of ZnO particles on polystyrene matrix was investigated.[277] They found an improvement in flexural strength and modulus and the glass transition temperature of ZnO/ PS nanocomposite increased with ZnO content. Zheng et al.[278] investigated the structure and morphology of the polyamide 6/ZnO nanocomposites. They reported that the ZnO nanoparticle can induce the crystallization of the γ-crystalline form PA 6 from the melt and during the annealing of the amorphous solid. Li et al.[279] reported transparent ZnO/epoxy nanocomposites with high visible light transparency and high UV light shielding efficiency. Poly (styrene butylacrylate) latex/nano ZnO composites were prepared.[280] The tensile strength, UV and NIR shielding properties of the nanocomposite polymers increased, and the T_g first increased and then decreased, with increasing ZnO content. Dong et al.[281] investigated effects of ZnO nanoparticles on the physical properties of polyacrylonitrile (PAN). The incorporation of ZnO nanoparticles decreased the crystallization temperature (T_c) from 285 to 272 °C and increased the heat of crytallization. This suggested that ZnO nanoparticles accelerate crystallization through heterogeneous nucleation and increased the degree of crystallinity. There was an improvement in thermal

stability of PAN and introduction of ZnO nanoparticles increased the tensile modulus but reduced the toughness of PAN.

The extent of reinforcement depends on factors such as particle size, size distribution, aspect ratio, degree of dispersion and orientation in the matrix, and the adhesion at the filler-matrix interface.[282]

1.11 Scope and objectives of the present work

The addition of nano fillers to polymers can have a dramatic effect on the properties of polymers as compared to micro scale fillers. Large part of this effect is due to the small size and the large surface area of nano scale fillers. The control of particle size, morphology and crystallinity of the particles during the preparation is essential to achieve the key properties. The search of novel methods to synthesize nano materials with controlled particle size and morphology still remains a challenge.

Many nano sized metal oxides such as SiO_2, TiO_2, Al_2O_3, V_2O_5 and ZnO have been synthesized on commercial scale. Compared to macro metal oxides, because of the unique morphologies that impart remarkable surface chemistry, nano sized materials can be used for any number of diverse applications ranging from remediation of hazardous chemical waste to increase the tensile strength of polymers. Among the metal oxides mentioned above, ZnO nano powder is one of the most attractive materials, because of their excellent performance in fields such as high corrosion resistant nano coating, highly transparent composites, semiconductors, cosmetics, sensors etc.

Various synthesis routes have been developed in recent years for the preparation of nanoparticles. One of those methods is polymer induced crystallization. The first objective of the present work was to prepare nano ZnO powder by polymer induced crystallization in chitosan solution and to characterize the material using different techniques like TEM, SEM, XRD, FTIR, UV spectroscopy, TGA, DSC etc.

The second object of the study is to prepare composites using nano ZnO. It has been undertaken to explore the potential of nano ZnO as reinforcement in engineering as well as commodity thermoplastics to widen their application spectra. We selected three engineering thermoplastics like [poly ethylene terephthalate, polyamide 6, and polycarbonate] and three commodity plastics like [polypropylene, high density polyethylene, and polystyrene] for the study. To date one of the few disadvantages associated with nanoparticle incorporation has concerned toughness and impact performance. Modification of polymers could reduce impact performance. The present study also focused on whether nano ZnO can act as a modifier for thermoplastics, without sacrificing their impact strength. The salient objectives of the current research are:

a   To disperse nano ZnO in polymer matrices

b   To investigate the effect of nano ZnO on the crystallization, mechanical, dynamic mechanical, rheological and thermal characteristics of polymers

c   To compare the performance of nano ZnO composites with those of commercial ZnO composites.

1.12 References

1.   Giannelius EP. Adv Mater 1996, 8, 29.

2.   Thomas Pinnavaia. American Chemical Society 1995.

3.   Gavin Buxton A, Anna Balazs C. Molecular Simulations 2004, 30(4), 249.

4.   Huynh WU, Dittmar JJ, Alivisatos AP. Science 2002, 295, 2425.

5.   Mitchell CA, Bahr JL, Arepalli S, Tour JM, Krishnamoorti R. Macromolecules 2002, 35, 8825.

6.   Leonard Sweet, Bradford Strohm. Human and Ecological Risk Assessment 2006, 12, 528.

7.   Gleiter H. Prog Mater Sci 1990, 33 (4), 223.

8.   Gell M. Mater Sci Eng 1995, A204 (1-2), 246.

9.   Min Zhi, Rong, Ming Qui, Zhang, Yong Xiang Zheng, Han Min Zeng, Walter R, Friedrich K. Polymer 2001, 1, 167.

10.   Sherman LM. Nanocomposites. Plastics Technology 1999, 6, 52.

11.   Bernie Miller. Plastics World 1997, 55, 36.

12. Kanny K, Moodley VK. Journal of Engineering Materials and Technology 2007, 129, 105.

13. Sur GS, Sun HL, Lyu SG, Mark JE. Polymer 2001, 42, 9783.

14. Sarat K Swain, Avraam I Isayev. Polymer 2007, 48, 281.

15. Akkapeddi MK. Annual Technical Conference Proceedings; Society of Plastics Engineers 1999, 45, 1619.

16. Wang Hua, Elkovitch Mark, Lee James L, Koelling Kurt W. Annual Technical Conference Proceedings; Society of Plastics Engineers 2000, 46, 2402.

17. Tzong-Ming Wu, Chein-Shiun Liao. Annual Technical Conference Proceedings, 48, 2002; Society of Plastics Engineers 2000, 46, 1514.

18. O'Neil Charles J, Acquarulo Lawrence A. Jr, Xu Jianwei. Annual Technical Conference Proceedings; Society of Plastics Engineers 2000, 46, 1518.

19. Bonner Sheanna, Sabandith Donesavanh, Swannack Charles, Zhou, Wennie. Annual Technical Conference Proceedings; Society of Plastics Engineers 2001, 47, 292.

20. Worley DC, II, Akkapeddi MK, Socci, EP. Annual Technical Conference Proceedings; Society of Plastics Engineers 2001, 47, 2120.

21. Bureau Martin N, Denault J, Glowacz Franck. Annual Technical Conference Proceedings; Society of Plastics Engineers 2001, 47, 2125.

22. Bagrodia Germinario S. Annual Technical Conference Proceedings; Society of Plastics Engineers 2001, 47, 2116.

23. Yalcin B, Cakmak M. Annual Technical Conference Proceedings; Society of Plastics Engineers 2001, 47, 2208.

24. Liang, Ying, Omachinski Scott, Logsdon Jason, Jae Whan Cho, Lan Tie. Annual Technical Conference Proceedings; Society of Plastics Engineers 2001, 47, 2218.

25. McBrearty Michael, Bur Anthony J, Roth Steven C. Annual Technical Conference Proceedings; Society of Plastics Engineers, 2002, 48, 3377.

26. Yalcin B, Cakmak M. Annual Technical Conference Proceedings; Society of Plastics Engineers 2002, 48, 2285.

27. Ergungor Zeynep, Cakmak Miko, Batur Celal. Annual Technical Conference Proceedings; Society of Plastics Engineers 2002, 48, 2280.

28. Bellemare Simon C, Bureau Martin N, Denault Johanne, Dickson J Ivan. Annual Technical Conference Proceedings; Society of Plastics Engineers 2002, 48, 2235.

29. Fabrication and characterization of polycarbonate/carbon nanotubes composites. Short Communication, Composites Part A: Applied Science and Manufacturing Volume 2006, 37(9), 1485.

30. Zhaobo Wang, Zhikun Zhang. J of Dispersion Sci and Tech 2007, 28(2), 309.

31. Nanocomposites 1999. Polymer Technology for the Next Century; Company Press Release, Principia Partners.

32. Chou Chai-jing, Read AE, Garcia-Meitin EI, Bosnyak CP. Annual Technical Conference Proceedings; Society of Plastics Engineers 2002, 48, 1452.

33. Mohammad M Hasan, Yuanxin Zhou, Hassan Mahfuz, Shaik Jeelani. Materials Science and Engineering: A 2006, 429(1-2), 181.

34. Ling Y, Omachinski S Logsdon J, Whan Cho J, Lan, T. (2004). Nano-Effects in In Situ Nylon-6 Nanocomposites. Retrieved February 28, 2005 from http://www.nanocor.com/tech_papers/antec2001.asp.

35. Eggnog Zeynep, Cokmak Miko, Batur Celal. Annual Technical Conference Proceedings; Society of Plastics Engineers 2002, 48, 1519.

36. Garcia-Rejon A, Derdouri A, Denault J, Bureau MN, Cole K. Annual Technical Conference Proceedings; Society of Plastics Engineers 2002, 48, 410.

37. Gilman Jeffrey W, Kashiwagi Takashi, Lichtenhan Joseph D. Nanocomposites: A Revolutionary New Flame Retardant Approach. 42nd International SAMPE Sumposium, 1997, 1078.

38. Goettler Lloyd A, Lysek Bruce A. Annual Technical Conference Proceedings; Society of Plastics Engineers 1999, 45, 3972.

39. Kressler Jorg, Thomann, Ralf. Annual Technical Conference Proceedings; Society of Plastics Engineers 1998, 44, 2400.

40. Lew CY, Murphy WR, McNally GM. Annual Technical Conference Proceedings; Society of Plastics Engineers 2002, 48, 1530–1534.

41. Dahman Sam J. Annual Technical Conference Proceedings; Society of Plastics Engineers 2000, 46, 2407.

42. Miller Joshua, Greene Joseph. Annual Technical Conference Proceedings; Society of Plastics Engineers 2002, 48, 3594.

43. McConaughy Shawn D. Annual Technical Conference Proceedings; Society of Plastics Engineers 2002, 48, 3587.

44. Puttarudraiah Amrutheswar H, Goettler Lloyd A. Annual Technical Conference Proceedings; Society of Plastics Engineers 2002, 48, 2930.

45. Lee JA, Gopakumar TG, Kontopoulou M, Parent JS. Annual Technical Conference Proceedings; Society of Plastics Engineers 2002, 48, 2230.

46. Martin Darren, Halley Peter, Truss Rowan, Murphy Michael Meusburger Simon. Annual Technical Conference Proceedings; Society of Plastics Engineers 2002, 48, 1292.

47. Murphy MJ, Martin DJ, Truss R, Halley P. Annual Technical Conference Proceedings; Society of Plastics Engineers 2002, 48, 1286.

48. Kening S, Ophir A, Shepelev O, Weiner F. Annual Technical Conference Proceedings; Society of Plastics Engineers 2002, 48, 794..

49. Chungchun, Zeng, James Lee L. Annual Technical Conference Proceedings; Society of Plastics Engineers 2001, 47, 2213.

50. Xiangmin Han, Changchun Zeng, James L, Lee Kurt W. Koelling, Tomasko David L. Annual Technical Conference Proceedings; Society of Plastics Engineers 2001, 47, 1915.

51. Brody. "Nano, Nano" Food Packaging Technology. Food Technology 2003, December 52.

52. Leaversuch. Nanocomposites Broaden Roles in Automotive, Barrier Packaging. Plastics Technology 2001, October, 64.

53. Lei SG, Hoa SV, M-T Ton-That. Composites Science and Technology 2006, 66 (10), 1274.

54. Mark JE. Polym Eng Sci 1996, 36, 2905.

55. Von Werne T, Patten TE. J Am Chem Soc 1999, 121, 7409

56. Calvert P. in "Carbon Nanotubes," edited by Ebbsen TW(CRC Press, Boca Raton, FL, 1997) p. 277.

57. Favier V, Canova G, Shrivastava SC, Cavaille JY. Polym Eng Sci 1997, 37, 1732.

58. Chazeau L, Cavalle JY, Canova G, Debdivel R, Bouthern B. J Appl Polym Sci 1999, 71, 1797.

59. Akexandre M, Dubois P. Mat Sci Eng 2000, 28, 1.

60. Ou Y, Yang F, Zhuang Y. Acta Polym Sin 1997, 2, 199.

61. Ryu Joung Gul, Kim Hyung Soo, Jae Wook. Annual Technical Conference Proceedings; Society of Plastics Engineers 2002, 48, 2240.

62. Caskey Terrence C, Lesser Alan J, McCarthy Thomas J. Annual Technical Conference Proceedings; Society of Plastics Engineers 2002, 48, 2260.

63. Tang NJ, Jiang HY, Zhong W, Wu XL, Zou WQ, Du YW. Journal of Alloys and Compounds 2006, 419(1-2), 145.

64. Zhaohui Han, Huaiyong Zhu, Jeffrey Shi, Lu GQ. Materials Letters 2006, 60(19), 2309.

65. Usuki A, Kojima Y, Kowarumi M, Okada A, Fukushima Y, Kurauchi T, Kamigaito OJ. Mater Res 1993, 8, 1179.

66. Usuki A, Koiwai A, Kojima Y, Kawasumi M, Okada A, Kurauchi T, Kamigaito O. J Appl Polym Sci 1995, 55, 119.

67. Kojima Y, Usuki A, Kawasumi M, Okada A, Kurauchi T, Kamigaito O. J Polym Sci Part A: Polym Chem 1993, 31, 1983.

68. Kojima Y, Usuki A, Kawasumi M, Okada A, Kurauchi T, Kamigaito O. J Appl Polym Sci 1993, 49, 1259.

69. Kojima Y, Fukumori K, Usuki A, Okada A, Kurauchi T. J Mater Sci Lett 1993, 12, 889.

70. Angell HW. Proced Forest Prod Res Soc 1951, 5, 107.

71. Guo-An Wang, Cheng-Chien Wang and Chuh-Yung Chen. Polymer Degradation and Stability 2006, 91(10), 2443.

72. Ming W, Jones FN, Fu S. Macrom Chem Phys 1998, 199, 1075.

73. Santanu R, Surekha D. Polymer 1997, 38, 3325.

74. Michael D, Bernd T. Langmuir 1998, 14, 800.

75. Xu XJ, Siow KS, Wong MK, Gan LM. Coll Polym Sci 2001, 279, 879.

76. Papp S, Dekany I. Coll Polym Sci 2001, 279, 449.

77. Bhawal S, Pokhriyal NK, Devi S. Euro Polym J 2002, 38, 735.

78. Du H, Chen P, Lin F, Meng FD, Li TJ, Tang XY. Mater Chem and Phys 1997, 51, 277.

79. Ferdinand Rodriguez. Principles of Polymer Systems, TMH Edition 1974.

80. Bauer F, Decker U, Ernst H, Findeisen M, Langguth H, Mehnert R, Sauerland V, Hinterwaldner R. International Journal of Adhesion and Adhesives 2006, 26(7), 567.

81. Wei S, Shiyi G, Changshui F, Dong X, Quan R. J Mater Sci 1999, 34, 5995.

82. Kyung Min Lee, Chang Dae Han. Polymer 2003, 44, 4573.

83. Chen B. British Ceramic Transactions 2004, 103(6), 241.

84. Liang Shen, Yijian Lin, Qiangguo Du, Wei Zhong. Composites Science and Technology 2006, 66(13), 2242.

85. Hedenqvist MS, Backman A, Gällstedt M, Boyd RH, Gedde UW. Composites Science and Technology 2006, 66(13), 2350.

86. González I, Eguiazábal JI, Nazábal J. Composites Science and Technology 2006, 66(11), 1833.

87. Jianwei Hao, Menachem Lewin, Charles A. Wilkie, Jianqi Wang. Polymer Degradation and Stability 2006, 91(10), 2482.

88. Lei Li, Leon M Bellan, Harold G Craighead, Margaret W Frey. Polymer 2006, 17(9), 6208.

89. Tianbin Wu, Yangchuan Ke. Polymer Degradation and Stability 2006, 91(9), 2205.

90. Peng He, Yong Gao, Jie Lian, Lumin Wang, Dong Qian, Jian Zhao, Wei Wang, Mark J Schulz, Xing Ping Zhou, Donglu Shi. Composites Part A: Applied Science and Manufacturing 2006, 37(9), 1270.

91. Avella M, Errico ME, Martelli S, Martuscelli. Applied Organometallic Chemistry 2001, 15, 435.

92. Siegel RW. Nanostruct Mater 1993, 3(1), 1.

93. Uyeda R. Prog Mater Sci 1991, 35 (1), 1.

94. Kear BH, Keem LE, Siegel RW, Spaepen F, Taylor KC, Thomas EL, Tu KN. Research Opportunities for Materials with Ultrafine Microstructures vol. NMAB-454, National Academy, Washington, DC, 1989.

95. Gleiter H. Nanostruct Mater 1992, 1 (1), 1.

96. Fakhru'l-Razi A, Atieh MA, Girun N, Chuah TG, El-Sadig M, Biak BRA. Composite Structures 2006, 75(1), 496.

97. Wang ZL. Characterization of Nanophase Materials;Wiley-VCH: Verlag Gmbh, Weinheim, Germany, 2000.

98. Khomutov GB, Gubin SP. Mater Sci Eng C 2002, 22, 141.

99. Kenneth Klabunde J. Nanoscale Materials In Chemistry. A John Wiley & Sons, Inc; Publication, p-10.

100. Katz JL, Miquel PF. Nanostruct Mater 1994, 4(5), 5551.

101. Gunther B, Kumpmann A. Nanostruct Mater 1992, 1 (1), 27.

102. Mizoguchi Y, Kagawa M, Suzuki M, Syono Y, Hirai T. Nanostruct Mater 1994, 4 (5), 591.

103. Vollath D, Sickafus KE. Nanostruct Mater 1992, 1(5), 427.

104. Petrov AE, Orlov AP, Ya K.Vaivads, Belogurov SV, Kuzyukevich AA. Sov Pow Met Met Ceram 1991, 30 (6), 445.

105. Martin CR. Science 1994, 266, 1961.

106. Martin CR. Acc Chem Res 1995, 28, 61.

107. Martin CR. Chem Mater 1996, 8, 1739.

108. http://www.azonano.com

109. Gaertner GF, Miquel PF. Nanostruct Mater 1993, 4 (3), 559.

110. Ajayan PM, Schadler LS, Braun PV. Nanocomposite Science and Technology. Wiley- VCH;2003

111. Charles Poole P, Jr., Frank Owens J. Introduction to nanotechnology. A John Wiley & Sons Inc; Publication 2003.

112. Brinker CJ, Scherer GW. Sol-Gel Science: The Physics and Chemistry of Sol-Gel Processing, Academic Press, San Diego, CA, 1990.

113. Brinker CJ, Scherer GW. Sol-gel Science; Academic Press Inc.: New York, 1990.

114. Hench LL, West JK. Chem Rev (Washington, D.C.) 1990, 90, 33.

115. Aegerter MA, Mehrota RC, Oehme I, Reisfeld R, Sakka S, Wolfbeis O, Jorgensen CK. Optical and electronic phenomena in Sol-Gel Glasses and Modern Applications; Springer- Verlag: Berlin,1996, Vol. 85.

116. Karthikeyan J, Berndt CC, Tikkanen J, Reddy S, Herman H. Materials Science and engineering 1997, A238, 275.

117. Nanoparticles and Nanostructured Films: Preparation, Characterization and Applications (J. H. Fendler, Ed.) John Wiley & Son Ltd, 1998.

118. Cullity BD. Elements of X-ray Diffraction, Reading, Addison- weslet publishing Co.Inc; 1978.

119. Ekstrom T, Chatfield C, Wruss W, Schreiber MM. J Mater Sci 1985, 20 (4), 1266.

120. Pradhan SK, Chakraborty T, Sen Gupta SP, Suryanarayana C, Frefer A, Froes FH. Nanostruct Mater 1995, 5(1), 53.

121. Gustavo M do Nascimento, Vera RL Constantino, Richard Landers, Marcia LA Temperini. Polymer 2006, 47(17), 6131.

122. Madhuchhanda Maiti, Anil K Bhowmick. Polymer 2006, 47 (17), 6156.

123. Nanomaterials: Technology, Characterisation and Application. Symposium organized by Indian Society of Analytical Scientists Kochi Chapter, 2006

124. Therberge JE. How mineral fillers improve plastics. Machine Design 52, 113–116.

125. Katz HS, Milewski JW. Handbook of Fillers and Reinforcements for Plastics; Van Nostrand Reinhold: New York, 1978.

126. Wilkes GL, Orler B, Huang H. Polym Bull 1985, 14, 557.

127. Seo YJ, Jung JH, Cho YS, Kim JC, Kang NK. J of American Ceramic Soc 2007, 90(2), 649.

128. Yamabe T. Synth Met 1995, 70, 1511.

129. Favier V, Canova GR, Shivastava SC, Cavaille JY. Polym Eng Sci 1997, 37, 1732.

130. Kojima Y, Usuki A, Kawasumi M, Okada A, Kurauchi T, Kamigaito O. J Polym Sci Part A: Polym Chem 1993, 31, 1755.

131. Ellsworth MW, Novak BM. J Am Chem Soc 1991, 113, 2756.

132. Wang S, Adanur S, Jang BZ. Compos B 1997, 28(4), 215.

133. Gachter R, Muller H. Plastics Additives, 4th Ed.; Hanser: New York, 1989; 525.

134. Rudolf Pfaendner. How will additives shape the future of plastics? Review Article, Polymer Degradation and Stability 2006, 91(9), 2249.

135. Sheldon RP. Composite Polymeric Materials, Applied Science Publishers; London and New York.

136. Marco C, Ellis G, Gomez MA. J Appl Polym Sci 2002, 84(13), 2440.

137. Chan CM, Wu JS, Li JX. Polymer 2002, 43(10), 2981.

138. Taubert A, Glasser G, Palms D. Langmuir 2002, 18(11), 4488.

139. Privalko VP, Karaman VM, Privalko EG, Walter R, Friedrich K, Zhang MQ, Rong MZ. J Macromol Sci—Phys 2002, B41 (3), 487.

140. Zhang ML, Liu YQ, Zhang XH, Gao JM, Huang F, Song ZH, Wei GS, Qiao JL. Polymer 2002, 43(19), 5133.

141. Gui QD, Xin Z, Zhu WP, Dai G. J Appl Polym Sci 2003, 88(2), 297.

142. Chung SC, Hahm WG, Im SS, Oh SG. Macromol Res 2002, 10(4), 221.

143. Ferrage E, Martin F, Boudet A. J Mater Sci 2002, 37(8), 1561.

144. Zweifel H. Plastics additives handbook. 5th ed. Munich: Hanser; 2001. p 963–4.

145. Wittmann JC, Lotz B. Prog Polym Sci 1990, 15(6), 909.

146. Chisholm BJ, Fong PM, Zimmer JG, Hendrix R. J Appl Polym Sci 1999, 74(4), 889.

147. Mercier JP. Polym Engng Sci 1990, 30(5), 70.

148. Monks R. Plast Technol 1989, 35, 65.

149. Jang GS, Cho WJ, Ha CS. J Polym Sci; Polym Phys Ed 2001, 39(10), 1001.

150. Song SS, White JL, Cakmak M. Polym Engng Sci 1990, 30(16), 944.

151. Shepard TA, Delsorbo CR, Louth RM, Walborn JL, Norman DA, Harvey NG, Spontak RJ. J Polym Sci; Polym Phys Ed 1997, 35(16), 2617.

152. Feng Y, Jin X, Hay JN. J Appl Polym Sci 1998, 69(10), 2089.

153. Muzarelli RAA. Chitin, Peragamon: Oxford 1977.

154. Roberts GAF. Chitin chemistry, Macmillan: London 1992.

155. McGahren WJ, Perkinson GA, Growich JA, Leese RA, Ellestard GA. Process Biochemistry 1984, 19, 88.

156. Paul DR, Barlow JW, Keskkula H. In: Mark HF, Bikales NM, Overberger ChG, Menges G, editors. Encyclopedia of polymer science and engineering, vol. 12. New York: Wiley; 1989.

157. Fakirov S, editor. Handbook of thermoplastic polyesters. Weinheim: Wiley–VCH; 2002.

158. Rieckmann Th, Volker S. In: Scheirs J, Long TE, editors. Modern polyesters. New York: Wiley; 2003.

159. Van Bennekom ACM, Gaymans RJ. Polymer 1997, 38, 657.

160. Bouma K, de Wit G, Lohmeijer JHGM, Gaymans RJ. Polymer 2000, 41, 3965.

161. Agarwal US, de Wit G, Lemstra PJ. Polymer 2002, 43, 5709.

162. Ou CF. J Appl Polym Sci 2003, 89, 3315.

163. Calcagno CIW, Mariani CM, Teixeira SR, Mauler RS. Polymer 2007, 48, 966.

164. Ke Y, Long C, Qi Z. J Appl Polym Sci 1999, 71, 1139.

165. Anoop Anand K, Agarwal US, Rani Joseph. Polymer 2006, 47, 3976.

166. Ming-Hai Qu, Yu-Zhong Wang, Chuan Wang, Xin-Guo Ge, De-Yi Wang, Qian Zhou. European Polymer Journal 2005, 41, 2569.

167. Xingyou Tian, Xian Zhang, Wentao Liu, Jin Zheng, Changjiu Ruan, Ping Cui. J of Macromolecular Sci Part B: Physics 2006, 45, 507.

168. Jiang-Ping He, Hua-Ming Li, Xia-Yu Wang, Yong Gao. European Polymer Journal 2006, 42, 1128.

169. Kojima Y, Usuki A, Kawasumi M, Okada A, Kurauchi T, Kamigaito O, Kaji K. J Polym Sci, Polym Phys Ed 1994, 32, 625.

170. Kojima Y, Usuki A, Kawasumi M, Okada A, Kurauchi T, Kamigaito O, Kaji K. J Polym Sci Polym Phys Ed 1995, 33, 1039.

171. Reynaud E, Jouen T, Gauthier C, Vigier G, Varlet J. Polymer 2001, 42, 8759.

172. Vlasveld DPN, Groenewold J, Bersee HEN, Picken SJ. Polymer 2005, 46, 12567.

173. Salame M. Plastic Film Sheet 1986, 2, 321.

174. Kojima Y, Usuki A, Kawasumi M, Okada O, Fukushima Y, Kurachi T, Kamigato O. J Mater Res 1993, 8, 1185.

175. Junrong Zheng, Richard W, Siegel C, Gregory Toney. J of Polym Sci: Part B: Polymer Physics 2003, 41, 1033.

176. Kohen MI et al. Nylon Plastics, Wiley, New York, 1973.

177. Fornes TD, Paul DR. Polymer 2003, 44, 3945.

178. Liang Shen, Yijian Lin, Qiangguo Du, Wei Zhong, Yuliang Yang. Polymer 2005, 46, 5758.

179. Srinath G, Gnanamoorthy R. J of Materials Sciences 2005, 40, 2897.

180. Douwe Homminga S, Bart Goderis, Vincent Mathot BF, Gabriel Groeninckx. Polymer 2006, 47, 1630.

181. Hedicke K, Wittich H, Mehler C, Gruber F, Altstadt V. Composite Science and Technology 2006, 66, 571.

182. Liang Shen, Yijian Lin, Qiangguo Du, Wei Zhong. Composite Science and Technology 2006, 66, 2242.

183. Pham HT, Weckle CL, Ceraso JM. Adv Mater 2000, 12, 1881.

184. Jiang W, Tjong SC. Poly Degrad Stab 1999, 66, 241.

185. Li ZM, Yang MB, Hang R. J Mater Sci 2001, 36, 2013.

186. Mekhilef N, Ait Kadi A, Ajji A. Eng Sci 1992, 32(13), 894.

187. Yoon PJ, Humter DL, Paul DR. Polymer 2003, 44, 5323.

188. Carrión FJ, Sanes J, Maria-Dolores Bermúdez. Wear 2007, 262, 1504.

189. Karger-Kocsis J, editor. Polypropylene: an A–Z reference. Dordrecht: Kluwer Academic Publishers; 1999.

190. Ng CB, Ash BJ, Schadler LS, Seigel RW. Adv Comp Lett 2001, 10, 101.

191. Ghase Naderi, Pierre G Lafleur, Charles Dubois. Polym Eng and Sci 2007, 47(3), 207.

192. Seigel RW, Chang SK, Ash BJ, Stone J, Ajayan PM, Doremus RW. Scripta Mater 2001, 44, 2061.

193. Okada O, Usuki A. Mater Sci Eng 1995, C3, 109.

194. Wang Z, Pinnavaria TJ. Chem Mater 1998, 19, 1820.

195. Kyriaki Kalaitzidou, Hiroyuki Fukushima, Lawrence T Drzal. Comp Part A: Appl Sci and Manu 2007, 38(7), 1675.

196. Kanny K, Moodley VK. Journal of Engineering Materials and Technology 2007, 129, 105.

197. Kornmann X, Lindberg H, Berglund LA. Polymer 2001, 42, 4493.

198. Gilman JW, Kashiwaga T, Brown JET, Lomankin S, Giannelis EP, Manias E. In: Proceedings of the 43rd international SAMPE symposium, Part I, 1998, 43, 1053.

199. Dasari A, Rohrmann J, Misra RDK. Mater Sci Eng 2004, A367, 248.

200. Dasari A, Rohrmann J, Misra RDK. Polym Eng Sci 2004, 44, 1738.

201. Ferrage E, Martin F, Boudet A, Petit S, Fourty G, Jouffret F. J Mater Sci 2003, 37, 1561.

202. Gonzalez J, Albano C, Ichazo M, Diaz B. Eur Polym J 2002, 38, 2465.

203. Hambir S, Bulakh N, Jog JP. Polym Eng Sci 2002, 42, 1800.

204. Fillon B, Thierry A, Lotz B, Wittman JC. J Therm Anal 1994, 42, 721.

205. Chatterjee AM, Price FP. J Polym Sci: Polym Phys Ed 1975, 13, 2385.

206. Schmidt H. J Non-Cryst Solids 1985, 73, 681.

207. Ulrich DR. J Non-Cryst Solids 1990, 121, 465.

208. Novak BM. Adv Mater 1993, 5, 422.

209. Fu Q, Wang GH, Shen JS. J of Appl Polym Sci 1993, 49, 673.

210. Farzana Hussain, Samit Roy, Narasimhan K, Vengadassalam K, Lu H. J of Therm Comp Mater 2007, 20(4), 411.

211. Avella M, Errico ME, Martuscelli E. Nanoletters 2001, 1, 213.

212. Avella M, Bondioli F, Cannello V, Cosco S, Errico ME, Ferrari AM. Macromol Symp 2004, 218, 201.

213. Sanchez C, Ribot F. New J Chem 1994, 18, 1007.

214. Di Lorenzo ML, Frigione M. J Polym Eng 1997, 17, 429.

215. Di Lorenzo ML, Avella M, Errico ME. J Mater Sci 2002, 37, 2351.

216. Avella M, Cosco S, Di Lorenzo ML, Di Pace E, Errico ME. J Therm Anal Calor 2005, 80, 131.

217. Kato M, Usuki A, Okada A. J Appl Polym Sci 1997, 66, 1781.

218. Oya A, Kurokawa Y. J Mater Sci 2000, 35, 1045.

219. Galgali G, Ramesh C, Lele A. Macromolecules 2001, 34, 852.

220. Kawasumi M, Hasegawa N, Kato M, Usuki A, Okada A. Macromolecules 1997, 30, 6333.

221. Treece MA, Oberhanser JP. Macromolecules 2007, 40(3), 571.

222. Weon J-I, Sue H-J. J Mater Sci 2006, 41, 2291.

223. Avella M, Cosco S, Di Lorenzo Ml, Di Pace E, Errico ME, Gentile G. European Polymer Journal 2006, 42, 1548.

224. Yuan Q, Misra RDK. Polymer 2006, 47, 4421.

225. Chaganti Srinivasa Reddy, Chapal Kumar Das. J of Appl Polym Sci 2006, 102, 2117.

226. Hadal RS, Misra RDK. Mater Sci Eng, A 2004, 374, 374.

227. Hadal RS, Misra RDK. Mater Sci Eng, A 2004, 380, 326.

228. Trotigon JP, Verdu J, Boissard RDe, Vallios ADe. In: Sedlaucek B, editor. Polymer composites: proceedings of prague IUPAC microsymposium on macromolecules. Berlin: De Grugter; 1985. p. 191.

229. Dasari A, Sarang S, Misra RDK. Mater Sci Eng, A 2004, 368, 191.

230. Dasari A, Rohrmann J, Misra RDK. Mater Sci Eng, A 2004, 364, 357.

231. Dasari A, Misra RDK. Acta Mater 2004, 52, 1683.

232. Yuan Q, Jiang W, Zhang HZ, Yin JH, An LJ, Li RKY. J Polym Sci, Part B: Polym Phys 2001, 39, 1855.

233. Deshmane C, Yuan Q, Misra RDK. Mater Sci Eng, A 2007, 452, 592.

234. Thio YS, Argon AS, Cohen RE, Weinberg M. Polymer 2002, 43, 3661.

235. Haworth B, Raymond CL, Sutherland I. Polym Eng Sci 2001, 41, 1345.

236. Wang Y, Wang JJ. Polym Eng Sci 1999, 39, 190.

237. Gonzalez J, Albano C, Ichazo M, Diaz B. Eur Polym J 2002, 38, 2465.

238. Price GJ, Ansari DM. Polym Int 2004, 53, 430.

239. Vollenberg PHTh, Heikens D. J Mater Sci 1990, 25, 3089.

240. Misra RDK, Nerlikar P, Bertrand K, Murphy D. Mater Sci Eng, A 2005, 384, 284.

241. Tanniru M, Misra RDK, Bertrand K, Murphy D. Mater Sci Eng, A 2005, 404, 208.

242. Tanniru M, Misra RDK. Mater Sci Eng, A 2005, 405, 178.

243. Rong MZ, Zhang MQ, Zheng YX, Zeng HM, Walter R, Friedrich K. Polymer 2001, 42, 167.

244. Dong Wook Chae, Kwang Jin Kim, Byoung Chul Kim. Polymer 2006, 47, 3609.

245. Ng CB, Schadler LS, Siegel RW. Nanostruct Mater 1999, 12, 507.

246. Pawlak A, Zinck P, Galeski A, Gerard JF. Macromol Symp 2001, 169, 197.

247. Okada O, Usuki A. Mater Sci Eng, C 1995, 3, 109.

248. Wang Z, Pinnavaia TJ. Chem Mater 1998, 10, 1820.

249. Chan CM, Wu J, Li JX, Cheng YK. Polymer 2002, 43, 2981.

250. Gilman JW, Kashiwaga T, Brown JET, Lomankin S, Giannelis EP, Manias E. Flammability studies of polymer layered silicate nanocomposites. Proceedings of the 43rd international SAMPE symposium. Part I, 1998, 43, 1053.

251. Gilman JW, Jackson CL, Morgan AB, Harris R, Manias E, Giannelis EP. Chem Mater 2000, 12, 1866-73.

252. Thompson MR, Yeung KK. Polymer Degradation and Stability 2006, 91, 2396.

253. Weihua Luo, Nanqiao Zhou, Zhihong Zhang, Hongwu Wu. Polymer Testing 2006, 25, 124.

254. Giannelis EP, Krishnamoorti R, Manias E, Adv Polym Sci 1998, 138, 108.

255. Hoffmann B, Dietrich C, Thomann R, Friedrich C, Mu"lhaupt R. Macromol Rapid Commun 2000, 21, 57.

256. Xaoan F, Qutubuddin S. Mater Lett 2000, 42, 12.

257. Okamoto M, Morita S, Taguchi H, Kim YH, Kotaka T, Tateyama H. Polym Commun 2000, 41, 3887.

258. Noh MW, Lee DC. Polym Bull 1999, 42, 619.

259. Olson BG, Peng ZL, McGervey JD, Jamieson AM, Manias E, Giannels EP. Mater Sci Forum 1997, 336, 255.

260. Wizel S, Margel S, Gedanken A. Polym Int 2000, 49, 445.

261. Kumar Vijaya R, Yu Koltypin, Palchik O, Gedanken A. J Appl Polym Sci 2002, 86, 160.

262. ǎjinóvić DS, ǎponjić ZVS, Cvjetićanin N, Marinović-Cincović M, Nedeljković JM. Chem. Phys Lett 2000, 329, 168.

263. Yu SH, Yoshimura M, Moreno JMC, Fujiwara T, Fujino T, Teranishi R. Langmuir 2001, 17, 1700.

264. Djoković V, Nedeljković JM. Macromol Rapid Commun 2000, 21, 994.

265. Sung Thae Kim, Hyoung Jin Choi, Soon Man Hong. Colloid & polymer Science 2007, 285, 593.

266. Xiao M, Sun L, Liu J, Li Y, Gong K. Polymer 2002, 43, 2245.

267. Zhu J, Liu S, Palchik O, Yu Koltypin, Gedanken A. J Solid State Chem 2000, 153, 342.

268. http://navbharat.co.in

269. Godovsky DY. Adv Polym Sci 2000, 153, 163.

270. Gangopadhyay R, De A. Chem Mater 2000, 12, 608.

271. Hong JI, Winberg P, Schadler LS, Siegel RW. Materials Letters 2005, 59, 473.

272. Peng Liu, Zhixing Su. J of Macromolecular Science, Part B: Physics 2006, 45, 131.

273. Mustafa Demir M, Mine Memosa, Patrie Castignolles, Gerhard Wegner. Macromol Rapid Commun 2006, 27, 763.

274. Hongxia Zhao, Robert KY Li. Polymer 2006, 47, 3207.

275. Tjong SC, Liang GD. Materials Chemistry and Physics 2006, 100, 1.

276. Tjong SC, Liang GD, Bao SP. J of Appl Polym Sci 2006, 102, 1436.

277. Chen-Chi Ma M, Yi-Jie Chen, Hsu-Chiang Kuan. Journal of Appl Polym Sci 2006, 100, 508.

278. Zheng JR, Siegel RW, Toney CG. J Polym Sci Part B: Polym Phys 2003, 41, 1033.

279. Yuan-Qing Li, Shao-Yun Fu, Yiu-Wing Mai. Polymer 2006, 47, 2127

280. Mingna Xiong, Guangxin Gu, Bo You, Limin Wu. J of Appl Polym Sci 2003, 90, 1923.

281. Dong Wook Chae, Byoung Chul Kim. J of Appl Polym Sci 2006, 99, 1854.

282. Ettlinger M, Ladwig T, Weise A. Progr Org Coating 2000, 40, 31.

MATERIALS AND EXPERIMENTAL TECHNIQUES

Abstract

This chapter gives a brief description of the materials and methods used for the preparation of composites. The polymers used for the preparation of composites have also been discussed. A brief description about the different analytical techniques used for the characterization of composites is also given in this chapter.

2.1 Polymers

2.1.1 Polyethylene terephthalate (PET) having 0.655 dl/g intrinsic viscosity when measured in phenol-1, 1, 2, 2-tetrachloroethane (3:2 by mass) and the corresponding viscosity molecular weight was 50 kg/mol was supplied by Reliance Industries Limited.

Melting point: 245 $^{\circ}$C

Density at 25 $^{\circ}$C: 1.31 g/cm^3

2.1.2 Polyamide 6 (PA 6) (M28 RC) was supplied by GSFC, India, having melting point 215 $^{\circ}$C and density 1.12 g/cm^3.

2.1.3 Polycarbonate (PC) (PK2870), with a melt flow index of 2.5 g/10min, was supplied by GE Polymerland having melting point 230 $^{\circ}$C and density 1.20 g/cm^3.

2.1.4 Polypropylene (PP) (REPOL H200MA), with a melt flow index of 20 g/10min, was supplied by Reliance Industries Limited having melting point 165 $^{\circ}$C and density 0.90 g/cm^3.

2.1.5 High density polyethylene (HDPE) (HD50MA 180), with a melt flow index of 18 g/10min was supplied by Haldia Petrochemicals having melting point 130-140 $^{\circ}$C and density 0.94 g/cm^3.

2.1.6 Polystyrene (PS) (GPPS LGG 102) with a melt flow index of 10 g/10min was supplied by M/s LG polymers, Mumbai, India having melting point 180 $^{\circ}$C and density 1.05 g/cm^3.

2.2 Nanocomposite preparation

A simple melt-compounding route was adopted for the preparation of polymer-ZnO nanocomposites.[1] The polymer and ZnO samples were vacuum dried at 120 $^{\circ}$C for 12 h to avoid moisture-induced degradation. The melt compounding was performed using Thermo Haake Rheocord 600 mixing chamber with a volumetric capacity of 69 cm^3 fitted with a roller type rotors operating at 40 rpm. Nanocomposites at different concentrations (0.0-3.0 wt%) of ZnO were prepared. For comparative purpose, samples of unfilled polymers

were also subjected to the same blending procedure so that unfilled polymer and the polymer matrix for the nanocomposites had experienced similar processing histories. In all cases the torque stabilized to a constant value during mixing time.[2] The hot mix from the mixing chamber was immediately passed through a laboratory size two-roll mill and the resulting sheets are cut to small pieces and the test specimens were prepared using a semi-automatic plunger type injection-moulding machine, with a corresponding barrel temperature.

The detais of mixing time, mixing temperature and barrel temperature of injection moulding machine are given in table 2.1. The photograph of Thermo Haake Rheocord 600 is given in figure 2.1.

Table 2.1 Melt-mixing parameters of nanocomposites

Nanocomposite samples	Mixing time (min)	Mixing temperature (°C)	Barrel temperature (°C)
PET-ZnO	4.0	255	255
PA 6-ZnO	10.0	230	230
PC-ZnO	10.0	240	240
PP-ZnO	8.0	180	180
HDPE-ZnO	10.0	150	150
PS-ZnO	8.0	180	180
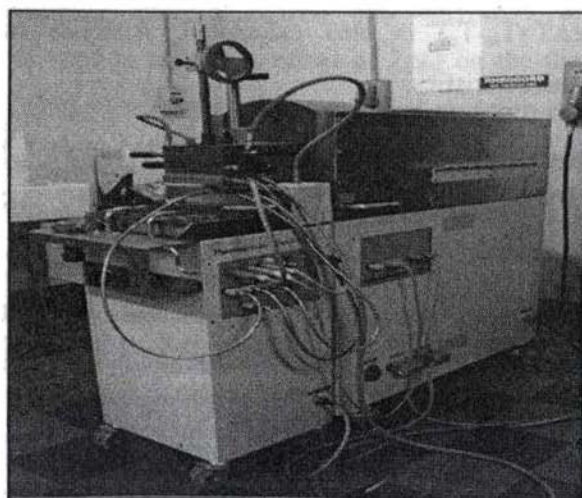
Figure 2.1 Thermo Haake Rheocord 600

2.3 Nanocomposite characterization
2.3.1 Thermal behaviour
2.3.1.1 Differential scanning calorimetry (DSC)

Heat flow, i.e., heat absorption (endothermic) or heat emission (exothermic), is measured, per unit time for the sample and the result is compared with that of thermally inert reference. Differential scanning calorimetry (DSC Q 100, TA instruments) equipped with a RCS cooling system was employed to study the crystallization characteristics of the nanocomposites. The photograph of DSC instrument is shown in figure 2.2. Indium was used for temperature calibration (T_m =156.6 °C, ΔH_m = 28.4 J/g). The sample weight was around 5 mg. All the samples were dried prior to the measurements and analysis was done in a nitrogen atmosphere using standard aluminum pans.

To study the nucleating effect of ZnO on polymer matrix, calorimetric measurements were done while the nanocomposite samples of PET, PA 6, PC, PP, HDPE and PS were exposed to the following temperature scans: heating at a rate 20 °C/min to 300 °C, holding for 10 min to erase thermal history effects and then cooling to 50 °C at the rate of 20 °C/min during which the peak of crystallization exotherm was taken as the crystallization temperature, (T_c). The heat of fusion (ΔH_m) and the heat of crystallization (ΔH_c) were determined from the areas of the melting and crystallization peaks respectively.[3] The degree of supercooling ($\Delta T = T_m - T_c$) is also calculated. Analysis of the isothermal crystallization characteristics:

PET –ZnO samples were subsequently reheated to 300 °C at a rate of 20 °C/min, held at 300 °C for 2 min, and then cooled rapidly (60 °C /min) to the desired temperature for isothermal crystallization (195 °C, 200 °C, 205 °C, 210 °C).

PA 6-ZnO samples were subsequently reheated to 300 °C at a rate of 20 °C/min, held at 300 °C for 2 min, and then cooled rapidly (60 °C /min) to the desired temperature for isothermal crystallization (190 °C, 195 °C, 200 °C, 205 °C).

PP-ZnO samples were subsequently reheated to 200 °C at a rate of 20 °C/min, held at 200 °C for 2 min, and then cooled rapidly (60 °C /min) to the desired temperature for isothermal crystallization (110 °C, 115 °C, 120 °C, 125 °C).

HDPE-ZnO samples were subsequently reheated to 200 °C at a rate of 20 °C/min, held at 200 °C for 2 min, and then cooled rapidly (60 °C /min) to the desired temperature for isothermal crystallization (120 °C, 125 °C, 130 °C, 135 °C).
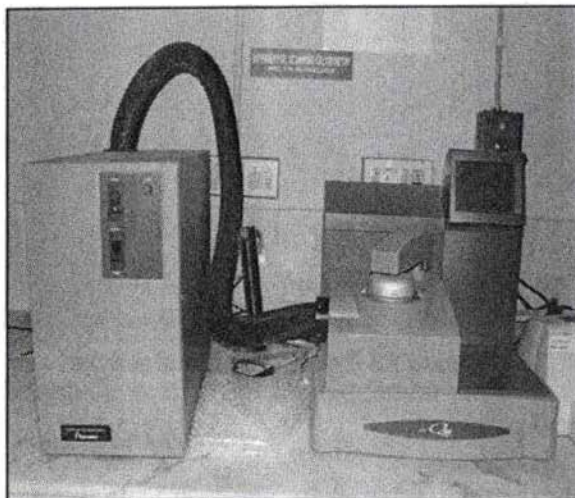
Figure 2.2 Differential scanning calorimeter

2.3.1.2 Thermo gravimetric analysis

Thermogravimetric analysis (TGA) and derivative thermogravimetric analysis (DTG) is used to study the effect of ZnO on the thermal stability of polymers. TGA, Q50 (TA Instruments) was used at a rate of 20 °C/min from room temperature to 800 °C. The chamber was continuously swept with nitrogen at a rate of 60 ml/min. Approximately 5 mg of the samples was heated.

2.3.1.3 Dynamic mechanical analysis (DMA)

The storage modulus, loss modulus and mechanical damping (tan delta) were measured using fixed dynamic analysis techniques. A dynamic mechanical analyzer (Q 800, TA Instruments) was made use of for this purpose. Rectangular specimens of 35 mm length, 4 mm breadth and 2 mm thickness were used. DMA tests were conducted at a constant frequency of 1 Hz. A temperature ramp was

run from 30 °C to 150 °C at 3 °C/min to get an overview of the thermo mechanical behaviour of polymer after the incorporation of ZnO nanoparticles. The photograph of DMA instrument is shown in figure 2.3.
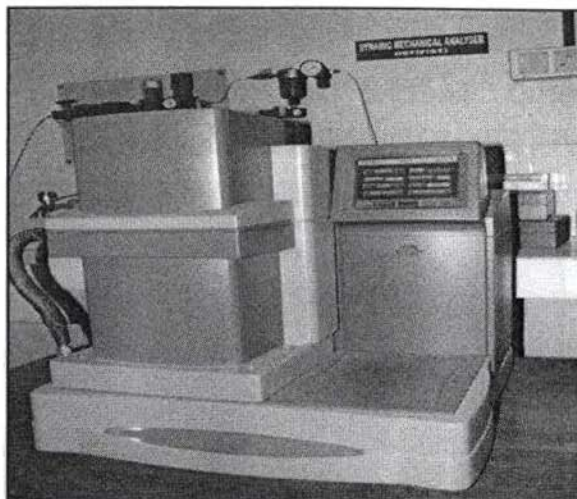
Figure 2.3 Dynamic mechanical analyzer

2.3.2 Mechanical properties
2.3.2.1 Tensile properties

The tensile properties of the samples were determined according to ASTM D − 638 using dumb-bell shaped specimens with a Universal Testing Machine (Shimadzu AG 1) at a crosshead speed of 50 mm/min. The length between the jaws at the start of each test was fixed to 40 mm and at least six concordant measurements are taken to represent each data point. The various parameters determined from the tensile testing are:

1. Tensile strength: It is the maximum tensile stress registered in the tensile loading operation. It corresponds to yield strength if the breaking strength is less than the yield stress. It is measured as the force measured by the load cell at the time of break divided by the original cross sectional area of the sample at the point of minimum cross section.

2. Tensile modulus: It is the slop of the linear portion of stress-strain curve.

3. Elongation at break: It is the elongation of the specimen at break. It was measured in terms of its initial length (L_0) and final length (L_1) and is given as,

$$\text{Elongation at break} = \frac{(L_1 - L_0)}{L_0} \times 100 \qquad \text{............................2.1}$$

Tensile toughness: It is energy to maximum /thickness of the sample.

2.3.2.2 Flexural properties

Flexural properties of the samples were measured by three-point loading system using Universal Testing Machine according to ASTM-D-790. The flexural properties were determined using rectangular shaped samples at a crosshead speed of 5 mm/min and a span length of 50.8 mm. Rectangular specimen of length 100 mm, width 10 mm and thickness 2-3 mm were used. The various flexural properties measured were:

Flexural strength: It is equal to the maximum stress at the outer layer of specimen at the moment of break.

Flexural modulus: It is the ratio of stress to corresponding strain within elastic limit.

Flexural strength (Kg/cm^2) = $3PL/2bd^2$ $\qquad$ --2.2

Flexural modulus (Kg/cm^2) = $L^3m/4bd^3$ $\qquad$ --2.3

Where P=maximum load at the moment of break, b= width of the specimen, L= length of the span and d= the thickness of the specimen.

2.3.2.3 Impact strength

The Izod impact strength (unnotched) of the rectangular samples was determined by Tinius Olsen Model 503 with a striking velocity of 3.5 m/s. Before the impact testing, the depth and the width of the specimens were measured with micrometer.

2.3.3 Melt rheology

The melt rheological measurements were carried out using Shimadzu (model AG1) capillary rheometer (50 KN) at different plunger speeds from 1-

500 mm/min. The capillary used was made of tungsten carbide with a length to diameter (L/D) ratio of 40 at an angle of entry 90°. The sample for testing was loaded inside the barrel of the extrusion assembly and forced down the capillary using a plunger. After giving a residence time of 5 min the melt was extruded through the capillary at 6 pre-determined plunger speeds. The initial position of the plunger was kept constant in all experiments and shear viscosities at different shear rates were obtained from a single charge of the material. The measurements were carried out at three different temperatures.

For,

PET nanocomposites, the temperatures were 250, 260 & 270 °C

PA 6 nanocomposites, the temperatures were 220, 230 & 240 °C

PC nanocomposites, the temperatures were 230, 240 & 250 °C

PP nanocomposites, the temperatures were 170, 180 & 190 °C

HDPE nanocomposites, the temperatures were 140, 150 & 160 °C

PS nanocomposites, the temperatures were 170, 180 & 190 °C

The forces and cross-head speeds were converted into apparent shear stress (τ_w) and shear rate ($\dot{\gamma}_w$) at wall. The wall shear stress τ_w can be calculated by using the following equation[4] involving the geometry of the capillary and the plunger,

$$\tau_w = F/4A_p \,(l_c/d_c) \qquad\qquad\qquad ....2.4$$

Where τ_w is the shear stress of the wall, F is the force acting on the plunger (kgf), A_p is the barrel diameter (mm^2), and d_c and l_c and are the capillary diameter and length (mm), respectively.

The apparent shear rate at the wall for Newtonian liquid can be estimated as follows:

$$\dot{\gamma}_{wa} = 32Q/\Pi d^3 \qquad\qquad\qquad ....2.5$$

Where $\dot{\gamma}_w$ is the shear rate, Q is the volumetric flow rate ($mm^3 s^{-1}$), d_c is the diameter of the capillary (mm).

With regard to non-Newtonian liquid, the wall shear rate will be different from that given above for the Newtonian liquid, and the Rabinowich correction needs to be performed as follows [5]:

$$\dot{\gamma}_w = (3n'+1/4\,n')\;\dot{\gamma}_{wa} \qquad\qquad ....2.6$$

Where n' is the flow behaviour index defined by the following equation:

$$n'= d\ln\tau_w / d\ln\dot{\gamma}_{wa} \qquad\qquad ....2.7$$

Thus by regression analysis of the graph of $\ln\tau_w$ versus $\ln\dot{\gamma}_w$, n' can be obtained.

The apparent viscosity, η was calculated using the equation

$$\eta= \tau_w/\dot{\gamma}_w \qquad\qquad ....2.8$$

2.3.4 Die swell measurements

The extrudates were carefully collected as they emerged from the capillary die, taking care to avoid any deformation. The diameter of the extrudate was measured after 24 h of extrusion using a travelling microscope. The die swell ratio was calculated using the relation,

$$\text{Die swell ratio}= \frac{\text{Diameter of the extrudate (de)}}{\text{Diameter of the capillary (dc)}} \qquad ....2.9$$

The ratio of the diameter of the extrudate to that of the capillary was calculated as die swell ratio (de/dc).[6]

2.3.5 Morphological studies-scanning electron microscopy

Scanning electron microscope (Cambridge Instruments, S 360 Stereoscanner-version V02-01, England) was used to investigate the morphology of the fractured surfaces. In this technique, an electron beam is scanned across the specimen resulting in back scattering of electrons of high energy, secondary electrons of

low energy and X-rays. These signals are monitored by detectors (photo multiplier tube) and magnified. An image of the investigated microscopic region of the specimen is thus observed in a cathode ray tube and photographed using black and white film. The SEM observations reported in the present study were made on the fracture surfaces of the tensile specimens. Thin specimens were prepared and mounted on a metallic stub with the help of a silver tape and conducting paint in the upright position. The stub with the sample was placed in an E-101 ion-sputtering unit for gold coating of the sample to make it conducting. The gold-coated sample was used for SEM analysis.

2.4 References

1. Anoop Anand K, Agarwal US, Rani Joseph. Polymer 2006, 47, 3976.

2. Thomas Abraham N, George KE. Plastic Rubber and Composites 2005, 33, No 9/10.

3. Lazzeri A, Zebarjad SM, Pracella M, Cavalier K, Rosa R. Polymer 2005, 46, 827.

4. Chen Dazhu, Yang Haiyang, He Pingsheng, Zhang Weian. Composites Science and Technology 2005, 65, 1593.

5. Shenoy AV. Rheology of filled polymer systems. Kluwer Academic Publishers; 1999, P. 99–102, 118–24, 317–2.

6. Oommen Z, Thomas S, Premalatha CK, Kuriakose B. Polymer 1997, 38, 5611.

PREPARATION AND CHARACTERIZATION OF NANO ZINC OXIDE

Abstract

Zinc oxide (ZnO) is prepared from zinc chloride and sodium hydroxide in chitosan solution by polymer induced crystallization. It is characterized using different analytical techniques. TEM and SEM studies revealed that zinc oxides are nanoparticles. The particle size of nano zinc oxide is much lower than that of commercial zinc oxide. TEM studies revealed that mode of preparation has a specific role in determining the size and shape of zinc oxide particle. This method has many advantages, such as simplicity, low cost, high input, high purity, high yield and little pollution in addition to superfine compounds that can be easily prepared.

3.1 Introduction

Nano zinc oxide, as one of the multifunctional inorganic nanoparticles, has drawn increasing attention in recent years due to its many significant physical and chemical properties, such as high chemical stability, low dielectric constant[1-6], large elecromechanical coupling coefficient, high luminous transmittance, high catalysis activity, intensive ultraviolet and infrared absorption etc. It is a semiconducting oxide with a wide and direct band gap of 3.4 eV and a large exciton binding energy of 60 meV.[7-11] Accordingly; ZnO is an important electronic and photonic material for UV light-emitters, varistors, gas sensors, acoustic wave devices, field emission displays and piezoelectric devices etc.[12-14]

Recent developments in nanotechnology have provided several routes for the preparation of zinc oxide of nano particle size. But the properties of ZnO was found to depend on dispersibility, morphology, crystallinity, purity and particle size.[15-18] Several studies have been conducted on the synthesis and the structural property of ZnO nanoparticles.[19-21] Basically there are two approaches in getting sub micron powders: one is top to bottom approach i.e., mechanical break process by attrition etc. and the other, bottom to top i.e., building up process for nucleation process. This involves the phase change from vapour or liquid to solid. These methods are broadly classified into (a) low temperature and (b) high temperature methods. Among the low temperature techniques, chemical precipitation and replication methods have been widely used. Chemical precipitation technique includes precipitation of solution from room temperature to 100 °C, hydrothermal synthesis (> 100 °C > 1 atm pressure), inverse micelle method, sol-gel synthesis etc. These methods are ideally suited for precise control of size and shape of nano particles. In addition, they are cost effective because of less energy consumption. The main drawback in the precipitation technique is chemical contamination. The replication method has been used to produce nano oxides or metals by carrying reactions in micro pores and meso pores of either crystalline or amorphous materials.

The high temperature method includes gas condensation, self-propagating high temperature synthesis, spray pyrolysis, laser ablation etc. In the gas condensation technique metal is volatilized in inert atmosphere to produce nano powders. Laser ablation method use pulsed laser to evaporate metal atoms to form hot plasma, which then condenses to form nanoclusters. Chemical methods give the ability to produce powders with an exceptionally small size (nanometer range).

To obtain ZnO nanoparticles with fine particle size, many synthesis methods have been used, including homogeneous precipitation[22], hydrothermal method[23], sol-gel[24], a combustion synthetic route[25], sonochemical process[26], oxidation of ZnS[27], mechanical milling[28], thermal decomposition[29-30], chemical method[31-33] etc. McBride et al.[34] and Oliveira et al.[35] had directly obtained microcrystalline zinc oxide by the reaction of zinc salts with sodium hydroxide. Qian et al.[36] reported a method for preparing nanometer-sized ZnO crystals via ultrasonic irradiation in absolute ethanol. Gao et al.[37] reported a method for preparing monodispersed ZnO nanoparticles.

Various ZnO nanostructure, including nanowires[38], nanobelts[39], nanotubes[40], nanorods[41-43], nanorings[44], nanosaws[45], cage-like[46], tetrapod-like[47-48], dendritic[49], hierarchical pattern[50], maize cod-based micron flowers[51-52] etc. have been prepared by different methods. Traditionally, fine and homogeneous zinc oxide powders are obtained by the decomposition of its hydroxides[53-54], oxalates[55], nitrates[56] etc. The search for novel methods to prepare nano ZnO with controlled size and morphology still remains a technical challenge. At present, two methods are generally being used to obtain nano-sized ZnO powder: vapour method and sol-gel method.[57-63] For the vapour method, the resulting powders are agglomerates rather than separated powders because the reaction condition during the process is difficult to control. In addition the method is time- and energy- consuming. The sol-gel method produces uniform ZnO powders. However, strict control of the reaction condition is necessary because of its violent hydrolysis reaction in air during the synthesis. In addition, this method has high material costs, and so it is not commercialized but done in small-

scale laboratories. So here, we made an easy attempt to prepare ZnO nano powder in chitosan medium by a method known as polymer induced crystallization.

3.1.1 Polymer induced crystallization

In order to control the size and morphologies of nanoparticles, colloidal solutions[64], porous glasses[65], certain polymers[66-67] and so on have been used as hosts for the preparation of nanosized materials. However, they are inefficient in generating clusters of uniform size. J. Liu et al. reported a method to prepare nano ZnO in presence of polyethylene glycol.[51] The nanosized calcium phosphate was synthesized by in-situ deposition technique by S. Mishra et al.[68] They prepared a complex of calcium chloride and polyethylene glycol to which they added ammonium phosphate solution. So polymer induced crystallization or polymer mediated growth of dispersed phase is a new technique, which has got more attention recently.[69] This has become an increasingly important area of research in the context of the production of smart materials, high performance composites and nano technology. In this method polymer plays an important role of controlling or modifying the growth habit of dispersed phase. The dispersed phase may be organic, inorganic, metal, or another polymer in the polymer matrix.

The in-situ growth and modification of crystalline phase, orientation, morphology, crystallite size of the additive will give special properties. The advantage of using this in-situ deposition technique is that, it would be able to control the overall morphology, growth, uniformity of size and dispersion, generation of orientation and better inter facial adhesion, which is achieved by a shorter, direct and easier route. Hence we thought it could be possible to prepare ZnO particle by this technique under controlled conditions. Here we used chitosan solution as a medium to grow the ZnO particle.[70]

3.2 Experimental
3.2.1 Materials

Chitosan samples of viscosities 55, 330 and 800 cps were supplied by India Sea Foods, Cochin, Kerala. The degree of deacetylation of the samples was greater than 85 %.

☞ Zinc chloride, sodium hydroxide and acetic acid were supplied from s.d. fine-chem. ltd, Mumbai, India.

Commercial zinc oxide:

Synonyms: Chinese white, zinc oxide

Supplied by M/s. Meta Zinc Ltd., Mumbai. Main properties and its values are given in table 3.1.

Table 3.1 Main properties and values of commercial ZnO

Properties	Value
Crystal form	Hexagonal
Lattice parameters	A=3.25, C=5.05
Particle size	40 nm
Colour	White
Hardness	mohs 4.5
Melting point	1975 °C
ZnO content	98.0 %
Acid content	0.4 % max.
Heat loss (2 hrs at 100 °C)	0.5 % max.

3.2.2 Preparation of zinc oxide in chitosan solution

ZnO was prepared from $ZnCl_2$ and NaOH using chitosan as a matrix. This method essentially consists of forming a complex of $ZnCl_2$ and chitosan by dissolving the two components in desired proportion in acetic acid. Vigorous stirring was maintained at this stage. This was allowed to react for 24 hours. Then stoichiometric amount of NaOH was added drop wise to the above complex with / without stirring. The whole mixture was allowed to digest for 12 hours at room temperature. During this period the OH⁻ and Cl⁻ ions diffused through the matrix and formed a precipitate of $Zn(OH)_2$. It was filtered and washed several times with water and dried at 100 °C. Then it was calcined at different temperatures like 350 °C, 450 °C and 550 °C in a silica crucible in a muffle furnace for 4 hours. The yield of the ZnO nanocrystals by this method is about 90 %. Figure 3.1 shows the schematic overview of the preparation of ZnO.

```
ZnCl₂-CH₃COOH          Chitosan-CH₃COOH
        |                       |
        ↓                       ↓
        |_____|
                    |
                    ↓
        ZnCl₂- Chitosan complex
                    |
                    ↓  NaOH Precipitation
                 Zn (OH)₂
                    |
                    ↓  550 °C
            Precipitated ZnO
```
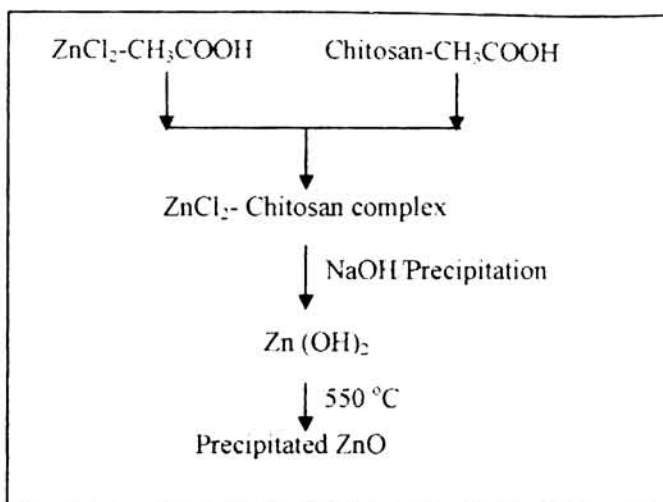
Figure 3.1 Schematic overview of the preparation of nano zinc oxide

To find synthetic fundamentals for this new approach, a number of preparative parameters were examined in detail. The process was repeated by taking different concentrations of zinc chloride, chitosan and sodium hydroxide solution and also by varying the time and temperature for complexation and precipitation. The conditions were optimized for the preparation of ZnO nanoparticles. Using the above method 18 batches of ZnO was prepared using different concentrations of chitosan of different viscosity and with / without stirring during the addition of NaOH. The photographs of precipitated zinc hydroxide with stirring and without stirring and zinc oxide are shown in figures 3.2 (a), (b) & (c) respectively.

(a)

(b)

(c)

Figure 3.2 The photographs of (a) precipitated zinc hydroxide prepared by stirring method (b) precipitated zinc hydroxide prepared by without stirring method (c) precipitated zinc oxide

Different batches of ZnO is given in table 3.2.
Amount of $ZnCl_2$ is constant in all batches.

Table 3.2 Different batches of ZnO

Sample name	Viscosity of chitosan in cps	% of chitosan solution	Mode of preparation
S1	55	1	Without stirring
S2	55	2	Without stirring
S3	55	5	Without stirring
S4	55	1	With stirring
S5	55	2	With stirring
S6	55	5	With stirring
S7	300	1	Without stirring
S8	300	2	Without stirring
S9	300	5	Without stirring
S10	300	1	With stirring
S11	300	2	With stirring
S12	300	5	With stirring
S13	800	1	Without stirring
S14	800	2	Without stirring
S15	800	5	Without stirring
S16	800	1	With stirring
S17	800	2	With stirring
S18	800	5	With stirring

3.3 Characterization
3.3.1 Bulk density (ASTM D 1895)

Apparent density-

Weight / unit volume of a material including voids inherent in the material.

Bulk density-

Bulk density is defined as the weight per unit volume of a material. It is primarily used for powders or pellets. The test can provide a gross measure of particle size and dispersion, which can affect material flow consistency and reflect packaging quantity.

Apparent density

Measuring cup, a cylindrical cup of $100 + 0.5$ ml capacity having a diameter equal to half of the height. For e.g. 39.9 mm inside diameter by 79.8 mm inside height.

Funnel, having a 9.5 mm diameter opening at the bottom and mounted at a height 38 mm above the measuring cup.

Specimen: Powder or Pellets
Procedure

Close the small end of the funnel with hand or a suitable flat strip and pour 115 ± 5 cm^3 samples into the funnel. Open the bottom of the funnel quickly and allow the material to flow freely into the cup. If caking occurs in the funnel, the material may be loosened with a glass rod. After the material has passed through the funnel immediately scrap off the excess on the top of the cup with a straight edge without shaking the cup. Weigh the material cup to the nearest 0.1g. Calculate the weight in grams of 1 cm^3 of the material.

Data: Apparent density value is recorded as g/cm^3

3.3.2 Element analysis (ICP-AES analysis)

Inductively coupled plasma atomic emission spectroscopic analysis is a highly successful multielemental analysis with inductively coupled plasma as the heating source and operating on atomic emission spectroscopic technique.

The ZnO sample is dissolved with 5ml HNO_3 and made up to 50 ml using distilled water. The filtered sample is analyzed with ICPAES system of Thermo Electron Corporation (Model: IRIS INTREPID II XSP).

3.3.3 Energy dispersive X-ray spectrometer

The chemical stoichiometry of ZnO nanoparticle is investigated with EDX, (EDS, HITACHI, S-2400).

3.3.4 Surface area

Surface area of the zinc oxide nanoparticles and commercial zinc oxide were measured using BET method. Surface area analysis was done using Micromeritics BJH surface analyser tristar 3000. Measurements were carried out at liquid nitrogen temperature.

3.3.5 X-ray diffraction (XRD)

Particle size of the sample was determined using X-ray diffraction (XRD) technique. XRD patterns were collected using Bruker, AXS D_k Advance diffractometer at the wavelength $CuK\alpha= 1.54$ Å, a tube voltage of 40 KV and tube current of 25 mA. Crystallite size is calculated using Scherrer equation,

$$CS = 0.9\lambda \, / \, \beta \, Cos \, \theta \qquad\qquad ....3.1$$

Where, CS is the crystallite size, β is full width at half-maximum (FWHM $_{hkl}$) of an *hkl* peak at θ value.[71]

3.3.6 Fourier transform infrared spectroscopy

Fourier transform infrared spectra are generated by the absorption of electromagnetic radiation in the frequency range 400 to 4000 cm^{-1} by organic molecules. Different functional groups and structural features in the molecule absorb at characteristic frequencies. The frequency and intensity of absorption are the indication of the band structures and structural geometry in the molecule. FTIR absorption spectra were collected using ThermoAvtar 370 spectrometer.

3.3.7 UV spectroscopy

Room temperature UV-vis absorption spectra were recorded on UV-2550 spectrophotometer.

3.3.8 Photoluminescence (PL) spectroscopy

The room temperature photoluminescence spectra were performed on a spectrophotometer Fluorolog-3-Tau using a He-Cd laser (λ_{ex}=325 nm) as the excitation source.

3.3.9 Transmission electron microscopy

The morphology and particle size of zinc oxide were observed using transmission electron microscope (TEM). The TEM images and selected area electron diffraction (SAED) patterns were taken on Philips TEM CM 200 model.

3.3.10 Scanning electron microscopy

Scanning electron microscope (Cambridge Instruments, S 360 Stereoscanner-version V02-01, England) was used to investigate the morphology of the zinc oxide samples.

3.3.11 Thermo gravimetric analysis

Thermo gravimetric analyzer (TGA, Q-50, TA Instruments) was used to study the thermal stability of ZnO. Approximately 5 mg of the samples were heated at a rate of 20 °C/min to 800 °C. The chamber was continuously swept with nitrogen gas at the rate of 60 ml/min.

3.3.12 Differential scanning calorimetry

(DSC Q 100, TA instruments) was employed to study the calorimetric measurements of ZnO nanoparticles. Indium was used for temperature calibration (T_m =156.6 °C, ΔH_m =28.4 J/g). All the samples were dried prior to the measurements and analysis were done in a nitrogen atmosphere using standard aluminum pans.

3.4 Results and discussions
3.4.1 Bulk density

The different types of ZnO prepared in the lab are characterized by determining the bulk density. Determining the bulk density of the sample does the primary identification. The bulk density of the prepared samples is shown in table 3.3.

Table 3.3 Bulk densities of the prepared ZnO samples

Sample name	Bulk density (g/cm^3)
Commercial	0.4234
S1	0.9034
S2	0.9038
S3	0.9043
S4	1.0742
S5	1.0738
S6	1.0778
S7	0.9053
S8	0.9088
S9	0.9067
S10	1.0589
S11	1.0921
S12	1.0323
S13	0.9056
S14	0.9069
S15	0.9105
S16	1.0845
S17	1.0529
S18	1.0723

From the bulk density results, it is seen that ZnO prepared in chitosan solution has high values when compared with the commercial ZnO. This may be due to the reduction in particle size and difference in structure. It is observed that particle size is lower for stirred batches (S4, S5, S6, S10, S11, S12, S16, S17, S18) than that of without stirred batches (S1, S2, S3, S7, S8, S9, S13, S14, S15).

From this study it is also found out that, particle size almost remains the same with change in viscosity of the medium. Only chitosan medium is important.

3.4.2 Element analysis (ICP-AES analysis)

The elements analyzed are Zn and Na and table 3.4 shows the amount of elements present in the sample.

Table 3.4 Element analysis

Elements	Avg	Units
Zn	99.1	%
Na	0.89	%

So the prepared ZnO has high purity.

3.4.3 Energy dispersive X-ray spectrometer

The chemical stoichiometry of ZnO nanoparticle was investigated with EDX (figure 3.3), which affirmed an atomic ratio of Zn:O $\cong$ 1:1.

Elmt	Element %	Atomic %
O	18.29	47.78
Zn	81.71	52.22
Total	100.00	100.00
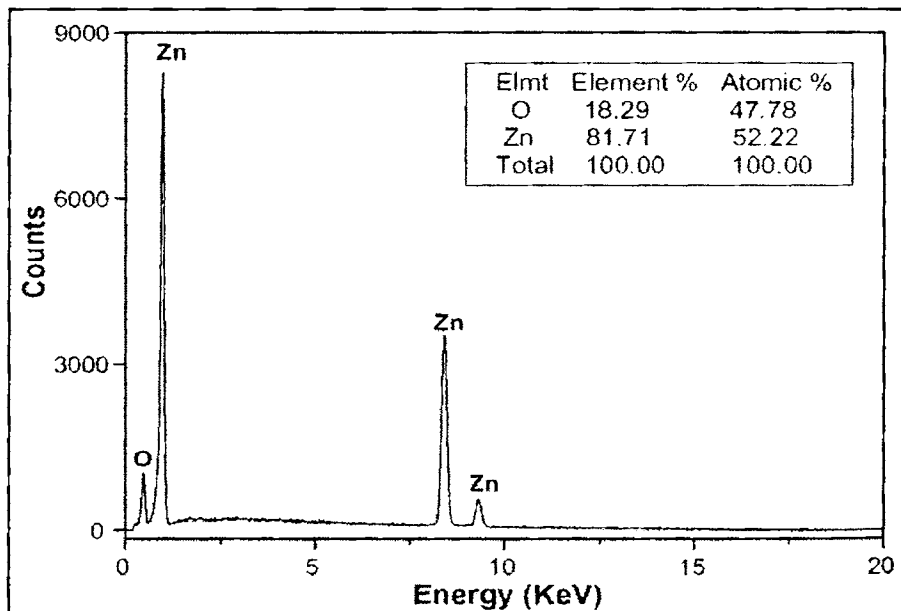
Figure 3.3 EDX patterns of ZnO nanoparticles

3.4.4 Surface area

Representative samples were selected from those prepared with stirring (S11) and without stirring (S8) for surface area determination. Table 3.5 shows surface area for commercial zinc oxide, S8 and S11 samples.

Table 3.5 Surface areas for different ZnO samples

Sl. No.	Samples	Surface area
1	Commercial zinc oxide	4.08 Sqm/g
2	S8	37.56 Sqm/g
3	S11	42.15 Sqm/g

The surface area is more for the ZnO samples prepared in the lab compared to commercial ZnO. It is also clear that ZnO prepared with stirring is having more surface area than ZnO prepared without stirring. This is due to the smaller particle size of S11 than S8.

3.4.5 XRD studies

Figures 3.4 (a), (b) and (c) shows the XRD patterns of commercial ZnO, S8 and S11 respectively.
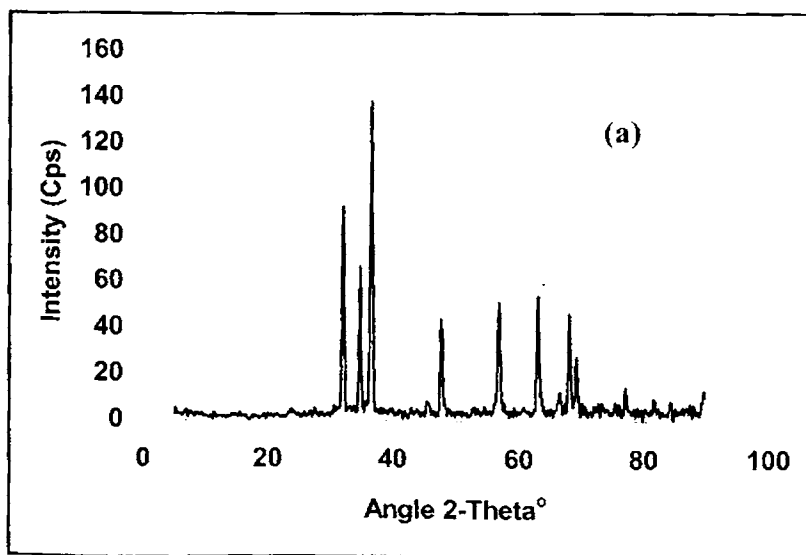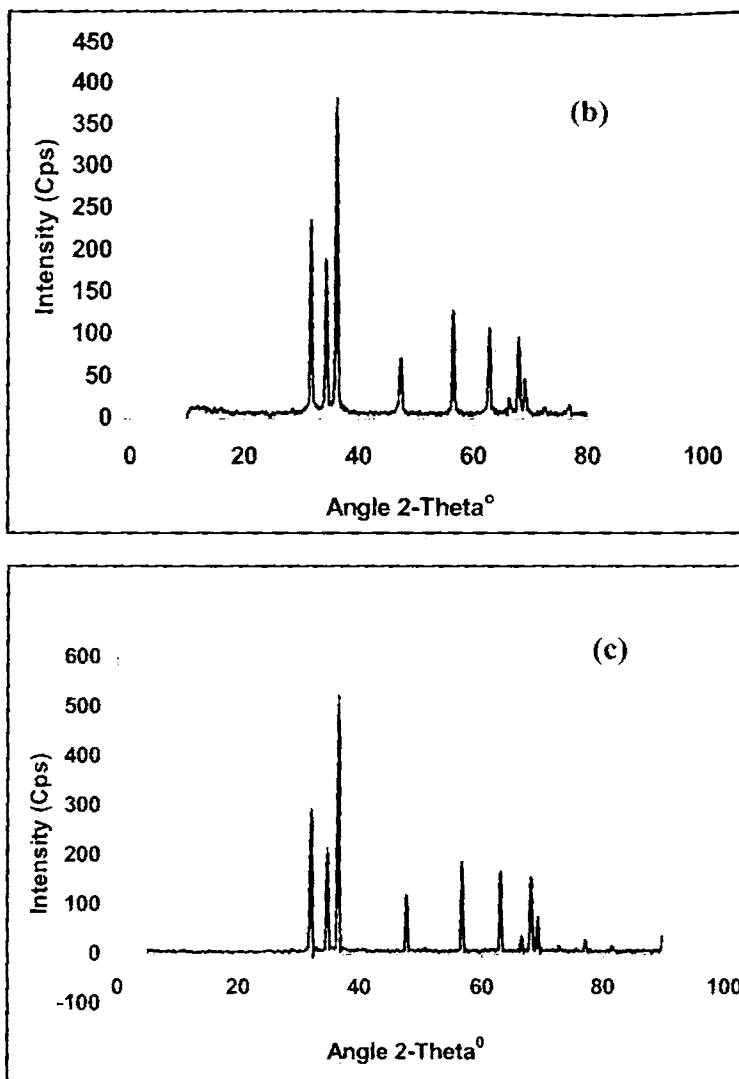
Figure 3.4 XRD patterns of (a) commercial ZnO (b) S8 & (c) S11

It is very clear from the above figure 3.4 (c) that the major reflections between $30°$ and $40°$ (2θ values) indicate more crystalline regions in the zinc oxide sample.

Also the less intense peaks at $47.5°$, $56°$ and $63°$ (2θ's) indicate the high crystallinity of zinc oxide samples. The detailed analysis of the XRD and the assignments of various reflections are given in table 3.6. Crystallite sizes of the ZnO are calculated using Scherrer's formula.

Table 3.6 Analysis of XRD and the assignments of various reflections of ZnO

Sample	d (Obs)	FWHM	Crystallite size (nm)
Commercial	2.4599	0.224	37.39
S8	2.4574	0.368	22.76
S11	1.9027	0.446	18.78

The full width at half-maximum of an *hkl* peak at θ value and crystallite size of all the zinc oxide samples shows that S11 have smaller crystal size compared to others. When the morphology of S8 changed to S11 from plate like structure to rod like structure, it was presumed that the distance of planar spacing was shortened.[72]

Figure 3.5 shows the XRD patterns of zinc oxide samples (S11) formed at different calcinations temperatures. The Bragg reflections of zincite are visible at all temperatures as shown in the figure. But at lower temperature, in the precursor, more amorphous regions are present, along with crystalline zinc oxide particles. When the temperature is increased, this amorphous region disappeared as shown in the XRD pattern of high temperature samples.

It is also clear from the figure that the increase in calcinations temperature, the crystallinity increases as indicated by the intensity of the XRD pattern. The zinc oxide sample calcined at 550 °C showed lower particle size as indicated by high peak intensity.
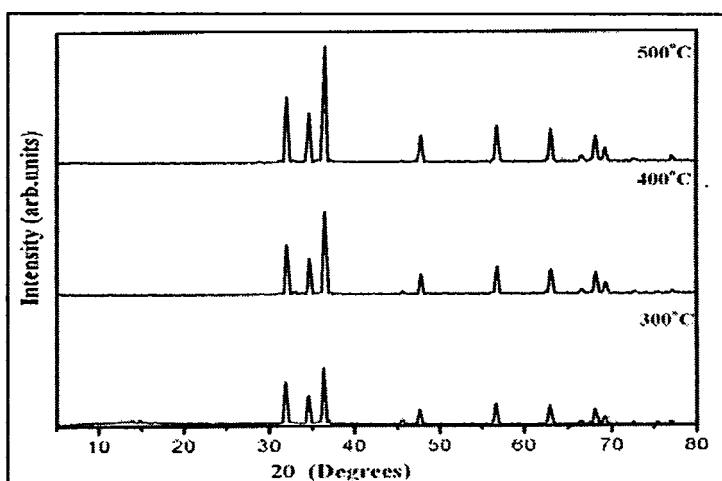
Figure 3.5 XRD patterns of zinc oxide samples formed at different calcinations temperatures

3.4.6 IR spectroscopy

Figure 3.6 (a) & (b) shows the IR spectrum of S11 and commercial ZnO samples respectively. A similar spectrum is obtained for sample S8.
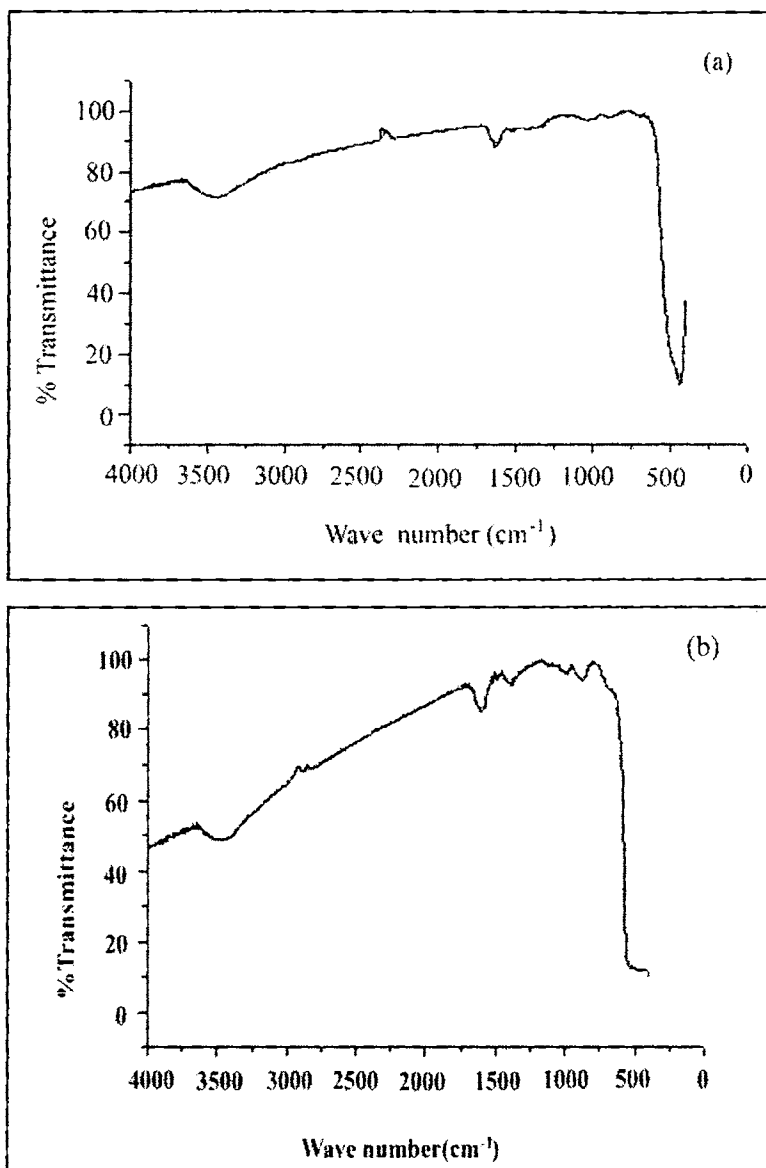
Figure 3.6 IR spectrums of (a) S11 & (b) commercial ZnO

The peak around $450\ cm^{-1}$ shows a distinct stretching mode of crystal zinc oxide. The shape of the IR spectrum of ZnO particles is generally influenced by

particle size and morphology, the degree of particle aggregation, or the crystal structure of ZnO polymorph. Hayashi et al.[73] compared the recorded and calculated spectra of ZnO. Serna and co-workers[74,75] considered the relationship between the shape of IR spectrum on one side, and the physical shape and aggregation of ZnO particles on the other. Tanigaki et al.[76] prepared ZnO particles by the high temperature oxidation of zinc powder and observed different shapes in the spectra.

Figure 3.7 shows the IR spectrum of intermediate products formed at different temperatures during calcination. A broad peak in the range $3250 - 3600$ cm^{-1} for the sample heated at 350 °C indicates the presence of –OH stretching vibrations, which is due to the presence of zinc hydroxide. It is seen from the spectra that this peak is disappeared for the samples calcined at higher temperatures.

It is also clear from the spectra that the intensity of the characteristic peaks of zinc oxide is in the range of 500-525 cm^{-1} is increased when the calcinations temperature is increased.
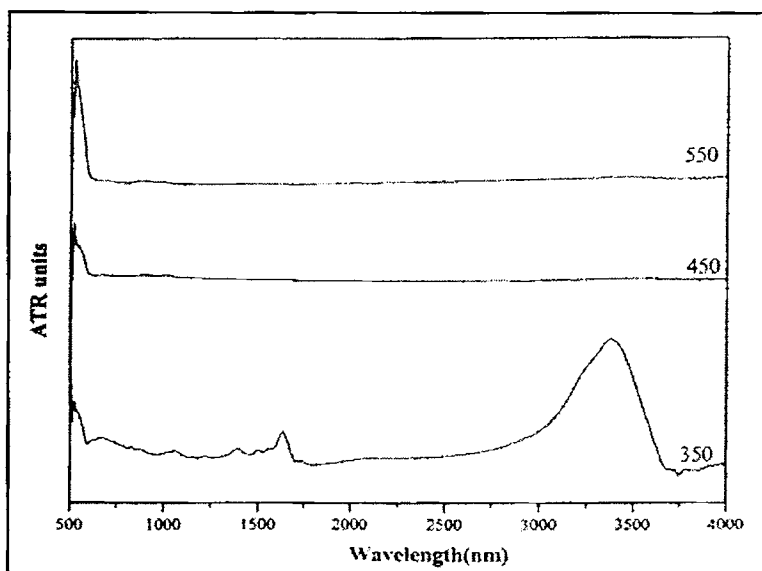
Figure 3.7 FTIR spectra of zinc oxide samples at different calcinations temperatures

3.4.7 UV spectroscopy

Figure 3.8 shows the UV-vis absorption spectrum of S11 sample. It exhibits a strong excitonic absorption feature at ~368 nm, which is blue shifted of ~7 nm with respect to the bulk absorption of 375 nm. A similar spectrum is obtained for sample S8 and commercial ZnO.
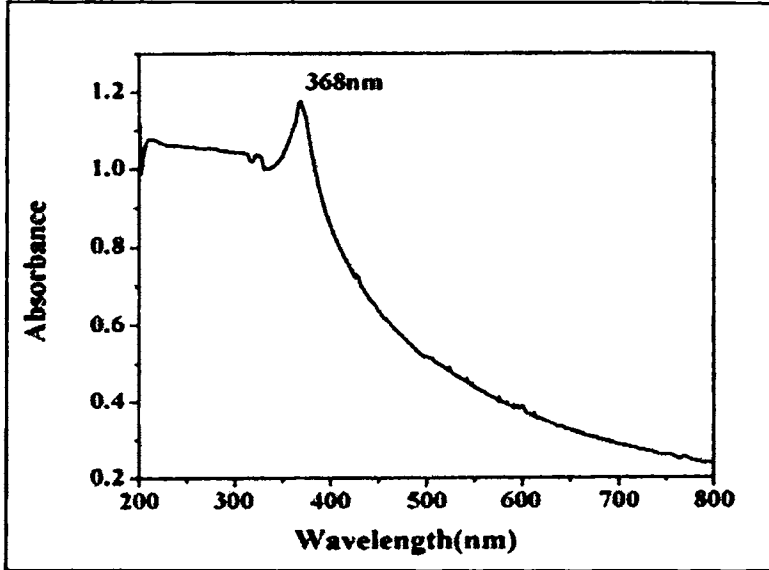
Figure 3.8 Absorption spectra of ZnO nanoparticle

3.4.8 Photoluminescence (PL) spectroscopy

Figure 3.9 reveals the room temperature PL spectra of S11 sample. A strong UV emission at ~384 nm, agreeing the near band edge emission can be detected. Generally, a green-yellow emission could be observed in the PL spectrum, which generally comes from the recombination of photo-generated hole with electrons in singly occupied oxygen vacancies. Unlike those reported in many ZnO nanostructure synthesis, the green emission band (around 510–515 nm) due to the presence of the singly ionized oxygen vacancies (or other point defects) [40] is barely observable in prepared samples. As reported in the literature [77,78] this finding may indicate that the ZnO nanorods synthesized by this novel method possess high crystalline perfection. A similar spectrum is obtained for sample S8.
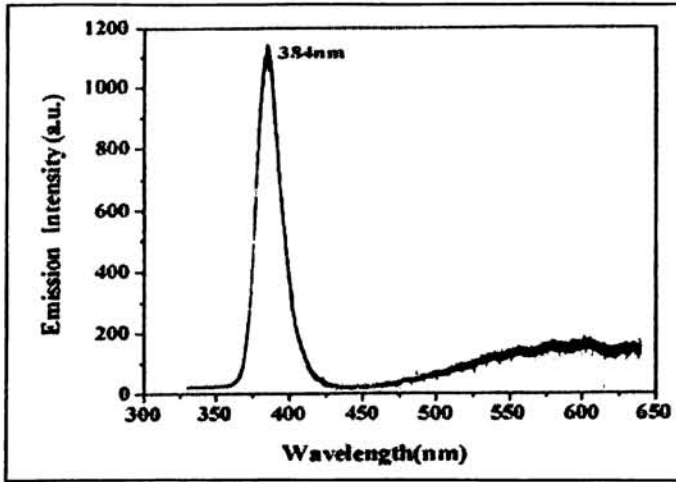
3.4.9 Transmission electron microscopy

Figures 3.10 (a) shows the TEM images of S11 sample and (b) shows its SAED patterns. It shows that zinc oxide particle of rod like structure having high aspect ratio, is obtained with constant stirring. From the TEM image it can be obtained that the rod diameter is in the range 12-25 nm and length is in the range 100 –250 nm. The corresponding SAED pattern indicates that the nanorods are consisted of hexagonal single crystal ZnO and amorphous ZnO nanoparticles. The clear diffraction spots indicate a high crystal quality of S11.[61] So the prepared ZnO nanorod is different from commercial ZnO in morphology [figure 3.11 (a)] and highly crystalline than commercial ZnO, which is clear from the SAED patterns shown figure 3.11 (b).

(a)   (b)
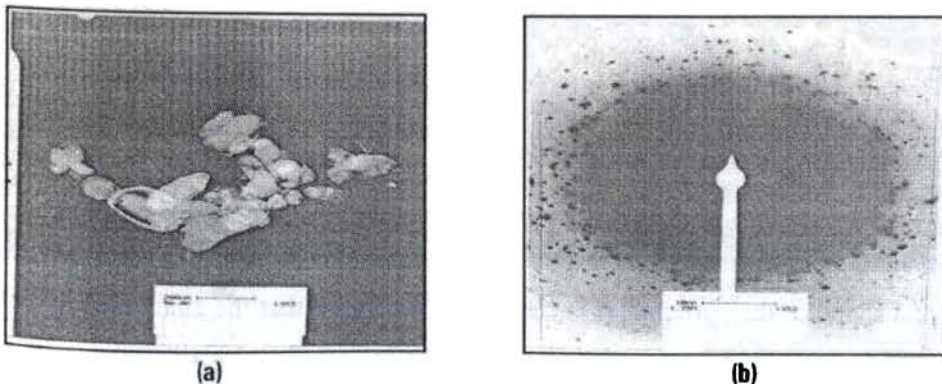
Figure 3.10 (a) TEM image and (b) SAED patterns of S11

TEM image of zinc oxide particle prepared without stirring (S8) is shown in figure 3.12 (a) and have specific plate or box like shape. Its particle size is 20-30 nm. It is also clear from the photograph that the zinc oxide formed is crystalline as its shape is changed from the coarse structure of commercial ZnO as shown in figure 3.11 (a). The nano ZnO prepared is highly crystalline than commercial ZnO. The particle size of commercial ZnO is 40-90 nm.

(a)   (b)
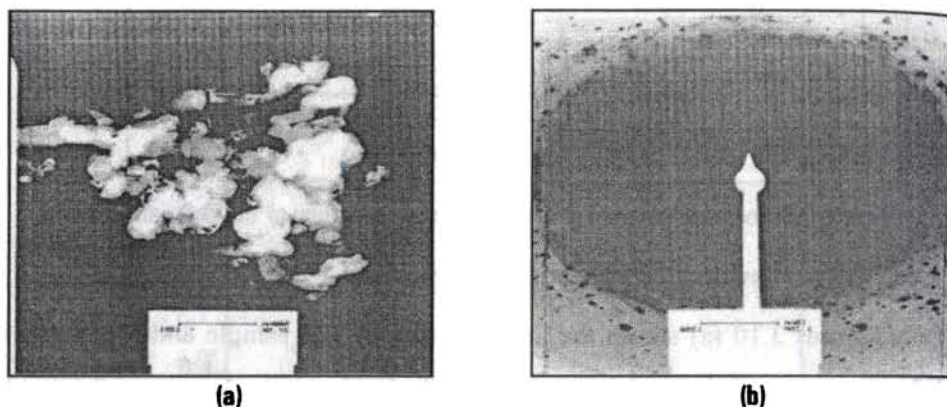
Figure 3.11 (a) TEM image and (b) SAED patterns of commercial ZnO

(a)   (b)
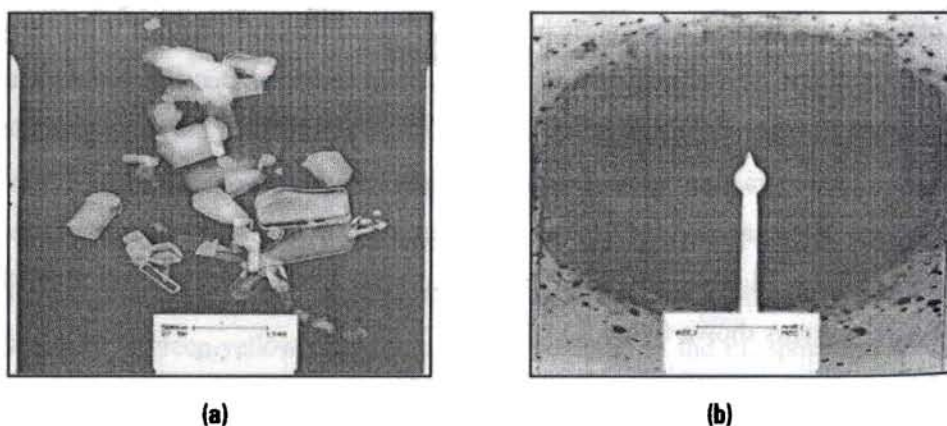
Figure 3.12 (a) TEM image and (b) SAED patterns of S8

3.4.10 Scanning electron microscopy

The surface morphology as determined by scanning electron microscopy reveals that the method of preparation has a significant effect on the structure and shape of the particles. It is clear from the figure that the zinc oxide particles (S8) formed by without stirring method have specific plate like shape [figure 3.13 (c & d)]. Precipitation carried out by vigorous stirring gave zinc oxide

particles (S11) with rod like structure [figure 3.13 (a & b)]. It is different from the structure of commercial ZnO [figure 3.13 (e & f)]. A remarkable change in particle size and morphology was observed for the ZnO samples precipitated in chitosan medium. The sample precipitated using chitosan medium shows a dramatic reduction in particle size.
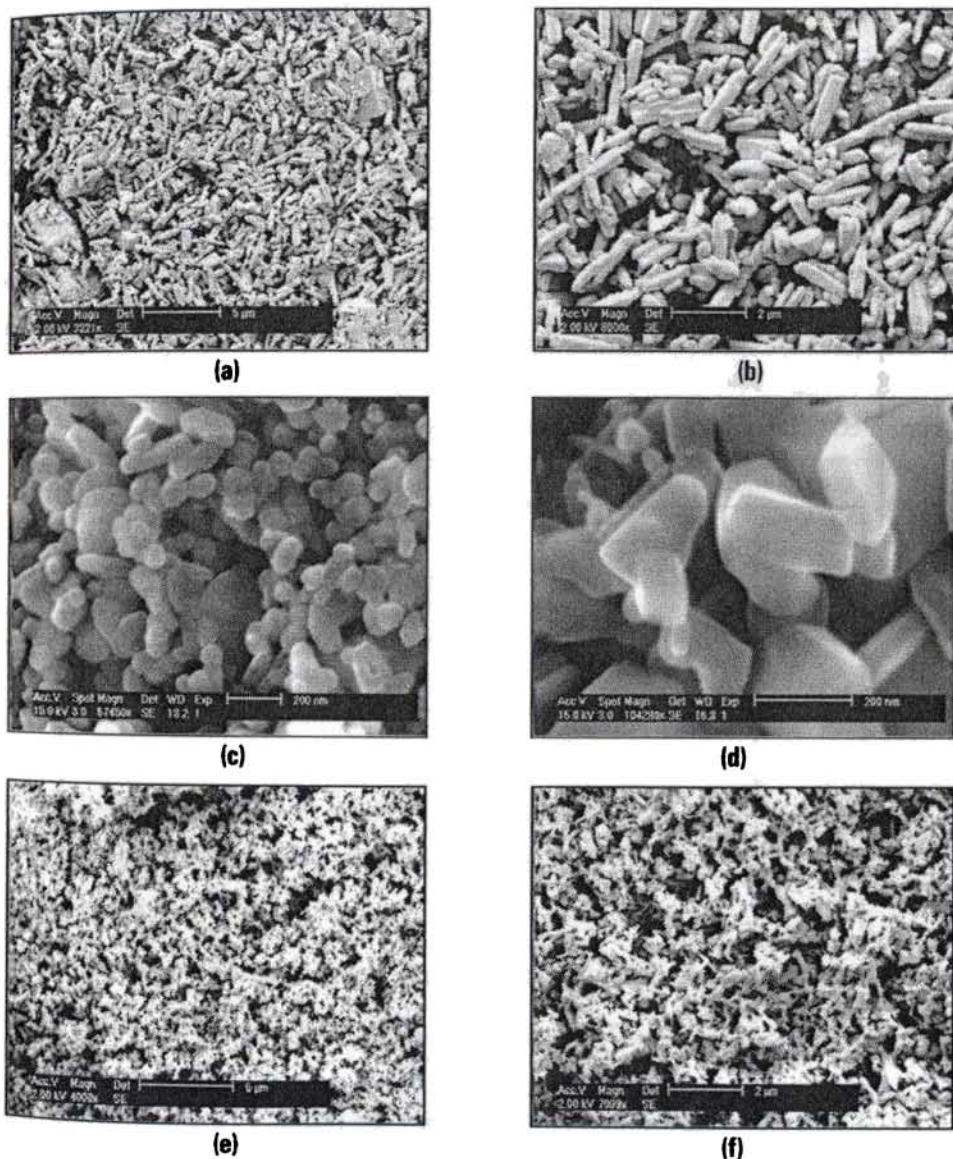
Figure 3.13 SEM images of different ZnO samples [(a) & (b) S11, (c) & (d) S8 and (e) & (f) commercial ZnO]

3.4.11Thermo gravimetric analysis

Thermal analysis of the prepared ZnO nanoparticles (nano ZnO) was carried out to know the possible changes occurring when the materials were subjected to heat treatment. Figure 3.14 (a) shows the corresponding TGA trace for the nano ZnO and (b) for commercial ZnO. From the figure it is seen that TGA curve for the nano ZnO is almost featureless except for a small endothermic peak at around 190 °C. The TG curve in the figure indicates that the sample weight begins to decrease slightly at 190 °C, and then levels off from 600 °C. As reported by Morishige et al.[79] and Chen et al.[80] the peaks at around 220 and 270 °C in TG figure may be caused by the decomposition of the condensation dehydration of the hydroxyls. This peak could not be associated with any phase change, as the corresponding XRD pattern [figure 3.4 (c)] also did not show any change in the phase of the material prepared. At the most, the peak can be attributed to complete crystallization of the sample.
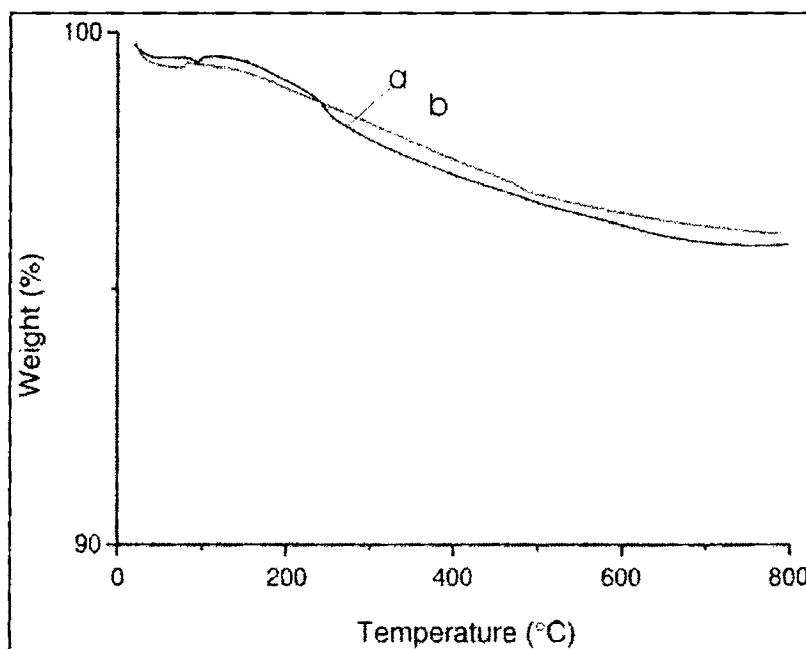
Figure 3.14 TGA trace for (a) nano ZnO and (b) commercial ZnO

3.4.12 Differential scanning calorimetry

No obvious peak was seen in DSC curve, as shown in figure 3.15, which may indicate that the nano ZnO is pure, hexagonal phase, which is associated with the XRD results. Similar behaviour is observed for commercial ZnO.
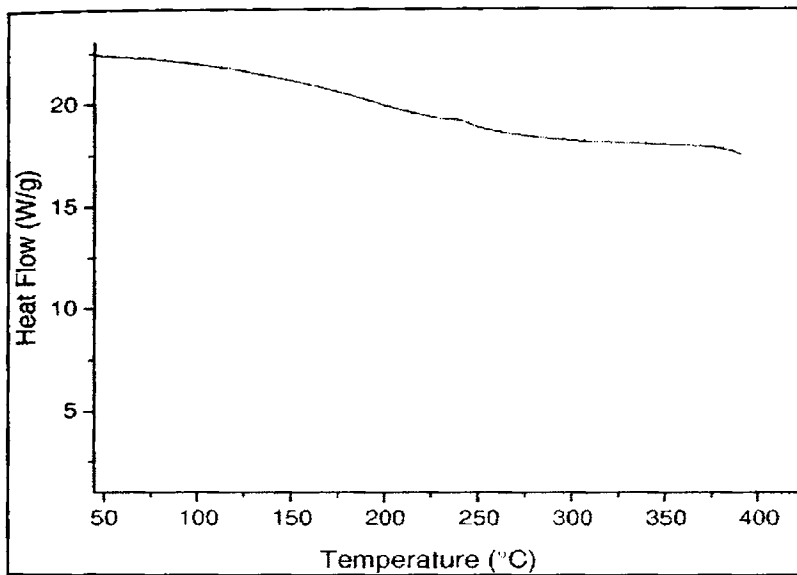
Figure 3.15 Differential scanning calorimetry (DSC) of nano ZnO

3.4.13 Formation of nanoparticles

Based on the above experimental results, we proposed a plausible mechanism for the formation of ZnO nanoparticles by polymer-induced crystallization as shown in figure 3.16. The influence of chitosan matrix is very important in forming nanoparticles of zinc hydroxide and hence on the zinc oxide obtained subsequently.

Formation of nanoparticles depends on many factors. The most important of these are:

- The stability of the complex formed between the particle and the surrounding polymer matrix and the proper diffusion of the reacting species are the most important criteria for the formation of nanoparticles. The surrounding polymer matrix should be able to hold the metal atom

at a particular space, for e.g. OH⁻ ions in chitosan and should not allow it to break away from the matrix.

- The proper diffusion of the second reactant also plays a major role in reduction in particle size of the particular particle. In the case of chitosan matrix stirring is required for proper diffusion of OH⁻ ions.

- The ratio between the polymer matrix used (chitosan) and the metal ion i.e., Zn^{+2} will also play an important role. For the same molecular weight, a lower ratio i.e., below 1 % of chitosan solution, the number of polymer chains available will be less and the metal ions can move freely along the chain reducing the stability. However, at higher ratio the number of polymer chains available is very high and the metal ion is bound strongly to the polymer, which is in turn surrounded by the matrix. Thus the stability of the bond is enhanced and this results in reduction in particle size. Also the interaction between different particles of the same type will be reduced, thus reducing cluster formation.

- Other factors are temperature, interaction of the particle with various systems around it, the method of synthesis. Higher the temperature, greater the chances of breaking the polymer- metal ion complex which will thus not have much effect on the particle size of the filler. Also the particle present in the system can interact with the solvent present, with the polymer matrix, another particle of the same type and other reactants. For efficient reduction in particle size, the interaction between the polymer matrix and the metal ion should be high when compared to other interactions.

This method essentially consists of forming a complex of zinc chloride with chitosan by dissolving the two components in desired proportions in acetic acid. Chemical linkages between OH⁻ions present in the chitosan medium and Zn ions in $ZnCl_2$ form the complex. There is no possibility of zinc hydroxide formation at this moment, since hydroxyl ions are strongly bond to the chitosan chain. On

adding sodium hydroxide without stirring, the OH⁻ ions present in it has to diffuse through the bulky medium in different directions to reach up to zinc ions. Since the polymer chains binds the zinc ions, the formation of zinc hydroxide can take place only at certain sites. Since low amount of hydroxyl ions reach up to zinc ions some of the zinc ion are left free and we are getting box or plate like nano zinc oxide particles, whereas ZnO nanorods were formed at high $[Zn^{2+}]/[OH^-]$ ratio. With vigorous stirring, hydroxyl ions diffuse in to the matrix from all the possible directions and nanorods are obtained. More OH⁻ions in solution were reactive with Zn^{2+} to form ZnO clusters. The formed ZnO clusters heterogeneously grow on the surface of ZnO nanocrystals as nucleation centre. During this course, the smaller nanocrystals in the solution shrink and the bigger ones continue their growth. As a result, the size of ZnO nanocrystals was increased, but crystals grew simultaneously in three dimensions. However, permanent dipole moment in nanocrystals has been enhanced with increasing the volume of ZnO nanocrystals. The facets terminated by negatively charged O atoms and positively charged Zn atoms have been reported.[81] As in the final stage of the process, nanocrystals grew almost exclusively along their long axis and both aspect ratio and volume of crystals increased rapidly with increasing the amount of Zn^{2+} and OH⁻ ions in solution. Henceforth, ZnO nanorods were formed. The formation of ZnO nanorods furthermore increased the polarity between particles. Even though there is stirring, only slow diffusion of the reactant takes place, which results in reduction in particle size. The viscosity of chitosan has no specific role in determining the size and shape of particles. The yield of zinc hydroxide is almost a constant with varying concentrations.

This new synthesis of zinc oxide particles has three advantages. (1) The reaction is carried out under moderate or even simple and crude conditions, which makes this method promising for large-scale production. (2) Particles of nanometer-size can be attained by this method. (3) With the change of reaction conditions, particles with different morphologies can be seen through TEM.
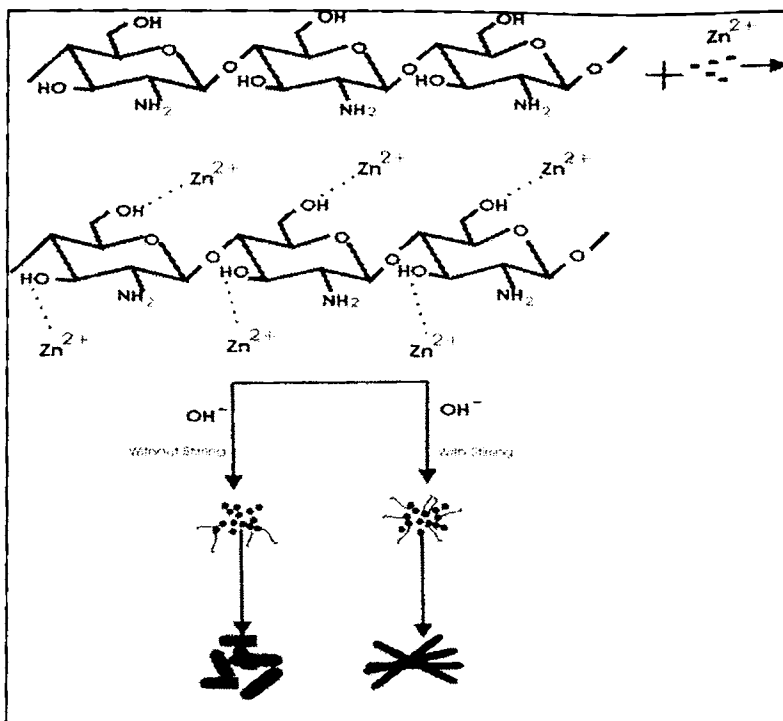
Figure 3.16 A possible mechanism for the growth of ZnO nanoparticles in chitosan medium

ZnO prepared by this method (S11) is hereafter called as nano zinc oxide which is used for the preparation of nanocomposites.

3.5 Conclusions

Zinc oxide with high crystalline nature can be prepared from zinc chloride in chitosan solution by in-situ deposition technique. TEM and SEM studies revealed that zinc oxide is having nanoparticle size. The particle size of nano zinc oxide is much lower than that of commercial zinc oxide. There is not much change in the particle size of nano zinc oxide with variation in viscosity of chitosan medium. SEM and TEM studies revealed that mode of preparation have a specific role in determining the size and shape of zinc oxide particle. Nano ZnO is having high purity as revealed by TGA and DSC studies. They have a very strong photoluminescence (PL) band at ultraviolet wavelength range. This method has many advantages, such as simplicity, low cost, high input, high purity, high yield and little pollution in addition to superfine compounds that can be easily prepared.

3.6 References

1. Takai M, Futsuhara G, Shimizu CP, Lungu J, Nozue. Thin solid films 1998, 318, 117.

2. Xu JQ, Pan QY, Shun YA, Tian ZZ. Sensors and Actuators 2002, B66, 227.

3. Lou XJ. Sens Trans Technol 1991, 3, 1.

4. Dong LF, Cui ZL, Zhang ZK. Nanostructure Mat 1997, 8(7), 815.

5. Van Dijken A, Miulenkamp EA, Vanmaekelbergh D, Meijerink A. J Luminescence 2000, 90, 123.

6. Vanheusden K, Warren WL, Seager CH, Tallant DR, Voigt JA, Gnade BE. J Appl Phy 1996, 79(1), 7983.

7. Jose J, Abdul Khadar M. Nanostructure Material 1999, 11(8), 1091.

8. Nan CW, Holten S, Birringer R, Gao H, Kliem H, Gleiter H. Phys Stat Sol (A) 1997, 164, R1.

9. Lee J, Hwang JH, Mashek JJ, Manson TO, Miller AE, Siegel RW. J Mater Res 1995, 10, 2295.

10. Li JF, Yao LZ, Ye CH, Mo CM, Cai WL, Zhang YL, Zhang D. J Crystal Growth 2001, 223, 535.

11. Liu YX, Liu Yc, Shen DZ, Zhang GZ, Fan XW, Kong XG, Mu R. Solid State Comm 2002, 121, 531.

12. Pearton SJ, Norton DP, Ip K, Heo YW, Steiner T. Prog Mater Sci 2005, 50, 293.

13. Anderson RA, Pike GE. J Mater Res 2003, 18, 994.

14. Snoke D. Science 1996, 273, 1351.

15. Cpllins IR, Taylor ES. J Mater Chem 1992, 2, 1277.

16. Spanhel L, Weller H, Henglein A. J Am Chem Soc 1987, 109, 6632-35.

17. Vogel R, Hoyer P, Weller H. J Phys Chem 1994, 98, 3183-88.

18. Koudelka L, Horak J. J Mater Sci 1994, 29, 1497-99.

19. Hwang CC, Wu TY. J Mater Sci 2004, 39, 6111.

20. Hwang CC, Wu TY. Mat Sci Eng B, Solid 2004, 111, 197.

21. Boyle TJ, Bunge SD, Andrews NL, Matzen LE, Sieg K, Rodiguez MA, Headley T. J Chem Mater 2004, 16, 3279.

22. Fujita K, Matsuda K, Mitsuzawa S. Bull Chem Soc Jpn 1992, 65, 2270.

23. Li WJ, Shi EW, Zheng YQ, Yin ZW. J Mater Sci Lett 2001, 12, 2301.

24. Meulenkamp EA. J Phys Chem B 1998, 102, 5566.

25. Pang Zw, Dai Zr, Wang ZL. Science 2001, 291, 1947.

26. Kumar RV, Diamant Y, Gendanken A. Chem Mater 2000, 12, 2301.

27. Li Y, You L, Duan R. Solid state Commun 2004, 129, 233.

28. Damonte LC, Mendoza Zelis LA, Mari Soucase B, Hernandez Fenollosa Ma. Powder technology 2004, 148, 15.

29. Liewhiran C, Seraphin S, Phanichphant S. Current Applied Physics 2006, 6499.

30. Hongmei Zhong, Jinbin Wang, Mei Pan, Shaowei Wang, Zhifeng Li, Wenlan Xu, Xiaoshuang Chen, Wei Lu. Materials Chemistry and Physics 2006, 97, 390.

31. Jingwei Zhang, Wei Wang, Pengli Zhu, Jianmin Chen, Zhijun Zhang, Zhishen Wu. Mat Lett 2007, 61, 592.

32. Changle Wu, Xueliang Qiao, Jianguo Chen, Hongshui Wang, Fatang Tan, Shitao Li. Mat Letters 2006, 60, 1828.

33. Wang L, Muhammed M. J Mater Chem 1999, 9, 2871.

34. McBride R, Kelly J, McCormack D. J Mater Chem 2003, 13, 1196.

35. Oliveira A, Hochepied J, Grillon F, Berger M. Chem Mater 2003, 15, 3202.

36. Qian D, Jiang J, Hansenm P. Chem Commun 2003, 2068.

37. Gao XD, Li XM, Yu WD. J Phys Chem.B 2005, 109, 1155.

38. Huang MH, Mao S, Feick H, Yan H, Wu Y, Kind H, Weber E, Russo R, Yang P. Science 2001, 292, 1897.

39. Pan ZW, Dai ZR, Wang ZL. Science 2001, 191, 1947.

40. Zhang J, Sun LD, Liao CS, Yan CH. Chem Commun 2002, 3, 262.

41. Guo L, Ji YL, Xu HB, Simon P, Wu ZY. J Am Chem Soc 2002, 124, 14864.

42. Lepot N, Van Bael MK, Van den Rul H, D'Haen J, Peeters R, Franco D, Mullens. Materials Letters 2007, 61, 2624.

43. Shengtai He, Hideaki Maeda, Masato Uehara, Masaya Miyazaki. Materials Letters, 2007, 61, 626.

44. Kong XY, Ding Y, Yang RS, Wang ZL. Science 2004, 1348, 303.

45. Yan HQ, He RR, Johnson J, Law M, Saykally RJ, Yang PD. J Am Chem Soc 2003, 125, 4728.

46. Fan HJ, Scholz R, Kolb FM, Zacharias M, Gosele U. Solid State Commun 2004, 130, 517.

47. Yan H, He R, Pham J, Yang PD. Adv Mater 2003, 15, 402.

48. Roy VAL, Djuri AB, Chan WK, Gao J, Lui HF, Surya C. Appl Phys Lett 2003, 83, 141.

49. Gao P, Wang ZL. J Phy Chem B 2002, 106, 12653.

50. Wen JG, Lao JY, Wang DZ, Kyaw TM, Foo Y, Ren ZF. Chem Phys Lett 2003, 372, 717.

51. Jinping Liu, Xintang Huang, Yuanyuan Li, Jinxia Duan, Hanhua Ai, Lu Ren. Mat Sci and Eng B 2006, 127, 85.

52. Xianhui Xia, Zhizhen Ye, Guodong Yuan, Liping Zhu, Binghui Zhao. Applied Surface Science 2006, 253, 909.

53. Sakohara S, Honda S, Yahai Y, Anderson MA. J Chem Eng Jpn 2001, 4, 15.

54. Kutty TRN, Padmini P. Mater Res Bull 1992, 27, 945.

55. Auffredic JP, Boultif A, Langford JI, Louer D. J Am Ceram Soc 1995, 78, 323.

56. Dhage SR, Renu Pasricha, Ravi V. Mat Letters 2005, 59, 779.

57. Mondelaers D, Vanhoyland G, Van den Rul H, Haen JD, Van Bael MK, Mullens J, Van Poucke LC. Mater Res Bull 2002, 37, 901.

58. Tokumoto MS, Pulcinelli SH, Santilli CV, Briois V. J Phys Chem B 2003, 107, 568.

59. Spanhel L, Anderson MA. J Am Chem Soc 1991, 113, 2826.

60. Chu S, Yan T, Chen S. J Mater Sci Lett 2000, 19, 349.

61. Xiaohong Liu, Jinqing Wang, Junyan Zhang, Shengrong Yang. Materials Science and Engineering 2006, A 430, 248.

62. Ristic M, Music S, Ivanda M, Popovic S. Journal of Alloys and Compounds Letter 2005, 397, L1.

63. Lakshmi BB, Dorhour PK, Martin CR. Chem Mater 1997, 9, 857.

64. Rossetti R, Hall R, Gibson JM, Brus LE. J Chem Phys 1985, 83, 1406.

65. Ekimov AI, Efros AIL, Onushcenko AA. Solid State Commun 1985, 56, 921.

66. Dalas E, Kallitsis J, Sakkopoulos S, Vitoratos E, Koutsoukos PG. J Colloid Interface Sci 1991, 14, 137.

67. Wei Zeng, Zhuo Wang, Xue-Feng Qian, Jie Yin a, Zi-Kang Zhu. Materials Research Bulletin 2006, 41, 1155.

68. Mishra S, Mukherji A, Sonawane SH. Polymer-Plastics Technology and Engineering 2006, 45, 641.

69. Radhakrishnan VV. M.Tech Project, CUSAT 2003.

70. Nisha VS. Ph.D Thesis, CUSAT 2006.

71. Jing LQ, Xu ZL, Sun XJ, Shang J, Cai WM. Appl Surf Sci 2001, 180, 308.

72. No-Kuk Park, Gi Bo Han, Jong Dae Lee, Si OK Ryu, Tae Jin Lee, Won Chul Chang, Chih Hung Chang. Current App Phys 2006, 6S1, 176.

73. Hayashi S, Nakamori N, Kanamori H, Yodogawa Y, Yamamoto K. Surf Sci 1979, 86, 665.

74. Andres-Verges M, Mifsud A, Serna CJ. J Chem Soc Faraday Trans 1990, 86, 959.

75. Andres-Verges M, Serna CJ. J Mater Sci Lett 1988, 7, 970.

76. Tanigaki T, Kimura S, Tamura N, Kaito C. Jpn J Appl Phys 2002, 41, 5529.

77. Wang JM, Gao L. J Mater Chem 2003, 13, 2551.

78. Zhong XH, Knoll WG. Chem Commun 2005, 1158.

79. Morishige K, Kittaka S, Moriyasu T. J C S Faraday 1980, 176, 728.

80. Chen J, Feng ZC, Ying PL, Li MJ. Phys Chem Chem Phys 2004, 6, 4473.

81. Rusen Y, Yong D, Zhonglin W. Nano Lett 2004, 4, 1309.

MODIFICATION OF ENGINEERING THERMOPLASTICS USING NANO ZINC OXIDE

Abstract

This chapter is divided into three parts. Modification of three engineering thermoplastics like [polyethylene terephthalate (PET), polyamide 6 (PA 6) and polycarbonate (PC)] using nano ZnO is discussed. Nanocomposites have been prepared through a simple melt compounding route. Melt compounded nano ZnOs have been shown to act as effective nucleating agents for PET and PA 6 crystallization. With increasing concentration of nano ZnO, the mechanical and dynamic mechanical properties improved, corresponding to an effective reinforcement. The rheological characteristics revealed that shear viscosity of the nano ZnO composites increased with increasing concentration of nano ZnO and decreased with increasing shear stress.

Part a

MODIFICATION OF POLYETHYLENE TEREPHTHALATE USING NANO ZINC OXIDE

4a.1 Introduction

Poly (ethylene terephthalate) (PET) was first prepared in 1946[1] and has become one of the most widely used polymers. Because of its low cost and high performance such as high transparency, high stability in dimension and good mechanical property, it can be used in lots of fields including film, bottle and fibre.[2,3,4] However, due to its higher melting point and lower crystallization rate, PET is not suitable very well for some processing such as injection moulding. However, the crystallization rate can be increased by the addition of polymeric nucleating agents such as thermo tropic liquid crystalline polymer (TLCP)[5-10] and inorganic fillers.[11-25]

Recently, the composites of polymer/inorganic nanoparticles have attracted more and more attention[26-34] and have made great progress. One of the most prevalent classes of composites is composed of materials containing an organic binding matrix with an inorganic material as the reinforcing filler, which comprise one of the most important class of synthetic engineering materials.[35-38] The incorporation of organic/inorganic hybrids can result in materials possessing high degrees of stiffness, strength and gas barrier properties with far less inorganic content than in conventional filled polymer composites. In addition, nanofillers can serve as a nucleating agent to speed up crystallization and to increase crystallinity.[39-42]

In this study we have used ZnO as a nucleating agent in PET matrix. The effect of ZnO on the crystallization behaviour, thermal stability, morphology, rheology, mechanical and dynamic mechanical property of the nanocomposites were analyzed. The properties were compared with that containing commercial ZnO.

4a.2 Experimental

Simple melt-compounding route was adopted for the preparation of PET-ZnO nanocomposites. The melt compounding was performed using Thermo Haake Rheocord 600 having mixing chamber with a volume capacity of 69 cm^3 fitted with roller type rotors operating at 40 rpm for 4 min at 255 °C. Nanocomposites at different concentrations (0.0-3.0 wt%) of ZnO were prepared. In all cases the torque stabilized to a constant value in this mixing time. The crystallization behaviour, thermal stability, morphology, rheology, mechanical and dynamic mechanical property of the nanocomposites using commercial and nano ZnO were analyzed according to the details summarized in sections 2.3 of this thesis.

4a.3 Results and discussion
4a.3.1 Differential scanning calorimetry
4a.3.1.1 Non-isothermal

PET is a semicrystalline polymer and its properties are related to its morphological features such as degree of crystallization, size and perfection of crystallites.[43] Nucleating agents that have been mentioned in the literature include metal oxides and hydrides, residual catalysts and diamide segments.[44,45,46] Several workers have reported the use of nanoparticles, such as organically modified nano clays as crystallization promoters for a variety of polymers[47,48] and nanotubes.[49] Previous investigations of PET-clay nanocomposites have demonstrated that the degree of crystallinity decreased while the rate of crystallization increased.[50] In literature only a few work have been reported on the use of ZnO. Crystallization temperature tends to shift to higher values with increasing ZnO nanoparticle content in PP matrix is reported by Zhao et al.[51] On adding 2.0 wt% of nano ZnO, there is an increase of 2 °C in crystallization temperature for PP matrix is observed by Tang et al.[52] and Zhao et al.[51] and on adding ZnO to PAN matrix crystallization temperature decreased.[53] In this section we compared the crystallization characteristics of PET matrix using nano and commercial ZnO.

The effect of nano ZnO on the crystallization characteristics of melt compounded PET-ZnO nanocomposite samples was analyzed first with non-isothermal DSC experiments. The crystallization temperatures (T_c), the apparent melting temperatures (T_m), the corresponding enthalpies (ΔH_c and ΔH_m) and the degree of super cooling ($\Delta T = T_m - T_c$) are also reported in table 4a.1.

Table 4a.1 Thermal characteristics for PET- ZnO nanocomposite from DSC

Concentration of ZnO (wt%)	T_c (°C)	ΔH_c (J/g)	T_m (°C)	ΔH_m (J/g)	ΔT (°C)
0.0	162.06	39.68	252.49	39.48	90.4
0.03	194.28	40.21	251.46	39.65	57.1
0.1	196.99	40.83	251.13	36.34	54.1
0.5	197.12	38.89	249.41	37.32	52.3
1.0	202.62	39.66	251.77	39.16	49.1
2.0	203.38	40.16	250.61	40.51	47.2
3.0	204.52	39.23	250.12	39.86	45.6

Figure 4a.1 shows the DSC cooling scans of PET-nano ZnO composite samples. During cooling from the melt, the ZnO containing samples show crystallization exotherms earlier than neat PET, as also seen from the corresponding T_c values indicated in table 4a.1. It is found that the composite sample containing nano ZnO at a concentration as low as 0.03 wt% enhances the rate of crystallization in PET as the cooling nanocomposites melt crystallizes at a temperature 32 °C higher as compared to neat PET. The T_c values continue to increase with increasing ZnO concentration, but at a slower rate, as with further 100 fold increase in ZnO concentration from 0.03 to 3.0 wt%, the additional T_c increase is only about 10 °C. In other words, there is a saturation of the nucleant effect at low ZnO concentrations, resulting in diminishing dependence on the increasing ZnO induced

nucleation, possibly because of large surface area and good dispersion of ZnO. The melting temperature and enthalpies of PET stay unaffected. The degree of supercooling ($\Delta T = T_m - T_c$) may be a measurement of a polymer's crystallizability: the smaller the ΔT, the higher the overall crystallization rate.[54] The ΔT values (figure 4a.2) for the PET-nano ZnO were 57-45 °C smaller than that of neat PET (90 °C). So nano ZnO content affects the crystallization rate and takes the role of a nucleating agent on PET crystallization due to its enormous surface area.[55-56] The results indicated that the incorporation of ZnO nanoparticles had little effect on the degree of crystallinity of PET. Furthermore, the glass transition temperature (T_g) of nanocomposites resulted in a slight increase in value from 71 °C in the case of neat PET to 74 °C. With increase in ZnO loading, T_g remains unaffected. This result suggests that the movement of PET chains is hindered by the introduction of ZnO nanoparticles.

Increasing ZnO concentration from 0.0-3.0 wt %

exo

150   160   170   180   190   200   210   220
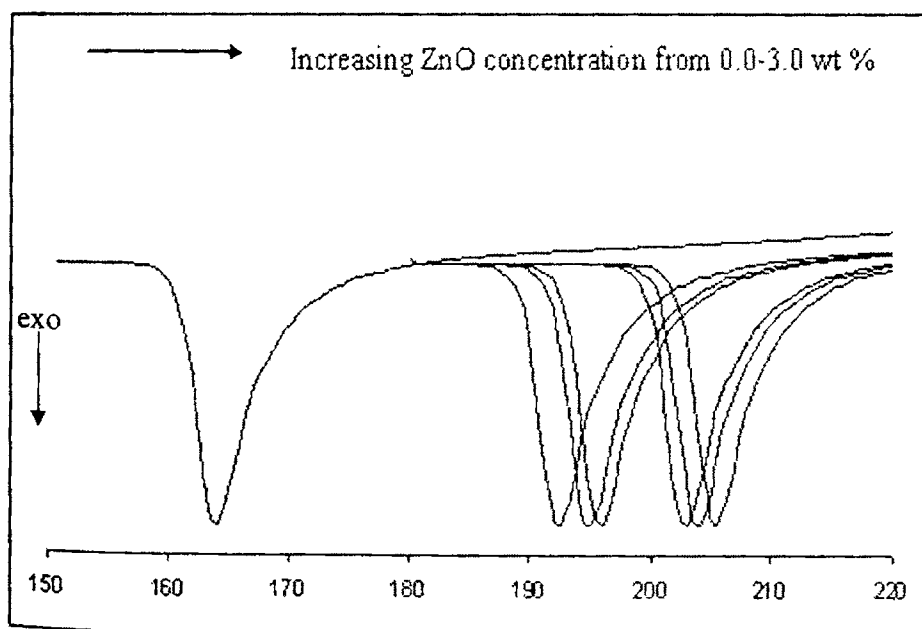
Figure 4a.1 DSC cooling scans (20 °C/min from 300 °C melt) of PET-nano ZnO composite samples
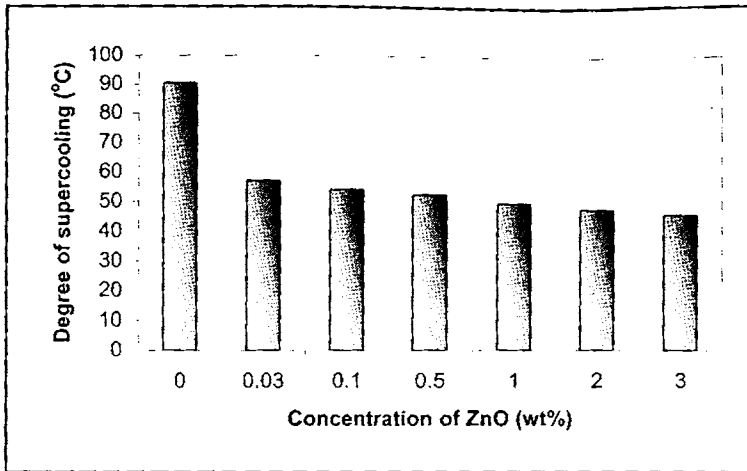
Figure 4a.2 Variation of degree of supercooling with concentration of ZnO

Figure 4a.3 shows the DSC cooling scans of PET-commercial ZnO composite samples. It is clear from the figure that on adding 0.03 wt% commercial ZnO the crystallization temperature increases by 7 °C, and with further addition there is not much change in the value. ΔH_c, ΔH_m, T_c and T_m values remains constant with ZnO loading. T_g of the composites slightly decreases from 71 °C for PET to 68 °C for composites. The ΔT values for the PET-commercial ZnO were 79-75 °C smaller than that of neat PET (90 °C).
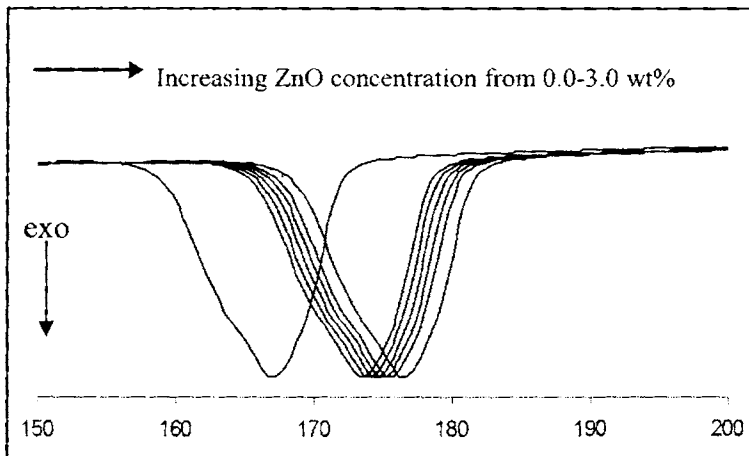
Figure 4a.3 DSC cooling scans of PET- commercial ZnO nanocomposite samples

On comparing the crystallization temperatures of PET-ZnO nanocomposites using two different ZnO samples, one with nano and another with commercial ZnO, (figure 4a.4) it can be seen that nano ZnO is a better nucleating agent than commercial ZnO. T_c increase is only about 10 °C on adding 3.0 wt% of commercial ZnO, but for nano ZnO the increase is about 40 °C.
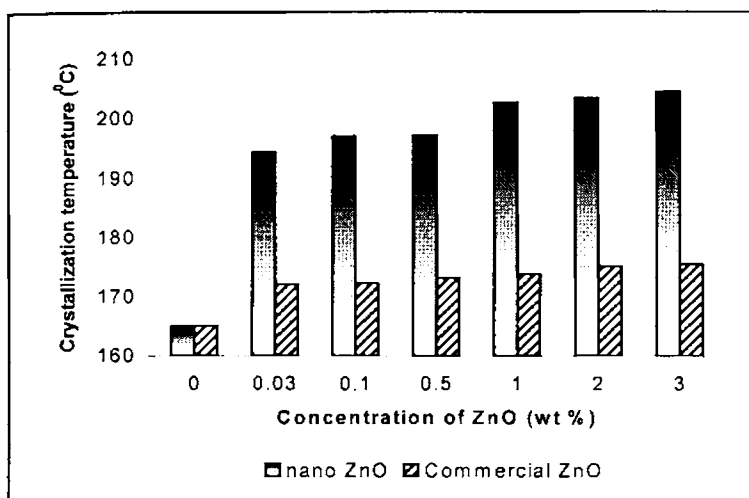
Figure 4a.4 Comparison of crystallization temperatures of PET- ZnO nanocomposites using nano and commercial ZnO

4a.3.1.2 Isothermal crystallization characteristics

Nano ZnO is found to be a better nucleating agent than commercial ZnO. Typical isothermal crystallization curves of the PET- nano ZnO composite samples at four temperatures (195 °C, 200 °C, 205 °C, 210 °C) is shown in figure 4a.5. The time corresponding to the maximum in the heat flow rate (exotherm) was taken as peak time of crystallization (t_{peak}). Such peaks are seen at each of the four isothermal crystallization temperatures for the 0.03 wt% ZnO containing nanocomposite, with the earlier or faster crystallization (smaller t_{peak}) corresponding to lower temperature of isothermal crystallization. In the case of neat PET, no exotherm is seen at the highest temperatures of 205 °C, 210 °C because crystallization is very slow and would require longer time than the 4 minutes employed in the DSC program. On the other hand, for the nanocomposite sample with 3.0 wt% ZnO, the rate of crystallization is so fast

near the lowest temperatures 195 °C, 200 °C, 205 °C that most crystallization occurs already during the cooling scan (60 °C/min) employed to reach those temperature, resulting in absence of exothermic peak in the heat flow curves at those temperatures.
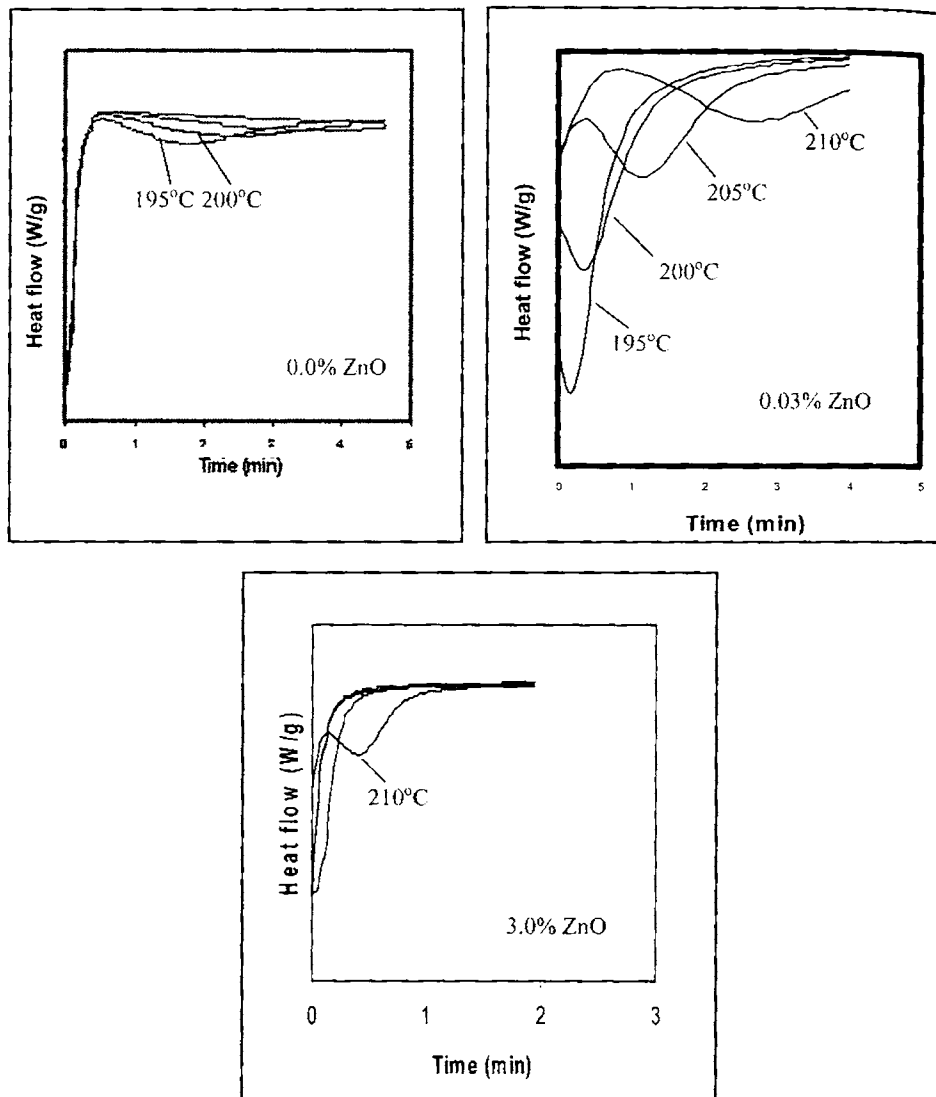
Figure 4a.5 Heat flow during isothermal crystallization of PET- nano ZnO composite samples

The peak time of crystallization at each of the temperatures for all the PET-ZnO nanocomposite samples is plotted against the isothermal crystallization temperature (figure 4a.6). We notice that the t_{peak} values for the nanocomposite

samples reduced to less than 50 % as compared to neat PET due to the presence of ZnO at concentration as low as 0.03 wt%. With the increasing ZnO concentration, there is further increase in the crystallization rate (as indicated by the decrease in t_{peak} value), demonstrating the role of ZnO in enhancing the rate of crystallization.
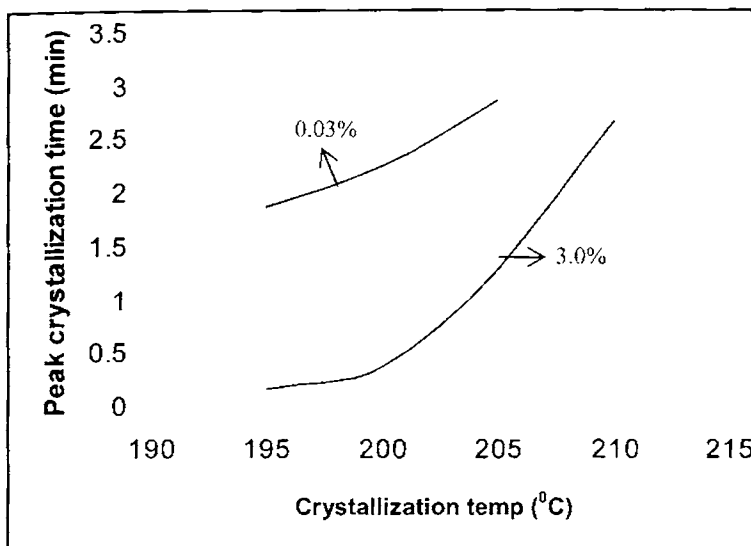
Figure 4a.6 Effect of nano ZnO concentration on the peak crystallization time of the nanocomposites at different isothermal crystallization temperatures

4a.3.2 Thermogravimetry

The thermal stability of a material usually assessed by TGA in which the sample mass loss because of volatilization of degraded byproducts is monitored by the function of a temperature ramp.[57] The TG and DTG curves of neat PET and its composites with nano ZnO are given in figures 4a.7(a)& (b) respectively: The temperature of onset of degradation (T_i) (^{o}C), the temperature at which the rate of decomposition is 10 % ($T_{10\%}$), the temperature at which the rate of decomposition is maximum (T_{max}) (^{o}C), the temperature at which the rate of decomposition is 50 % ($T_{50\%}$), the peak degradation rate and the residue at 800 ^{o}C are given in table 4a.2. PET degrades in a single step. The degradation starts at a temperature of 358.69 ^{o}C and the peak rate of degradation is 2.024 %/min at corresponding T_{max} 443 ^{o}C and in

nanocomposites, T_i is 383 °C on adding 3.0 wt% of nano ZnO, indicating improved thermal stability of the nanocomposite. The T_{max} temperature also shows slight improvement in thermal stability. Residue at 800 °C is only about 10.43 % for PET. On adding 3.0 wt% of ZnO, residue increased to 12.05 % from 10.43 % and the peak rate of decomposition decreased from 2.024 to 1.749 %/min. This increase in the thermal stability of the nanocomposites may result from the strong interaction between the nano ZnO and PET. On adding commercial ZnO, thermal stability remains unchanged.
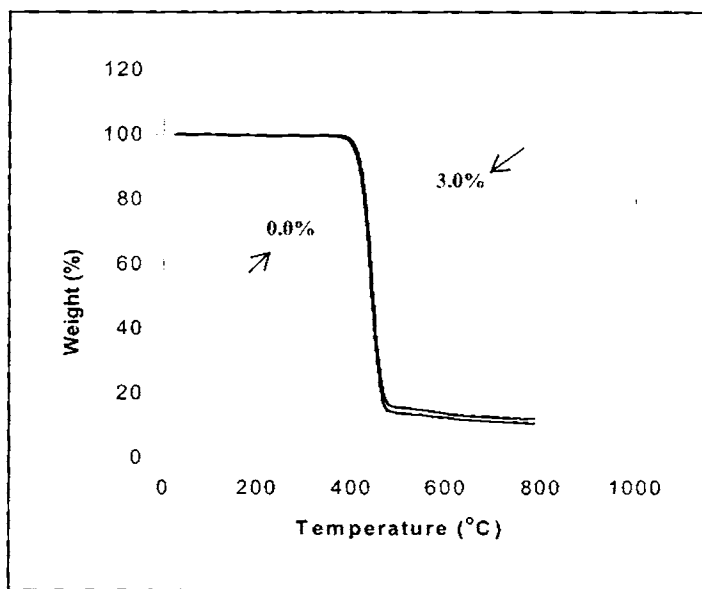
(a)

Figure 4a.7 Thermogravimetric traces of PET- nano ZnO composite samples (lower curves with increasing ZnO concentrations 0.0, 0.03, 1.0 and 3.0 wt%)

Table 4a.2 Degradation characteristics of PET and its nanocomposites

Concentration of ZnO	T_i (°C) Onset temp	$T_{10\%}$ (°C)	Peak temperature (T_{max}) (°C)	Residue at 800 °C (%)	$T_{50\%}$ (°C)	Peak rate of decomposition (%/min)
0.0	358.69	401	443.01	10.43	443.19	2.024
0.03	379.04	405	443.76	10.43	443.30	1.849
1.0	379.04	405	444.51	12.05	444.66	1.783
3.0	383.95	405	445.43	12.05	444.66	1.749
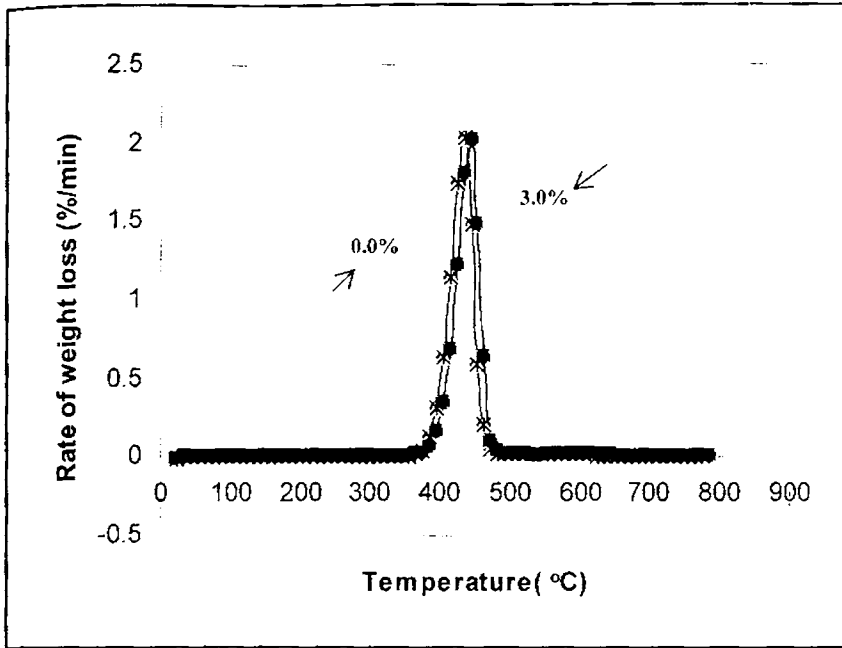
(b)

Figure 4a.7 Differential thermogravimetric traces of PET-ZnO nanocomposites

4a.3.3 Mechanical properties
4a.3.3.1 Torque studies

The variation of mixing torque with time of mixing at different ZnO loading is shown in figure 4a.8. A mixing time of 4 minutes was fixed since the torque stabilized to a constant value during this time. The temperature of the mixing was fixed as 255 °C. The stabilization of the torque may be related to the attainment of a stable structure after a good level of mixing. The initial and final torque values increase with increase in ZnO loading. Initially torque increases with the charging of PET, but decreases with melting. After homogenization of PET, ZnO is added. There is no change in torque on continued mixing with ZnO. This may be due to low concentration of ZnO. It is clear from figure that there is no degradation taking place during mixing.
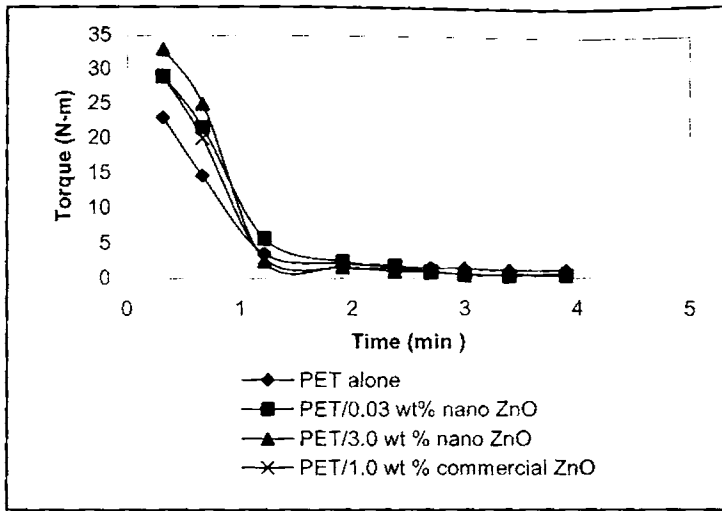
Figure 4a.8 Torque-time curves of PET nanocomposites

4a.3.3.2 Tensile properties

The most important property of nanocomposites is the enhancement in mechanical properties even at low percentages of the nano filler loading. The tensile strength may vary strongly depending on the nature of the interactions between the filler and the matrix. Zhao et al.[51] observed the effect of ZnO in PP matrix on tensile properties and an increase in tensile values was reported. The effect of the nano ZnO on the tensile properties in PET matrix is summarized in table 4a.3.

Table 4a.3 Tensile properties of PET-nano ZnO composite

Concentration of ZnO (wt%)	Tensile strength (MPa)	Tensile modulus (GPa)	Elongation (%)	Shore D hardness	Energy to max (J)	Tensile toughness (J/m)
0.0	39.99	1.156	5.47	51	0.5342	258.4
0.03	40.86	1.193	4.79	58	0.6158	324.9
0.1	43.26	1.241	4.25	62	0.7856	381.3
0.5	44.79	1.273	3.61	67	0.8465	457.7
1.0	45.83	1.314	3.15	73	0.8912	489.2
2.0	49.44	3.546	3.01	82	0.9566	503.4
3.0	54.42	3.752	2.96	91	1.284	675.8

The results in table 4a.3 shows an increase in the tensile modulus and strength of PET with an increasing concentration of ZnO content from 0.0 to 3.0 wt%. From 0.0 to 1.0 wt% the change in tensile strength is about 15 % and modulus is about 13 %. But from 1.0 to 3.0 wt% there is a rapid increase in tensile strength (about 20 %) and modulus (about 185 %). The tensile strength shows an increment of about 38 % and modulus of about 225 % on adding 3.0 wt% of nano ZnO (figure 4a.9 & 4a.10 respectively). The hardness increases from 51 to 91 Shore D with the addition of 3.0 wt% of ZnO. The elongation to break is found to decrease with the increasing loading of ZnO, indicating that the nanocomposites become somewhat brittle. Energy to max and tensile toughness (energy/thickness of the sample) values (figure 4a.11) increases with filler loading (161 % on adding 3.0 % ZnO). Since there is an increase in energy absorption some modification has taken place, which is clear from the increase in tensile toughness. These results demonstrate that even a small fraction of ZnO provide effective reinforcement to the PET matrix. This is due to better interaction between the PET matrix and ZnO nanoparticles. Table 4a.4 shows the tensile properties of PET-commercial ZnO nanocomposites. From the table it is clear that commercial ZnO does not provide any reinforcement to the PET matrix. The tensile strength, energy and tensile toughness decreases with increasing amount of comm. ZnO and modulus remains almost constant.

So composites prepared from nano ZnO can attain superior performance over commercial ZnO. This high reinforcement effect implies a strong interaction between the matrix and nano ZnO interface that can be attributed to the nanoscale and uniform dispersion of the ZnO in the PET matrix.

Table 4a.4 Tensile properties of PET-commercial ZnO composite

Concentration of ZnO (wt%)	Tensile strength (MPa)	Tensile modulus (GPa)	Elongation (%)	Shore D hardness	Energy (J)	Tensile toughness (J/m)
0.0	39.99	1.156	5.47	51	0.5342	258.1
0.03	39.61	0.961	5.25	58	0.4982	191.9
0.1	37.92	0.851	5.01	62	0.4367	189.4
0.5	37.65	0.847	4.12	65	0.4358	216.6
1.0	35.29	0.839	4.79	69	0.4138	205.3
2.0	35.01	0.821	4.25	69	0.3561	166.7
3.0	34.98	0.805	3.82	68	0.3906	191.2
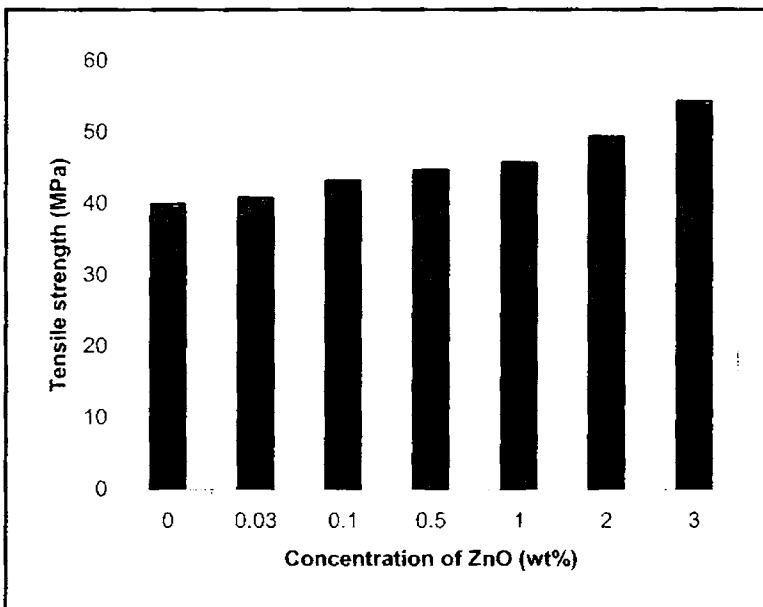
Figure 4a.9 Variation of tensile strength with concentration of nano ZnO
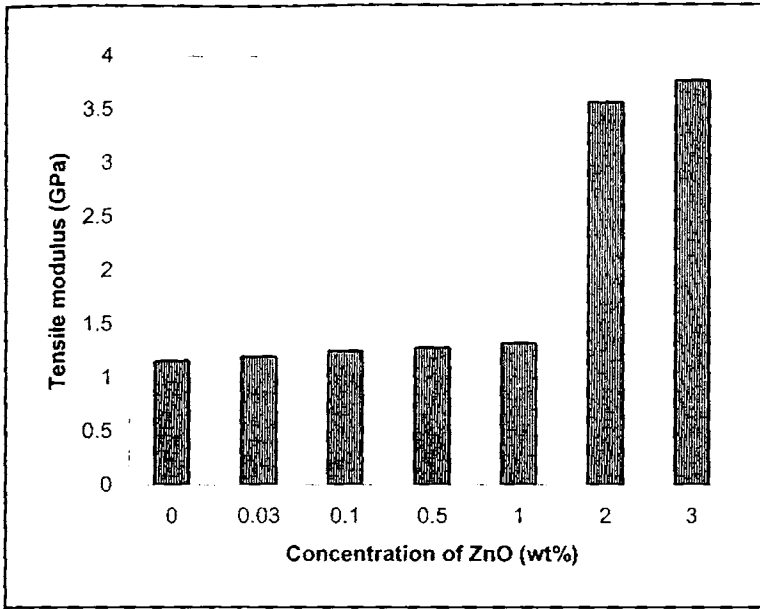
Figure 4a.10 Variation of tensile modulus with concentration of nano ZnO
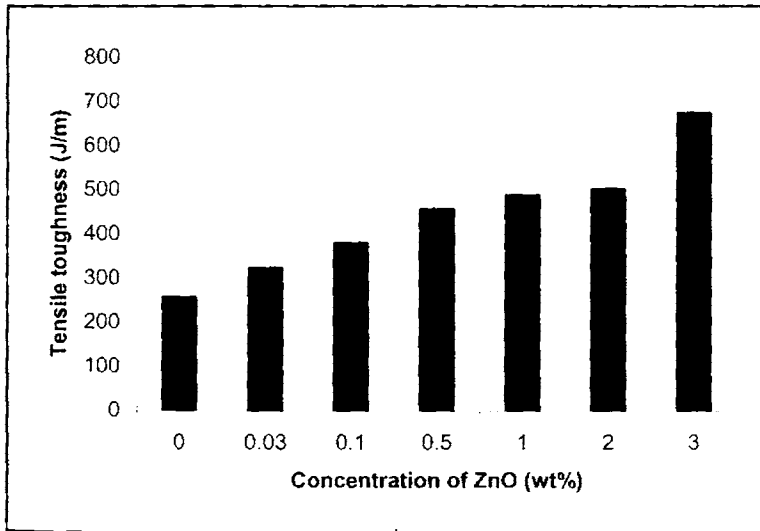
Figure 4a.11 Variation of tensile toughness with concentration of nano ZnO

Stress-strain curves for PET and its nanocomposite is shown in figure 4a.12. From the stress-strain curve it is clear that with nano ZnO loading the elongation (%) decreases. This shows the brittle nature of the nanocomposites. Area under the stress-strain curve increased due to energy absorption. So it is clear that modification has taken place in PET matrix.
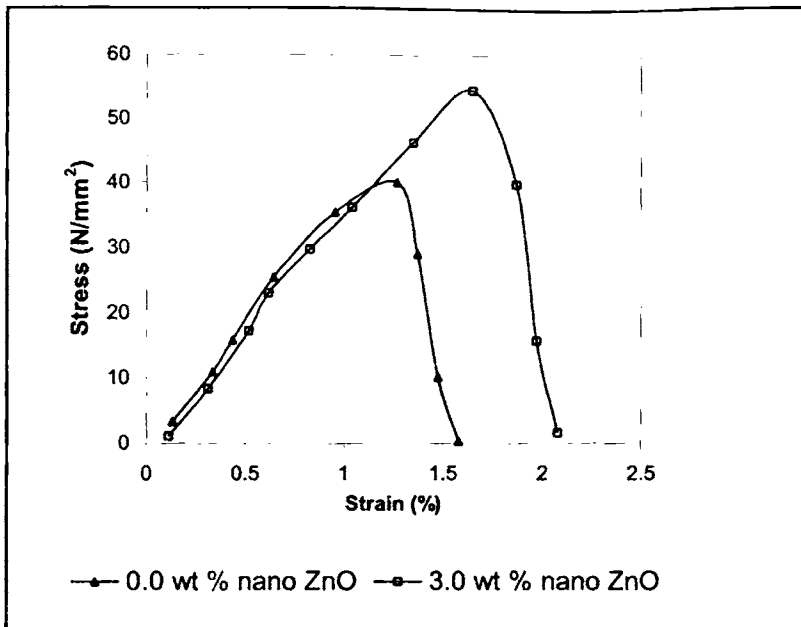
Figure 4a.12 Stress-strain curve for PET and its nanocomposite

4a.3.3.3 Morphology of the fractured surfaces

The morphological structure of polymer nanocomposites is important because it ultimately determines many properties of the polymer nanocomposites. The scanning electron micrographs of the fractured surfaces of the tensile test specimens have been studied to acquire an insight into the mechanism of reinforcement. Figure 4a.13 (a) shows the fracture surface for unmodified PET. It contains plane areas without any sign of significant plastic deformation. From figure 4a.13 (b), it is clear that nano ZnO exist as dispersed particles and the morphology gets substantially modified. SEM images are in good agreement with the observed mechanical properties, which is due to shear yielding. Figure shows that, in different project positions of the matrices of PET-ZnO, nanoscale ZnO particles are homogeneously dispersed in the PET matrices. Nano ZnO loading leading to stress whitening is prevalent in this figure, indicating localized plastic deformation. Indeed, stress whitening is due to the scattering of visible light and can be attributed to the various processes that can take place in the polymer, such as matrix crazing, matrix shear yielding, and filler/matrix debonding.[58] In PET-ZnO nanocomposites; shear yielding

is the reinforcement mechanism. There is complete stress transfer from the PET matrix to nano rod having high aspect ratio. There is no sign of extensive particle agglomeration as compared to PET-commercial ZnO nanocomposite fracture surface shown in figure 4a.13 (c), where we can see large agglomerates and the dispersion is inhomogeneous.

(a)

(b)

(c)
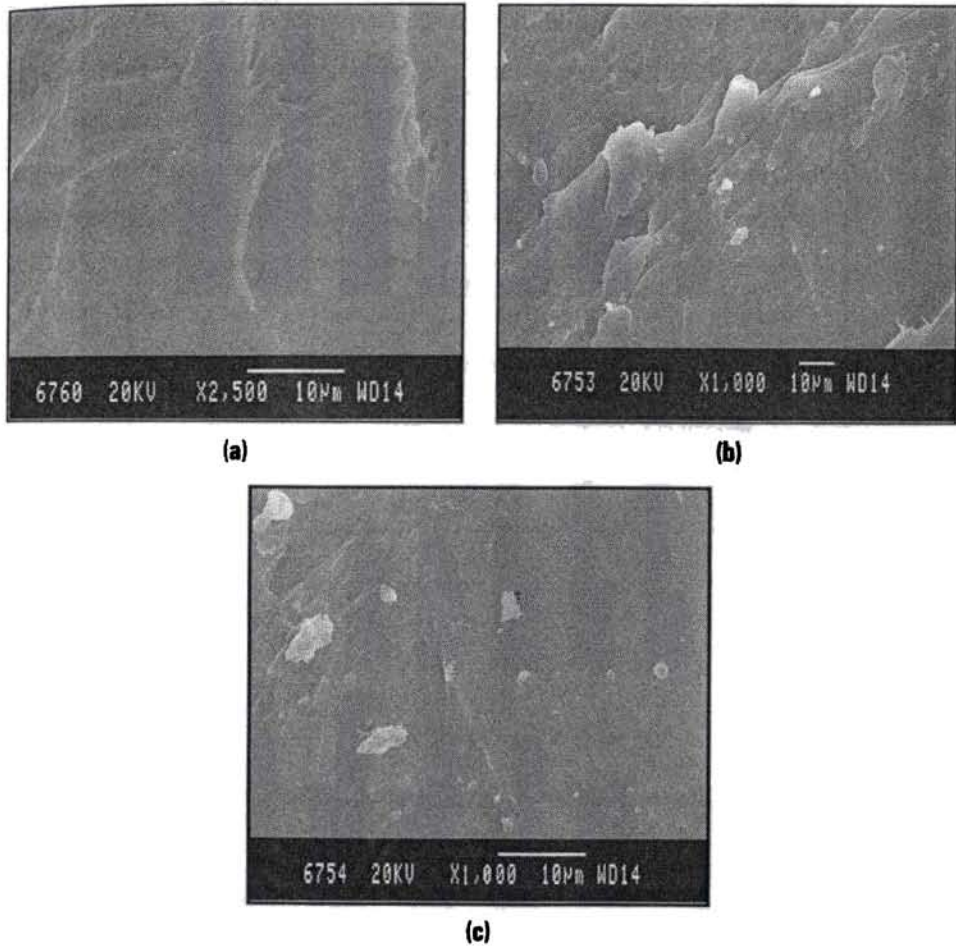
Figure 4a.13 Fracture surface for (a) pure PET (b) PET-nano ZnO composite
(c) PET-commercial ZnO composite

4a.3.3.4 Flexural properties

A comparison of flexural strength and modulus of PET-ZnO nanocomposites using nano and commercial ZnO is shown in figure 4a.14 (a) & 4a.14 (b) respectively. With nano ZnO, the flexural modulus as well as the

strength of PET increases considerably. For example, incorporation of nano ZnO at the level of 3.0 wt% modulus increases by around 286 % and strength by around 20 %. With commercial ZnO, the flexural modulus remains almost constant and a slight increase in strength is observed.
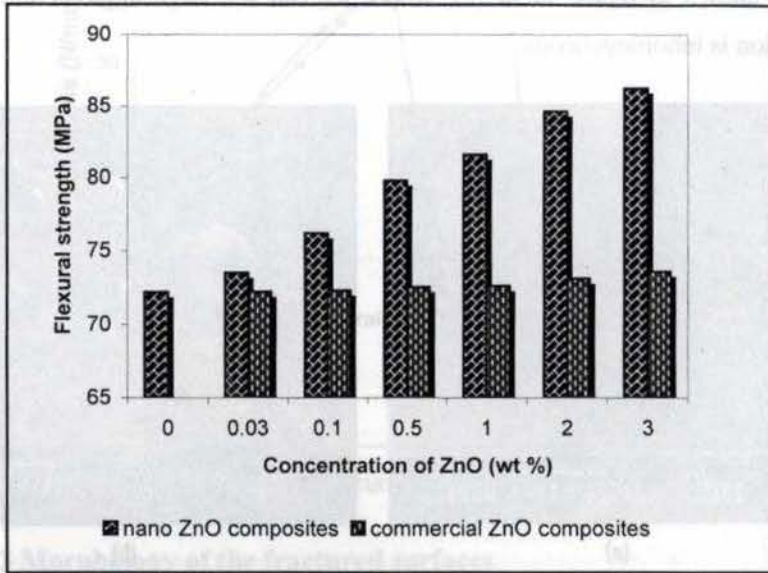
(a)
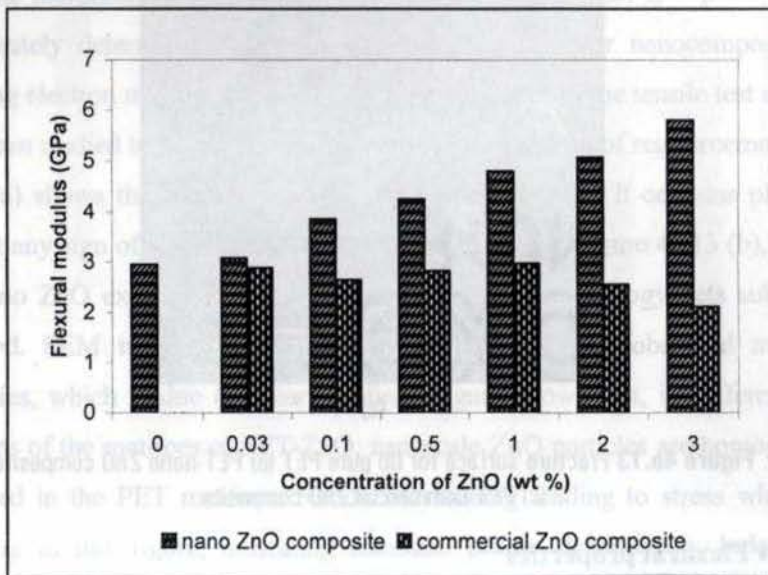
(b)

Figure 4a.14 (a) Comparison of flexural strength of PET-ZnO nanocomposites and (b) comparison of flexural modulus of PET-ZnO nanocomposites

4a.3.3.5 Impact strength

Izod impact strength (unnotched) of PET-ZnO nanocomposites with nano and commercial ZnO is compared in figure 4a.15. With commercial ZnO, the impact strength slightly decreases, but on adding 3.0 % nano ZnO, the increase in impact strength is about 160 %. The reinforcement with nano ZnO did not increase the percentage crystallinity, so there is a positive effect on impact strength.[59] The increase in impact strength is evidenced by the tensile toughness values (table 4a.3) and from the area of the stress strain curve (figure 4a.12). So the toughness of the nanocomposite improved with nano ZnO addition. The decrease in impact strength for PET- commercial ZnO nanocomposite is due to poor dispersion and weak interaction of ZnO with the matrix.
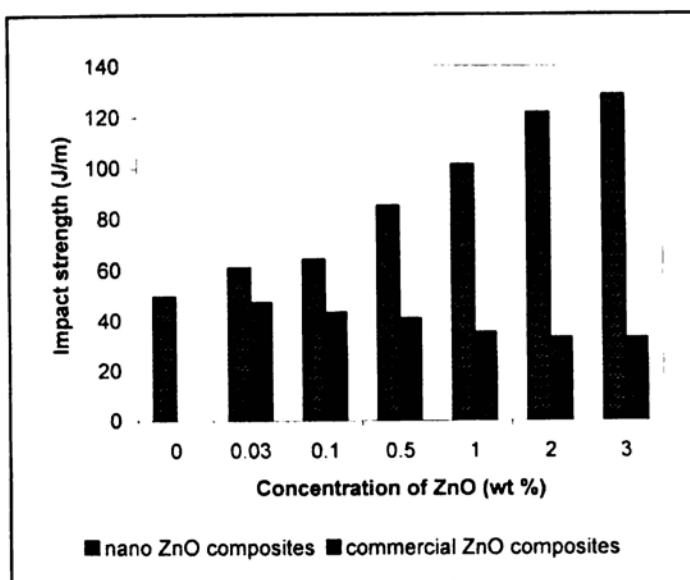
Figure 4a.15 Comparison of Izod impact strength of PET- ZnO nanocomposites

4a.3.4 Dynamic mechanical analysis (DMA)

Dynamic storage modulus (E') is the most important property to assess the load- bearing capability of a nanocomposite material, which is very close to the flexural modulus.[60] It is usually used to study the relaxations in polymers. The ratio of the loss modulus (E'') to the storage modulus (E') is known as mechanical loss factor (tan δ). This quantity is the measure of balance between

the elastic phase and the viscous phase in the polymeric structure. This is related to the impact properties of a material. It represents the ratio of the dissipated energy to the stored energy and is related to the glass transition temperature of the polymer. It has been suggested[61-62] that the enhancement of the storage modulus and glass transition temperature results from the strong interfacial interactions between the polymer and filler and the restricted segmental motions of polymer chains at the organic–inorganic interface. An increase in storage modulus of PP matrix was observed by adding ZnO particle by Zhao et al.[51] This is expected owing to the stiffness improvement effect of inorganic ceramic particles.

The DMA results for the dynamic storage modulus of the PET-ZnO nanocomposite samples as a function of temperature at 1 Hz are shown in figure 4a.16. Following a slow decrease of the modulii with temperature in the glassy state, a rapid decrease in modulii is observed corresponding to the glass-rubber transition at about 75 °C. The storage modulii of the nanocomposite samples below glass transition increases substantially with the nano ZnO concentration (about 25 % increase with 1 wt% and about 40 % increase with 3 wt% nano ZnOs) due to the stiffening effect of ZnO, and indicating efficient stress transfer between the PET matrix and ZnOs. But with commercial ZnO, the storage modulus decreases, i.e. nanocomposite is more soft and flexible. The storage modulus of nanocomposites at 35 °C, 50 °C & 80 °C is given in table 4a.5.

Table 4a.5 Storage modulus of PET- ZnO nanocomposites at 35 °C, 50 °C & 80 °C

Sample	Storage modulus at 35 °C (MPa)	Storage modulus at 50 °C (MPa)	Storage modulus at 80 °C (MPa)
PET alone	1176	1121	468
PET-0.03 wt% nano ZnO	1445	1405	469
PET-3.0 wt% nano ZnO	1586	1543	432
PET-1.0 wt% commercial ZnO	1128	1101	397

Figure 4a.17 shows tan δ versus temperature plots for PET-ZnO nanocomposites. It is evident from the figure that there is not much difference in the height of the tan δ peak. This indicates that they possess the same order of damping capabilities. It is obtained in many cases that the improvement of stiffness markedly reduces the ductility. But PET-ZnO nanocomposite is prepared with increased stiffness without sacrificing ductility. From the tan δ peak it is clear that with nano ZnO only a slight increase in glass transition temperature is observed, but it decreases by around 10 °C with commercial ZnO. Loss modulus curves for the PET- nano ZnO composite is given in figure 4a.18. T_g, loss modulus and tan δ values of PET- ZnO nanocomposite are given in table 4a.6. It is clear from tabling that loss modulus increases with modification. The glass transition temperatures are consistent with the DSC results given in section 4a.3.1.1. A slightly higher T_g value of DMA than that of DSC is due to the frequency difference between these two measurements.
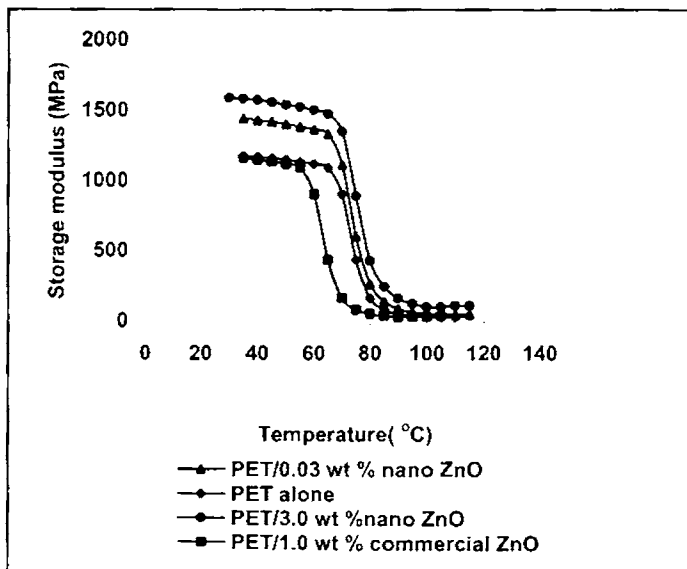
Figure 4a.16 Effect of ZnO concentration on the storage modulus of PET-ZnO nanocomposite samples
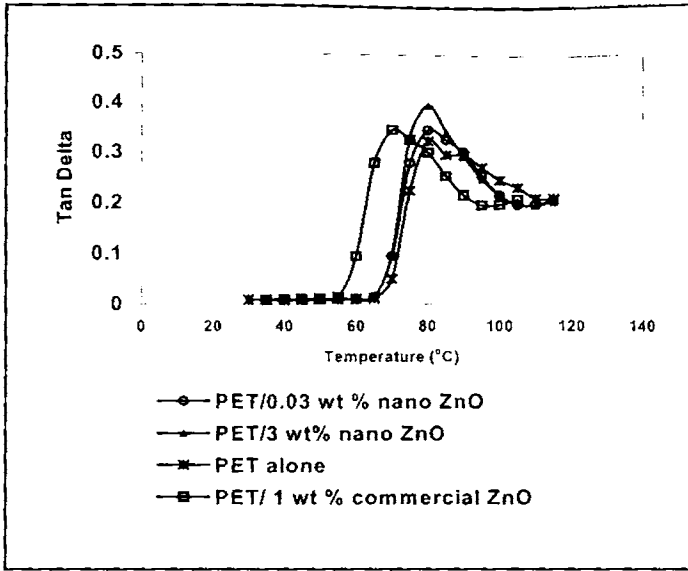
Figure 4a.17 Effect of ZnO concentration on the tan δ of PET-ZnO nanocomposite samples
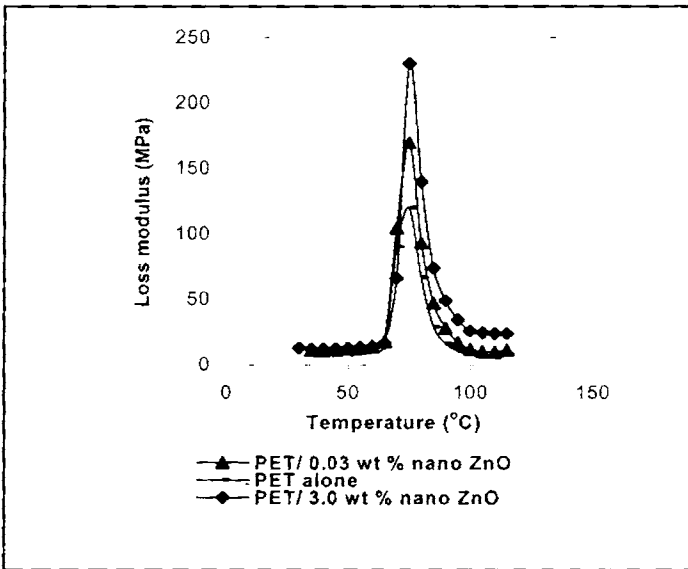
Figure 4a.18 Loss modulus curves of PET- nano ZnO composites

With the addition of nano ZnO, loss modulus values increases and on adding commercial ZnO, modulii remains constant.

Table 4a.6 T$_g$, loss modulus and tan δ values of PET-ZnO nanocomposite samples

Sample	Loss modulus (MPa)	T$_g$ °C (from tan δ peak)	Peak values of tan δ at T$_g$
PET alone	146.6	78.03	0.3241
PET-0.03 wt% nano ZnO	169.7	79.40	0.3452
PET-3.0 wt% nano ZnO	199.2	79.27	0.4031
PET- 1.0 wt% commercial ZnO	146.3	70.2	0.3455

It was observed that the modulus, $E^* = $ (loss modulus ^{2} + storage modulus ^{2}) $^{1/2}$ for the neat PET is numerically consistent with the tensile modulus reported by the Dow Chemical Co. PET chains are severely entangled and the function of nanoparticles as physical anchorage points is relatively insignificant. The mobility of molecular chain segments is largely determined by entangling conditions. Therefore, T$_g$ of PET does not have a clear variation with the addition of nano ZnO. The T$_g$ of PET- nano ZnO composites slightly increases with ZnO content, because ZnO nanorods having larger aspect ratio can restrict the segmental motion of PET molecules and reduce the free volume of polymer chain folding. But in the case of commercial ZnO nanocomposites, due to the coarse nature of ZnO, T$_g$ value decreases.

Reportedly, any molecular process that promotes distribution and dissipation of energy would enhance the impact resistance of polymers, because viscoelastic relaxation of polymers is an important mechanism of energy dissipation. Correlation of impact and dynamical properties in terms of tan δ peak values of the nanocomposites has been done. The variation of the impact strength as a function of the total loss tangent peak values for PET-nano ZnO composites and PET-commercial ZnO composites is shown in figure 4a.19 & 4a.20 respectively. The curves show a non-linear shape and features similar to those of curve depicting the variation of impact strength with concentration of ZnO. The increase in impact strength with the total loss tangent peak values indicated the role of viscoelastic energy dissipation mechanism in the impact enhancement of nano ZnO composites.
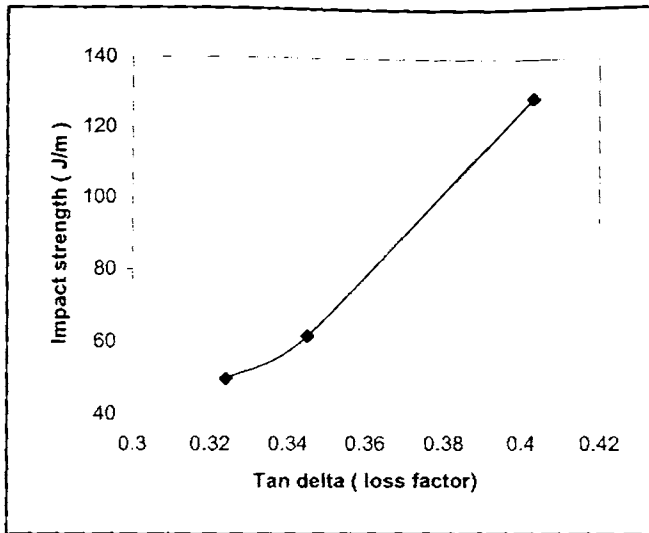
Figure 4a.19 Variation of the impact strength of PET- nano ZnO composites as a function of the total loss tangent peak values
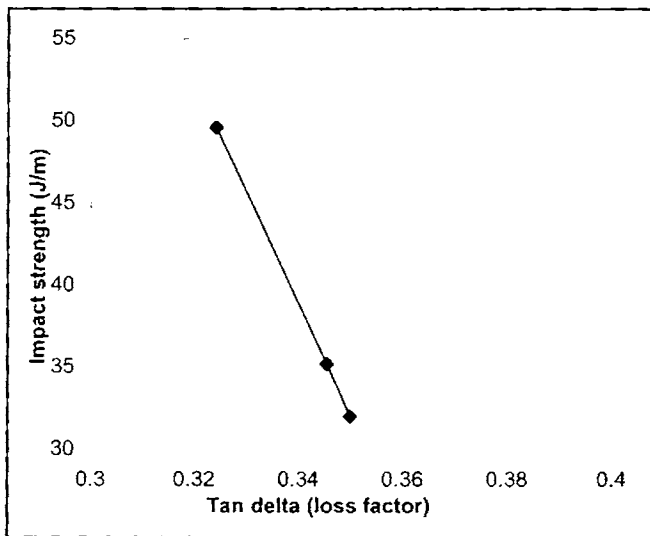
Figure 4a.20 Variation of the impact strength of PET- commercial ZnO composites as a function of the total loss tangent peak values

4a.3.5 Melt rheology

It is believed that the rheometry has been recognized as a powerful tool for investigating the internal microstructures of nanocomposites[63-66] such as the state of dispersion of filler and the confinement effect of fillers on the motion of polymer chains. Moreover, it may provide some useful guidance to overcome the possible

difficulties resulting from the large changes in melt viscoelastic properties observed in the nanocomposites. The measurement of rheological behaviours of nanocomposites has received prominent attention recently because most fabrication techniques involve flow of the polymer melt. Rheological studies were done on polymer layered silicate nanocomposites. Giannelis[67] and Manias[68] found that the steady- state shear viscosity of a series of polydimethylsiloxane nanocomposites at low shear rates increased due to the introduction of clay, but Newtonian-type behaviour was still observed even at reasonably high silicate loadings. Moreover, they attributed the shear thinning behaviour observed for PNCs to the orientation of the filler under shear and polymer coils. Galgali et al.[69] investigated creep behavior of molten polypropylene/organoclay nanocomposites, revealing that the solid-like rheologial response of the nanocomposite originates from large frictional interactions of the clay crystallites. The influence of matrix molecular weight in the case of nylon 6/clay nanocomposites was also examined by Fornes et al.[70] via dynamic and steady shear capillary tests. They found that high molecular weight nylon 6 nanocomposites exhibited solid-like, non-Newtonian behaviour while the nanocomposites with lower molecular weight nylon 6 displayed Newtonian plateaus at low shear frequencies. The melt viscosity as well as the shear stress increased with increasing molecular weight of nylon 6, which was considered as the major contributor to exceptional exfoliation of clay platelets in the higher molecular weight matrix. More recently, Kim et al.[71,72] investigated the rheology of polystyrene nanocomposites based on either inorganical montmorillonite or organically modified montmorillonite and also observed a shift from liquid-like to solid-like behaviour, proving the formation of a supermolecular structure in the nanocomposites. Beyond the work mentioned above, Lim et al.[73] examined the preference of the intercalating competition in a binary polymer blend of poly (ethylene oxide) (PEO) and poly (methyl methacrylate) (PMMA), confirming better affinity of PMMA for organoclay than PEO. Kim et al.[74] prepared high impact polystyrene (HIPS)/organoclay nanocomposites by in situ polymerization and found that the organoclay prefers to disperse into the rubber phase. SWNTs and MWNTs also improved melt viscosity of PET matrix.[49]

The rheological behaviour of PET-ZnO nanocomposites is studied at three different temperatures 250, 260 & 270 °C. Effect of shear stress, filler loading and temperature on rheological behaviour is also investigated.

4a.3.5.1 Effect of shear stress on shear viscosity

Figure 4a.21 present the shear viscosity vs. shear stress curves of PET-nano ZnO composites at 260 °C with increasing ZnO concentration from 0.0-3.0 wt%. We also examined the flow behaviour of PET nanocomposites filled with 1.0 % commercial ZnO. As shear stress increases, the viscosity of PET-ZnO composites decreases in all cases, indicating the pseudoplastic flow behaviour. At zero shear, the molecules are randomly oriented and highly entangled and therefore exhibited high viscosity. Under the application of shearing force, the polymer chains orient, resulting in the reduction of shear viscosity and thus exhibit shear-thinning (pseudoplastic behaviour).[75,76] It is just this pseudoplasticity that makes the nanocomposites to be easily melt-processed. Effect of temperature on shear viscosity of PET nanocomposites filled with 1.0 % nano ZnO is given in figure 4a.22. With a rise in temperature from 260 to 270 °C the value of shear viscosity decreases, especially at relatively lower apparent shear stress. The melt viscosity increases when the temperature decreases to 250 °C.
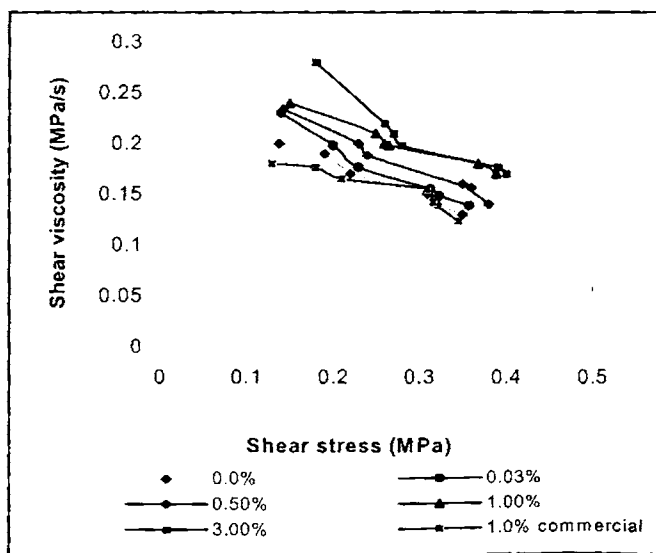
Figure 4a.21 Effect of shear stress on shear viscosity of PET-ZnO nanocomposites
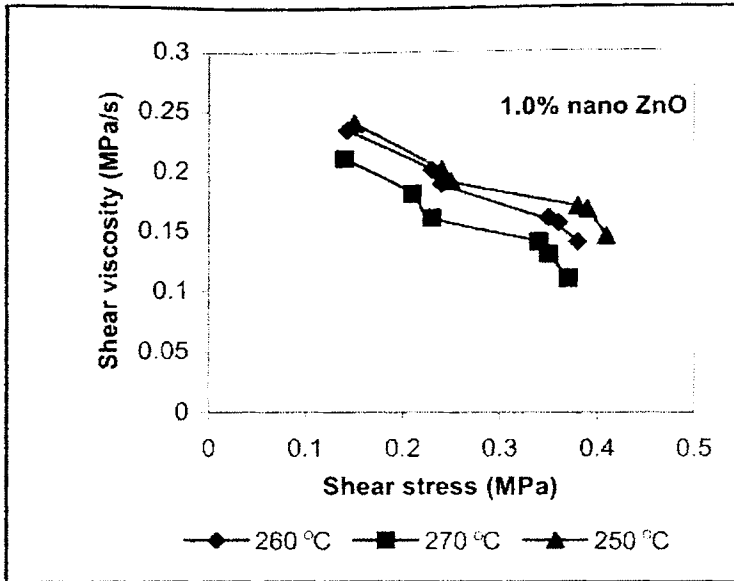
Figure 4a.22 Effect of temperature on shear stress vs. shear viscosity

4a.3.5.2 Effect of filler loading

Since entanglement of polymer chains and arrangement of ZnO are not permanent and altered by flow and relaxation processes, any disturbance of this steady state, such as shear, will disrupt the structure of the polymer matrix. Figure 4a.23 shows the variation of shear viscosity with increasing concentration of nano ZnO from 0.0-3.0 wt% at six different shear rates. It is clear from the figure that shear viscosity increases with nano ZnO addition and this increase is more prominent at low ZnO concentration. With further increase of ZnO content from 1.0 to 3.0 wt% the shear viscosity almost remains constant. Also it can be seen from the figure that shear viscosity decreases substantially with increasing shear rate, but increases monotonically with increasing nano ZnO loading at a given shear rate.[71,72]
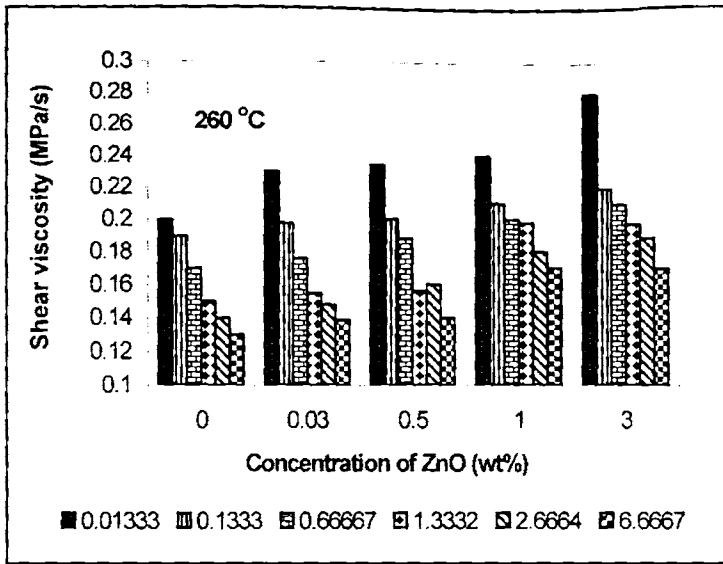
Figure 4a.23 Variation of shear viscosity with concentration of ZnO and shear rates at 260 °C

Figure 4a.24 examines the variation of shear viscosity of PET nanocomposites with concentration of commercial ZnO at four different shear rates. It is clear from the figure that viscosity decreases with ZnO loading.
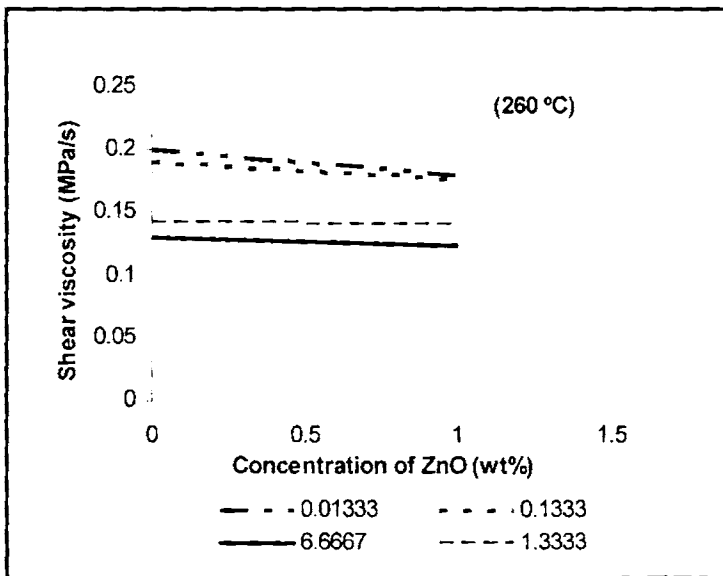
Figure 4a.24 Variation of shear viscosity with concentration of commercial ZnO at four different shear rates at 260 °C

4a.3.5.3 Effect of temperature

An understanding of the mechanism of polymer flow processes in relation to the nature and composition of the material can be elucidated by a study of the temperature dependence of shear viscosity. Namely, the temperature sensitivity of the shear viscosity has a profound effect on the choice of processing conditions as well as on the quality of the end products. Shear viscosities of pure PET and nanocomposite melts decreased with increasing extrusion temperature in the range of 250–270 °C, demonstrating that increasing temperature improves the flow behavior of the polymer melts. However, the effect of temperature on shear viscosity changes with the shear rate. The data indicate that the temperature sensitivity of shear viscosity is high in lower shear rate region, and drops at higher shear rates. This phenomenon is in agreement to the fact that elevating shear rate always accompanied by a rapid decrease of the entanglement density of macromolecules and the melt viscosity.[77] The temperature dependence of shear viscosity can be stated by Arrhenius–Eyring equation,[78]

$$\eta_a = A_o \exp (E_a/RT) \text{ ------------------------------------- 4a.1}$$

Where η_a is the melt viscosity at temperature T, R the universal gas constant, A_o a frequency term depending on the entropy of activation for flow, and E_a is taken to be the activation energy for viscous flow. The Arrhenius plots of PET-nano ZnO composites at two different shear rates are given in figure 4a.25 (a) & (b). A good linear correlation was found in the plot of ln η_a vs. 1/T, which has proved the appropriateness of the Arrhenius–Eyring equation. Values of E_a obtained from the slopes of these plots are given in table 4a.7. The activation energy of a material provides valuable information on the sensitivity of the material towards the change in temperature. The higher the activation energy, the more temperature sensitive the material will be. Therefore, such information is highly useful in selecting the processing temperature of polymeric materials.

From the table 4a.7 it can be observed that the activation energy of flow of the composites increases with modification at lower shear rates, while, it remains a constant at higher shear rate.
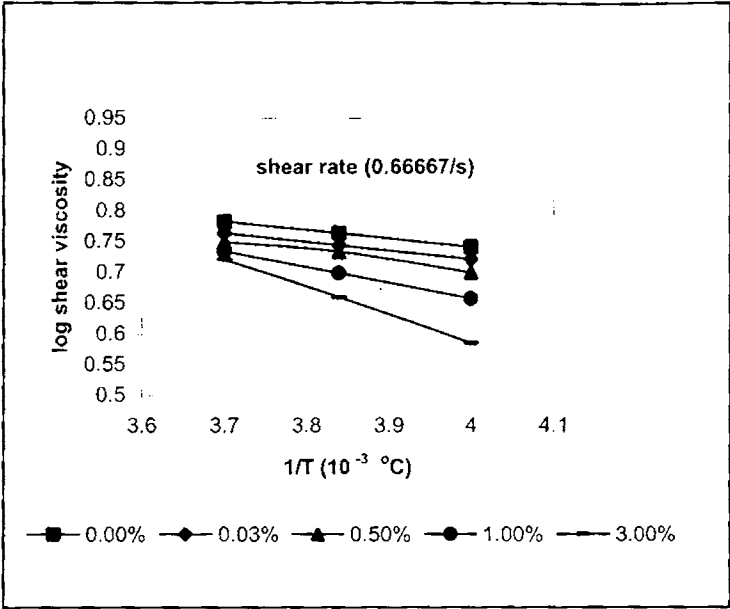
(a)
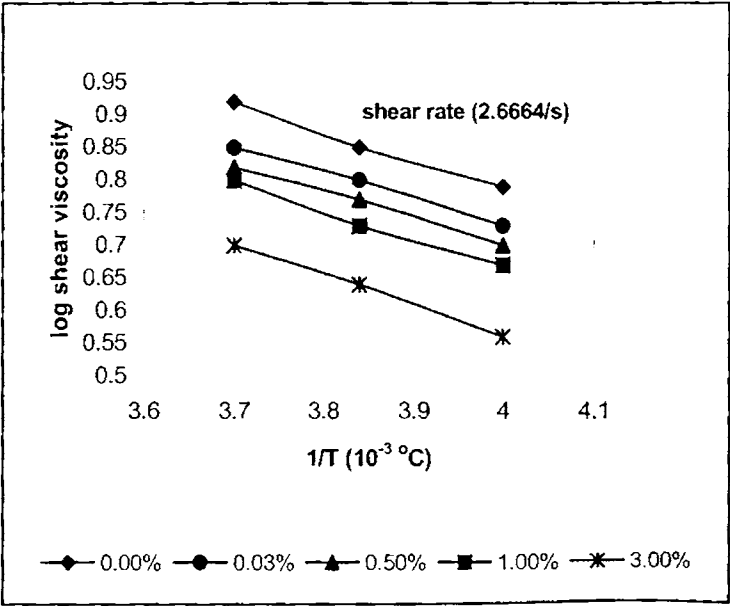
(b)

Figure 4a.25 (a) & (b) Variation of log viscosity with 1/T for the PET- nano ZnO composites

Table 4a.7 Activation energies of PET- nano ZnO composites at two shear rates

Concentration of ZnO (wt%)	Activation energy (KJ/mol)	
	0.66667/s	2.6664/s
0.0	13.7	43.2
0.03	14.2	40.1
0.5	16.7	40.1
1.0	25.6	43.2
3.0	45.6	46.7

4a.3.5.4 Flow behaviour index (n′)

The effects of temperature and concentration of ZnO on the flow behaviour indices of the samples have been studied in detail. The extent of pseudoplasticity or non-Newtonian behaviour of the materials can be understood from n′ values. Pseudoplastic materials are characterized by n′ below 1. Flow behaviour index values of PET- nano ZnO composites at 260 °C and 270 °C are given in figure 4a.26. It is clear from the figure that n′ decreases with increasing concentration of ZnO and with increasing temperature. This suggests that the system becomes more pseudoplastic as the ZnO content and temperature increases. A similar trend of decreasing values of n′ with an increase in temperature has been reported.[75,79,80]
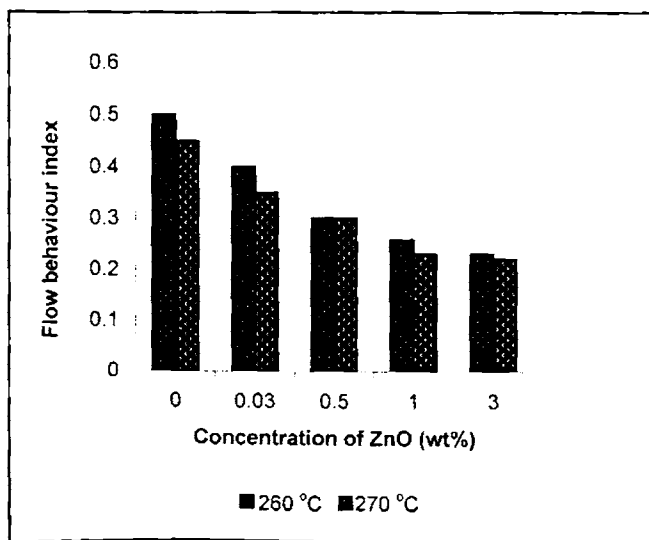
Figure 4a.26 Variation of melt flow index with concentration of ZnO at two temperatures

4a.3.5.5 Die swell

Die swell, called Barus effect is an important parameter for characterizing polymer melt elasticity in an extrusion flow and is related to the quality of the end products.[81,82]

4a.3.5.5.1 Effect of shear rate and concentration of ZnO

Figure 4a.27 shows the plots of the die swell ratio, de/dc for PET and PET-ZnO nanocomposites at 260 °C at six different shear rates. The die swell ratio increases obviously with increasing shear rate at a constant ZnO content. From the viewpoint of the microrheology, the action of an outside shear field leads to the extension, orientation, and arrangement of polymer chains along the flow direction. Furthermore, the elastic energy stored in the melts increases correspondingly with increasing shear rates. When the melt leaves the die exit, the extended and oriented polymer chains exhibit an elastic recovery and tend to recover to their original random states, due to the disappearance of an outside force field.[82] It is noticeable that at a constant shear rate, the die swell ratio decreases slightly with a rise of ZnO content. Similar phenomena of nonlinear decrease were also observed in the cases of carbon black-filled polybutadiene (or butadiene–styrene copolymer) [83], TiO_2-filled HDPE composite[84] and glass bead-filled LDPE composite.[85] Li et al.[77] supposed it is the combined effect of the melt elasticity of the continuous phase, the extent of deformation of the dispersed phase and the difference in the volume contraction between the two phases due to the increase of density after the strand cools to room temperature that affects the die swell. It is generally believed that not only the polymer but also the filler particles oriented under shear and the latter will unavoidably limit the elastic recovery of the confined molecule chains in a plane vertical to the extrusion direction after leaving the capillary die. In other words, the oriented ZnO particles counteract at a certain degree, the positive contribution of the continuous phase to die swell. The more the ZnO content, the stronger the hindrance to the release of elastic energy of the composite melts, and as a result, the lower the extent of die swell. This effect is usually described as a decrease of melt elasticity.[86] On the other hand, increasing shear rate will inevitably enlarge the degree of

orientation of the ZnO particles i.e., strong shear is unfavorable to die swell. This hypothesis has been confirmed by the fact that the die swell ratio drops more sharply with increasing ZnO loading at a high level of the shear rate, compared to that in the region of lower shear rate (figure 4a. 27).

Figure 4a.28 shows the variation of die swell ratio of PET nanocomposites filled with 1.0 % commercial ZnO at different shear rates. Here also die swell ratio decreases with ZnO loading.
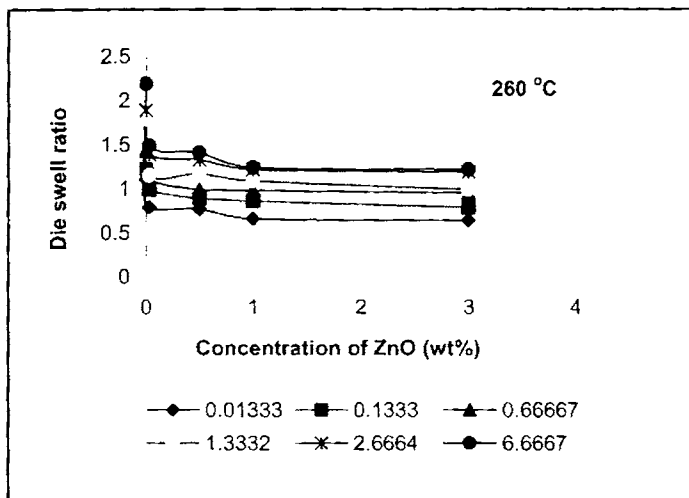
Figure 4a.27 Variation of die swell ratio of PET-nano ZnO composites with concentration of ZnO at different shear rates
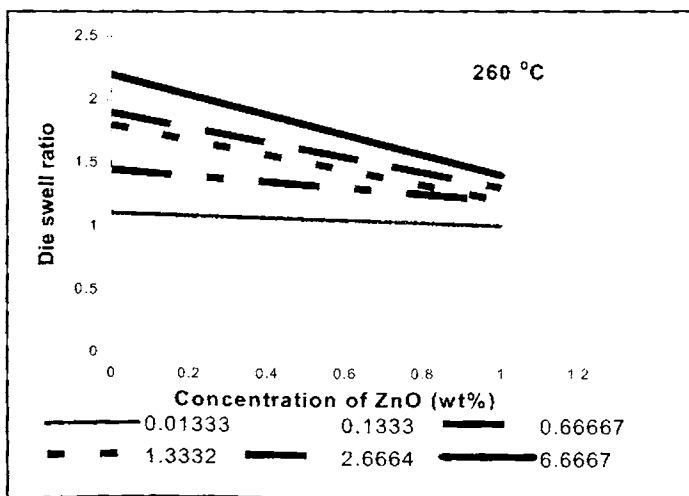
Figure 4a.28 Variation of die swell ratio of PET-commercial ZnO composites with concentration of ZnO at different shear rates

4a.3.5.5.2 Effect of temperature

Variation of die swell ratio of PET-nano ZnO composites at 3 different temperatures is given in figure 4a.29. It is clear from the figure that die swell ratio decreases with temperature.
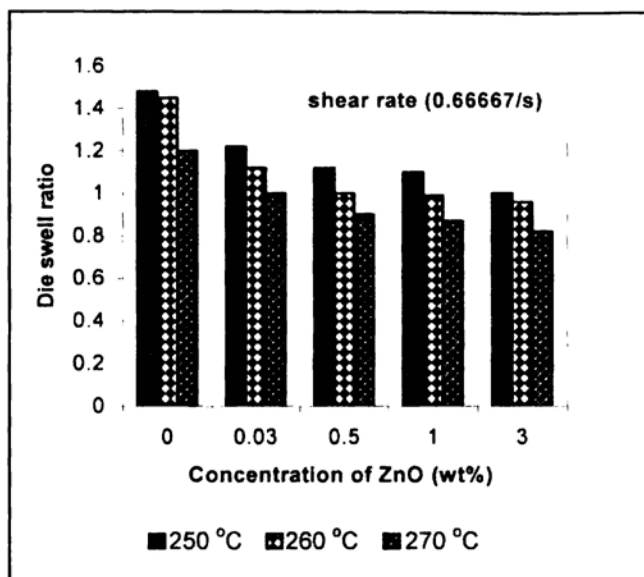
Figure 4a.29 Variations of die swell ratio of PET-nano ZnO composites with temperature

4a.3.5.6 Extrudate deformation studies

The appearance of the extrudate of neat PET and composites with 1.0 % nano ZnO at six different shear rates is shown in figure 4a.30 (a) and (b) respectively. From the figure it is clear that the extrudate distortion tendency increases with the shear rate. At a low shear rate, the extrudate has a smooth surface; however, at a higher shear rate, the surface becomes rougher. The ZnO content of the nanocomposite also plays a major role in determining the surface characteristics. As the ZnO content increases, the surface roughness also increases. Several factors contribute towards surface irregularity. It has been conclusively shown by photographic techniques[87,88] that a fracturing or breaking of the elastically deformed flowing polymer stream occurs at the entrance to the capillary itself at some critical shear stress. Another factor contributing towards extrudate distortion is the successive sticking and slipping of the polymer layer

at the wall in the capillary.[89,90] Moreover, there may be an effect at the exit as well. Shear thinning behaviour of the nanocomposites is clearly visible in these photographs.

Figure 4a. 30 Extrudate photographs of (a) neat PET and (b) PET- nano ZnO composites filled with 1.0 % ZnO at six different shear rates (a) 0.01333/s (b) 0.1333/s (c) 0.66667/s (d) 1.3332/s (e) 2.6664/s (f) 6.6667/s

MODIFICATION OF POLYAMIDE 6 USING NANO ZINC OXIDE

4b.1 Introduction

Advanced polymer composites are replacing metals in many bearing and gear applications owing to its lightweight and economic fabrication. Polymers have poor mechanical strength compared with metals and are reinforced with fillers to improve the mechanical properties.[91] Among engineered thermoplastic polymers, polyamides have a wide and continuously growing market spread, due to their favourable properties (chemical and mechanical resistance, low permeability respect to gases and vapours, high optical transparency, printability etc.). Polyamide 6 (PA 6) is a semicrystalline polymer material with low cost and high performance: it is currently used in fibre- reinforced thermal plastic composites. The main applications of PA 6 are in fibres, films and as injection-moulded engineering plastics.[92-95] The mechanical properties and the crystallization rate can be modified by the addition of inorganic fillers.[96] Fillers widely used are calcium carbonate, talc, silica, clay, glass fibre etc. which play an important role in the plastic filler market.[97-99] The influence of these fillers on the polyamide strongly depends on their shape, particle size, distribution and surface characteristics. A composite with improved properties and a low particle concentration (to preserve properties of pure matrix) is desired.[100]

This study is aimed at producing PA 6 nanocomposites with varying ZnO concentration and analyzing them for their crystallization, mechanical, dynamic mechanical and rheological properties.

4b.2 Experimental

A simple melt-compounding route was adopted for the preparation of PA 6-ZnO nanocomposites. The melt compounding was performed using Thermo Haake Rheocord 600 mixing chamber with a volume capacity of 69 cm^3 fitted with a roller type rotors operating at 40 rpm for 10 min at 230 °C. Nanocomposites at different concentrations (0.0–3.0 wt%) of ZnO were

prepared. In all cases the torque stabilized to a constant value in this mixing time. The crystallization behaviour, thermal stability, morphology, melt rheology, mechanical and dynamic mechanical property of the nanocomposites using commercial and nano ZnO were analyzed according to the details summarized in sections 2.3 of this thesis.

4b.3 Results and discussion
4b.3.1 Differential scanning calorimetry
4b.3.1.1 Non-isothermal

There are a few publications in the research literature that focus on polymer crystallization via nanoparticles of zinc oxide.[101] Recently, Zheng et al. investigated the structure and morphology of the PA 6- ZnO nanocomposites. They reported that ZnO nanoparticle can induce the crystallization of the Υ-crystalline form of PA 6 from the melt.[95]

In this section we compared the crystallization characteristics of PA 6 matrix using nano and commercial ZnO. The effect of nano ZnO on the crystallization characteristics of melt compounded PA 6-ZnO nanocomposite samples was analyzed first with non-isothermal DSC experiments. The crystallization temperatures (T_c), the apparent melting temperatures (T_m), the corresponding enthalpies (ΔH_c and ΔH_m) and the degree of supercooling ($\Delta T = T_m - T_c$) are also reported in table 4b.1.

Table 4b.1 DSC determined thermal characteristics of PA 6-nano ZnO composite samples

Concentration of ZnO (wt%)	T_c ($^\circ$C)	ΔH_c (J/g)	T_m ($^\circ$C)	ΔH_m (J/g)	ΔT ($^\circ$C)
0.0	182.31	61.95	215.72	62.55	33.4
0.03	192.65	61.55	217.83	60.08	25.2
0.1	194.56	62.36	216.60	59.63	22.0
0.5	196.21	62.02	217.35	60.79	21.1
1.0	197.89	63.51	216.23	62.61	18.3
2.0	198.05	51.58	217.80	62.86	19.7
3.0	200.23	52.58	219.58	59.96	19.3

Figure 4b.1 shows the DSC cooling scans of PA 6-nano ZnO composite samples. During cooling from the melt, the ZnO containing samples show crystallization exotherms earlier than neat PA 6, as also seen from the corresponding T_c values indicated in table 4b.1. It is found that the nanocomposite sample containing nano ZnO at a concentration as low as 0.03 wt% enhances the rate of crystallization in PA 6 as the cooling nanocomposites melt crystallizes at a temperature 10 °C higher as compared to neat PA 6. The T_c values continue to increase with increasing ZnO concentration, but at a slower rate, as with further 100 fold increase in ZnO concentration from 0.03 to 3.0 wt%, the additional T_c increase is only about 8 °C. In other words, there is a saturation of the nucleant effect at low ZnO concentrations, resulting in diminishing dependence on the increasing ZnO induced nucleation, possibly because of large surface area and good dispersion of ZnO. Khanna et al.[102], Aharoni et al.[103] and Fornes et al.[97] have reported an increase in crystallization temperature. The melting temperature and enthalpies of PA 6 stay unaffected.

The ΔT values for the PA 6-nano ZnO were 25-18 °C smaller than that of neat PA 6 (33 °C) (figure 4b.2). From these results nano ZnO content affects the crystallization rate and takes the role of a nucleating agent on PA 6 crystallization due to its enormous surface area. The results indicated that the incorporation of ZnO nanoparticles had little effects on the degree of crystallinity of PA 6. Tjong et al. also observed this behaviour in LDPE- ZnO nanocomposites.[104] Furthermore, the glass transition temperature (T_g) of nanocomposites resulted in a slight increase in value from 83 °C in the case of neat PA 6 to 84 °C. With increase in ZnO loading, T_g remains unaffected. This result suggests that the movement of PA 6 chains is hindered by the introduction of ZnO nanoparticles.
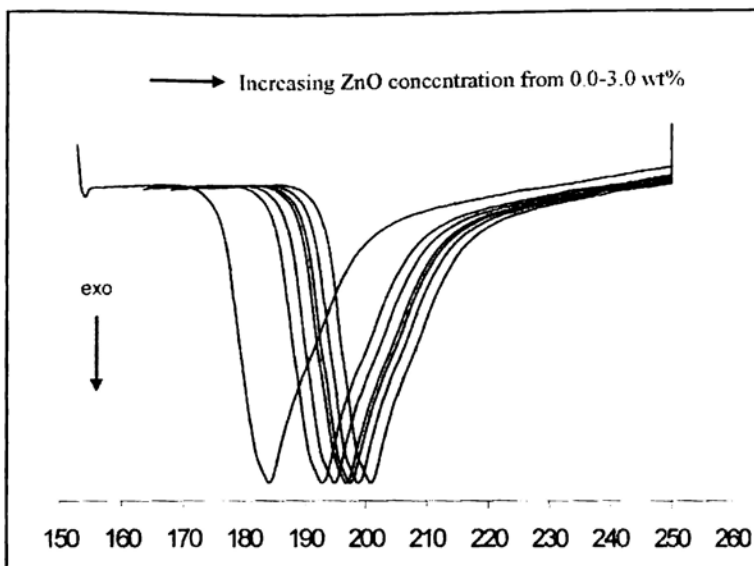
Figure 4b.1 DSC cooling scans (20 °C/min from 300 °C melt) of PA 6-ZnO nanocomposites samples
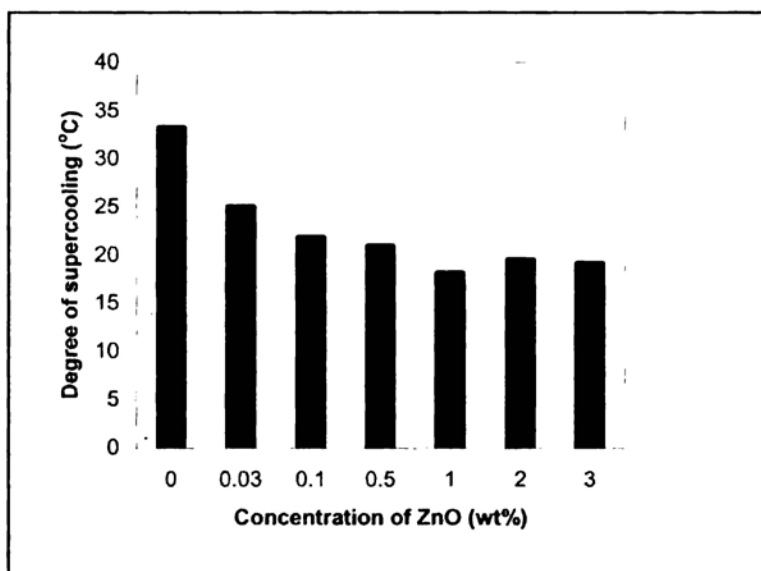
Figure 4b.2 Variation of degree of supercooling with concentration of ZnO
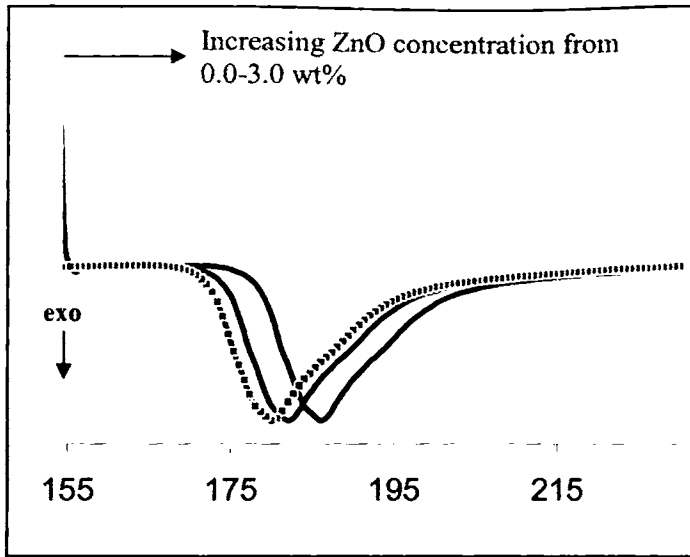
Figure 4b.3 DSC cooling scans of PA 6-commercial ZnO nanocomposite samples

Figure 4b.3 shows the DSC cooling scans of PA 6-commercial ZnO nanocomposite samples. On adding commercial ZnO, the total increase in crystallization temperature were 1 $^{\circ}$C and ΔH_c, ΔH_m, T_c and T_m values remains constant with ZnO loading. T_g of the nanocomposites slightly decreased from 83 $^{\circ}$C in the case of neat PA 6 to 81 $^{\circ}$C. The ΔT values for the PA 6-commercial ZnO composites remain a constant near the neat PA 6 value (33 $^{\circ}$C). So it is clear that commercial ZnO is not a nucleating agent for PA 6 matrix since there is no change in the crystallization rate of PA 6 on adding commercial ZnO.

Figure 4b.4 compares the crystallization temperatures of PA 6 nanocomposites using commercial and nano ZnO. It can be seen that nano ZnO is a better nucleating agent than commercial ZnO. T_c increase is only about 1°C on additing 3.0 wt% commercial ZnO, but for nano ZnO addition, the value is about 18 $^{\circ}$C. This is because, interactions between the filler surface and the matrix substantially decreased and the particles do not show to behave as nucleating agents, in the case of commercial ZnO.
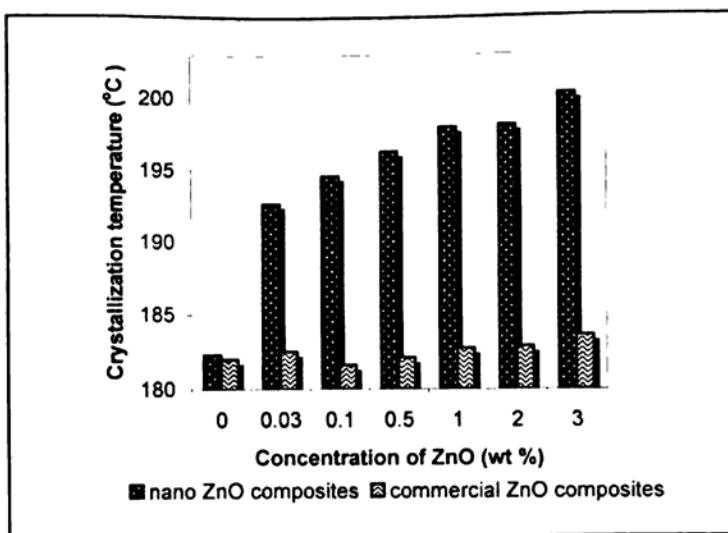
Figure 4b.4 Comparison of crystallization temperatures of PA 6- ZnO nanocomposites using nano and commercial ZnO

4b.3.1.2 Isothermal crystallization characteristics

Figure 4b.5 shows the typical isothermal crystallization curves of the PA 6-nano ZnO composite samples at four temperatures (190 °C, 195 °C, 200 °C and 205 °C). The time corresponding to the maximum in the heat flow rate (exotherm) was taken as peak time of crystallization (t_{peak}). Such peaks are seen at each of the four isothermal crystallization temperatures for the 0.03 wt% ZnO containing nanocomposite, with the earlier or faster crystallization (smaller t_{peak}) corresponding to lower temperature of isothermal crystallization. For the case of neat PA 6, no exotherm is seen at the highest temperatures of 195 °C, 200 °C , 205 °C, because crystallization is very slow and would require longer time than the 4 minutes employed in the DSC program. On the other hand, for the nanocomposite sample with 3.0 wt% ZnO, the rate of crystallization is so fast near the lowest temperatures 190 °C, 195 °C that most crystallization occurs already during the cooling scan (60 °C/min) employed to reach those temperature, resulting in absence of exothermic peaks in the heat flow curves at those temperatures.

Zheng et al.[95] gave possible nucleation mechanism for PA 6-ZnO nanocomposites. They reported that there are no chemical reaction between the ZnO nanoparticles and nylon 6. The possible nucleation mechanism of crystalline nylon 6

on the ZnO surfaces may be the epitaxial growth of nylon 6 crystals for matching the lattice parameters of ZnO. ZnO can apparently supply a sufficiently ordered surface to form hydrogen bonding with nylon 6 and, therefore, reduce its surface energy.

The peak time of crystallization at each of the temperatures for all the PA 6- ZnO nanocomposite samples is plotted against the isothermal crystallization temperature (figure 4b.6). We notice that due to the presence of ZnO the t_{peak} values for the nanocomposite samples reduced to less than 50 % as compared to neat PA 6 at concentration as low as 0.03 wt%. With the increasing ZnO concentration there is further increase in the crystallization rate (as indicated by the decrease in t_{peak}), demonstrating the role of ZnO in enhancing the rate of crystallization.
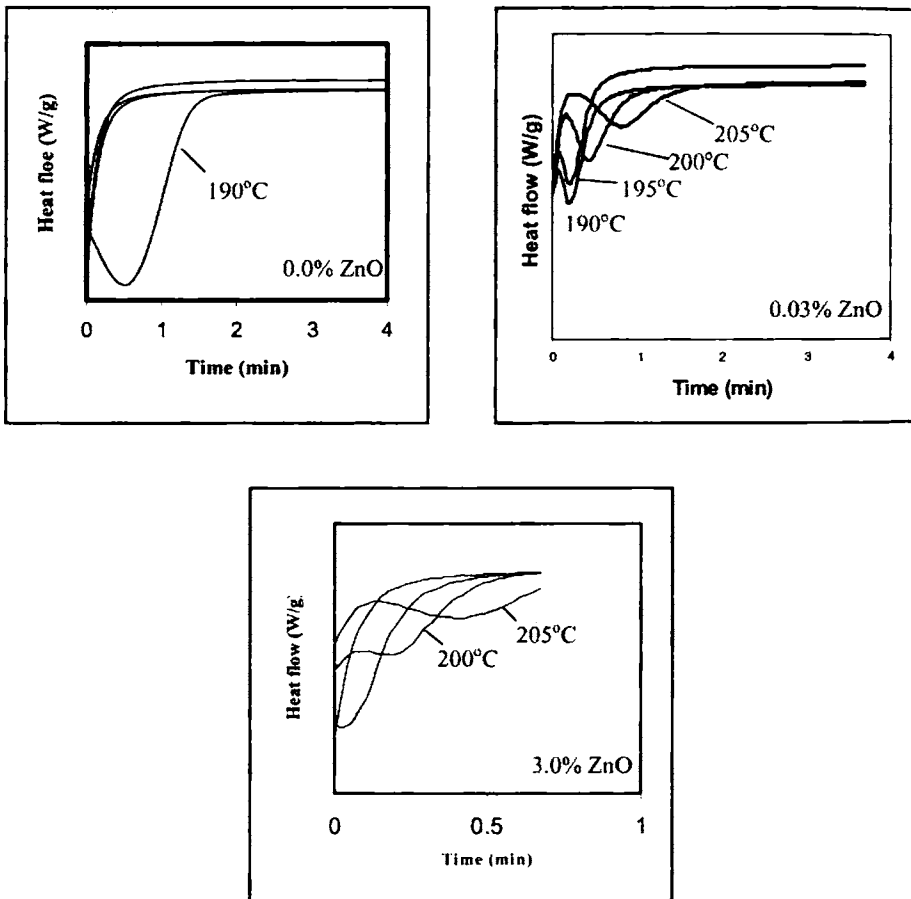
Figure 4b.5 Typical isothermal crystallization curves of the PA 6- nano ZnO composite samples at four temperatures (190 ºC, 195 ºC, 200 ºC and 205 ºC)
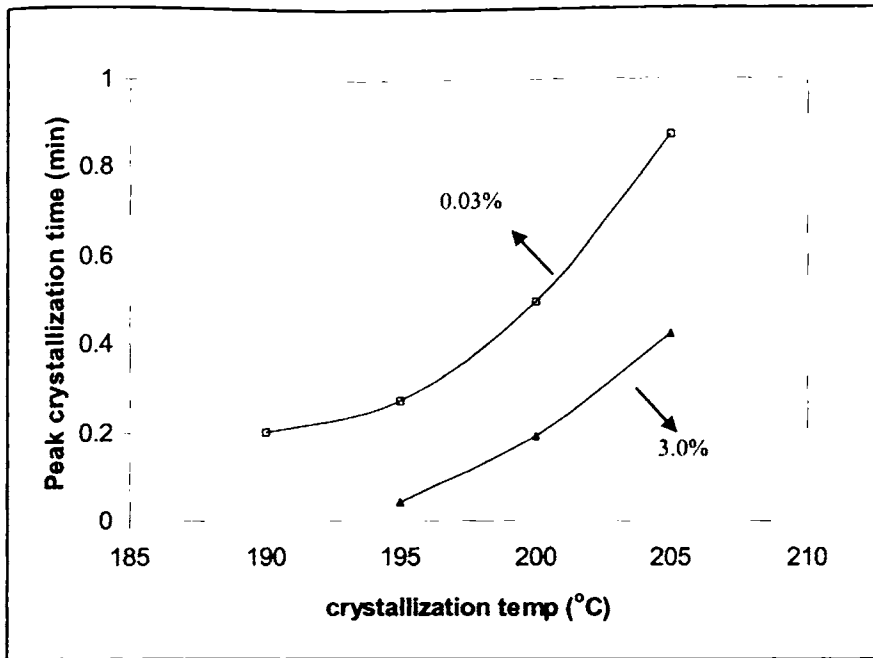
Figure 4b.6 Effect of nano ZnO concentration on the peak crystallization time of the nanocomposites at different isothermal crystallization temperatures

4b.3.2 Thermogravimetry

The TG and DTG curves of neat PA 6 and its composites using nano ZnO are given in figures 4b.7 & 4b.8 respectively. The temperature of onset of degradation T_i ($^{\circ}$C), the temperature at which the rate of decomposition is 10 % ($T_{10\%}$) ($^{\circ}$C), the temperature at which the rate of decomposition is maximum (T_{max}) ($^{\circ}$C), the temperature at which the rate of decomposition is 50% ($T_{50\%}$) ($^{\circ}$C), the peak degradation rate and the residue at 800 $^{\circ}$C are given in table 4b.2. PA 6 degrades in a single step. The degradation starts at a temperature of 315 $^{\circ}$C and the peak rate of degradation is 2.914 %/min at corresponding T_{max} 431 $^{\circ}$C and in nanocomposites, T_i is 330 $^{\circ}$C on adding 3.0 wt% of nano ZnO, indicating improved thermal stability of the nanocomposites. The T_{max} temperature also showed improvement in thermal stability. Residue at 800 $^{\circ}$C is only about 0.2531 % for PA 6. On adding 3.0 wt% of ZnO, residue increased to 5.415 %. Peak rate of decomposition decreased from 2.914 to 1.915 %/min. This increase in the thermal stability of the nanocomposites may result from the strong interaction between the nano ZnO and PA 6 molecules.

But on adding commercial ZnO, themal stability slightly decreases (figure 4b.9). The T_{max} temperature decreases from 431 °C to 426 °C on adding 1.0 wt% commercial ZnO.
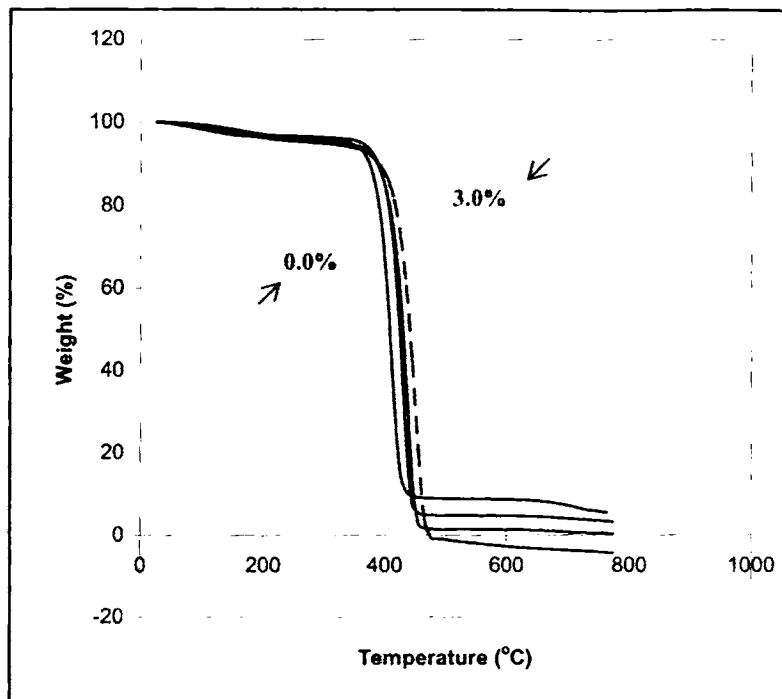
Figure 4b.7 Thermogravimetric traces of PA 6 - ZnO nanocomposite samples (lower curves with increasing ZnO concentrations 0.0, 0.03, 1.0, 3.0 wt%)

Table 4b.2 Degradation characteristics of PA 6 and its nanocomposites

Concentration of ZnO	T_i (°C) Onset	$T_{10\%}$ (°C)	Residue at 800 °C (%)	Peak rate of decomposition (%/min)	$T_{50\%}$ (°C)	T_{max} (°C)
0	315	332	0.2531	2.914	428	431
0.03	330	343	3.199	2.058	434	442
1.0	351	363	4.443	2.172	439	460
3.0	378	372	5.415	1.915	451	489
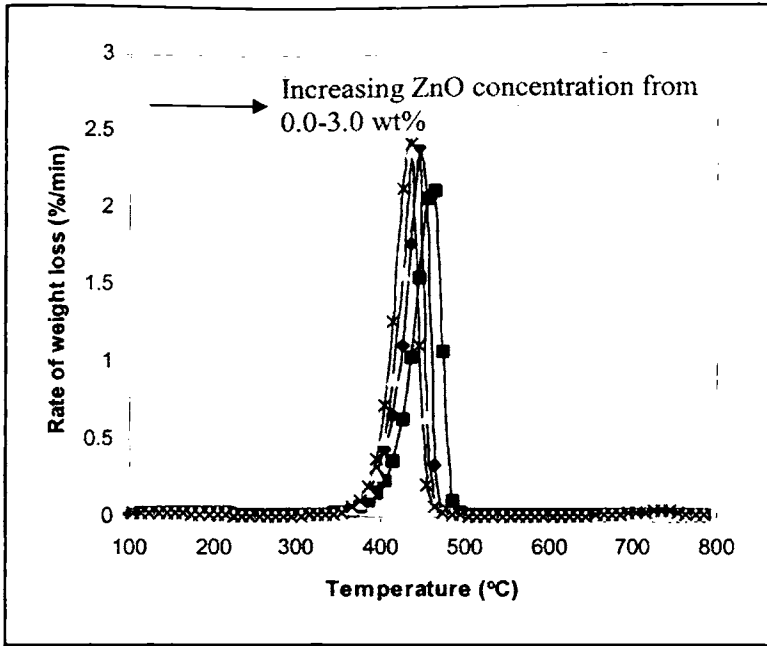
Figure 4b.8 Differential thermogravimetric traces of PA 6- nano ZnO composites
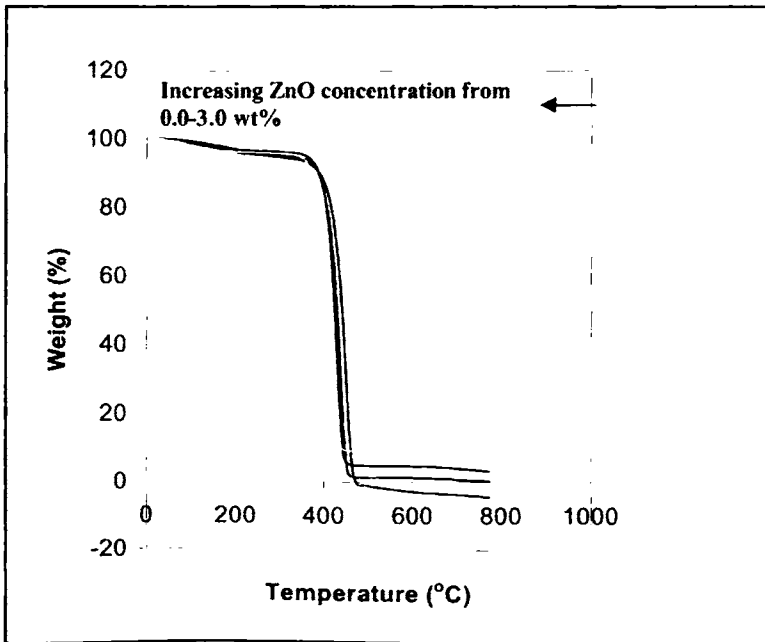
Figure 4b.9 Thermogravimetric traces of PA 6 ·commercial ZnO nanocomposites

4b.3.3 Mechanical properties
4b.3.3.1 Torque studies

The variation of mixing torque with time of mixing at different ZnO loading is shown in figure 4b.10. A mixing time of 10 minutes was fixed since the torque stabilized to a constant value during this time. The temperature of the mixing chamber was fixed as 230 °C. The stabilization of the torque may be related to the attainment of a stable structure after a good level of mixing. The initial and final torque values increase with increase in ZnO loading. Initially torque increases with the charging of PA 6, but decreases with melting. After homogenization of PA 6, ZnO was added at 4 min. There is a little increase in torque on continued mixing with ZnO. After mixing, the torque value is found to be steady. It is clear from figure that there is no degradation taking place during the mixing stage. Similar trend in torque is observed when commercial ZnO is mixed with PA 6.
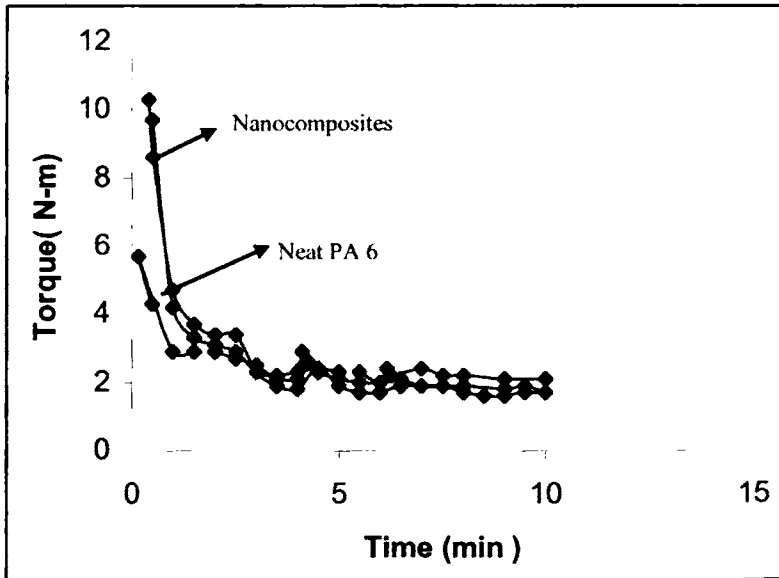
Figure 4b.10 Torque-time curves of PA 6 nanocomposites

4b.3.3.2 Tensile properties

The effects of the nano ZnO on the mechanical properties are summarized in table 4b.3.

Table 4b.3 Tensile properties of PA 6- nano ZnO composites

Concentration of ZnO (wt%)	Tensile strength (MPa)	Tensile modulus (GPa)	Elongation (%)	Shore D hardness	Energy to max (J)	Tensile toughness (J/m)
0.0	64.91	1.307	18.98	70	1.118	527.3
0.03	71.60	1.422	16.23	73	1.951	965.8
0.1	76.42	1.639	12.91	80	2.253	1062.7
0.5	80.22	1.691	11.02	81	3.001	1200.0
1.0	82.32	1.786	11.22	85	3.254	1301.6
2.0	84.67	1.790	10.43	90	3.489	1585.9
3.0	85.60	1.801	9.55	92	3.678	1599.1

The necking phenomenon was observed in pure PA 6 and its composites at about 1.0 wt% ZnO. Table 4b.3 shows an increase in the tensile modulus and strength of PA 6 with an increasing concentration of ZnO content from 0.0 to 3.0 wt%. From 0.0 to 1.0 wt% the change in tensile strength is about 27 % and modulus is about 37 %. But from 1.0 to 3.0 wt%, the increase in tensile strength is only about 4 % and modulus is about 1 %. The tensile strength showed an increment of about 38 % and modulus of about 38 % on adding 3.0 wt% of nano ZnO. So, for effective reinforcement only less than 1% ZnO is necessary. The Shore D hardness also supports the reinforcement. The elongation to break is found to decrease with increasing loading of ZnO, indicating that the ductility of neat PA 6 is reduced. Energy to maximum and tensile toughness (energy/ thickness of the sample) values increases (figure 4b.11) with filler loading. These results demonstrate that even a small fraction of ZnO provide effective reinforcement to the PA 6 matrix. This is due to better interaction between the PA 6 matrix and ZnO nanoparticles. As aspect ratio of ZnO is high, it has a large surface area available for adhesion between the polymer molecules and ZnO particles. This facilitates better load transfer to the reinforcing phase and contributes to the improved strength and modulus.[105]

Comparison of tensile srength and modulus of PA 6 nanocomposites using commercial and nano ZnO (figure 4b.12 & 4b.13 respectively) showed that nano ZnO gave better reinforcement to PA 6 matrix than commercial ZnO. The improvement in tensile strength and modulus is about 7 % and 8 % respectively on using 3.0 wt% commercial ZnO. Elongation, energy to maximum and tensile toughness of PA 6-commercial ZnO nanocomposites decreases (table 4b.4).
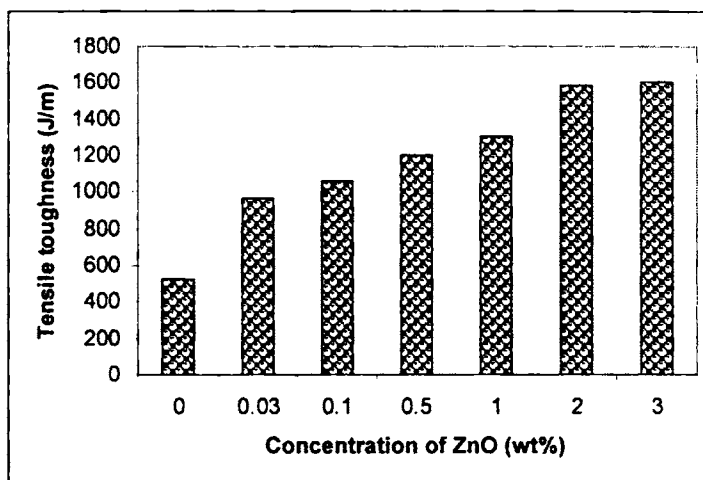
Figure 4b.11 Variation of tensile toughness of PA 6- ZnO composites
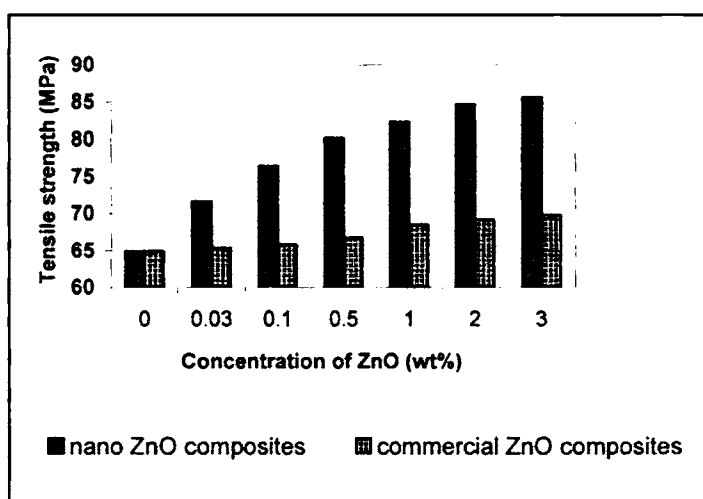
Figure 4b.12 Comparison of tensile strength of PA 6 nanocomposites using nano and commercial ZnO
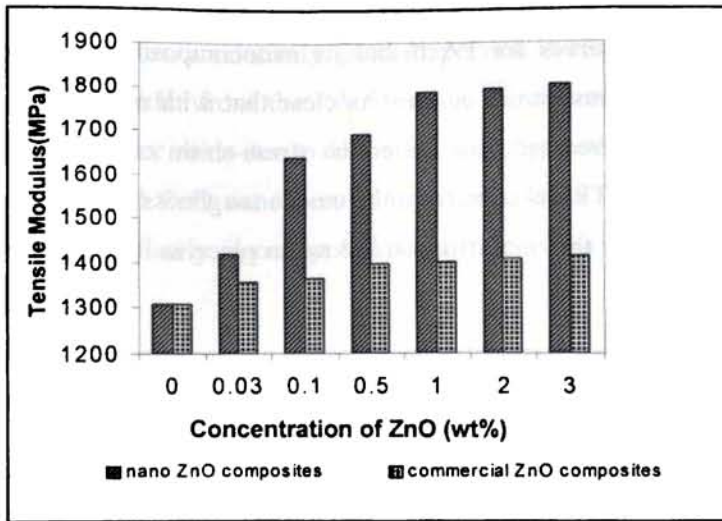
Figure 4b.13 Comparison of tensile modulus of PA 6 nanocomposites using nano and commercial ZnO

Table 4b.4 Tensile properties of PA 6- commercial ZnO nanocomposites

Concentration of ZnO (wt%)	Elongation (%)	Shore D hardness	Energy (J)	Tensile toughness (J/m)
0.0	18.98	70	1.118	527.3
0.03	18.67	72	1.109	433.2
0.1	16.82	73	1.112	427.6
0.5	16.87	76	1.076	446.4
1.0	16.21	83	1.001	357.9
2.0	15.90	87	0.987	346.2
3.0	15.23	88	0.785	331.0

So composites prepared from nano ZnO can attain superior performance over commercial ZnO. This high reinforcement effect implies a strong interaction between the matrix and nano ZnO interface that can be attributed to the nanoscale and uniform dispersion of the ZnO in the PA 6 matrix.

Stress-strain curves for PA 6 and its nanocomposite is shown in figure 4b.14. From the stress-strain curve it is clear that with nano ZnO loading the elongation (%) decreases. Area under the stress-strain curve increases due to energy absorption. This is clear from the tensile toughness values given in figure 4b.11. So it is clear that modification has taken place in PA 6 matrix on adding nano ZnO.
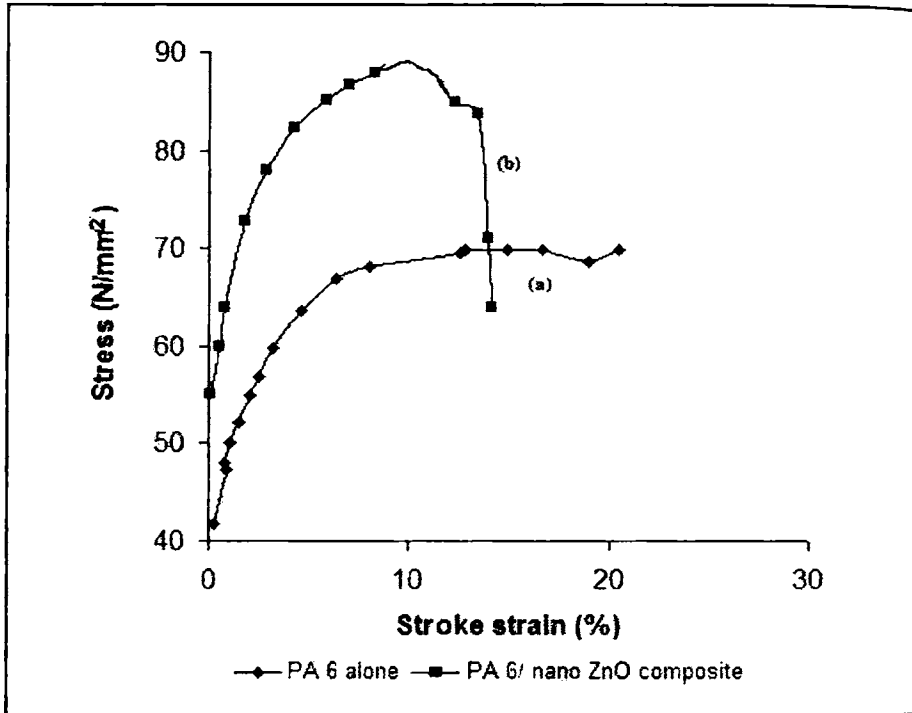
Figure 4b.14 Stress-strain curves for (a) neat PA 6 (b) PA 6- ZnO nanocomposites

4b.3.3.3 Morphology of the fractured surfaces

The scanning electron micrographs of the fractured surfaces of the tensile test specimens have been studied to acquire an insight into the mechanism of reinforcement. Figure 4b.15 (a) shows the fracture surface of neat PA 6 which shows the ductile behaviour. Figure 4b.15 (b) shows the fracture surface for PA 6-nano ZnO composites. From the image it is clear that nano ZnO exist as dispersed particles and the morphology gets substantially modified. Figure shows that, in different project positions of the matrices of PA 6-ZnO, nano ZnO particles are homogeneously dispersed in the PA 6 matrices. Apart from some

agglomerated particles, a relatively good dispersion is clearly visible. There is complete stress transfer from the PA 6 matrix to nanorod having high aspect ratio. Some cavities or voids due to debonding are observed in these figures. But in PA 6-commercial ZnO nanocomposites [figure 4b.15 (c)], the particles are pulled away immediately upon application of stress, as this may reduce the elastic modulus.
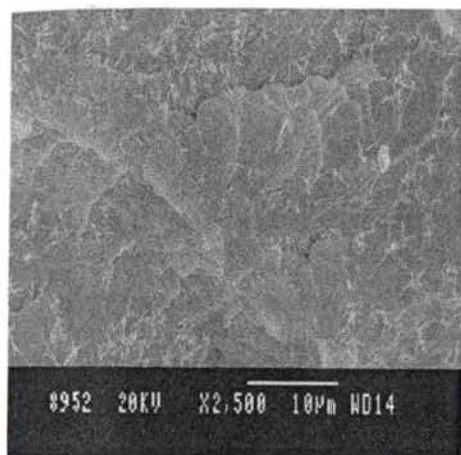
(a)
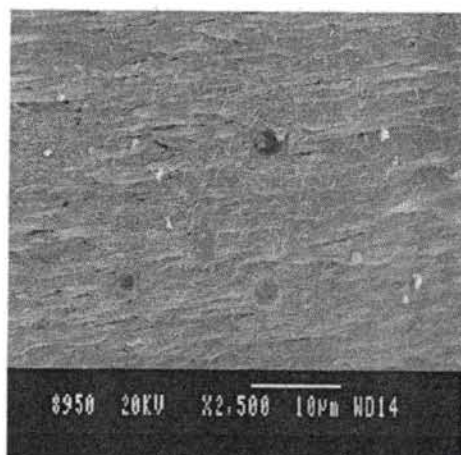
(b)

(c)

Figure 4b.15 SEM images of (a) neat PA 6 (b) PA 6- nano ZnO composite (c) PA 6- commercial ZnO composite

4b.3.3.4 Flexural properties

A comparison of flexural strength and modulus of PA 6-ZnO nanocomposites using nano and commercial ZnO is shown in Figure 4b.16 (a) & 4b.16 (b) respectively. With nano ZnO, the flexural modulus as well as the strength of PA 6 increases remarkably. For example, incorporation of nano ZnO at the level of 3.0 wt%, modulus almost increases five times the value of neat PA 6 and strength increases by around 17 %. The reinforcement is due to smaller particle size, high surface area, uniform dispersion and good interfacial interaction of nano ZnO with PA 6 matrix. With commercial ZnO, the flexural modulus and strength decreases.
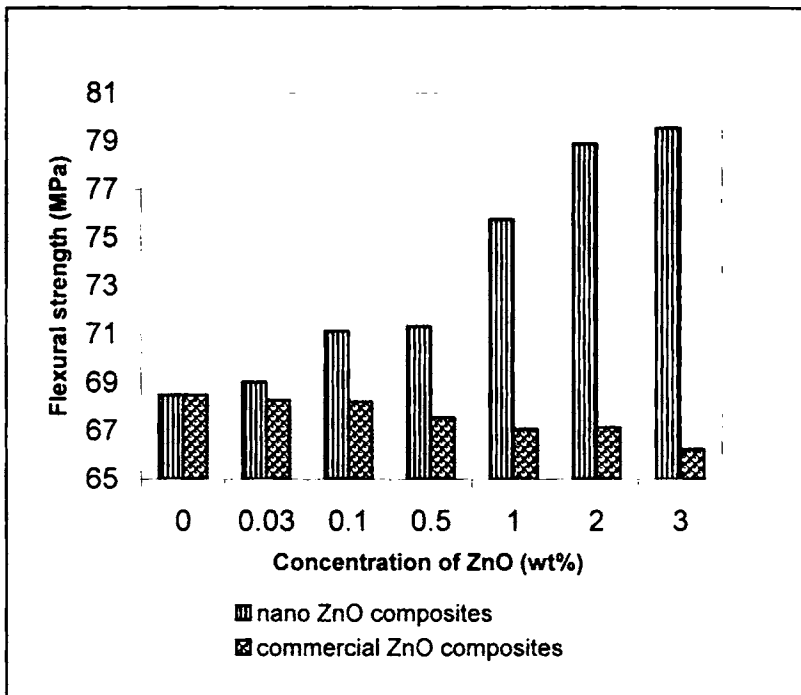
4b.16 (a) Comparison of flexural strength of PA 6 nanocomposites using nano and commercial ZnO
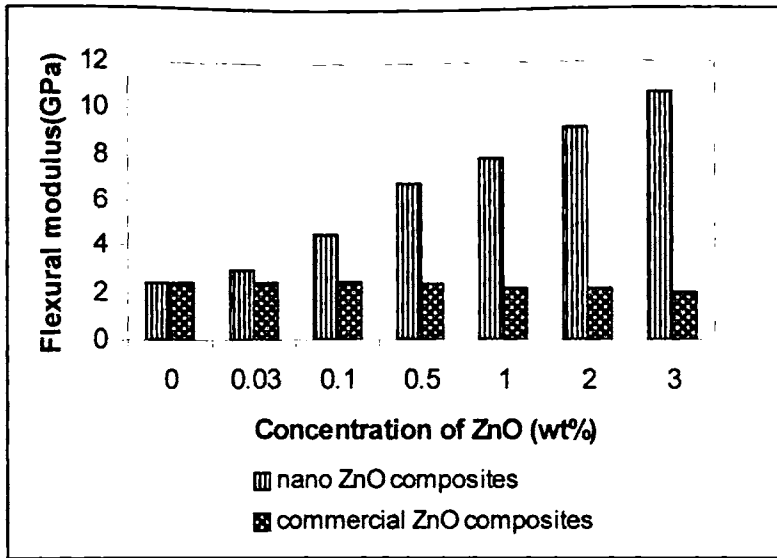
4b.16 (b) Comparison of flexural modulus of PA 6 nanocomposites using nano and commercial ZnO

4b.3.3.5 Impact strength

Polyamide 6 possess very high impact strength, composites require more strength and energy to break. Izod impact strength (unnotched) of PA 6-ZnO nanocomposites using nano and commercial ZnO is compared in figure 4b.17. With commercial ZnO, the impact strength, maintain at the same level but with nano ZnO, the increase is about 53 % on adding 3 wt% of ZnO. The addition of nano ZnO did not increase the percentage crystallinity, so there is a positive effect on impact strength.[59] The increase in impact strength is evidenced by the tensile toughness values given in figure 4b.11. So the toughness of the nanocomposite improved with nano ZnO addition.

The enhancement of impact strength of nano ZnO reinforced composites, is due to particle induced cavitation[106] which is clear from the SEM images shown in figure 4b.15 (b). This process was encouraged by the amorphous nature of the particle-matrix interface. In comparison to crazing-tearing, particle induced cavitation process released plastic constraint and encouraged plastic deformation of the matrix. Similar to the requirement of void creation via cavitation, Argon and Cohen proposed that for improvement in impact strength, the particle must

debond from the matrix creating voids around the particles and allowing the interparticle ligaments to deform plastically.[107-110] In fact, the stretching of the matrix ligaments between cavitated or debonded particles is the main adsorbing energy mechanism. On the other hand, voids reduce the macroscopic plastic resistance of the material and void coalescence also potentially decreases the fracture strain and the overall toughness achievable by the material. Ideally, the voids should not form immediately upon application of stress as this may reduce the elastic modulus.[111] This is the reason for decrease in mechanical properties of PA 6- commercial ZnO nanocomposites which is clear from the SEM images [figure 4b.15(c)]. So to improve toughness, it is necessary to obtain a low particle matrix adhesion (to favour debonding) but at the same time it is also necessary to prevent particle agglomeration and void coalescence.

The impact strength improvement obtained in the samples indicate that the effect of nucleation on the impact strength is smaller compared with that of the interfacial adhesion, considering that most nucleating agents decrease the impact when they increase the crystallization temperature, it is interesting that the prepared ZnO nanoparticles increases both properties at the same time.
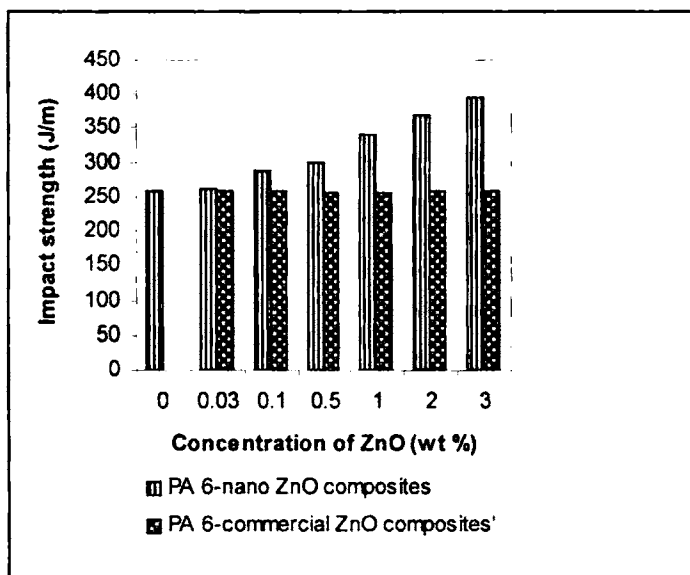
Figure 4b.17 Comparison of impact strength of PA 6 nanocomposites using nano and commercial ZnO

4b.3.4 Dynamic mechanical analysis (DMA)

The DMA results for the dynamic storage modulus of the PA 6-ZnO nanocomposite samples as a function of temperature at 1 Hz are shown in figure 4b.18. A slow decrease in modulii is observed for the nanocomposites. The storage modulii of the nanocomposite increases substantially with the nano ZnO concentration showing the stiffening effect of nano ZnO. But modulii decreases with addition of commercial ZnO. The storage modulus of nanocomposites at 35 °C, 50 °C & 80 °C is given in table 4b.5.

Table 4b.5 Storage modulus of PET- ZnO nanocomposites at 35 °C, 50 °C & 80 °C

Sample	Storage modulus at 35 °C (MPa)	Storage modulus at 50 °C (MPa)	Storage modulus at 80 °C (MPa)
PA 6 alone	396	334	287
PA 6/0.03 wt% nano ZnO	467	403	283
PA 6/1.0 wt% nano ZnO	492	431	295
PA 6/3.0 wt% nano ZnO	1373	1235	855
PA 6/0.03 wt% commercial ZnO	354	314	256
PA 6/1.0 wt% commercial ZnO	312	264	237

From the table it is clear that storage modulii of PA 6-nano ZnO composites increases to about 25 % at 35 °C on adding 1.0 wt % nano ZnO. From 1.0 wt% to 3.0 wt% there is an improvement of about 180 % in storage modulii. This showed the stiffness of the nanocomposite sample. On adding 1.0 wt % commercial ZnO, modulii decreased to about 21 %.
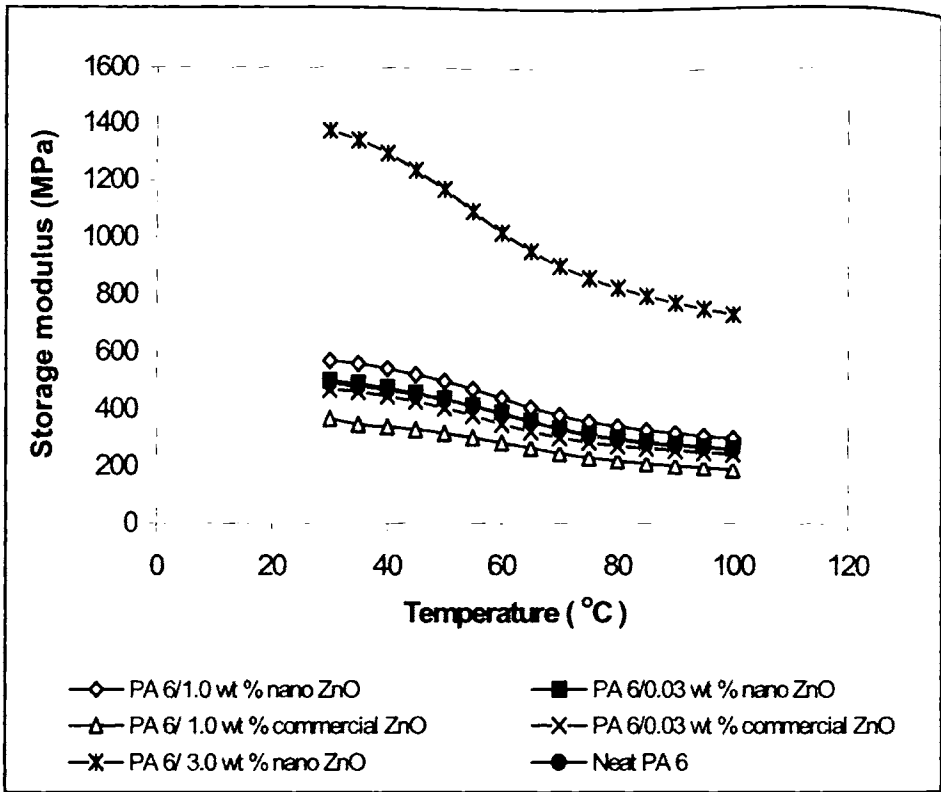
Figure 4b.18 Effect of ZnO concentration on the storage modulus of PA 6- ZnO nanocomposite samples

Figure 4b.19 shows tan δ versus temperature plots for PA 6-ZnO nanocomposites. It is evident from the peak broadening that some compatability is achieved on adding both commercial and nano ZnO. From the tan δ peak it is clear that with ZnO addition there is no significant change in glass transition temperature. Loss modulus curves for the PA 6-ZnO composite are given in figure 4b.20. T_g, loss modulus and tan δ values of PA 6- ZnO nanocomposite are given in table 4b.6.
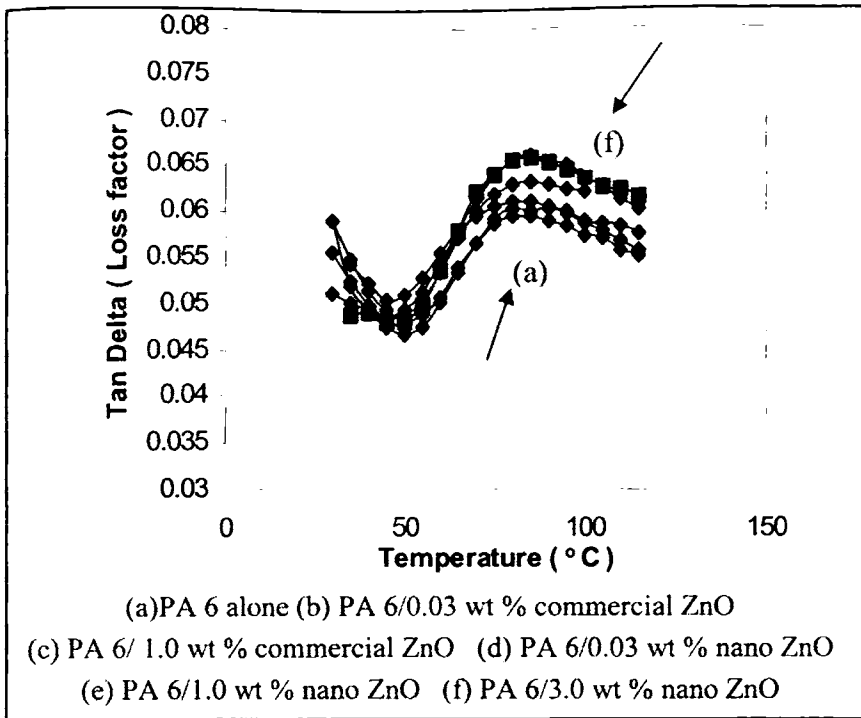
Figure 4b.19 Effect of ZnO concentration on the tan δ of PA 6- ZnO nanocomposite samples [lower curves with (a) to (f)]
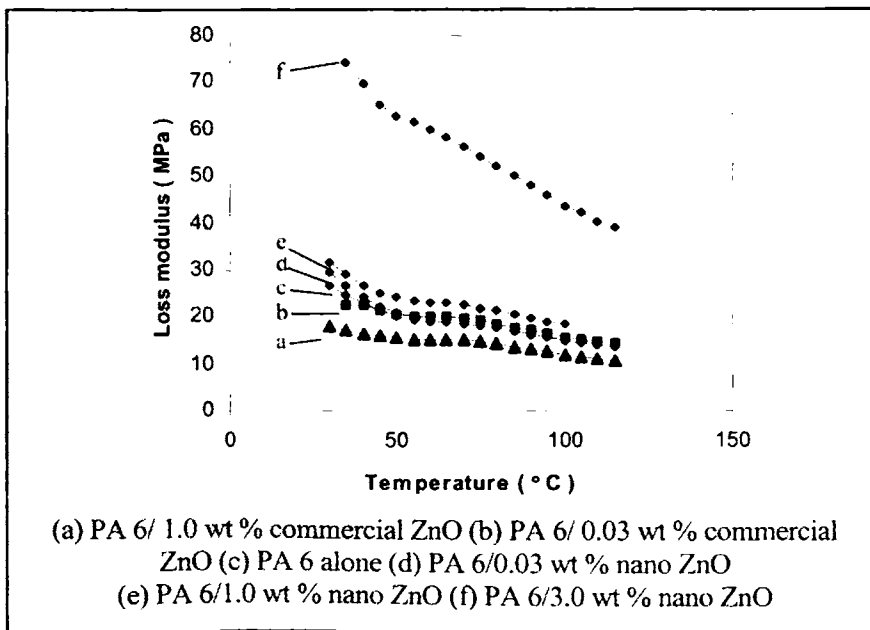
Figure 4b.20 Loss modulus of PA 6- ZnO nanocomposites [lower curves with (a) to (f)]

With the addition of nano ZnO loss modulus values increases. T_g values slightly increases on adding nano ZnO. On adding commercial ZnO, T_g value and loss modulus decreases.

Table 4b.6 T_g, loss modulus and tan δ values of PA 6-ZnO nanocomposite samples

Sample	Loss modulus (MPa) at 80 °C	T_g (°C) (from tan δ peak)	tan δ
PA 6 alone	16.9	83.25	0.0589
PA 6/0.03 wt% commercial ZnO	15.3	82.45	0.0601
PA 6/1.0 wt% commercial ZnO	14.4	82.95	0.0608
PA 6/0.03 wt% nano ZnO	17.8	84.90	0.0632
PA 6/1.0 wt% nano ZnO	19.3	84.97	0.0656
PA 6/3.0 wt% nano ZnO	56.2	84.67	0.0658

We note the modulus, $E^* = $ (loss modulus ^{2} + storage modulus ^{2}) $^{1/2}$ for the neat PA 6 is numerically consistent with the tensile modulus reported by the Dow Chemical Co. PA 6 chains are severely entangled and the function of nanoparticles as physical anchorage points is relatively insignificant. The mobility of molecular chain segments is largely determined by entangling conditions. Therefore, T_g of PA 6 does not have a clear variation by introduction of the nano ZnO particles. The T_g of PA 6-nano ZnO composites slightly increases with ZnO content, because ZnO nanorods having larger aspect ratio can restrict the segmental motion of PA 6 molecules and reduce the free volume of polymer chain folding. But in the case of commercial ZnO nanocomposites due to the coarse nature of ZnO, T_g value decreases.

Correlation of impact and dynamical properties in terms of tan δ peak values of the nanocomposites has been done. The variation of the impact strength as a function of the total loss tangent peak values for PA 6-nano ZnO composite and PA 6-commercial ZnO nanocomposites is shown in figure 4b.21 & 4b.22 respectively. The curves show a non-linear shape and features similar to

those of curve depicting the variation of impact strength with concentration of ZnO. The increase in impact strength with the total loss tangent peak values indicated the role of viscoelastic energy dissipation mechanism in the impact enhancement of nano ZnO composites.
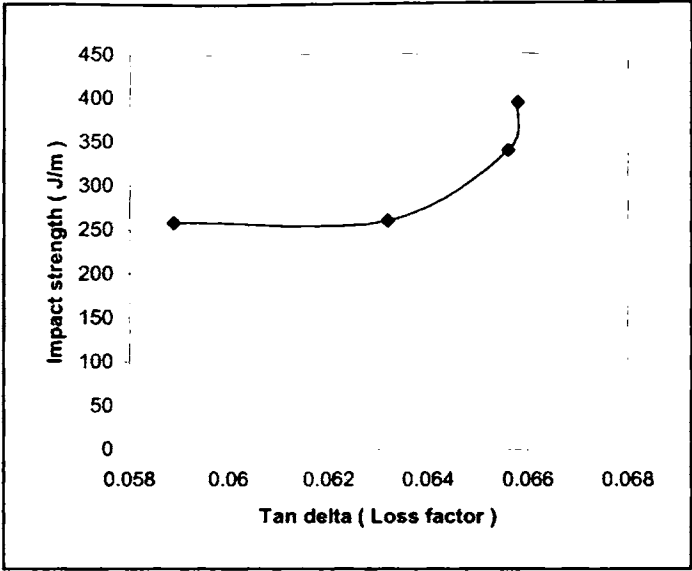
Figure 4b.21 Variation of the impact strength using nano ZnO as a function of the total loss tangent peak values
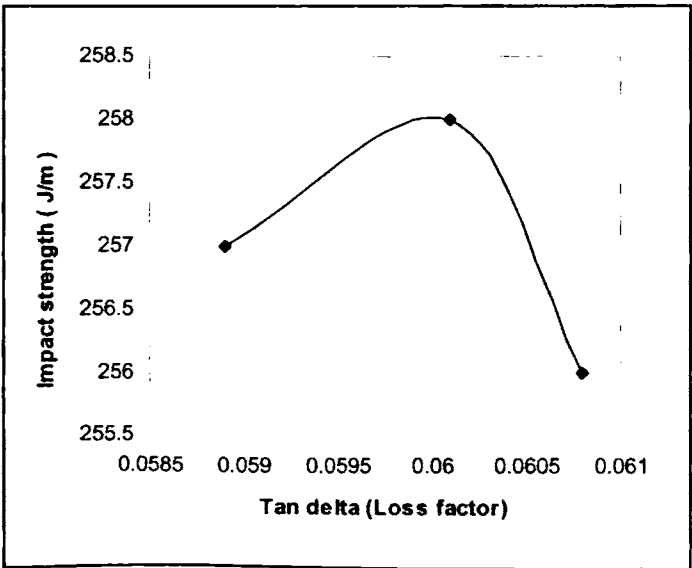
Figure 4b.22 Variation of the impact strength using commercial ZnO as a function of the total loss tangent peak values

4b.3.5 Melt rheology

The rheological behaviour of PA 6- ZnO nanocomposites is studied at three different temperatures 220, 230 & 240 °C. Effect of shear stress, filler loading and temperature on rheological behaviour is investigated.

4b.3.5.1 Effect of shear stress on shear viscosity

Figure 4b.23 present the shear viscosity vs. shear stress curves of PA 6- ZnO nanocomposites at 230 °C with an increasing ZnO concentration from 0.0-3.0 wt%. We also examined the flow behaviour of PA 6 nanocomposites filled with 1.0 % commercial ZnO. As shear stress increases, the viscosity of PA 6- ZnO composites decreases in all cases, indicates the pseudoplastic flow behaviour. At zero shear, the molecules are randomly oriented and highly entangled and therefore exhibit high viscosity. Under the application of shearing force, the polymer chains orient, resulting in the reduction of shear viscosity and thus exhibit shear-thinning (pseudoplastic behaviour).[75,76] It is just this pseudoplasticity that makes the nanocomposites to be easily melt-processed. Effect of temperature on shear viscosity of PA 6 nanocomposites filled with 1.0 % nano ZnO is given in figure 4b.24. With a rise of temperature from 230 to 240 °C the value of shear viscosity decreases, especially at relatively lower apparent shear stress. The melt viscosity increases when the temperature decreases to 220 °C.
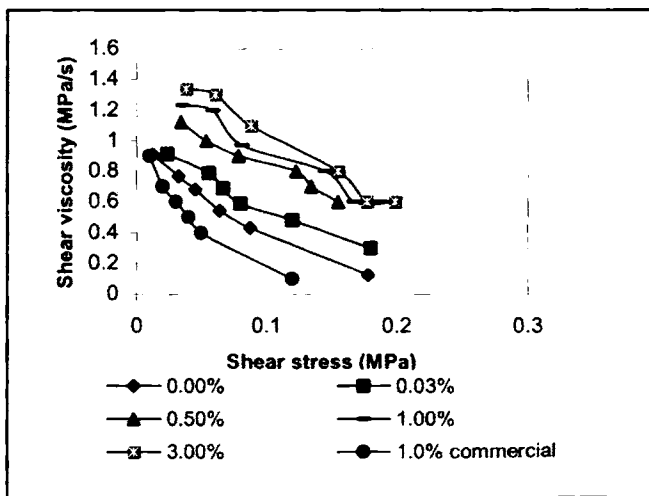
Figure 4b.23 Effect of shear stress on shear viscosity of PA 6- ZnO nanocomposites
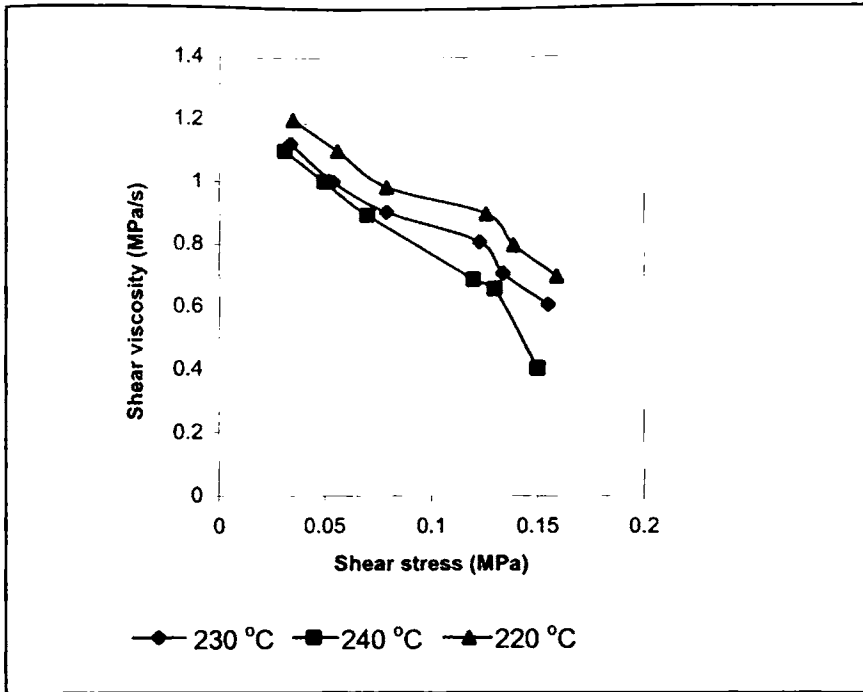
Figure 4b.24 Effect of temperature on shear stress vs. shear viscosity plots

4b.3.5.2 Effect of filler loading

Since entanglements of polymer chains and arrangement of ZnO are not permanent and altered by flow and relaxation processes, any disturbance of this steady state, such as shear, will disrupt the structure of the polymer matrix. Figure 4b.25 shows the variation of shear viscosity with increasing concentration of nano ZnO from 0.0-3.0 wt% at six different shear rates. It is clear from the figure that shear viscosity increases with nano ZnO addition and this increase is more prominent at low shear rates and low ZnO concentration. Also it can be seen from the figure that shear viscosity decreases substantially with increasing shear rate, but increases monotonically with increasing nano ZnO loading at a given shear rate.[71,72]
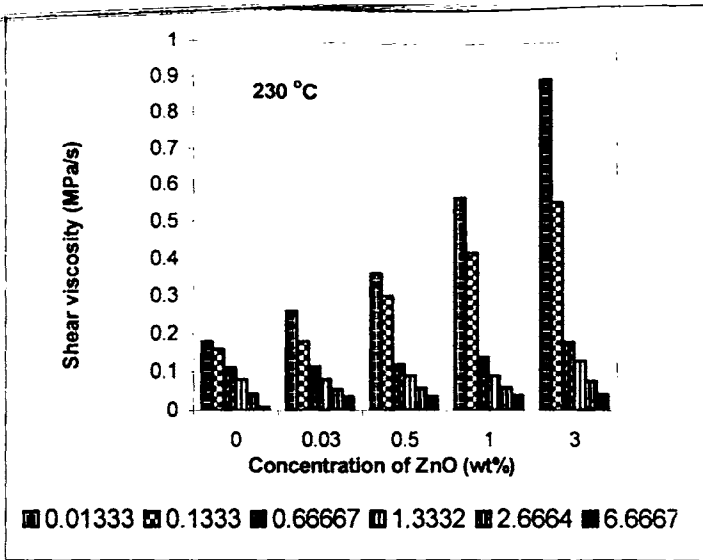
Figure 4b.25 Variation of shear viscosity with concentration of ZnO and shear rates at 230 °C

Figure 4b.26 examines the variation of shear viscosity of PA 6 nanocomposites with concentration of commercial ZnO at six different shear rates. It is clear from the figure that viscosity decreases with ZnO loading.
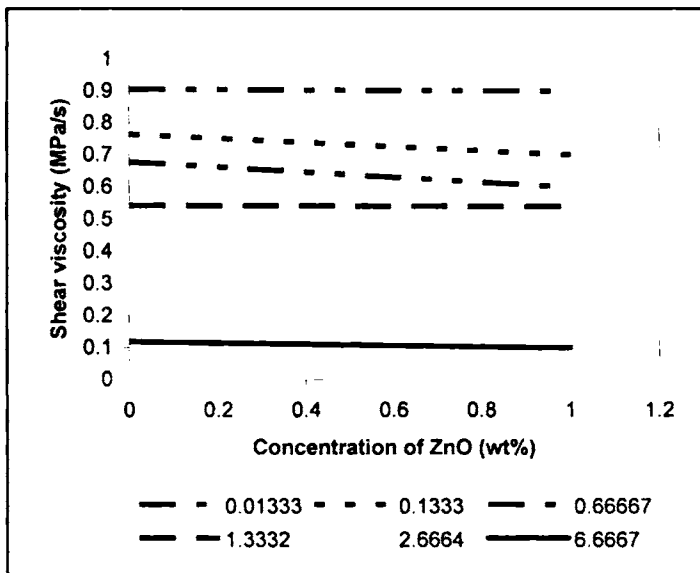
Figure 4b.26 Variation of shear viscosity with concentration of commercial ZnO at six different shear rates at 230 °C

170

4b.3.5.3 Effect of temperature

An understanding of the mechanism of polymer flow processes in relation to the nature and composition of the material can be elucidated by a study of the temperature dependence of shear viscosity. Namely, the temperature sensitivity of the shear viscosity has a profound effect on the choice of processing conditions as well as on the quality of the end products. Shear viscosities of pure PA 6 and nanocomposite melts decrease with increasing extrusion temperature in the range of 220–240 °C, demonstrating that increasing temperature improves the flow behavior of the polymer melts. However, the effect of temperature on shear viscosity changes with the shear rate. The data indicate that the temperature sensitivity of shear viscosity is higher in lower shear rate region, and drops at higher shear rates. This phenomenon is in agreement to the fact that elevating shear rate always accompanied by a rapid decrease of the entanglement density of macromolecules and the melt viscosity.[77] The Arrhenius plots of PA 6- nano ZnO composites at two different shear rates is given in figure 4b.27 (a) & (b). A good linear correlation was found in the plot of $\ln \eta_a$ vs. $1/T$, which has proved the appropriateness of the Arrhenius–Eyring equation. Values of E_a obtained from the slopes of these plots are given in table 4b.7. The activation energy of a material provides valuable information on the sensitivity of the material towards the change in temperature. The higher the activation energy, the more temperature sensitive the material will be. Therefore, such information is highly useful in selecting the processing temperature of polymeric materials.

From table 4b.7 it can be observed that the activation energy of flow of the nanocomposites remains constant up to 1.0 % addition of ZnO and increases with ZnO loading.
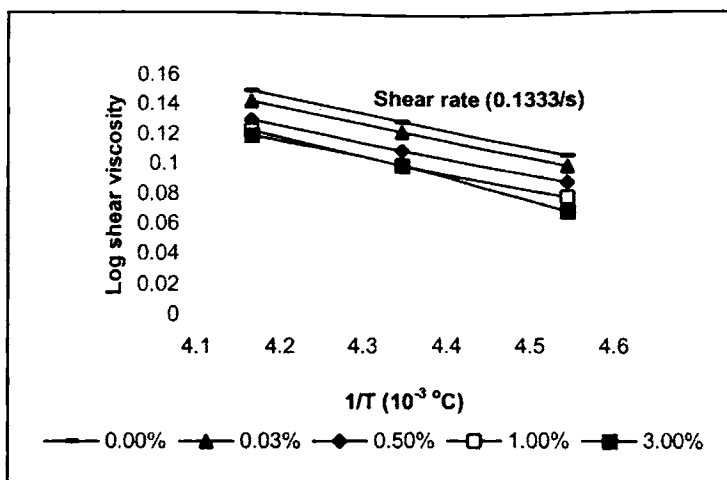
(a)
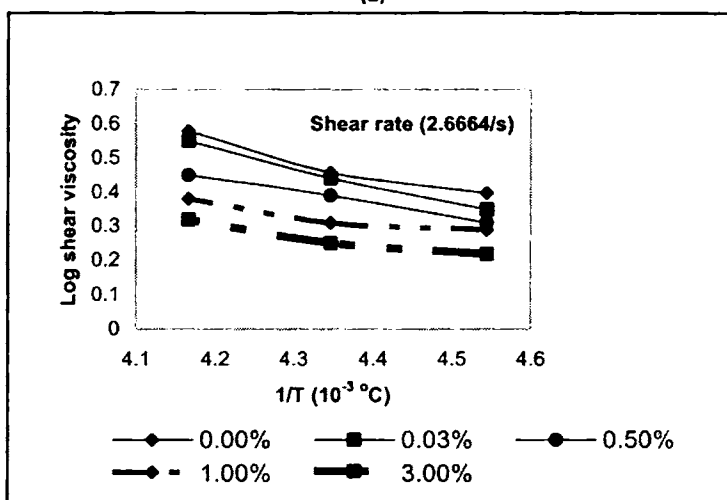
(b)

Figure 4b.27 (a) & (b) Variation of log viscosity with 1/T for the PA 6- nano ZnO composites at two shear rates

Table 4b.7 Activation energies of PA 6- nano ZnO composites at two shear rates

Concentration of ZnO (wt%)	Activation energy (KJ/mol)	
	0.1333/s	2.6664/s
0.0	11.11	47.99
0.03	11.12	52.65
0.5	11.52	36.99
1.0	11.72	23.55
3.0	13.22	26.21

4b.3.5.4 Flow behaviour index (n')

The effects of temperature and concentration of ZnO on the flow behaviour indices of the samples have been studied in detail. The extent of pseudoplasticity or non-Newtonian behaviour of the materials can be understood from n' values. Pseudoplastic materials are characterized by n' below 1. Flow behaviour index values of PA 6- nano ZnO composites at 230 °C and 240 °C are given in figure 4b.28. It is clear from the figure that n' decreases with increasing concentration of ZnO and also with increasing temperature. This suggests that the system becomes more pseudoplastic as the ZnO content and temperature increases. A similar trend of decreasing values of n' with an increase in temperature has been reported.[75,79,80]
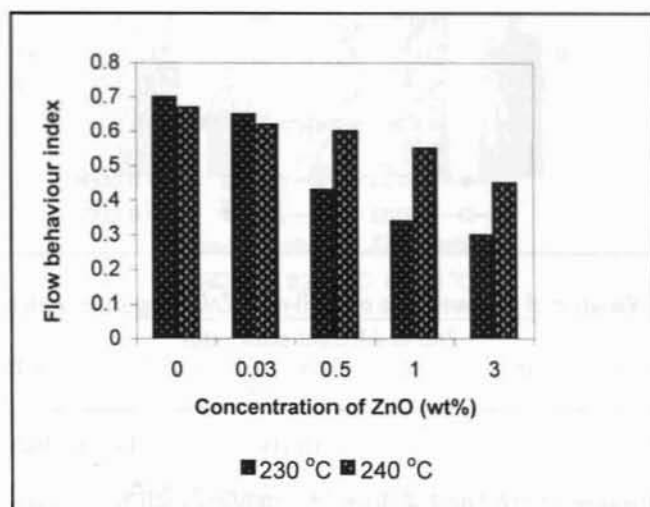
Figure 4b.28 Variation of melt flow index with concentration of ZnO at two temperatures

4b.3.5.5 Die swell

Die swell, called Barus effect is an important parameter for characterizing polymer melt elasticity in an extrusion flow and is related to the quality of the end products.

4b.3.5.5.1 Effect of shear rate and concentration of ZnO

Figure 4b.29 shows the plots of the die swell ratio, de/dc for PA 6 and PA 6- ZnO nanocomposites at 230 °C at six different shear rates. The die swell ratio increases obviously with increasing shear rate at a constant ZnO content. It is

noticeable that at a constant shear rate, the die swell ratio decreases slightly with a rise of ZnO content. Figure 4b.30 shows the variation of die swell ratio of PA 6 nanocomposites filled with 1.0 % commercial ZnO at different shear rates. Die swell ratio remains constant with ZnO loading.
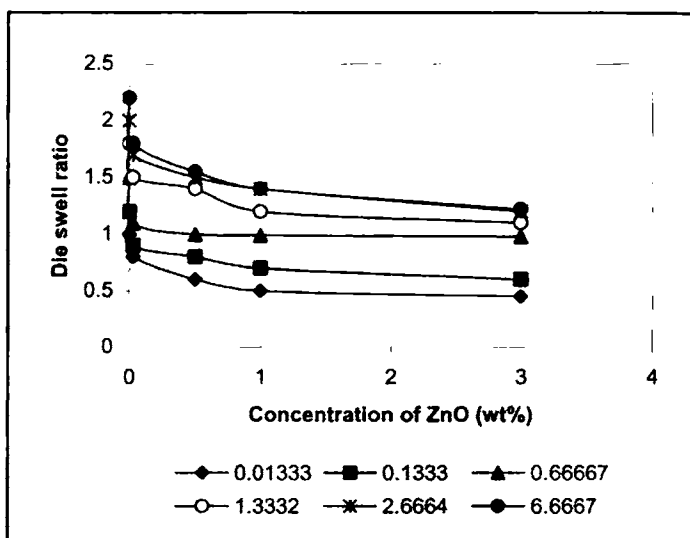
Figure 4b.29 Variation of die swell ratio of PA 6-nano ZnO composites with concentration of ZnO at different shear rates
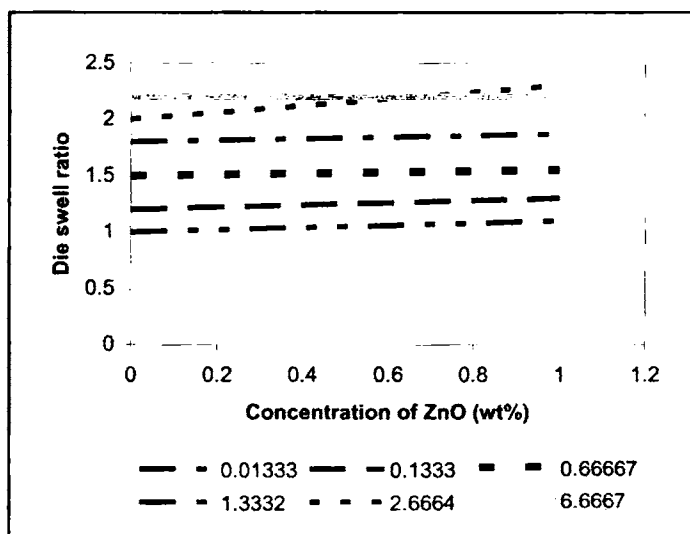
Figure 4b.30 Variation of die swell ratio of PA 6- commercial ZnO composites with concentration of ZnO at different shear rates

4b.3.5.5.2 Effect of temperature

Variation of die swell ratio of PA 6-nano ZnO composites at 3 different temperatures is given in figure 4b.31. It is clear from the figure that die swell ratio decreases with temperature. At low concentration of ZnO, die swell ratio remains same with increasing temperature.
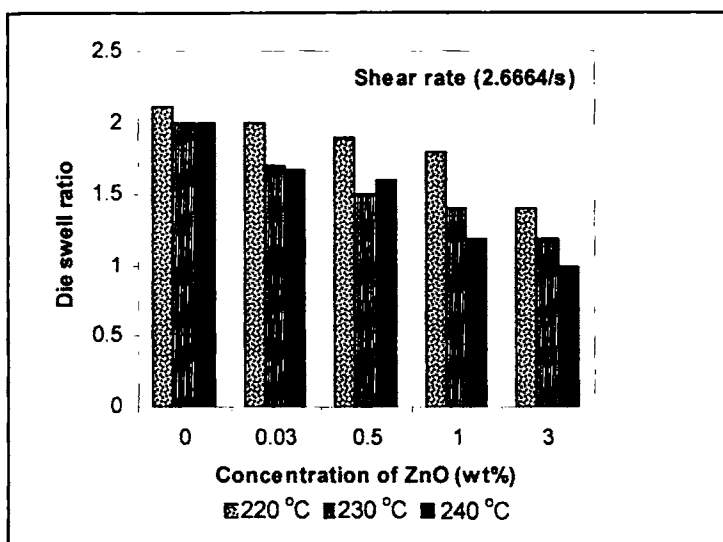
Figure 4b.31 Variation of die swell ratio of PA 6- nano ZnO composites with temperature

4b.3.5.6 Extrudate deformation studies

The appearance of the extrudate of neat PA 6 and nanocomposites with 1.0 % ZnO at six different shear rates is shown in figure 4b.32 (a) and (b) respectively. From the figure it is clear that the extrudate distortion tendency increases with the shear rate. At a low shear rate, the extrudate has a smooth surface; however, at a higher shear rate, the surface becomes rougher. The ZnO content of the nanocomposite also plays a major role in determining the surface characteristics. As the ZnO content increases, the surface roughness also increases. Several factors contribute towards surface irregularity. It has been conclusively shown by photographic techniques [87,88] that a fracturing or breaking of the elastically deformed flowing polymer stream occurs at the entrance to the capillary itself at some critical shear stress. Another factor contributing towards extrudate

distortion is the successive sticking and slipping of the polymer layer at the wall in the capillary.[89,90] Moreover, there may be an effect at the exit as well. Shear thinning behaviour of the nanocomposites is clearly visible in these photographs.

Figure 4b.32 Extrudate photographs of (a) neat PA 6 and (b) PA 6- nano ZnO composites filled with 1.0 % ZnO at six different shear rates (a) 0.01333/s   (b) 0.1333/s   (c) 0.66667/s (d) 1.3332/s (e) 2.6664/s (f) 6.6667/s

MODIFICATION OF POLYCARBONATE USING NANO ZINC OXIDE

4c.1 Introduction

Polycarbonate (PC) is bisphenol-A based polyester, which is an amorphous polymer, is one of the most important engineering thermoplastics used for a wide variety of applications, distinguished by its versatile combination of toughness, stiffness, transparency, heat resistance, ductility, and impact resistance.[112] These properties gave it uses in many applications like compact discs, riot shields, baby feeding bottles, electrical components, safety helmets and headlamp lenses. However, the limitations of PC, such as high notch sensitivity, high melt viscosity, and poor chemical resistance; need to be improved to extend its engineering applications.[113] PC was modified in many different ways, particularly by blending with polyolefin resin such as polyethylene (PE), polypropylene (PP) for use in demanding applications when its outstanding notched impact strength is important.[114-116] Unfortunately, the enhancement of the toughness is obtained at the expense of strength and thermal resistance. In principle, addition of well-dispersed nanofillers of layered silicate clay to PC could improve stiffness, modulus, and heat resistance, which makes a compelling case for exploring PC nanocomposites, particularly if toughness is needed to be preserved.[117,118] There is very little information available in the literature relating to polycarbonate nanocomposites. In principle, addition of well-dispersed nanofillers to polycarbonate could preserve the optical clarity of this amorphous polymer. The promise of transparency plus improved stiffness and scratch resistance make a compelling case for exploring polycarbonate nanocomposites, particularly if toughness could also be preserved. Recently, Huang et al. reported polycarbonate-layered silicate nanocomposites prepared by two different methods.[119]

In this chapter we report the preparation of PC nanocomposites with varying ZnO concentration and analyzing them for their crystallization, mechanical, dynamic mechanical and rheological properties.

4c.2 Experimental

A simple melt-compounding route was adopted for the preparation of PC-ZnO nanocomposites. The melt compounding was performed on a Thermo Haake Rheocord 600 mixing chamber with a volume capacity of 69 cm^3 fitted with a roller type rotors operating at 40 rpm for 10 min at 240 °C. Nanocomposites at different concentrations (0.0–3.0 wt%) of ZnO were prepared. In all cases the torque stabilized to a constant value in this mixing time. The crystallization behaviour, thermal stability, morphology, melt rheology, mechanical and dynamic mechanical property of the nanocomposites using commercial and nano ZnO were analyzed according to the details summarized in sections 2.3 of this thesis.

4c.3 Results and discussion
4c.3.1 Differential scanning calorimetry

Bisphenol-A polycarbonate (PC), possess extremely slow thermal crystallization kinetics. PC undergoes thermal-induced crystallization very slowly because of its chain rigidity, which retards chain diffusion. At 190 °C, one full day is necessary for the first crystallites to develop and a week or more to obtain a well-developed spherulite.[120] The half time of crystallization of PC with a molecular weight higher than 17,000 is more than a week.[121] Both solvents[122,123] and vapours [124,125] have been used to induce crystallization in PC. However, due to the higher residue of solvents in the crystallized materials as well as the associated environmental considerations, this method is only used in the basic research. The evident increase in crystallinity of PC-clay nanocomposites indicates that the addition of nano-scale clays can enhance the crystallization of PC in the presence of supercritical carbon dioxide ($SCCO_2$).[126] In the absence of CO_2, clay itself does not change the crystallization behaviour of PC under experimental conditions. In the presence of CO_2, the nano-scale clay is still an efficient nucleating agent and enhances the crystallization of PC. The incorporation of POSS molecules into PC matrix could not induce crystallinity.[127]

We analysed the crystallization behaviour of PC-ZnO nanocomposites using nano ZnO and commercial ZnO. It is of interest to point out that no crystalline melting endothermic peaks were observed in the DSC curves of PC- ZnO composites, and only a glass transition was identified for these composites with 0.03–3 wt% ZnO composition; the composite T_g values were very close to that of the PC control on adding nano ZnO (figure 4c.1) and the value increases with the increase of the commercial ZnO concentration (figure 4c.2). The T_g value of PC is 157 °C. On adding 1.0 wt % commercial ZnO T_g value decreases to 150 °C. It is clear that the system is more compatable with nano ZnO.

(a) PC alone
(b) PC/0.03 wt % nano ZnO composite
(c) PC/1.0 wt % nano ZnO composite
(d) PC/3.0 wt % nano ZnO composite
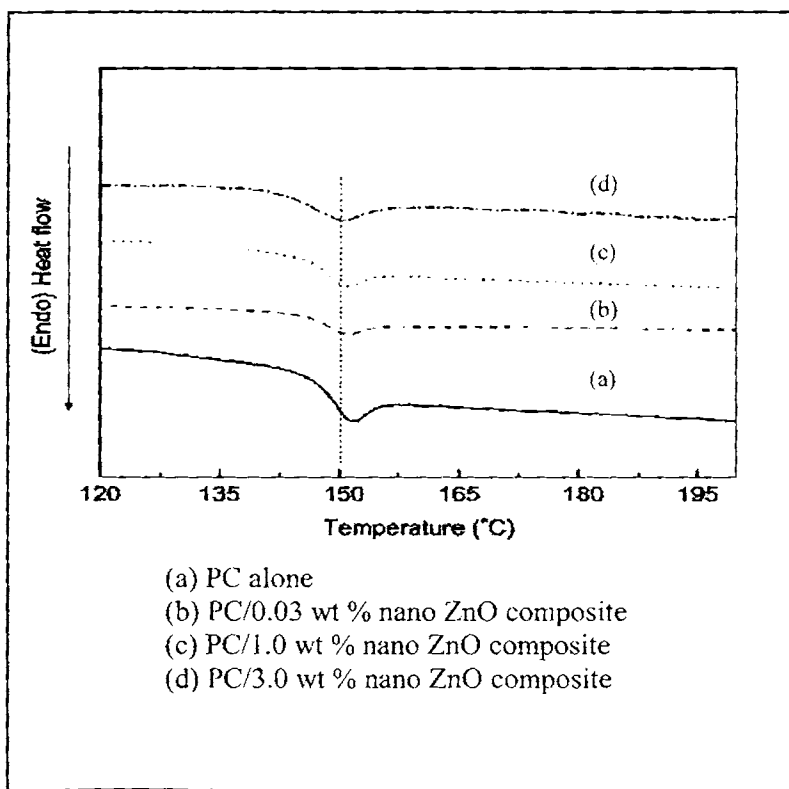
Figure 4c.1 DSC curves of PC- nano ZnO composites
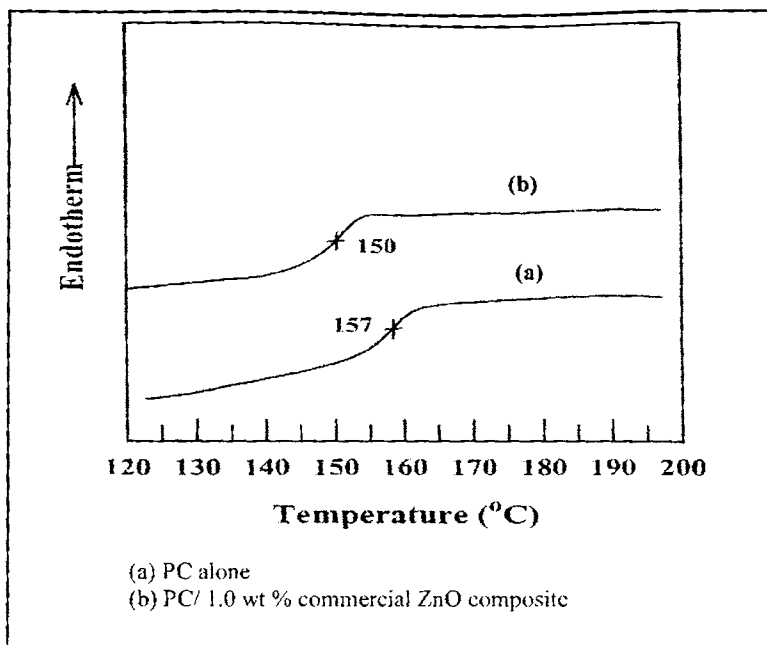
Figure 4c.2 DSC curves of PC- commercial ZnO composites

4c.3.2 Thermogravimetry

The TG and DTG curves of neat PC and its composites using nano ZnO are given in figures 4c.3 & 4c.4 respectively. The temperature of onset of degradation T_i ($^{\circ}$C), the temperature at which the rate of decomposition is 10 % [$T_{10\%}$ ($^{\circ}$C)], the temperature at which the rate of decomposition is maximum (T_{max}) ($^{\circ}$C), the temperature at which the rate of decomposition is 50% [$T_{50\%}$ ($^{\circ}$C)], the peak degradation rate and the residue at 800 $^{\circ}$C are given in table 4c.1. PC degrades in a single step. The degradation starts at a temperature of 264 $^{\circ}$C and the peak rate of degradation is 3.032 %/min at corresponding T_{max} 430.22 $^{\circ}$C and in nanocomposites, T_i is 283 $^{\circ}$C on adding 3.0 wt% of nano ZnO, indicating improved thermal stability of the nanocomposites. The T_{max} temperature also showed improvement in thermal stability. Residue at 800 $^{\circ}$C is 15.31 % for PC. On adding 3.0 wt% of ZnO, residue increased to 19.36 %. Peak rate of decomposition decreased from 3.032 to 1.128 %/min. This increase in the thermal stability of the nanocomposites may result from the strong interaction between the nano ZnO and PC molecules. On adding commercial ZnO, thermal stability of PC remains unaffected (figure 4c.5).
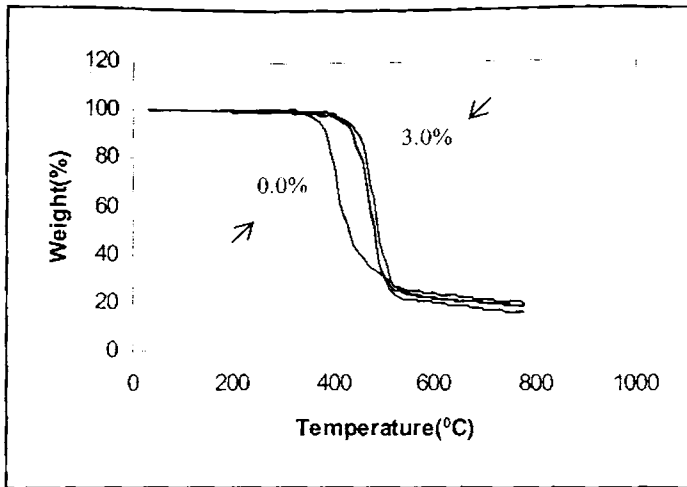
Figure 4c.3 Thermogravimetric traces of PC- nano ZnO composite samples (lower curves with increasing ZnO concentrations 0.0, 0.03, 1.0, 3.0 wt%)

Table 4c.1 Degradation characteristics of PC and its nanocomposites

Concentration of ZnO	T_i (°C) Onset	$T_{10\%}$ (°C)	Residue at 800 °C (%)	Peak rate of decomposition (%/min)	$T_{50\%}$ (°C)	(T_{max}) (°C)
0	264	377	15.31	3.032	420	430
0.03	267	381	15.55	1.039	421	426
1.0	273	421	18.07	1.172	472	480
3.0	283	426	19.36	1.128	478	490
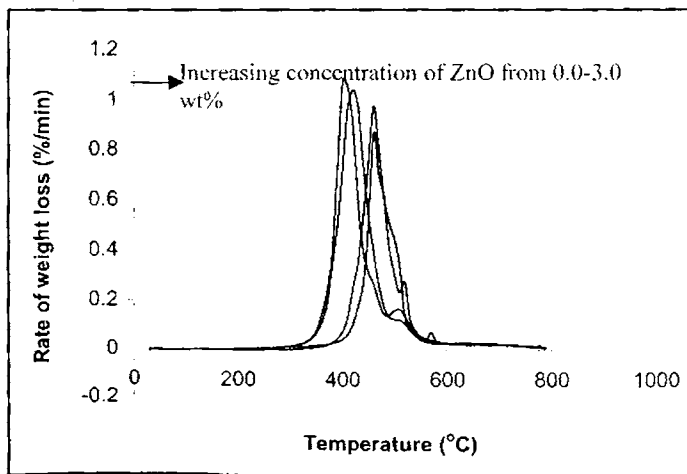
Figure 4c.4 Differential thermogravimetric traces of PC- nano ZnO composites
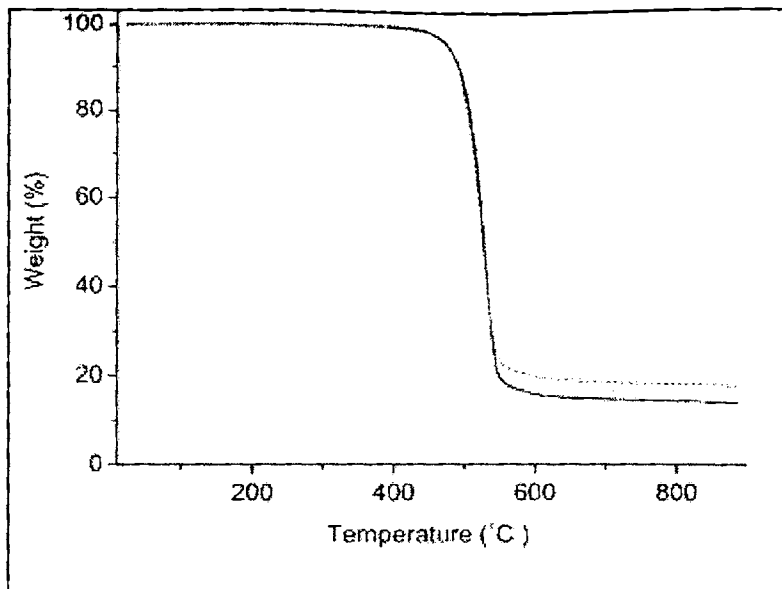
Figure 4c.5 Thermogravimetric traces of PC- commercial ZnO composite

4c.3.3 Mechanical properties
4c.3.3.1 Torque studies

The variation of mixing torque with time of mixing at different ZnO loading is shown in figure 4c.6. A mixing time of 10 minutes was fixed since the torque stabilized to a constant value during this time. The temperature of the mixing chamber was fixed as 240 °C. The stabilization of the torque may be related to the attainment of a stable structure after a good level of mixing. The initial torque value of PC is high because of its high melt viscosity. Initially torque increases with the charging of PC, but decreases with melting. After homogenization of PC, ZnO was added at 2.5 min. There is a little increase in torque on continued mixing with ZnO. After mixing, the torque value is found to be steady. It is clear from figure that there is no degradation taking place during the mixing stage. Similar trend in torque is observed when commercial ZnO is mixed with PC.
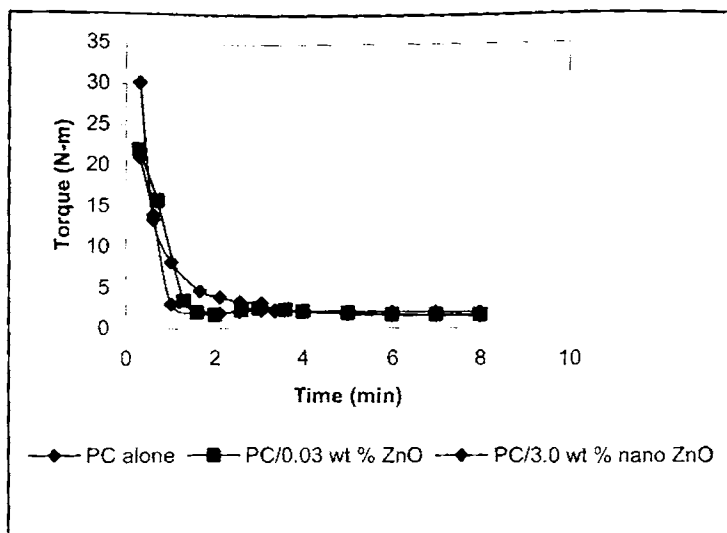
Figure 4c.6 Torque-time curves of PC- ZnO nanocomposites

4c.3.3.2 Tensile properties

The effects of the nano ZnO on the mechanical properties are summarized in table 4c.2.

Table 4c.2 Tensile properties of PC-nano ZnO composites

Concentration of ZnO (wt%)	Tensile strength (MPa)	Tensile modulus (GPa)	Elongation (%)	Shore D hardness	Energy to max (J)	Tensile toughness (J/m)
0.0	72.2	2.308	7.185	75	1.112	529.5
0.03	72.8	2.365	6.817	76	1.11	528.8
0.1	73.5	2.391	6.712	76	0.987	429.7
0.5	73.9	2.398	6.658	77	0.965	403.8
1.0	80.2	2.451	6.598	80	0.943	419.9
2.0	81.51	2.469	6.272	83	0.936	390.6
3.0	83.26	2.523	6.20	89	0.850	368.9

The necking phenomenon was observed in pure PC and its composites at about 1.0 wt% ZnO. The results in table 4c.2 shows an increase in the tensile modulus and strength of PC with an increasing concentration of ZnO content

from 0.0 to 3.0 wt%. From 0.0 to 1.0 wt% the change in tensile strength is about 11 % and modulus is about 6 %. From 1.0 to 3.0 wt% the increase in tensile strength is only about 4 % and modulus is about 3 %. The tensile strength showed an increment of about 15 % and modulus of about 9 % on adding 3.0 wt % of nano ZnO. So, for effective reinforcement only less than 1% ZnO is necessary. The Shore D hardness also supports the reinforcement. The elongation to break is found to decrease with the increasing loading of ZnO, indicating that the ductility of neat PC is somewhat reduced. Energy to maximum and tensile toughness (energy/ thickness of the sample) values (figure 4c.7) decreases with filler loading. These results demonstrate that even a small fraction of ZnO provide effective reinforcement to the PC matrix. This is due to better interaction between the PC matrix and ZnO nanoparticles. As aspect ratio of ZnO is high, it has a large surface area available for adhesion between the polymer molecules and ZnO particles. This facilitates better load transfer to the reinforcing phase and contributes to the improved strength and modulus.
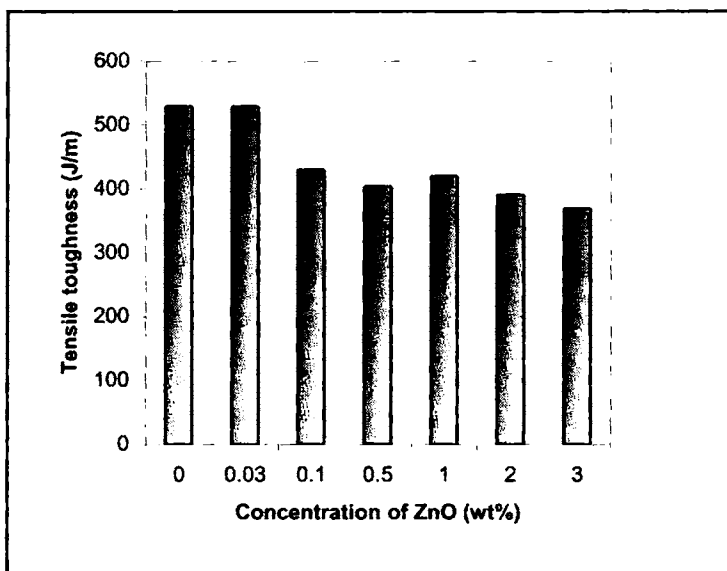
Figure 4c.7 Variation of tensile toughness with concentration of ZnO

Comparison of tensile srength and modulus of PC nanocomposites using commercial and nano ZnO (figure 4c.8 & 4c.9 respectively) shows that only

nano ZnO gives better reinforcement to PC matrix. On adding commercial ZnO, modulus as well as strength almost remains constant. Elongation, energy to maximum and tensile toughness of PC-commercial ZnO nanocomposites also decreases similar to PC- nano ZnO composites.
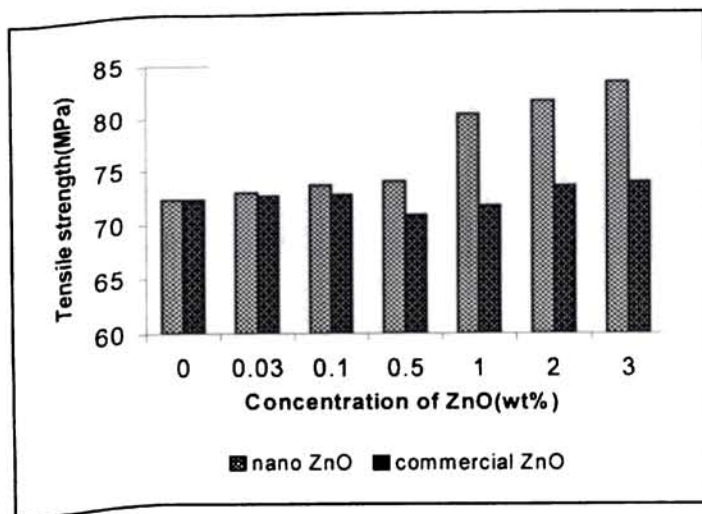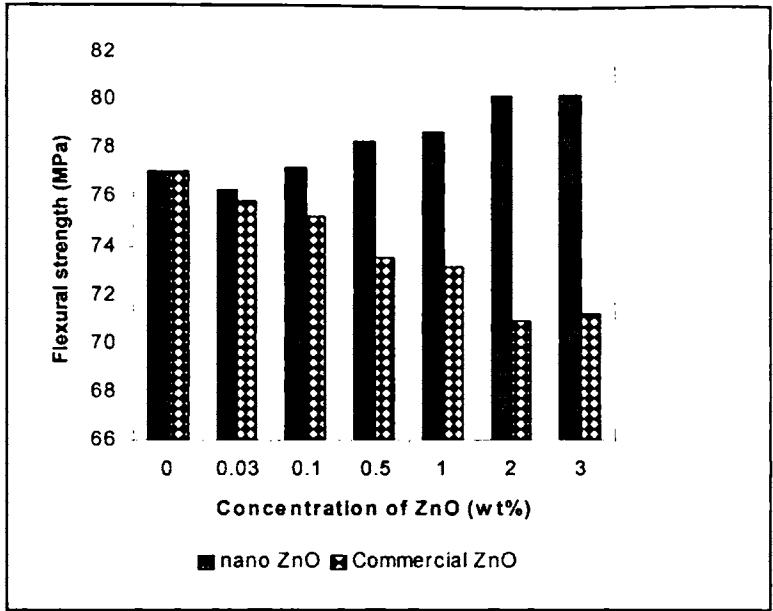

Figure 4c.8 Comparison of tensile strength of PC- ZnO nanocomposites
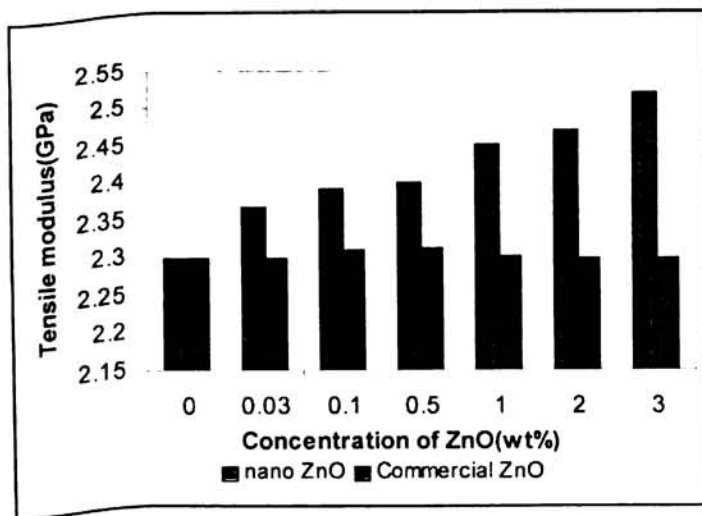
Figure 4c.9 Comparison of tensile modulus of PC- ZnO nanocomposites

Stress-strain curves for PC and its nanocomposite is shown in figure 4c.10. From the stress-strain curve it is clear that with nano ZnO loading the elongation (%) decreases, indicating that the composite becomes somewhat brittle

compared with neat PC. The decrease in the toughness of PC matrix can be seen from the area under the stress-strain curve.
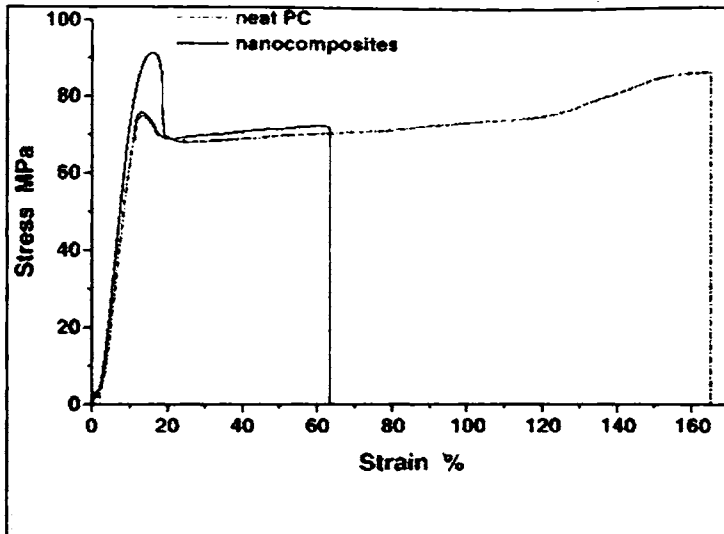
Figure 4c.10 Stress-strain curves for PC- ZnO nanocomposites

4c.3.3.3 Morphology of the fractured surfaces

The scanning electron micrographs of the fractured surfaces of the tensile test specimens have been studied to acquire an insight into the mechanism of reinforcement. Figure 4c.11 (a) shows the fracture surface of neat PC, which showed the ductile behaviour. Figure 4c.11 (b) shows the fracture surface for PC- nano ZnO composites. From the image it is clear that nano ZnO exist as dispersed particles and the morphology gets substantially modified. SEM images are in good agreement with the observed mechanical properties, which is due to shear yielding. Figure shows that, in different project positions of the matrices of PC-ZnO, nanoscale ZnO particles are homogeneously dispersed in the PC matricx. Apart from some agglomerated particles, a relatively good dispersion is clearly visible. There is complete stress transfer from the PC matrix to nanorod having high aspect ratio. There is no sign of extensive particle agglomeration compared to PC-commercial ZnO nanocomposite fracture surface shown in figure 4c.11(c) where we can see large agglomerate and the dispersion is inhomogeneous.
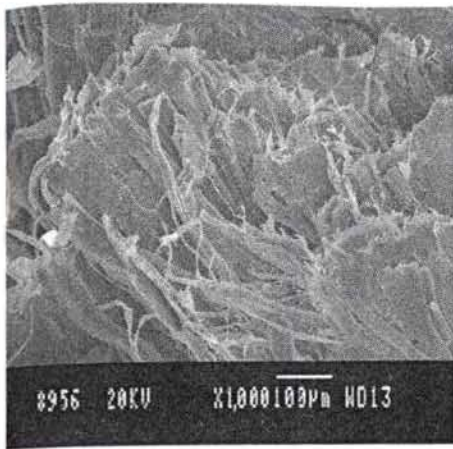
(a)
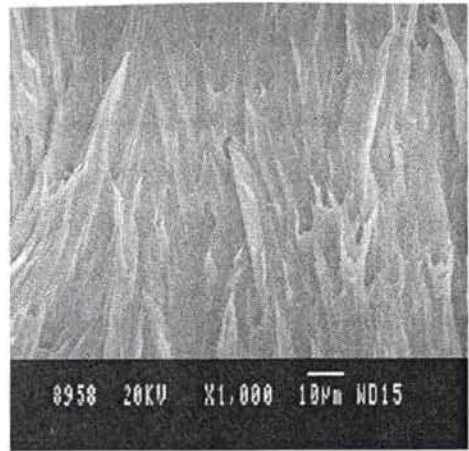
(b)
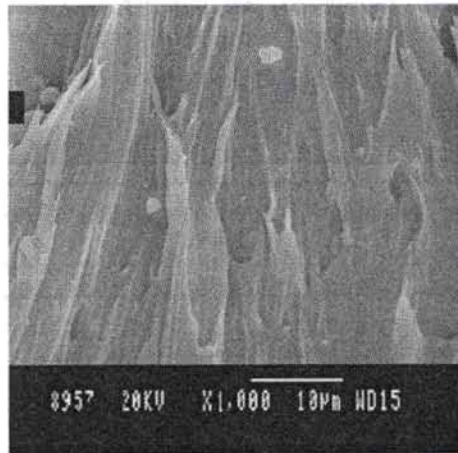
(c)

Figure 4c.11 SEM images of (a) neat PC, (b) PC- nano ZnO composite
(c) PC- commercial ZnO composite

4c.3.3.4 Flexural properties

A comparison of flexural strength and modulus of PC-ZnO nanocomposites using nano and commercial ZnO is shown in figure 4c.12 (a) & 4c.12 (b) respectively. With nano ZnO, the flexural modulus as well as the strength of PC increases considerably. For example, incorporation of nano ZnO at the level of 3.0 wt%, modulus increases by only 5 % and strength increases by around 5 %. The reinforcement is due to smaller particle size, high surface area, uniform dispersion and good interfacial interaction of nano ZnO with PC matrix. On

adding 3.0 wt% commercial ZnO, the flexural modulus and strength decreased to about 12 % and 7 % respectively.

Figure 4c.12 (a) Comparison of flexural strength of PC- ZnO nanocomposites
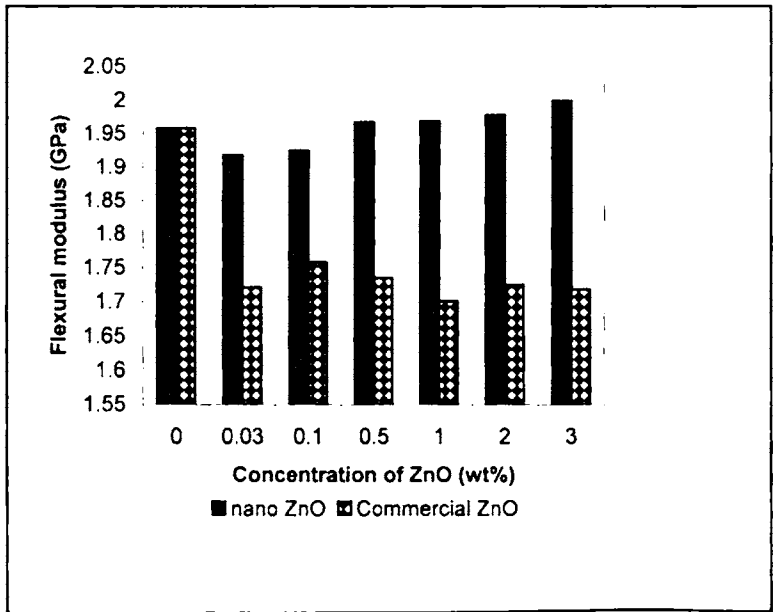
Figure 4c.12 (b) Comparison of flexural modulus of PC- ZnO nanocomposites

4c.3.3.5 Impact strength

PC is a ductile polymer and possesses very high impact strength. PC nanocomposites exbites lower impact strength than neat PC (table 4c.3). This is evident from the area under the stress-strain curve given in figure 4c.10. The most likely explanation for the decreased impact properties is that ZnO material is less well dispersed in the PC matrix. The decrease in impact strength of PC-poss nanocomposite is also reported by Zhao et al.[127] Loading 1.0 wt% nano ZnO and commercial ZnO, the impact strength decreases to about 6% and to about 15 % respectively. So the decrease in toughness is less for PC- nano ZnO composites compared to PC-commercial ZnO composites.

Table 4c.3 Impact strength of PC nanocomposites

Concentration of ZnO (wt%)	Impact strength (J/m) (nano ZnO composites)	Impact strength (J/m) (commercial ZnO composites)
0.0	298.1	298.1
0.03	287.2	284.9
0.1	283.9	289.7
0.5	284.7	255.7
1.0	280.7	254.2
2.0	267.5	243.4
3.0	254.0	242.9

4c.3.4 Dynamic mechanical analysis (DMA)

The DMA results for the dynamic storage modulus of the PC-ZnO nanocomposite samples as a function of temperature at 1 Hz are shown in figure 4c.13. A slow decrease in modulii below glass transition temperature and an abrupt decrease in modulii is observed for the nanocomposites. The storage modulii of the nanocomposite increases substantially with the nano ZnO concentration showing the stiffening effect of nano ZnO.
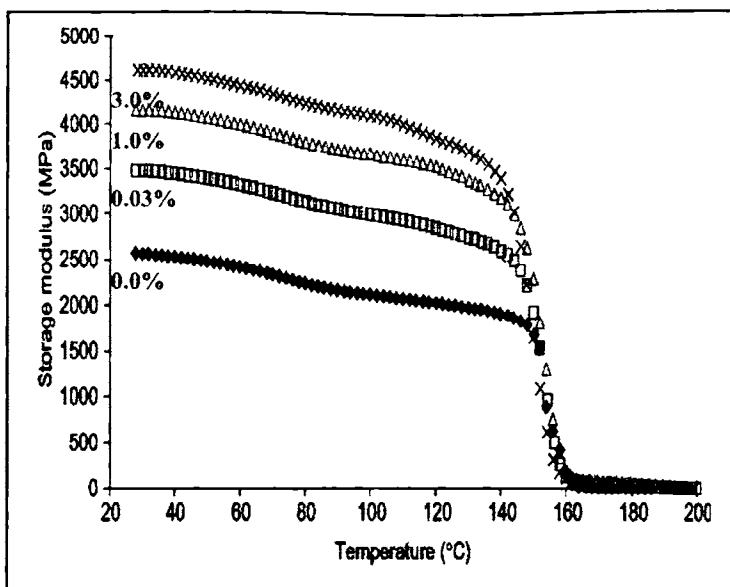
Figure 4c.13 Variation of storage modulii of PC- nano ZnO composites (lower curves with increase in concentration from 0.0 to 3.0 wt% ZnO)

The storage modulus of nanocomposites at 40 °C, 80 °C & 120 °C is given in table 4c.4.

Table 4c.4 Storage modulus of PC-ZnO nanocomposites at 40 °C, 80 °C & 120 °C

Sample	Storage modulus at 40 °C (MPa)	Storage modulus at 80 °C (MPa)	Storage modulus at 120 °C (MPa)
PC alone	2500	2200	2100
PC/0.03 wt% nano ZnO	3500	3190	3050
PC/1.0 wt% nano ZnO	4200	3980	3901
PC/3.0 wt% nano ZnO	4500	4258	4213

Figure 4c.14 shows tan δ versus temperature plots for PC-ZnO nanocomposites. It is obtained in many cases that the improvement of stiffness markedly reduces the ductility. But PC-ZnO nanocomposite is prepared with increased stiffness without sacrificing ductility. From the tan δ peak, it is observed that with nano ZnO addition, there is an increase in glass transition temperature; it is increased by around 7 °C with 3 % nano ZnO. Tan delta peak

value of the nanocomposite decreases with ZnO concentration showing that the composite is more compatibile.
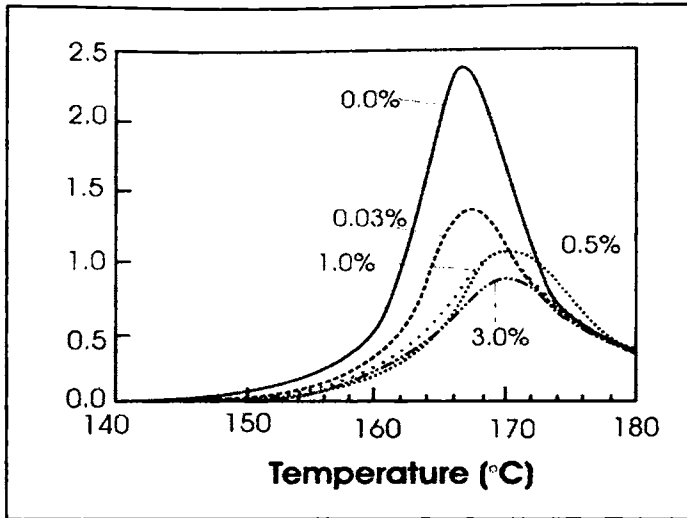
Figure 4c.14 Variation of tan delta of PC- nano ZnO composites (lower curves with decreasing concentration of ZnO)

Loss modulus curves for the PC- nano ZnO composite is given in figure 4c.15. T_g, and tan δ values of PC-ZnO nanocomposite are given in table 4c.5. The DMA glass transition temperatures are consistent with the DSC results. On adding nano ZnO, loss modulus values increases.
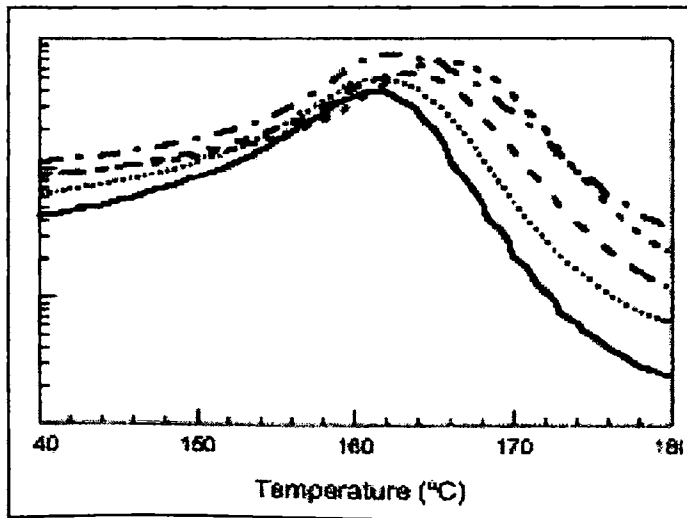

Figure 4c.15 Variation of loss modulus of PC- ZnO nanocomposites (lower curves with increasing concentration of ZnO from 0.0-3.0 wt%)

**Table 4c.5** T_g and tan δ values of PC-nano ZnO composite samples

Sample	T_g °C (from tan δ peak)	Peak values of tan δ at T_g
PC alone	165	2.4
PC/0.03 wt% nano ZnO	166	1.2
PC/0.5 wt% nano ZnO	169	1.1
PC/ 1.0 wt% nano ZnO	170	1.1
PC/3.0 wt% nano ZnO	172	0.7

We note the modulus, $E^* = (\text{loss modulus}^2 + \text{storage modulus}^2)^{1/2}$ for the neat PC is numerically consistent with the tensile modulus reported by the Dow Chemical Co. The T_g of PC-nano ZnO composite increases with ZnO content.

Figure 4c.16 shows the variation of storage modulus of PC- commercial ZnO composites and it is clear that modulii decreased by about 56 % on adding 3.0 % commercial ZnO. There is no significant change in loss modulus values of PC- commercial ZnO composites (figure 4c.17). The height of the tan delta peak (figure 4c.18) maintains the same level on adding commercial ZnO, but the peak value (1.3) is less than the value of neat PC (2.4). The glass transition temperature decreased to 152 °C in PC- commercial ZnO composites.
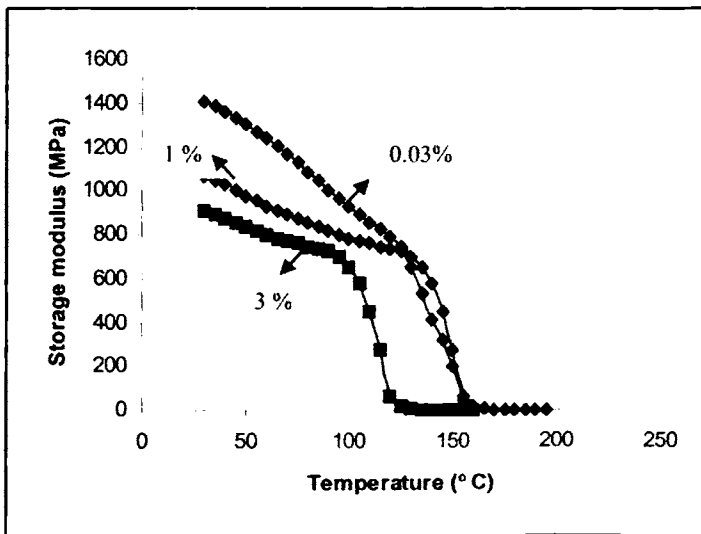
Figure 4c.16 Variation of storage modulus of PC-commercial ZnO composites
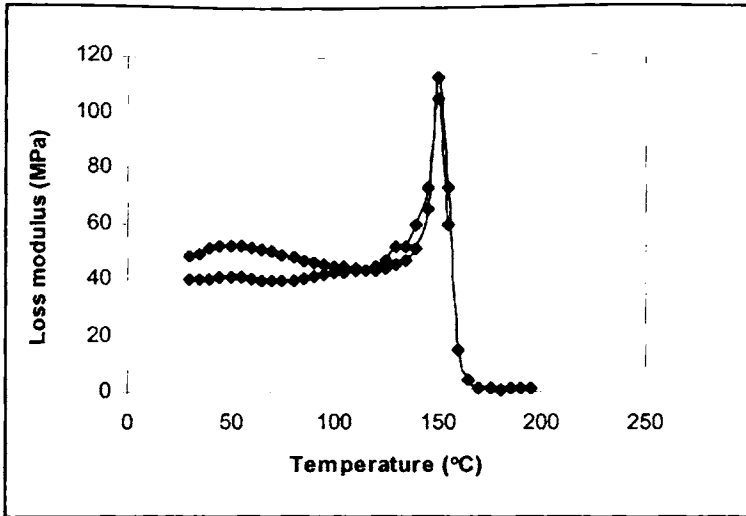
Figure 4c.17 Variation of loss modulus of PC- commercial ZnO composites (lower curves with increasing concentration of ZnO)
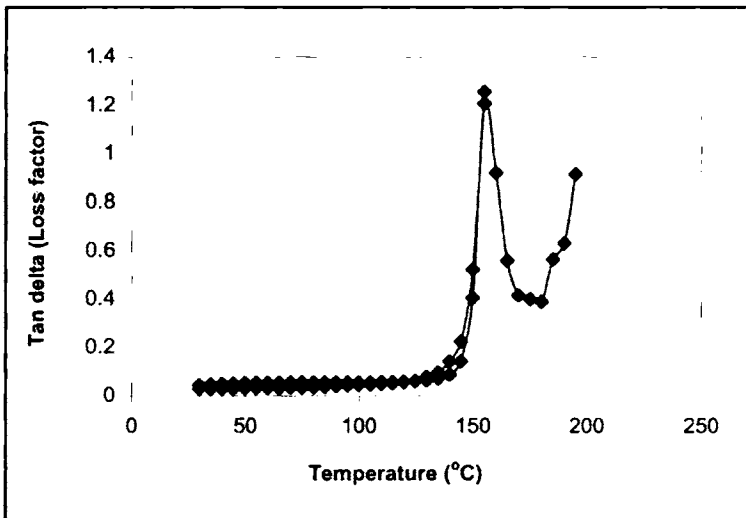
Figure 4c.18 Variation of Tan delta of PC- commercial ZnO composites

Correlation of impact and dynamical properties in terms of tan δ peak values of the nanocomposites has been done. The variation of the impact strength as a function of the total loss tangent peak values for PC- nano ZnO composites and PC- commercial ZnO composites is shown in figure 4c.19 & 4c.20 respectively.
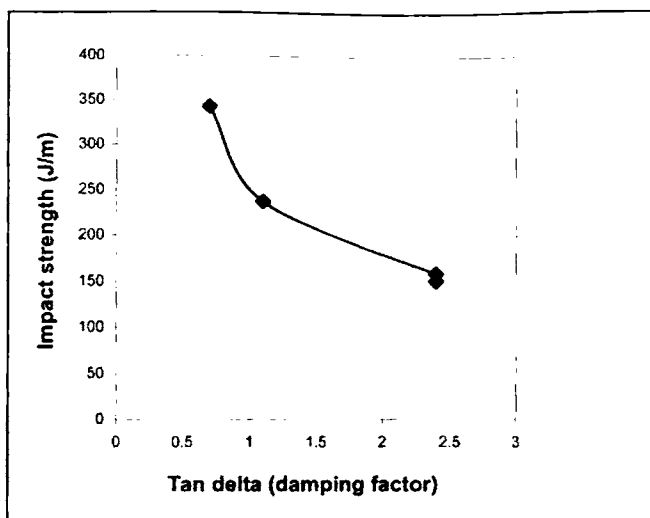
Figure 4c.19 Variation of tan delta with impact strength of PC- nano ZnO composites
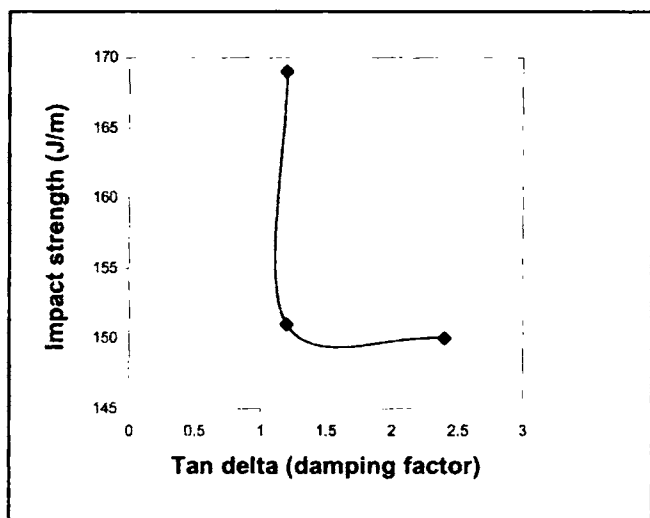
Figure 4c.20 Variation of tan delta with impact strength of PC- commercial ZnO composites

4c.3.5 Melt rheology

The rheological behaviour of PC-ZnO nanocomposites is studied at three different temperatures 230, 240 & 250 °C. Effect of shear stress, filler loading and temperature on rheological behaviour is investigated.

4c.3.5.1 Effect of shear stress on shear viscosity

Figure 4c.21 present the shear viscosity vs. shear stress curves of PC- ZnO nanocomposites at 240 °C with an increasing ZnO concentration from 0.0-3.0 wt%.

We also examined the flow behaviour of PC nanocomposites filled with 1.0 % commercial ZnO. As shear stress increases, the viscosity of PC-ZnO composites decreases in all cases, indicating the pseudoplastic flow behaviour. Effect of temperature on shear viscosity of PC nanocomposites filled with 0.5 % nano ZnO is given in figure 4c.22. With a rise of temperature from 240 to 250 °C the value of shear viscosity decreases, especially at relatively lower apparent shear stress. The melt viscosity increases when the temperature decreases to 230 °C.
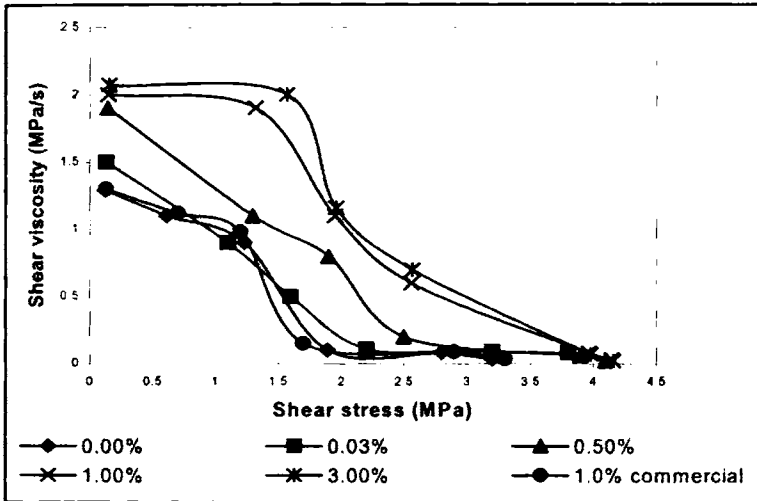
Figure 4c.21 Effect of shear stress on shear viscosity of PC- ZnO nanocomposites
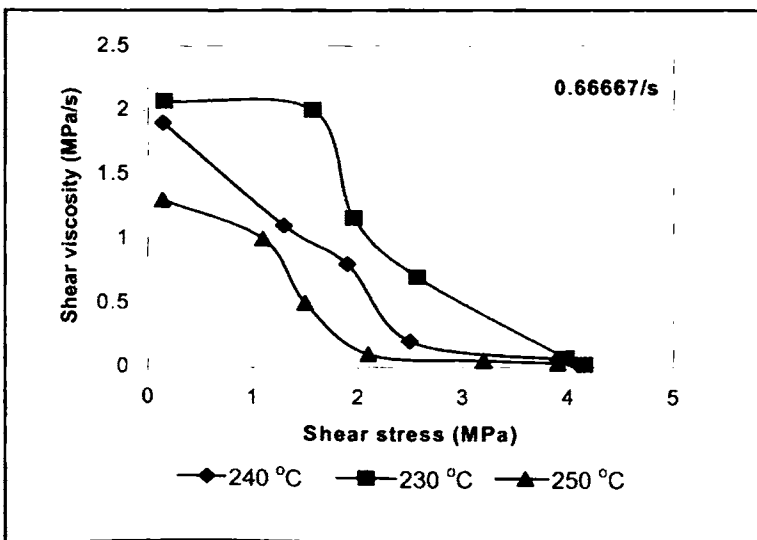
Figure 4c.22 Effect of temperature on shear stress vs. shear viscosity plots of PC-nano ZnO composites filled with 0.5 % ZnO

4c.3.5.2 Effect of filler loading

Figure 4c.23 shows the variation of shear viscosity with increasing concentration of nano ZnO from 0.0-3.0 wt% at six different shear rates. It is clear from the figure that shear viscosity increases with nano ZnO addition and this increase is more prominent at low shear rates and low ZnO concentration. Also it can be seen from the figure that shear viscosity decreases substantially with increasing shear rate, but increases monotonically with increasing nano ZnO loading at a given shear rate.[71,72]

Figure 4c.24 examines the variation of shear viscosity of PC nanocomposites with concentration of commercial ZnO at four different shear rates. It is clear from the figure that viscosity remains constant with ZnO loading. Shear viscosity decreases substantially with increasing shear rate and this decrease in viscosity is more at higher shear rates.
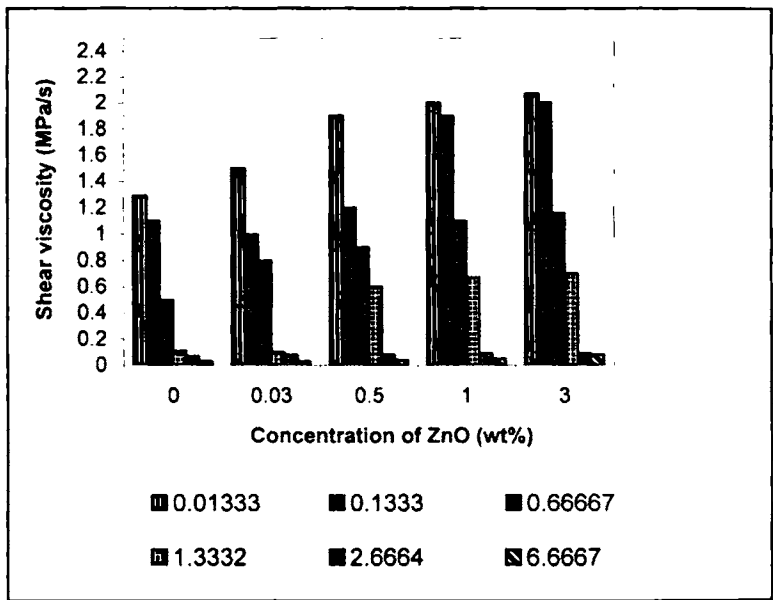
Figure 4c.23 Variation of shear viscosity with concentration of ZnO and shear rates at 240 °C
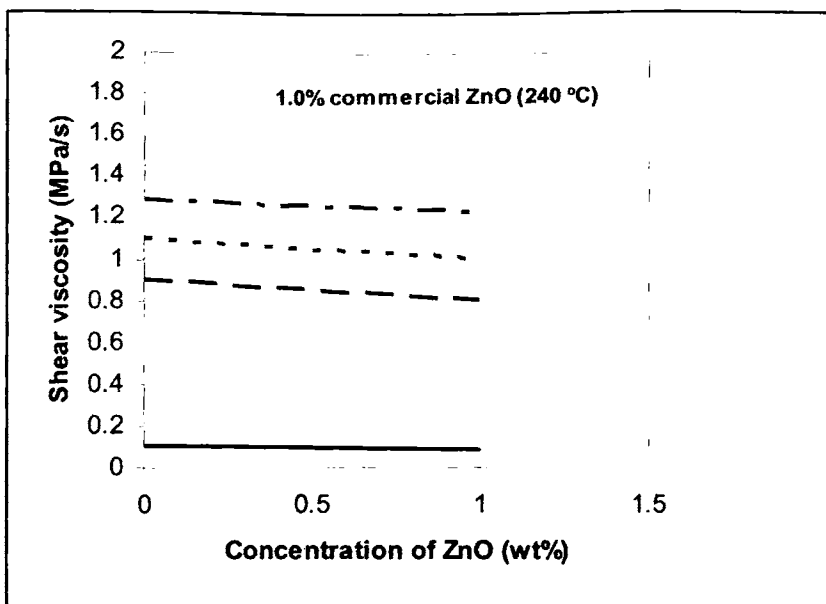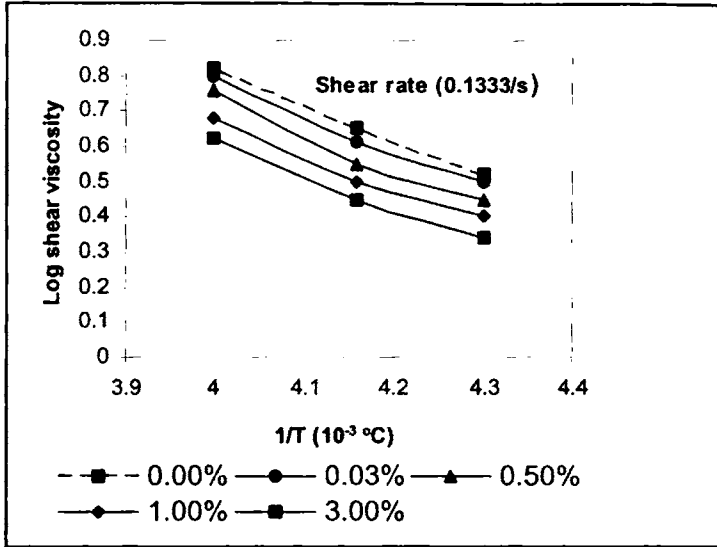
Figure 4c.24 Variation of shear viscosity with concentration of commercial ZnO at four different shear rates at 240 °C [lower curves with decreasing shear rate]

4c.3.5.3 Effect of temperature

Shear viscosities of pure PC and nanocomposite melts decrease with increasing extrusion temperature in the range of 230–250 °C, demonstrating that increasing temperature improves the flow behavior of the polymer melts. However, the effect of temperature on shear viscosity changes with the shear rate. The data indicate that the temperature sensitivity of shear viscosity is higher in lower shear rate region, and drops at higher shear rates. This phenomenon is in agreement to the fact that elevating shear rate always accompanied by a rapid decrease of the entanglement density of macromolecules and the melt viscosity.[77] The Arrhenius plots of PC- nano ZnO composites at two different shear rates is given in figure 4c.25 (a) & (b). A good linear correlation was found in the plot of ln η_a vs. 1/T, which has proved the appropriateness of the Arrhenius–Eyring equation. Values of E_a obtained from the slopes of these plots are given in table 4c.6. The activation energy of a material provides valuable information on the sensitivity of the material towards the change in temperature. The higher the activation energy, the more temperature sensitive the material

will be. Therefore, such information is highly useful in selecting the processing temperature of polymeric materials. From the table 4c.6, it can be observed that the activation energy of flow of the nanocomposites increases upto 0.5 % addition of ZnO and thereafter decreases at lower shear rates and at higher shear rates, it remains constant.


(a)
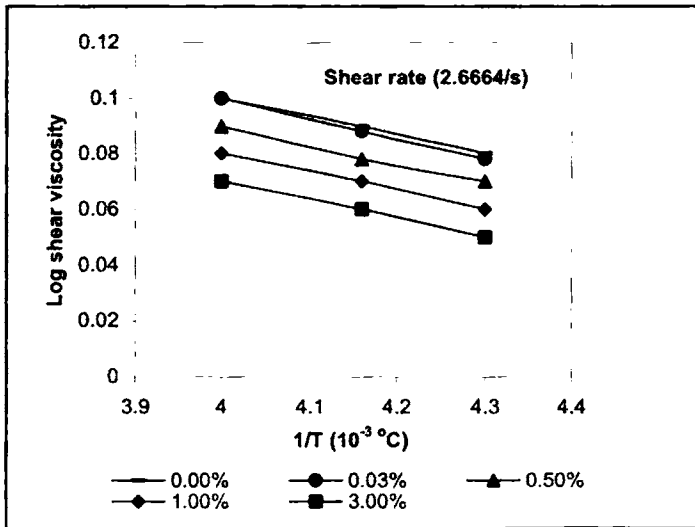
(b)

Figure 4c.25 (a) & (b) Variation of log viscosity with 1/T for the PC- nano ZnO composites

Table 4c.6 Activation energies of PC-nano ZnO composites at two shear rates

Concentration of ZnO (wt%)	Activation energy (KJ/mol)	
	0.1333/s	2.6664/s
0.0	1001.4	66.57
0.03	1004.4	66.57
0.5	1039.9	66.57
1.0	937.80	66.86
3.0	936.39	73.34

4c.3.5.4 Flow behaviour index (n′)

The effects of temperature and concentration of ZnO on the flow behaviour indices of the samples have been studied in detail. The extent of pseudoplasticity or non-Newtonian behaviour of the materials can be understood from n′ values. Pseudoplastic materials are characterized by n′ below 1. Flow behaviour index values of PC-nano ZnO composites at 240 °C and 250 °C are given in figure 4c.26. It is clear from the figure that n′ decreases with increasing concentration of ZnO and also with increasing temperature. This suggests that the system becomes more pseudoplastic as the ZnO content and temperature increases. A similar trend of decreasing values of n′ with an increase in temperature has been reported.[75,79,80]
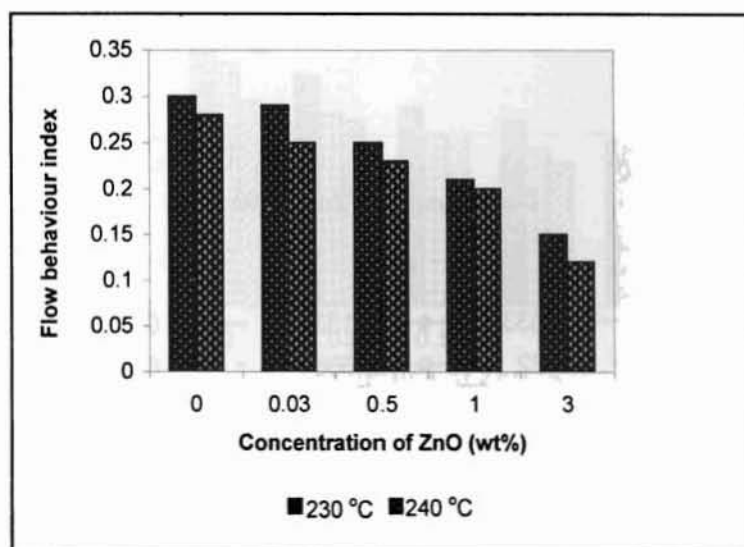
Figure 4c.26 Variation of melt flow index with concentration of ZnO at two temperatures

4c.3.5.5 Die swell

Die swell, called Barus effect is an important parameter for characterizing polymer melt elasticity in an extrusion flow and is related to the quality of the end products.

4c.3.5.5.1 Effect of shear rate and concentration of ZnO

Figure 4c.27 shows the plots of the die swell ratio, de/dc for PC and PC-ZnO nanocomposites at 240 °C at six different shear rates. The die swell ratio increases obviously with increasing shear rate at a constant ZnO content. It is noticeable that at a constant shear rate, the die swell ratio decreases slightly with a rise of ZnO content. At lower shear rates the decrease in die swell ratio is more compared to the decrease at higher shear rates. Figure 4c.28 shows the variation of die swell ratio of PC nanocomposites filled with 1.0 % commercial ZnO at different shear rates. Die swell ratio slightly increases with ZnO loading.
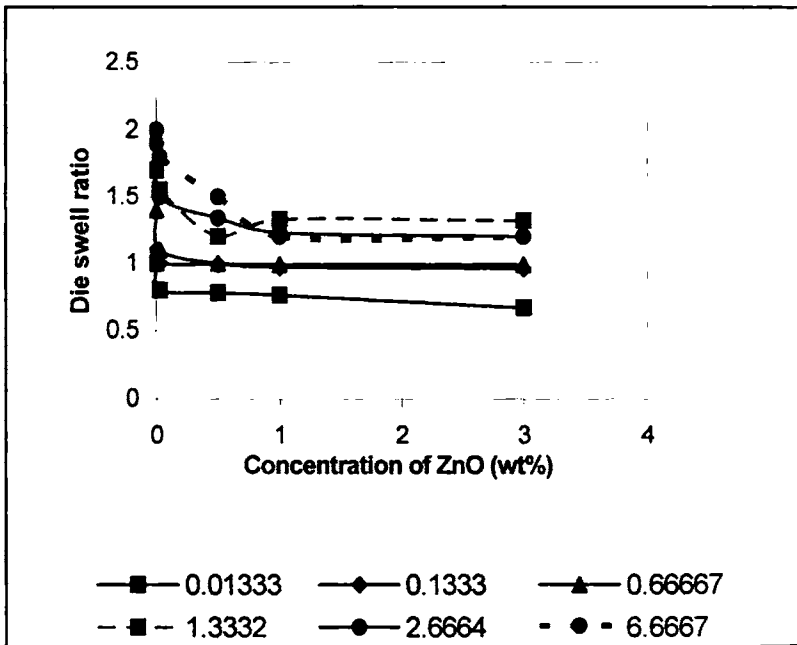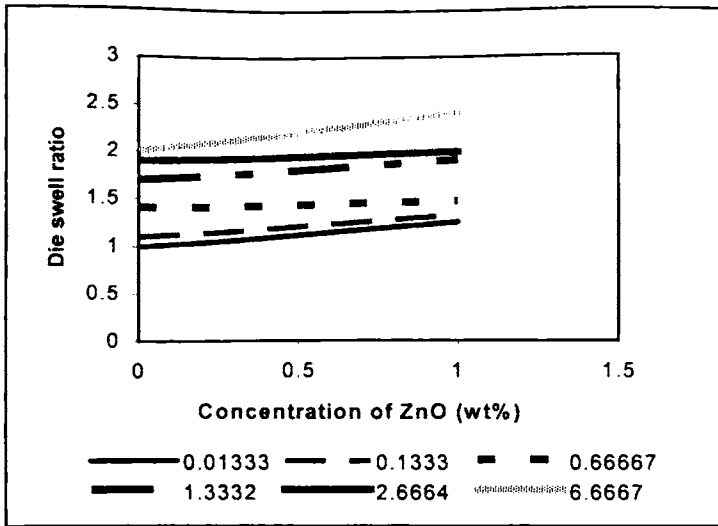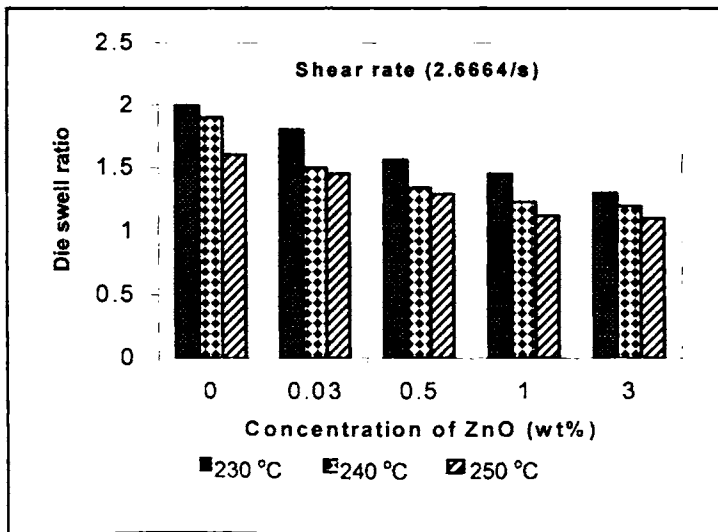

Figure 4c.27 Variation of die swell ratio of PC- nano ZnO composites with concentation of ZnO at different shear rates

Figure 4c.28 Variation of die swell ratio of PC- commercial ZnO composites with concentration of ZnO at different shear rates

4c.3.5.5.2 Effect of temperature

Variation of die swell ratio of PC-nano ZnO composites at 3 different temperatures is given in figure 4c.29. It is clear from the figure that die swell ratio decreases with temperature.
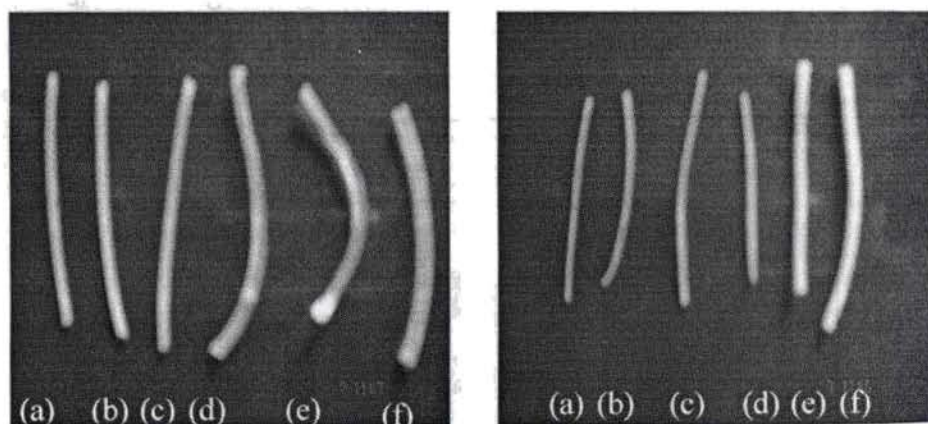

Figure 4c.29 Variation of die swell ratio of PC- nano ZnO composites with temperature

4c.3.5.6 Extrudate deformation studies

The appearance of the extrudate of neat PC and nanocomposites with 1.0 % ZnO at six different shear rates is shown in figure 4c.30 (a) and (b) respectively. From the figure it is clear that the extrudate distortion tendency increases with the shear rate. At a low shear rate, the extrudate has a smooth surface; however, at a higher shear rate, the surface becomes rougher. The ZnO content of the nanocomposite also plays a major role in determining the surface characteristics. As the ZnO content increases, the surface roughness also increases. Several factors contribute towards surface irregularity. It has been conclusively shown by photographic techniques[87,88] that a fracturing or breaking of the elastically deformed flowing polymer stream occurs at the entrance to the capillary itself at some critical shear stress. Another factor contributing towards extrudate distortion is the successive sticking and slipping of the polymer layer at the wall in the capillary.[89,90] Moreover, there may be an effect at the exit as well. Shear thinning behaviour of the nanocomposites is clearly visible in these photographs.

Figure 4c.30 Extrudate photographs of (a) neat PC and (b) PC-nano ZnO composites filled with 1.0 % ZnO at six different shear rates (a) 0.01333/s (b) 0.1333/s (c) 0.66667/s (d) 1.3332/s (e) 2.6664/s (f) 6.6667/s

4c.4 Conclusions

This study showed that nano ZnO is a good modifier for engineering thermoplastics like PET, PA 6 and PC. Nanocomposites have been prepared through a simple melt compounding route. Melt compounded nano ZnOs have been shown to act as effective nucleating agents for PET and PA 6 crystallization. The nano ZnO at a concentration as low as 300 ppm enhanced the crystallization temperature during melt cooling by 32 °C in PET matrix and 10 °C in PA 6 matrix, and reduced melt's isothermal crystallization time by more than 50 % in PET matrix and 20 % in PA 6 matrix. No crystalline melting endothermic peaks were observed in the DSC curves of PC-ZnO composites. A comparison of the nucleation ability of nano ZnO with commercial ZnO also revealed that nano ZnOs are potentially very attractive candidate as nucleating agents. Thermogravimetric analysis showed improved thermal stability for nano ZnO composites than their counterparts. The improved mechanical properties (tensile, flexural and impact) of the nano ZnO composites revealed that a small concentration of nano ZnO could substantially reinforce all the three matrices. In PC matrix impact strength and modulus decreased. Scanning electron microscope studies revealed that the reinforcement mechanism of nano ZnO is shear yielding in PET and PC matrix, and cavitation in PA 6 matrix. The dynamic mechanical analysis indicated an improvement in storage and loss modulus of nano ZnO composites than commercial ZnO composites. The rheological characteristics revealed that shear viscosity of the nano ZnO composites increased with concentration of nano ZnO and decreased with increasing shear stress. Melt flow index value and die swell ratio decreased with nano ZnO concentration indicating pseudoplastic behaviour of the flow. Activation energies of the nanocomposites increased with modification at lower shear rates. Apparently, nano ZnO is a good modifier compared to commercial ZnO for engineering thermoplastics.

4c.5 References

1. Whinfield JR, Dickinson JT. UK Patent No. 578079 (1946).

2. Lim JY, Kim SY. J Polym Sci Polym Phys 2001, 39, 964.

3. Lim JY, Kim SY. J Appl Polym Sci 1999, 71, 1283.

4. Rim PB, Nelson CJ. Properties of PET fibres with high modulus and low shrinkage (HMLS).

5. Joseph EG, Wilkes GL. Prepr Am Chem Soc Div Polym Chem 1983, 24, 304.

6. Sukhadia AM, Done D, Baird DG. J Polym Eng Sci 1990, 30, 519.

7. Battacharya SK, Tendokar A, Misra A. Mol Cryst Liq Cryst 1987, 153, 501.

8. Sharma SK, Tendokar A, Misra A. Mol Cryst Liq Cryst 1988, 157, 597.

9. Ou CF, Huang SL. J Appl Polym Sci 2000, 76, 587.

10. Ou CF, Li WC, Chen YH. J Appl Polym Sci 2002, 86, 1599.

11. Zhu P, Ma D. Eur Polym J 2000, 36, 2471.

12. Reinsch VE, Rebenfeld L. J Appl Polym Sci 1994, 52, 649.

13. Anoop Anand K, Agurwal US, Rani Joseph. J of Appl Polym Sci 2007, 104 (5), 3090.

14. Ke Y, Yang Z, Zhu C. J Appl Polym Sci 2002, 85, 2677.

15. Saujanya C, Imai Y, Tateyama H. Polym Bull 2002, 49, 69.

16. Murthy NS, Grubb DT, Zero K, Nelson CJ, Chen G. J Appl Polym Sci 1998, 42, 2527.

17. Wu G, Yoshida T, Cuculo JA. Polymer 1998, 39, 6473.

18. Jang LW, Kang CM, Lee DC. J Polym Sci Polym Phys 2001, 39, 719.

19. Hsu YG, Lin FJ. J Appl Polym Sci 2000, 75, 275.

20. Lee DC, Jang, LW. J Appl Polym Sci 1996, 61, 1117.

21. Yano K, Usuki A, Okada A. J Polym Sci Part A: Polym Chem 1997, 35, 2289.

22. Wang D, Zhu J, Yao Q, Wilkie CA. Chem Mater 2002, 14, 3837.

23. LeBaron PC, Wang Z, Pinnavaia TJ. Appl Clay Sci 1999, 12, 11.

24. Qureshi N, Stepanov EV. J Polym Sci Polym Phys 2000, 38, 1679.

25. Wu TM, Chang CC. J Polym Sci Polym Phys 2000, 38, 15.

26. Polyakova A, Stepanov EV. J Polym Sci Polym Phys 2001, 39, 1911.

27. Ming-Hai Qu, Yu-Zhong Wang, Chuan Wang, Xin-Guo Ge, De-Yi Wang, Qian Zhou. European Polymer Journal 2005, 41, 2569.

28. Lee A, Lichtenhan JD. J Appl Polym Sci 1999, 73, 1993.

29. Hwang SH, Paeng SW, Kim JY, Huh W. Polym Bull 2003, 49, 329.

30. Wang D, Zhu J, Yao Q, Wilkie CA. Chem Mater 2002, 14, 3837.

31. Li GZ, Wang L, Toghiani H, Daulton TL, Pittman Jr CU. Polymer 2002, 43, 4167.

32. Joseph EG, Wilkes GL. Prepr Am Chem Soc Div Polym Chem 1983, 24, 304.

33. Sukhadia AM, Done D, Baird DG. J Polym Eng Sci 1990, 30, 519.

34. Pawlak A, Zinck P, Galeski A, Gerard JF. Macromol Symp 2001, 169, 197.

35. Rong JF, Jing ZH, Li HQ, Sheng M. Macromol Rapid Commun 2001, 22, 329.

36. Sumita M, Shizuma T, Miyasaka K, Ishikawa K. J Macromol Sci Phys 1983, B22, 601.

37. Sumita M, Tsukurmo T, Miyasaka K, Ishikawa K. J Mater Sci 1983, 18, 1758.

38. Zhu P, Ma D. Eur Polym J 2000, 36, 2471.

39. Reinsch VE, Rebenfeld L. J Appl Polym Sci 1994, 52, 649.

40. Dong Wook Chae, Byong Chul Kim. Composites Science and Techology 2007, 67 (7-8), 1348.

41. Morgan AB, Jeffrey WG. Journal of Applied Polymer Science 2003, 87, 1329.

42. Uksuki A, Tukigase A, Kato M. Polymer 2002, 43, 2185.

43. Jiang-Ping He, Hua-Ming Li, Xia-Yu Wang, Yong Gao. European Polymer Journal 2006, 42, 1128.

44. Van Bennekom ACM, Gaymans RJ. Polymer 1997, 38, 657.

45. Bouma K, de Wit G, Lohmeijer JHGM, Gaymans RJ. Polymer 2000, 41, 3965.

46. Agarwal US, G de Wit, Lemstra PJ. Polymer 2002, 43, 5709.

47. Ou CF. J Appli Polym Sci 2003, 89, 3315.

48. Ou CF, J Polym Sci Part B: Polym Phys 2003, 41, 2902.

49. Anoop Anand K, Agarwal US, Rani Joseph. Polymer 2006, 47, 3976.

50. Wu T, Ke Y. Thin Solid Films 2007, 515 (13), 5220.

51. Hongxia Zhao, Robert KY Li. Polymer 2006, 47, 3207.

52. Jianguo Tang, Yao Wang, Haiyan Liu, Laurence A Belfiore. Polymer 2004, 45, 2081.

53. Dong Wook Chae, Byong Chul Kim. J of Appl Polym Sci 2006, 99, 1854

54. Cheng-Fang Ou. J of Polym Phys Part B: Polymer Physics 2003, 41, 2902.

55. Ke YC, Long CF, Qi ZN. J Appl Polym Sci 1999, 71, 1139.

56. Wan T, Chen L, Chua YC, Lu XH. J Appl Polym Sci 2004, 94, 1381

57. Wang S, Hu Y, Song L, Wang Z, Chen Z, Fan W. Polym Degrad Stab 2002, 77, 423.

58. Lazzeria A, Zebarjadb SM, Pracellac M, Cavalierd K, Rosad R. Polymer 2005, 46, 827.

59. Yuan Q, Misra RDK. Polymer 2006, 47, 4421.

60. Saha AK, Das S, Bhatta D, Mitra BC. J of Appl Polym Sci 1999, 71, 1505.

61. Okamoto M, Morita S, Taguchi H, Kim Y, Kotaka T, Tateyama H. Polymer 2000, 41, 3887.

62. McNally T, Murphy WR, Lew C, Turner R, Brennan G. Polymer 2003, 44, 2761.

63. Lim YT, Par OO. Rheol Acta 2001, 40(3), 220.

64. Krishnammoorti R, Giannelis EP. Macromolecules 1997, 30, 4097.

65. Wang Z, Zhang Z. J of Dispersion Sci and Tech 2007, 28 (2), 309.

66. Li J, Zhou CX, Wang G. J Appl Polym Sci 2003, 89, 3609.

67. Giannelis EP. Appl Organometal Chem 1998, 12, 675.

68. Manias E, Hadziioannou G, Brinke GT. Langmuir 1996, 12, 4587.

69. Galgali G, Ramesh C, Lele A. Macromolecules 2001, 34, 852.

70. Fornes TD, Yoon PJ, Keskkula H, Paul DR. Polymer 2001, 42, 9929.

71. Kim TH, Jang LW, Lee DC, Choi HJ, Jhon MS. Macromol Rapid Commun 2002, 23, 191.

72. Kim TH, Lim ST, Lee CH, Choi HJ, Jhon MS. J Appl Polym Sci 2003, 87, 2106.

73. Lim SK, Kim JW, Chin I, Kwon YK, Choi HJ. Chem Mater 2002, 14, 1989.

74. Kim KY, Lim HJ, Park SM, Lee SJ. Polymer-Korea 2003, 27, 377.

75. Asaletha R, Groeninckx G, Kumaran MG, Sabu Thomas. J Appl Polym Sci 1998, 69, 2673.

76. Oommen Z, Thomas S, Premalatha CK, Kuriakose B. Polymer 1997, 38, 5611.

77. Li SC, Jarvela PK, Jarvela PA. J Appl Polym Sci 1999, 71, 1641.

78. Eyring HJ. J Chem Phys 1936, 4, 283.

79. Thomas S, Kuriakose B, Gupta BR, De SK. Plast Rubber Process Appl 1986, 6, 85.

80. Saini DR, Shenoy AV. J Macromol Sci Phys 1983, B22, 437.

81. Choi HJ, Kim SG, Hyun YH, Jhon MS. Macromol Rapid Commun 2001, 22, 320.

82. Mendelson RA. Polym Eng Sci 1976, 16, 690.

83. White JL, Crowder JW. J Appl Polym Sci 1974, 18, 1013.

84. Minagawa N, White JL. J Appl Polym Sci 1976, 20, 501.

85. Liang JZ, Li RKY, Tang CY, Cheung SW. J Appl Polym Sci 2000, 76, 419.

86. Shenoy AV. Rheology of filled polymer systems. Kluwer Academic Publishers; 1999. p. 99–102, 118–24, 317–21.

87. Tordella JP. J Appl Phys 1956, 27, 454.

88. Bagley EB, Birks AM. J Appl Phys 1960, 31, 556.

89. Tordella JP. J Appl Polym Sci 1963, 7, 215.

90. Benbow JJ, Lamb P. SPE Trans 1963, 3, 7.

91. Peter C, Lebaron, Zhen Wang, Thomas Pinnavaia J. Appl Clay Sci 1999, 15, 11.

92. Vlasveld DPN, Groenewold J, Bersee HEN, Picken SJ. Polymer 2005, 46, 12567.

93. Salame M. Plastic Film Sheet 1986, 2, 321.

94. Kojima Y, Usuki A, Kawasumi M, Okada O, Fukushima Y, Kurachi T, Kamigato O. J Mater Res 1993, 8, 1185.

95. Junrong Zheng, Richard W, Siegel C, Gregory Toney. J of Polym Sci Part B: Polymer Physics 2003, 41, 1033.

96. Kohen MI et al. Nylon Plastics, Wiley, New York, 1973.

97. Fornes TD, Paul DR. Polymer 2003, 44, 3945.

98. Liang Shen, Yijian Lin, Qiangguo Du, Wei Zhong, Yuliang Yang. Polymer 2005, 46, 5758.

99. Srinath G, Gnanamoorthy R. J of Materials Sciences 2005, 40, 2897.

100. Yang F, Ou Y, Yu Z. J Appl Polym Sci 1998, 69, 355.

101. Taubert A, Glasser G, Palms D. Langmuir 2002, 18(11), 4488.

102. Khanna YP, Kumar R, Reimschuessel AC. Polym Eng Sci 1988, 28(24), 1601.

103. Aharoni SM. n-Nylons, their synthesis, stricture, and properties. Chichester, New York, Wiley, 1997.

104. Tjong SC, Liang GD, Bao SP. J of Appl Polym Sci 2006, 102, 1436.

105. Pinnavaia TJ, Beall GW. Polymer-Clay Nanocomposites, John Wiley 2001, 3.

106. Tanniru M, Misra RDK. Mater Sci Eng A 2005, 405, 178.

107. Argon AS, Bartczak Z, Cohen RE, Muratog'lu OK. Novel mechanisms of toughening semi-crystalline polymers. In: Pearson RA, Sue HJ, Yee AF, editors. Toughening of plastics advances in modeling and experiments, Symposium series 759. Washington, DC, ACS, 2000. p.98.

108. Bartczak Z, Argon AS, Cohen RE, Weinberg M. Polymer 1999, 40, 2347.

109. Wilbrink MWL, Argon AS, Cohen RE, Weinberg M. Polymer 2001, 42, 10155.

110. Thio YS, Argon AS, Cohen RE, Weinberg M. Polymer 2002, 43, 3661.

111. Bucknall CB. Toughened plastics. London: Applied Science, 1977.

112. Pham HT, Weckle CL, Ceraso JM. Adv Mater 2000, 12, 1881.

113. Balakrishnan S, Neelakantan NR, Jaisankar SN. J Appl Polym Sci 1999, 74, 2102.

114. Jiang W, Tjong SC. Poly Degrad Stab 1999, 66, 241.

115. Li ZM, Yang MB, Hang R. J Mater Sci 2001, 36, 2013.

116. Mekhilef N, Ait Kadi A, Ajji A. Eng Sci 1992, 32(13), 894.

117. Yoon PJ, Humter DL, Paul DR. Polymer 2003, 44, 5323.

118. Zhou J, Liu N, Li Y, Ma YJ. Silicate Bull 1999, 6, 50.

119. Huang X, Lewis S, Brittain WJ, Vaia RA. Macromolecules 2000, 33, 2000.

120. Vonfalka B, Rellensman W. Makromolekulare Chemie 1965, 75, 122.

121. Alizadeh A, Sohn S, Quinn J, Marand H, Shank LC, Iler HD. Macromolecules 2001, 34, 4066.

122. MacNulty B. J Polym 1968, 9, 41.

123. Kambour RP, Gruner CL, Romagosa EE. Macromolecules 1974, 7, 248.

124. Mercier JP, Groeninckx G, Lesne M. J Polym Symp 1967, 16, 2059.

125. Jonza JM, Porter RS. J Polym Sci Part B: Polym Phys 1986, 24, 2459.

126. Xianbo Hu, Alan J Lesser. Polymer 2004, 45, 2333.

127. Yiqiang Zhao, David A Schiraldi. Polymer 2005, 46, 11640.

MODIFICATION OF COMMODITY THERMOPLASTICS USING NANO ZINC OXIDE

Abstract

This chapter is divided into three parts. Modification of three commodity thermoplastics like [polypropylene (PP), high density polyethylene (HDPE), polystyrene (PS)] with nano ZnO is discussed. Commodity thermoplastics based nanocomposites have been prepared with nano ZnO through a simple melt-compounding route. Melt compounded nano ZnOs have been shown to act as effective nucleating agents for PP and HDPE crystallization. Reinforcement of commodity thermoplastics by ZnO nanoparticles was tremendous compared to commercial ZnO. The dynamic mechanical analysis indicated an improvement in storage and loss modulus of nano ZnO composites than commercial ZnO composites. The rheological characteristics revealed that shear viscosity of the nano ZnO composites increased with concentration of nano ZnO and decreased with increasing shear stress. Melt flow index value and die swell ratio decreased with nano ZnO concentration, indicating pseudoplastic behaviour of the flow. Nano ZnO is found to be a good modifier compared to commercial ZnO, for commodity thermoplastics.

MODIFICATION OF POLYPROPYLENE USING NANO ZINC OXIDE

5a.1 Introduction

Polypropylene (PP) is a semi-crystalline commodity thermoplastic and is known for its balance of strength, modulus and chemical resistance. It have many potential applications in automobiles, appliances and other commercial products in which creep resistance, stiffness and some toughness are demanded in addition to weight and cost savings. The main attraction of PP is its high performance-to-cost ratio. However, its inadequate stiffness and brittleness limits its versatile application to some extent. PP can be easily modified to achieve greatly enhanced properties. The incorporation of inorganic particulate fillers has been proved to be an effective way of improving the mechanical properties, and in particular the toughness, of polypropylene. For example, Stamhuis[1] has shown that talc filler can significantly increase the impact resistance of polypropylene if it is physically blended with either an SBS or an EPDM elastomer. Hadal and Misra[2] have reported that modulus of polypropylene has been improved by talc and wollastonite. Radhakrishnan and Saujanya[3] have reported that the needle-shaped $CaSO_4$ filler can improve the properties of polypropylene with its high aspect ratio. However, the typical filler content needed for significant enhancement of these properties can be as high as 10–20 % by volume. At such high particle volume fractions, the processing of the material often becomes difficult, and since the inorganic filler has a higher density than the base polymer, the density of the filled polymer is also increased. The advantages of polymers, i.e., their ease of processing and lightweight, get therefore lost, and which limits various applications of polypropylene composite. To overcome this drawback, a composite with improved properties and lower particle concentration is highly desired. With regard to this, the newly developed nanocomposites would be competitive candidates.

Nanoparticle filled polymers are attracting considerable attention since they can produce property enhancement that are sometimes even higher than the conventional filled polymers at volume fractions in the range of 1–5 %. Rong et al. have reported tensile performance improvement of low nanoparticle filled polypropylene composite.[4] Wu et al.[5] have investigated tensile behaviour of nanophased polypropylene. With regard to reinforcement effects, considerable research can be found in recent literature[6-19] on improving mechanical properties of PP using various kinds of inorganic fillers. It is now well recognized that the use of inorganic fillers is a useful tool for improving stiffness, toughness, hardness, chemical resistance, dimensional stability and gas barrier properties of PP.[6-9] The effects of inorganic fillers on the mechanical and physical properties of the PP composites strongly depend on the filler size, shape, aspect ratio, interfacial adhesion, surface characteristics and degree of dispersion.[10-16] Typically, the physical and mechanical properties of the polymers that contain nano-sized particles are superior to those containing micron-sized particles of the same filler type.[17-19] A large number of inorganic materials, such as glass fibre, talc, calcium carbonate, and clay minerals has been successfully used as additives to improve the strength of polymers.[20-25] Improvement in various properties of PP composites were reported in literature.[26-31]

This study is aimed at producing PP nanocomposites with varying ZnO (0.0-3.0 wt%) concentration and analyzing them for their crystallization, thermal, mechanical, dynamic mechanical performances and melt rheology.

5a.2 Experimental

A simple melt-compounding route was adopted for the preparation of PP-ZnO nanocomposites. The melt compounding was performed using Thermo Haake Rheocord 600 mixing chamber with a volume capacity of 69 cm^3 fitted with a roller type rotors operating at 40 rpm for 8 min at 180 °C. Nanocomposites at different concentrations (0.0–3.0 wt%) of ZnO were prepared. In all cases the torque stabilized to a constant value in this mixing

time. The crystallization behaviour, thermal stability, morphology, melt rheology, mechanical and dynamic mechanical property of the nanocomposites using commercial and nano ZnO were analyzed according to the details summarized in sections 2.3 of this thesis.

5a.3 Results and discussion
5a.3.1 Differential scanning calorimetry
5a.3.1.1 Non-isothermal

There are only 10–15 investigations in the research literature that focus on nanoscale-size nucleating agents for polymers, in general, and even fewer that employ nanoparticles of zinc oxide.[32] This contribution describes how zinc oxide nanoparticles affect the morphology and crystallization temperature of polypropylene. In a crystalline polymer composite, crystallization may have a major influence on the structure of composites and thereby on the mechanical properties, such as tensile and impact strength. For example, Maiti et al.[33] noted that the extent of intercalation increased with the crystallization temperature, and the size of spherulites decreased with increase in clay content in maleic anhydride grafted PP–clay nanocomposites.

Nonisothermal crystallization behaviour of PP nanocomposites has been studied extensively for different systems PP–carbon nanotubes, PP-surface-treated SiO_2, isotactic PP–CaCO$_3$, PP–montmorillonite clay.[34-36]

In this section we compared the crystallization characteristics of PP matrix using nano and commercial ZnO. The effect of nano ZnO on the crystallization characteristics of melt compounded PP-ZnO nanocomposite samples was analyzed first with non-isothermal DSC experiments. The crystallization temperatures (T_c), the apparent melting temperatures (T_m), the corresponding enthalpies (ΔH_c and ΔH_m) and the degree of supercooling ($\Delta T = T_m - T_c$) are also reported in table 5a.1.

**Table 5a.1** DSC-determined thermal characteristics of PP-nano ZnO composite samples

Concentration of ZnO (wt%)	T_c (°C)	ΔH_c (J/g)	T_m (°C)	ΔH_m (J/g)	ΔT (°C)
0.0	104.53	87.1	165.1	87.3	60.57
0.03	110.64	86.0	167.3	86.7	56.66
0.1	112.10	85.2	165.8	85.6	53.7
0.5	113.36	85.9	167.5	86.4	54.14
1.0	114.26	84.0	166.0	85.3	51.7
2.0	116.41	86.3	166.9	85.1	50.49
3.0	117.23	87.3	167.9	86.9	50.67

Figure 5a.1 shows the DSC cooling scans of PP-ZnO nanocomposite samples. During cooling from the melt, the ZnO containing samples show crystallization exotherms earlier than neat PP, as also seen from the corresponding T_c values indicated in table 5a.1. It is found that the nanocomposite sample containing ZnO at a concentration as low as 0.03 wt% enhances the rate of crystallization in PP as the cooling nanocomposites melt crystallizes at a temperature 6 °C higher as compared to neat PP. The T_c values continue to increase with increasing ZnO concentration, but at a slower rate, as with further 100 fold increase in ZnO concentration from 0.03 to 3.0 wt%, the additional T_c increase is only about 7 °C. In other words, there is a saturation of the nucleant effect at low ZnO concentrations, resulting in diminishing dependence on the increasing ZnO induced nucleation, possibly because of large surface area and good dispersion of ZnO. The melting temperature slightly increases and one possible reason for the increase in the melting temperature is that the processed nanocomposite has a smaller particle size, thus has a larger specific surface and a larger interfacial area, resulting in a stronger interaction between the polymer matrix and the more finely dispersed particles. The stronger interaction constrains the movement of molecular chains, leading to a higher melting point. The enthalpies of PP and nanocomposites stay unaffected. The ΔT values for the PP-nano ZnO were 56-50 °C smaller than that of neat PP (60 °C) [figure 5a.2]. From

these results it is clear that nano ZnO content affects the crystallization rate and takes the role of a nucleating agent on PP crystallization due to its enormous surface area. The results indicated that the incorporation of ZnO nanoparticles had little effects on the degree of crystallinity of PP.
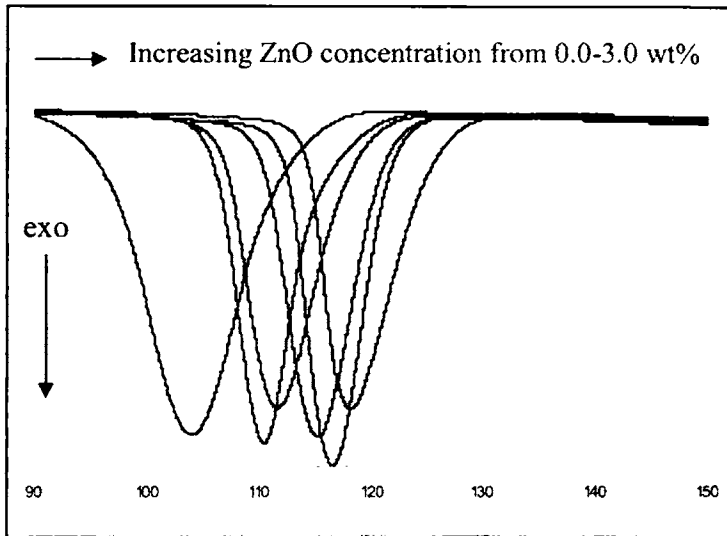
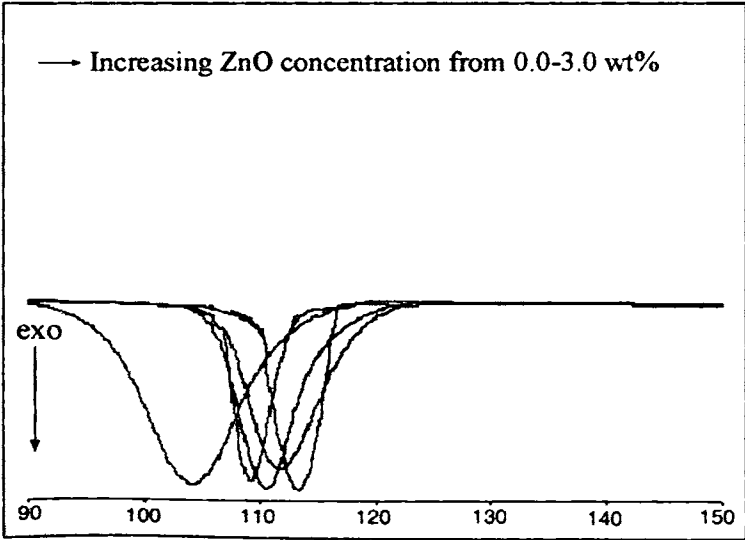**Figure 5a.1** DSC cooling scans of PP-ZnO nanocomposite samples
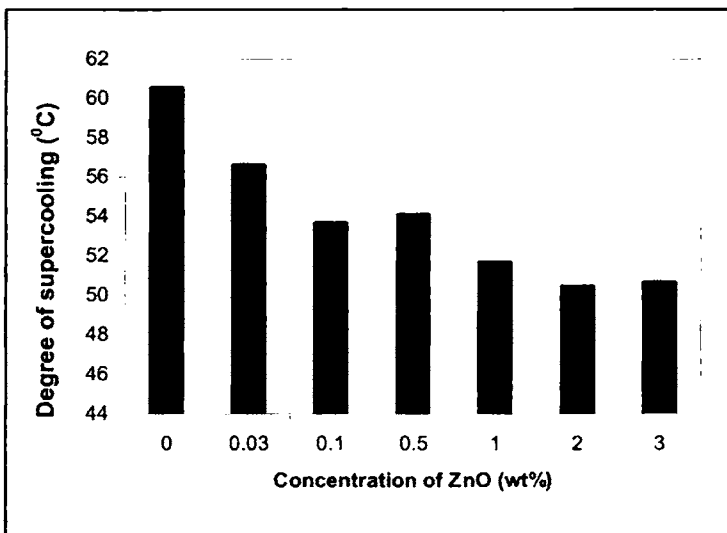
**Figure 5a.2** Variation of degree of supercooling with concentration of nano ZnO

Tang et al.[32] reported an increase in crystallization temperature marginally by 2 or 3 °C in the presence of 2 wt% MicroZn or NanoZn. Nanoparticles of

SiO_2 increased the crystallization temperature of PP by 3– 4 °C and reduced spherulite size. Marco et al.[37] observed an increase in the nucleation density (i.e., 71 % efficiency), an increase in the degree of crystallinity. Zhao et al.[38] observed that the melting behaviour of PP and enthalpies were not affected by increasing ZnO nanoparticle content. However, the crystallization temperature tends to shift to higher values with increasing ZnO nanoparticle content. This implies that the existence of ZnO nanoparticles facilitates the crystallization of PP and this effect becomes more evident with higher nanoparticle content.

Change in T_c is only about 7 °C when commercial ZnO is loaded from 0.0-3.0 wt%, but, in the case of nano ZnO the value is about 13 °C. DSC cooling scans of PP- commercial ZnO nanocomposites is given in figure 5a.3. ΔH_c, ΔH_m, T_c and T_m values remains a constant with commercial ZnO loading. The ΔT values for the PP-commercial ZnO composites remains a constant near the neat PP value (60 °C). Figure 5a.4 compares the crystallization temperatures of PP nanocomposites. From this figure it is clear that nano ZnO is a good nucleating agent for PP matrix than commercial ZnO.

Figure 5a.3 DSC cooling scans of PP- commercial ZnO nanocomposite samples
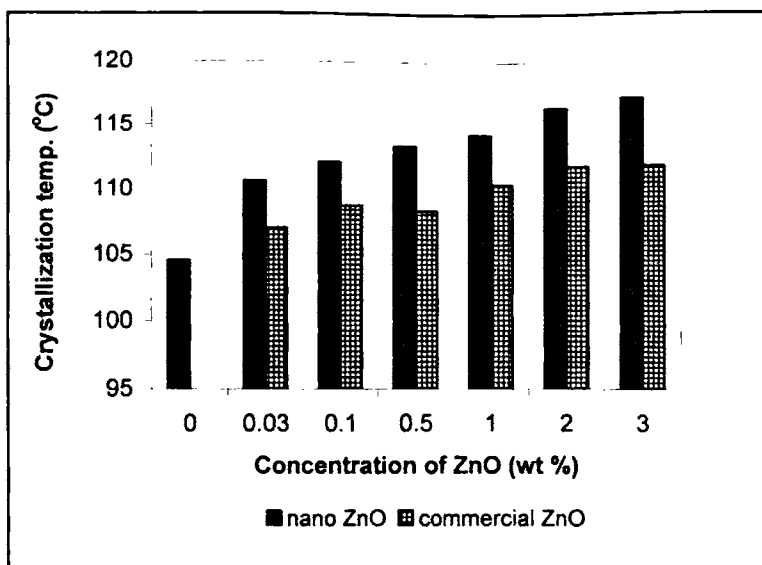
Figure 5a.4 Comparison of crystallization temperatures of PP matrix using nano and commercial ZnO

The interfacial interaction plays a critical role in the free energy of cluster formation and the rate of nucleation; the weak interaction lowers the rate of nucleation. This may be the reason for decrease in nucleating ability of commercial ZnO compared to nano ZnO.

5a.3.1.2 Isothermal crystallization characteristics

Figure 5a.5 shows the typical isothermal crystallization curves of PP-nano ZnO composite samples at four temperatures (110 °C, 115 °C, 120 °C and 125 °C). The time corresponding to the maximum in the heat flow rate (exotherm) was taken as peak time of crystallization (t_{peak}). Such peaks are seen at each of the four isothermal crystallization temperatures for the neat polymer, with the earlier or faster crystallization (smaller t_{peak}) corresponding to lower temperature of isothermal crystallization. In the case of neat PP, no sharp peak is seen at the highest temperature of 125 °C because crystallization is very slow and would require longer time than the 4 minutes employed in the DSC program. On the other hand for the nanocomposite sample with 3.0 wt% ZnO, the rate of crystallization is so fast that no exotherm peak is seen at these temperatures,

because crystallization occurs already during the cooling scan (60 °C/min) employed to reach those temperature, resulting in absence of exothermic peak in the heat flow curves at those temperature. In the case of 0.03 wt% nanocomposite, no peak is seen at the lowest temperature of 110 °C.
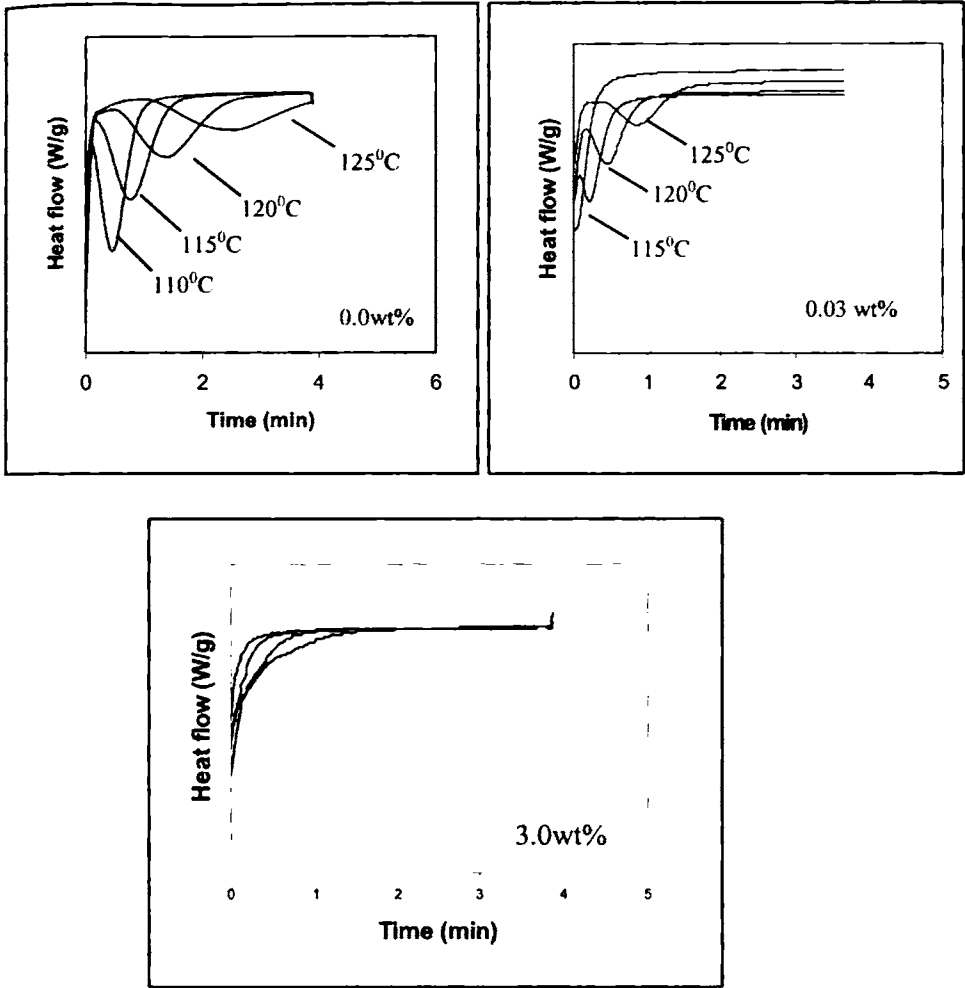
Figure 5a.5 Isothermal crystallization curves of PP-ZnO nanocomposite samples at four temperatures (110 ºC, 115 ºC, 120 ºC and 125 ºC)

The peak time of crystallization at each of the temperatures for all the PP-nano ZnO composite samples are plotted against the isothermal crystallization temperature (figure 5a.6). We notice that the t_{peak} values for the nanocomposite samples reduced to less than 50 % as compared to neat PP in presence of ZnO at a concentration as low as 0.03 wt%. With an increasing ZnO concentration there

is further increase in the crystallization rate, demonstrating the role of ZnO in enhancing the rate of crystallization.
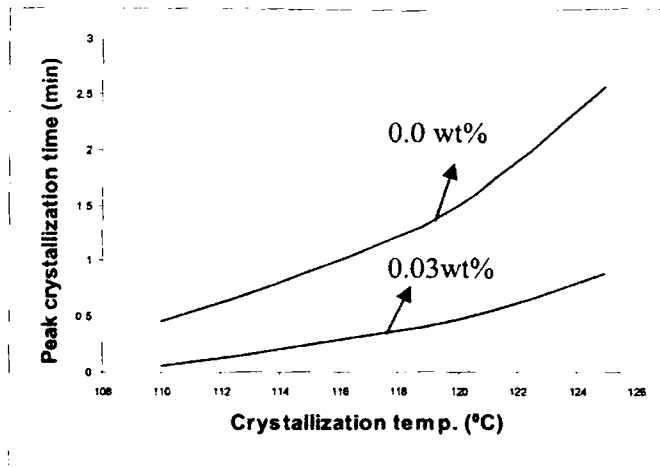
Figure 5a.6 Effect of nano ZnO concentration on the peak crystallization time of the nanocomposites at different isothermal crystallization temperatures

Gutzow et al.[39] developed a theory to explain why inorganic particles nucleate crystallization in linear polyolefins. Nucleation efficiencies are related to (i) bond energies between the nucleating agent and the polymeric crystals, and (ii) crystallographic mismatches between the substrate and polymer.

5a.3.2 Thermogravimetry

Thermal stability is an important property and the nanocomposite morphology plays an important role.[40] TGA studies shows that inorganic fillers, which are widely used industrially to improve the mechanical properties of polymer materials, have different effects on the thermal oxidation of PP. The decomposition temperature of PP was increased by adding nano silica[41], clay[42], $CaCO_3$[43] etc.

The TG and DTG curves of neat PP and its composites using nano ZnO are given in figures 5a.7 & 5a.8 respectively. The temperature of onset of degradation T_i ($^\circ$C), the temperature at which the rate of decomposition is 10 % [$T_{10\%}$ ($^\circ$C)], the temperature at which the rate of decomposition is maximum

(T_{max}) (°C), the temperature at which the rate of decomposition is 50% [$T_{50\%}$ (°C)], the peak degradation rate and the residue at 800 °C are given in table 5a.2. PP degrades in a single step. The thermal degradation profiles of PP and PP-nano ZnO composites exhibit that most of the degradation events occur between 270 and 500 °C. The nanocomposites degrade over a much narrower temperature range than the pure polymer because the onset point of degradation shifts to higher temperature. The degradation starts at a temperature of 285 °C and the peak rate of degradation is 2.914%/min at corresponding T_{max} 419.0 °C for PP and in nanocomposites, T_i is 331 °C on adding 3.0 wt% of nano ZnO, indicating improved thermal stability of the nanocomposites. The T_{max} temperature also showed an improvement in thermal stability. Residue at 800 °C is only about 1.665 % for PP. Adding 3.0 wt% of ZnO, residue increased to 2.460 %. The peak rate of decomposition decreased from 1.471 to 1.054 %/min in nanocomposites. This increase in the thermal stability of the nanocomposites may result from the strong interaction between the nano ZnO and PP molecules. Gilman[44] suggested that the thermal stability of polymers in the presence of fillers is due to the hindered thermal motion of polymer molecular chains.
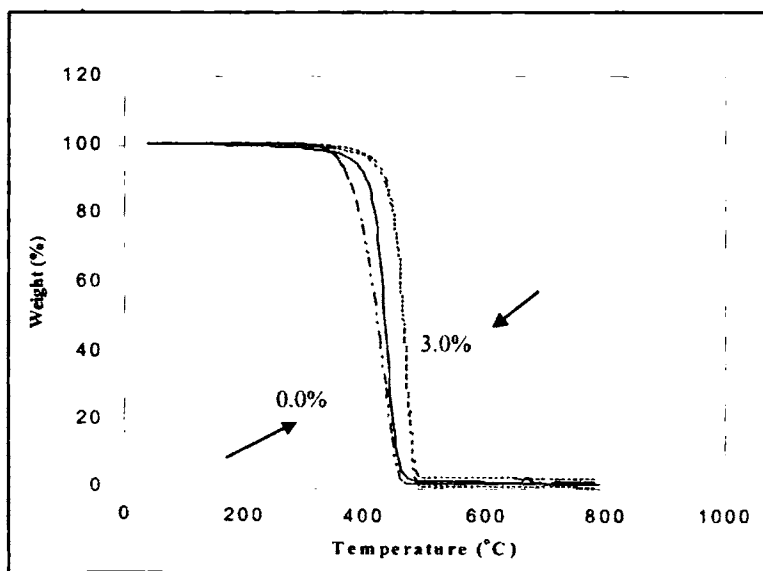
Figure 5a.7 Thermogravimetric traces of PP– nano ZnO composite samples (lower curves with increasing ZnO concentrations 0.0, 0.03, 1.0, 3.0 wt%)
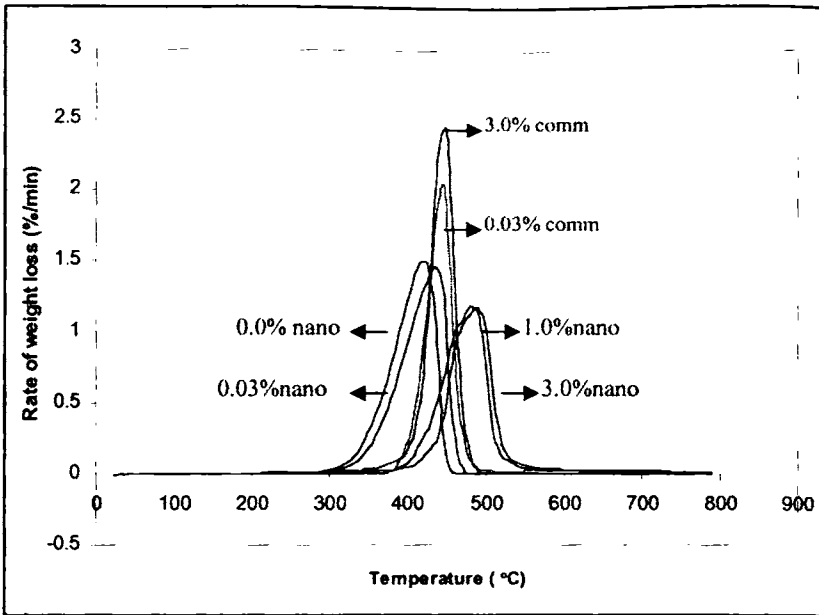
Figure 5a.8 Differential thermogravimetric traces of PP-ZnO composites

Table 5a.2 Degradation characteristics of PP and its nanocomposites

Concentration of ZnO	T_1 (°C) onset	$T_{10\%}$ (°C)	Residue at 800 °C (%)	Peak rate of decomposition (%/min)	$T_{50\%}$ (°C)	T_{max} (°C)
0	285	367.5	1.665	1.471	400.2	419.0
0.03	294	398.4	1.863	1.456	412.7	436.9
1.0	329	402.3	2.232	1.163	432.1	454.8
3.0	331	412.7	2.460	1.054	458.1	470.7

On adding commercial ZnO, themal stability increases (figure 5a.9). The T_{max} temperature increases from 419 °C to 450 °C on adding 3.0 wt% commercial ZnO. But the peak rate of decomposition increased from 1.471 to 2.436 %/min, which is clear from the DTG graph (figure 5a.8).
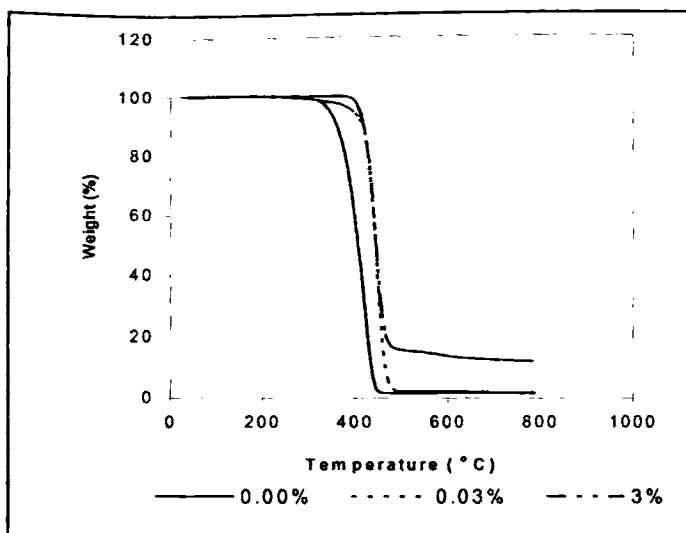
Figure 5a.9 Thermogravimetric traces of PP– commercial ZnO composite samples (lower curves with increasing ZnO concentrations 0.0, 0.03, 1.0 and 3.0 wt%)

5a.3.3 Mechanical properties
5a.3.3.1 Torque studies

It has been widely established that the mechanical properties of crystalline polymeric materials strongly depend on processing conditions and techniques used to process the materials. The same polymeric material can be processed into a soft and flexible product or a strong and stiff product under different conditions. The variation of mixing torque with time of mixing at different ZnO loading is shown in figure 5a.10. A mixing time of 8 minutes was fixed since the torque stabilized to a constant value during this time. The temperature of the mixing chamber was fixed as 180 °C. The stabilization of the torque may be related to the attainment of a stable structure after a good level of mixing. Initially torque increases with the charging of PP, but decreases with melting. After homogenization of PP, ZnO was added at 2.5 min. There is a little increase in torque on continued mixing with ZnO. After mixing, the torque value is found to be steady. It is clear from figure that there is no degradation taking place during the mixing stage. Similar trend in torque is observed when commercial ZnO is mixed with PP.
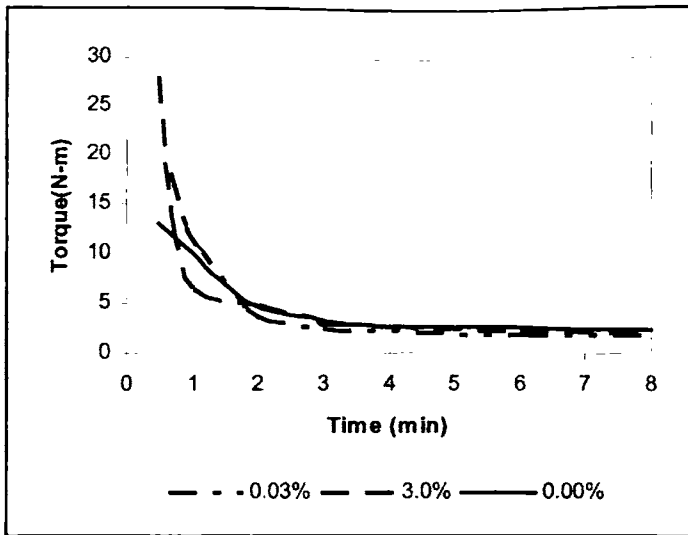
Figure 5a.10 Variation of mixing torque with time of mixing at different ZnO loading

5a.3.3.2 Tensile properties

The most important property of nanocomposites is the enhancement in mechanical properties even at low percentages of nano ZnO loading.

The effects of the nano ZnO on the mechanical properties of PP are summarized in table 5a.3.

Table 5a.3 Tensile properties of PP-nano ZnO composites

Concentration of ZnO (wt%)	Tensile strength (MPa)	Tensile modulus (GPa)	Elongation (%)	Shore D hardness	Energy to max (J)	Tensile toughness (J/m)
0.0	29.94	0.977	8.147	55	0.899	408.6
0.03	31.66	1.078	7.972	57	0.948	469.3
0.1	32.71	1.099	7.043	58	0.989	466.5
0.5	32.96	1.144	6.825	62	1.082	527.8
1.0	33.09	1.201	6.129	65	1.151	523.1
2.0	34.56	1.255	5.998	69	1.292	642.7
3.0	36.59	1.323	5.892	70	1.309	654.9

The results in table 5a.3 show an increase in the tensile modulus and strength of PP with an increasing concentration of ZnO from 0.0 to 3.0 wt%. From 0.0 to 1.0 wt% the change in tensile strength is about 10 % and modulus is about 23 %. From 1.0 to 3.0 wt% the same improvement in tensile strength (about 10 %) is observed, and modulus (about 10 %). The Shore D hardness also supports this reinforcement. The elongation to break is found to decrease with an increasing loading of ZnO, indicating that the nanocomposites become somewhat brittle. This behaviour is also observed when talc and calcium carbonate are added to PP matrix, which also provided an effective reinforcement to PP matrix.[45] Energy to max and tensile toughness (energy/ thickness of the sample) values increases by about 45 % and 60 % respectively with 3.0 wt% ZnO loading. Area under the stress-strain curve is directly proportional to the energy absorbed. Since there is an increase in energy absorption some modification has taken place, which is clear from the increase in tensile toughness values (figure 5a.11). These results demonstrate that even a small fraction of ZnO provide effective reinforcement to the PP matrix. This is due to better interaction between PP matrix and ZnO nanoparticles.
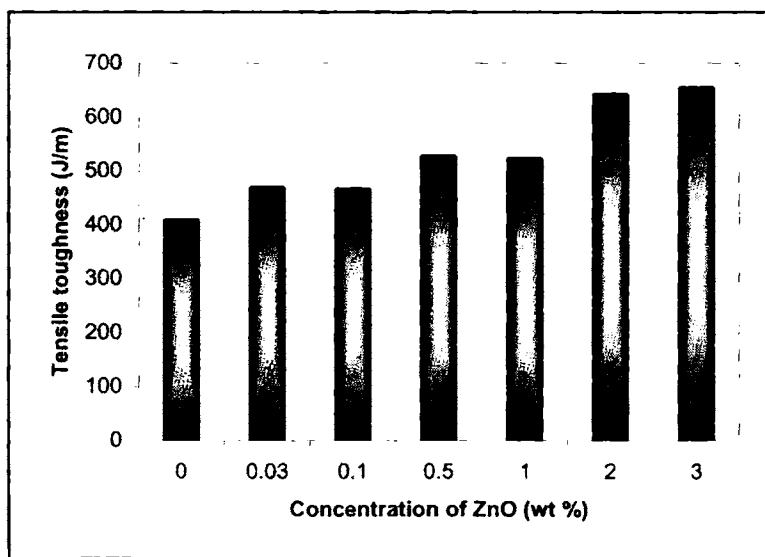
Figure 5a.11 Variation of tensile toughness values with nano ZnO concentration

Reinforcement of PP matrix is also achieved by mixing with commercial ZnO. Figure 5a.12 and 5a.13 compares the tensile strength and modulus of PP-ZnO composites using nano and commercial ZnO. The increase in tensile strength and modulus is about 7 % and 5 % respectively on adding 3.0 % commercial ZnO.
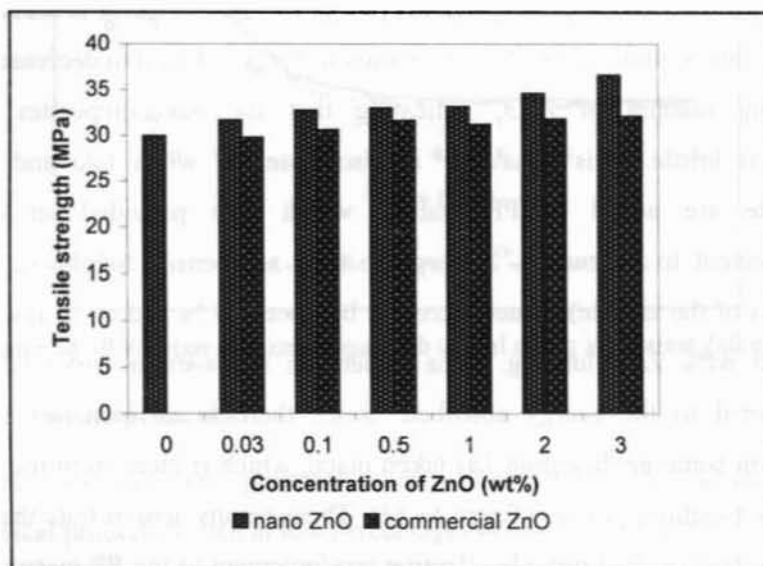

Figure 5a.12 Comparison of tensile strength of PP- ZnO composites using nano and commercial ZnO
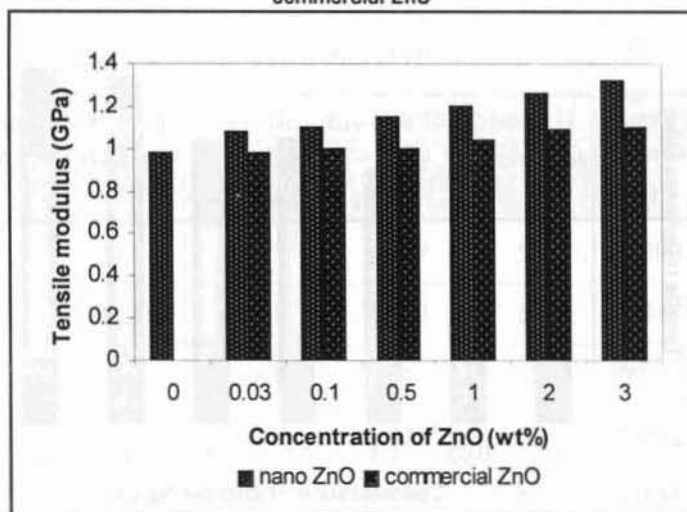

Figure 5a.13 Comparison of tensile modulus of PP- ZnO composites using nano and commercial ZnO

Energy to maximum, tensile toughness and elongation to break of PP-commercial ZnO nanocomposite is given in the table 5a.4. Elongation to break of nanocomposites decreases, energy to maximum and tensile toughness values increases to about 13 % and 18 % respectively on adding 3.0 % commercial ZnO. For the PP-clay nanocomposite by Kodgire et al.[46], the increase in tensile modulus was about 35 %, whereas the increase in the strength was about 10 % on adding 4 % clay.

Table 5a.4 Tensile properties of PP-commercial ZnO nanocomposites

Concentration of ZnO (wt%)	Elongation (%)	Shore D hardness	Energy to max (J)	Tensile toughness (J/m)
0.0	8.147	55	0.899	408.6
0.03	7.180	57	0.901	412.9
0.1	6.367	59	0.923	409.3
0.5	6.260	61	0.938	423.5
1.0	4.294	63	1.001	451.5
2.0	3.841	65	1.075	460.1
3.0	3.450	68	1.021	484.2

This study showed that the dispersion of the nanoparticles will have a significant effect on the mechanical properties of the nanocomposite. It is reasonable to propose that there is an intimate contact between the polymer molecules and the nanoparticles, so the strong interaction between the polymer and filler increases the mechanical properties. As for commercial ZnO particles, the contact is weak, because the particles aggregate in the polymer, so the extent of improvement in mechanical properties are lower when compared to the properties of PP-nano ZnO composites.

Stress-strain curves for PP and its nanocomposite is shown in figure 5a.14. From the stress strain curve it is clear that with nano ZnO loading the elongation (%)

decreases, indicating that the composite becomes somewhat brittle compared with neat PP.
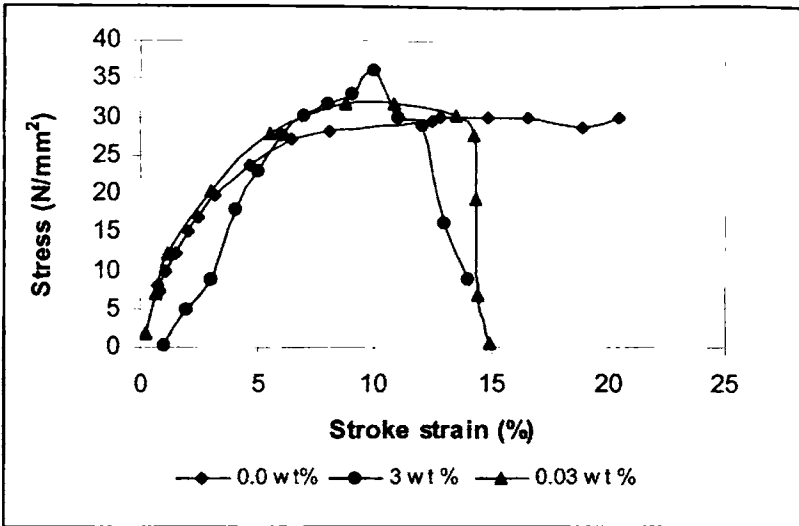

Figure 5a.14 Stress-strain curve for PP and its nanocomposites

5a.3.3.3 Morphology of the fractured surfaces

The scanning electron micrographs of the fractured surfaces of the tensile test specimens have been studied to acquire an insight into the mechanism of reinforcement. Figure 5a.15 (a) shows the fracture surface for unmodified PP. It indicates the necking phenomena of PP molecule, because of its ductility. There is no sign of significant plastic deformation. From figure 5a.15 (b), it is clear that nano ZnO exist as dispersed particles and the morphology gets substantially modified. Nano ZnO loading leading to stress whitening is prevalent in this figure, indicating localized plastic deformation. In PP- ZnO nanocomposites shear yielding is the reinforcement mechanism. There is complete stress transfer from the PP matrix to nano rod having high aspect ratio. There is no sign of extensive particle agglomeration as compared to PP-commercial ZnO nanocomposite fracture surface shown in figure 5a.15(c), where we can see large agglomerates and the dispersion is inhomogeneous.
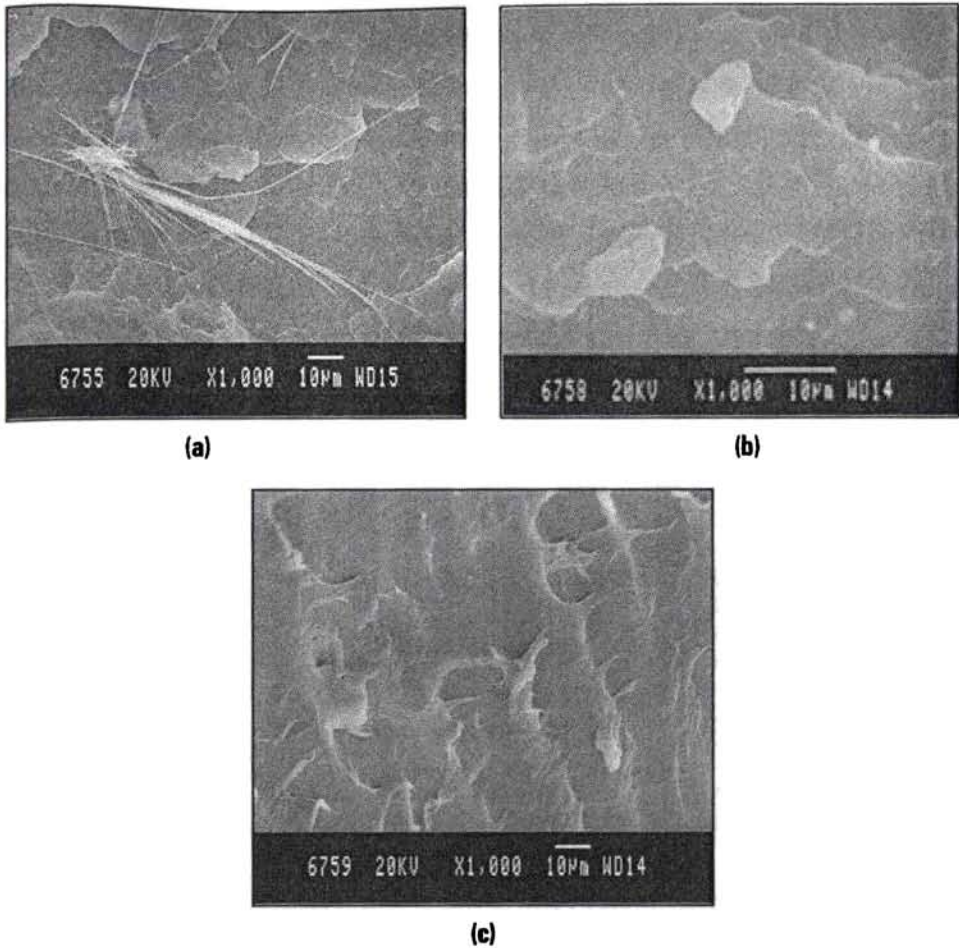
Figure 5a.15 Fracture surface of (a) unmodified PP matrix showing necking phenomena (b) PP-nano ZnO composite showing stress whitening (c) PP- commercial ZnO composite

5a.3.3.4 Flexural properties

A comparison of flexural strength and modulus of PP-ZnO nanocomposites using nano and commercial ZnO is shown in figure 5a.16 (a) & 5a.16 (b) respectively. With nano ZnO, the flexural modulus as well as the strength of PP increases considerably. For example, incorporation of nano ZnO at the level of 3.0 wt%, modulus increases by around 45 % and strength by around 42 %. With commercial ZnO, the flexural modulus and strength increases by around 2 % and 11 % respectively. The effective reinforcement is due to smaller particle size, high surface area, uniform dispersion and good interfacial interaction of nano ZnO with PP matrix. Nano ZnO has a unique structure, and so it is easily

inserted into the matrix, increasing the contact area between the ZnO and matrix. Moreover, from the perspective of reinforcement of composite, nano ZnO will increase the flexural strength and flexural modulus than commercial ZnO, because it has a higher aspect ratio. Chen et al.[47] also reported the reinforcement by ZnO. For the PP-clay nanocomposite by Kodgire et al.[46] the increase in flexural modulus was about 25 %, whereas the increase in the strength was about 30% on adding 4 % clay.
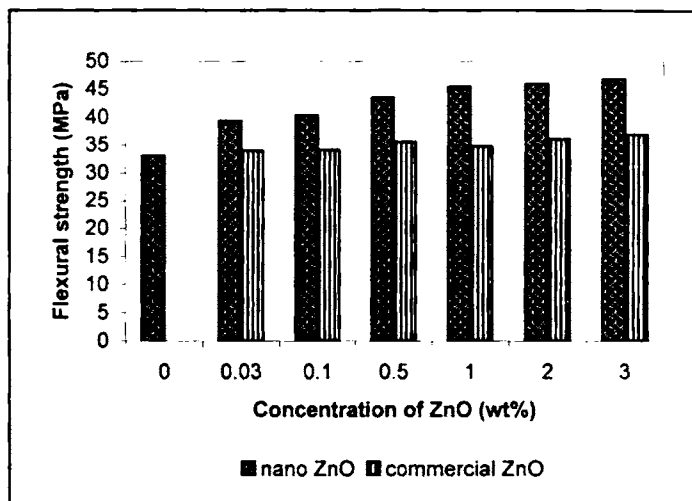
Figure 5a.16 (a) Comparison of flexural strength of PP- ZnO nanocomposites using nano and commercial ZnO
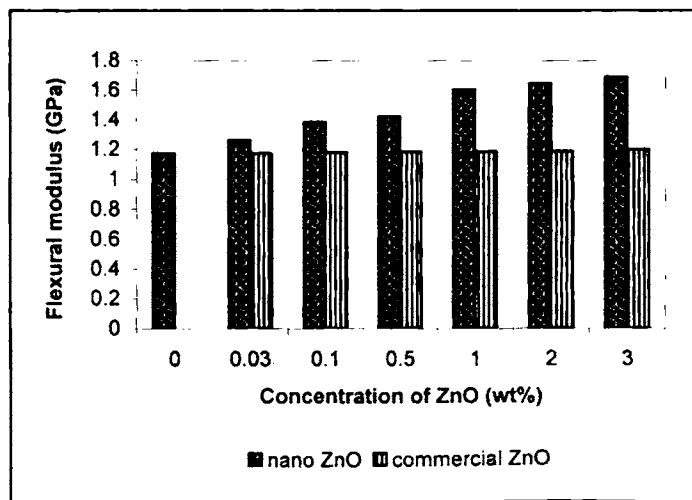
Figure 5a.16 (b) Comparison of flexural modulus of PP- ZnO nanocomposites using nano and commercial ZnO

5a.3.3.5 Impact strength

Unnotched Izod impact strength of PP-ZnO nanocomposites using nano and commercial ZnO is compared in figure 5a.17. With commercial ZnO, the impact strength increases by about 75 %, but with nano ZnO, the increase is about 210 % on adding 3 wt% of ZnO. The addition of ZnO does not increase percentage crystallinity, so there is a positive effect on impact strength. The increase in impact strength is evidenced by the tensile toughness values given in figure 5a.11. So the toughness of PP is improved with ZnO addition.
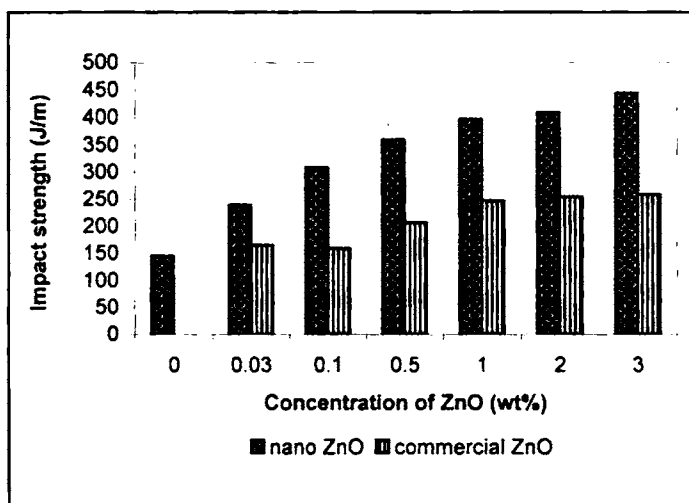
Figure 5a.17 Comparison of unnotched Izod impact strength of PP- ZnO nanocomposites using nano and commercial ZnO

Thio et al.[48] reported that the introduction of micrometer-scale $CaCO_3$ particles led to an improvement in the Izod impact strength of PP by up to four times. It was found that the main toughening mechanisms were crack deflection and interfacial debonding and plastic deformation of interparticle matrix ligaments. Recently, Chan et al.[25] reported that the fracture toughness of PP increased five-fold by incorporating nanometer-scale (ca. 40 nm) $CaCO_3$ particles, and the $CaCO_3$ nanoparticles acted as stress concentrators to promote toughening mechanisms. In our case ZnO acts as stress concentrators to promote toughening mechanism. Nanoclay exhibited a striking variation in impact toughness behaviour.[49]

5a.3.4 Dynamic mechanical analysis (DMA)

An increase in storage modulus was observed in PP- ZnO nanocomposites by Zhao et.al.[38] This is expected owing to the stiffness improvement effect of inorganic ceramic particles.

The DMA results for the dynamic storage modulus of the PP-ZnO nanocomposite samples at room temperature as a function of temperature at 1 Hz are shown in figure 5a.18. It shows a slow decrease of the modulii with temperature after the glass transition temperature. The storage modulii of the nanocomposite samples increases substantially with the nano ZnO concentration (about 37 % increase with 1 wt% and about 73 % increase with 3 wt% nano ZnOs) due to the stiffening effect of ZnO, and indicating efficient stress transfer between the PP matrix and ZnOs. But the storage modulus decreases,(about 27 % with 1 wt% and 55 % with 3 wt % ZnOs) on adding commercial ZnO. The storage modulus of nanocomposites at 50 °C & 100 °C is given in table 5a.5.

a. 3.0% commercial ZnO b. 0.03% commercial ZnO c. 0.0% d. 0.03% nano ZnO
e. 1.0% nano ZnO f. 3.0% nano ZnO
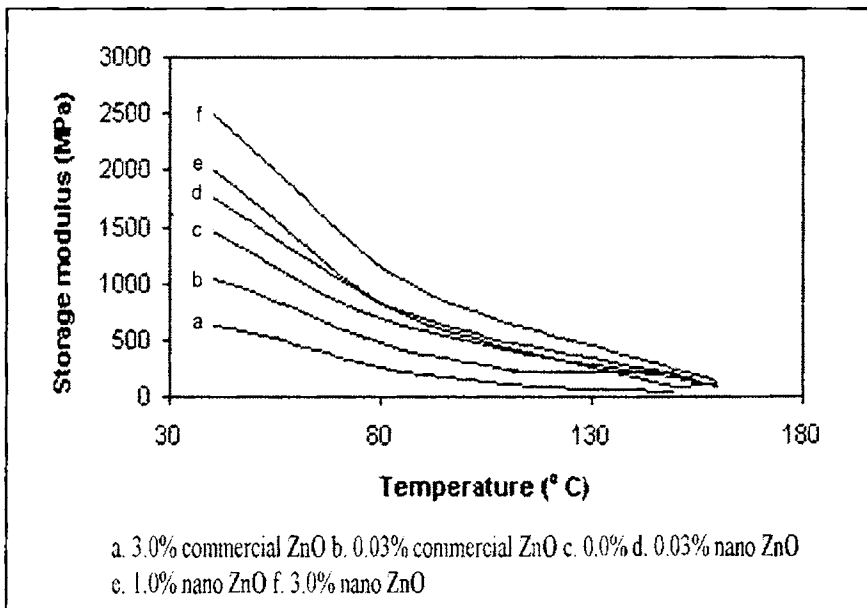
Figure 5a.18 Variation of storage modulus of PP- ZnO nanocomposites at room temperature

Table 5a.5 Storage modulus of PP- ZnO nanocomposites at 50 °C & 100 °C

Sample	Storage modulus at 50 °C (MPa)	Storage modulus at 100 °C (MPa)
PP alone	1263	490
PP/0.03 wt% nano ZnO	1524	499
PP/1.0 wt% nano ZnO	1732	574
PP/3.0 wt% nano ZnO	2188	776
PP/0.03 wt% commercial ZnO	921	304
PP/3.0 wt% commercial ZnO	559	148

The DMA results for the loss modulus of the PP-ZnO nanocomposite samples as a function of temperature at 1 Hz are shown in figure 5a.19. On modifying with both ZnOs, loss modulus value increases. This increase in loss modulus value is more for PP-nano ZnO composites than that of PP- commercial ZnO composites.
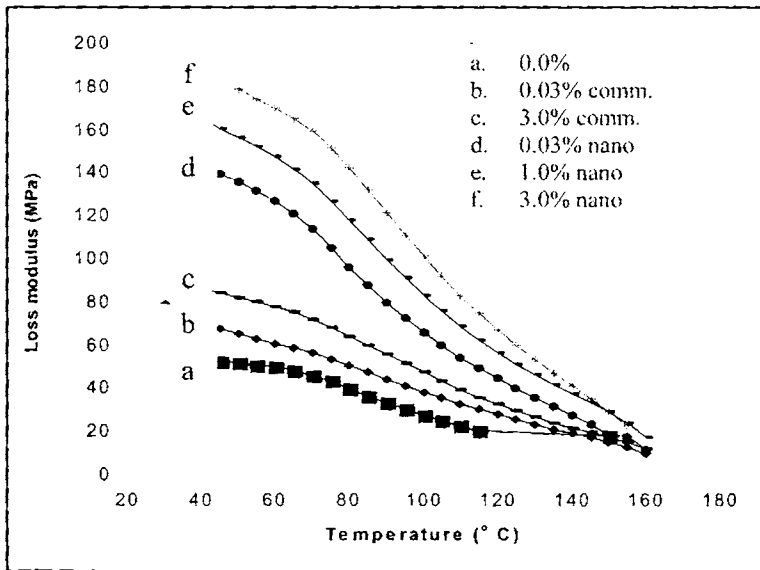
Figure 5a.19 Variation of loss modulus of PP- ZnO nanocomposites

` is observed at higher temperatures. Sangeetha et al.[42] reported an increase in storage and loss modulus of PP-clay nanocomposites. Zhao et al.[38] reported

an increase in storage and loss modulus of PP nanocomposites by ZnO nanoparticles.

Figure 5a.20 shows tan δ versus temperature plots for PP-ZnO nanocomposites. From the tan delta peak it is clear that some compatibility is achieved as a result of mixing PP with nano ZnO that is evident from peak broadening. PP-ZnO nanocomposite is prepared with increased stiffness. Tan δ value decreases with modification and the decrease is more in the case of commercial ZnO nanocomposites. Tan δ values of PP-ZnO nanocomposite are given in table 5a.6.
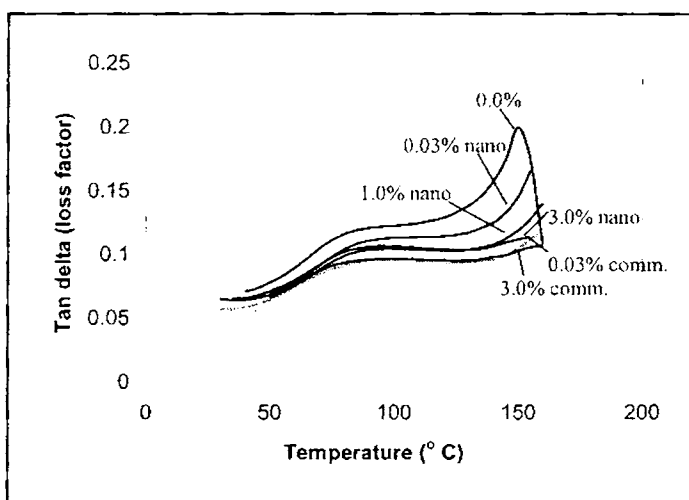
Figure 5a.20 Variation of tan delta of PP- ZnO nanocomposites

Table 5a.6 Tan δ values of PP-ZnO nanocomposite

Sample	Peak values of tan δ at 150 °C
PP alone	0.2002
PP/0.03 wt% nano ZnO	0.1456
PP/1.0 wt% nano ZnO	0.1192
PP/3.0 wt% nano ZnO	0.1124
PP/0.03 wt% commercial ZnO	0.1053
PP/3.0 wt% commercial ZnO	0.1030

Correlation of impact and dynamical properties in terms of tan δ peak values of the nanocomposites has been done. The variation of the impact strength as a function of the total loss tangent peak values for PP- nano ZnO composites and PP-commercial ZnO composites is shown in figure 5a.21 & 5a. 22 respectively. The curves show a non-linear shape.
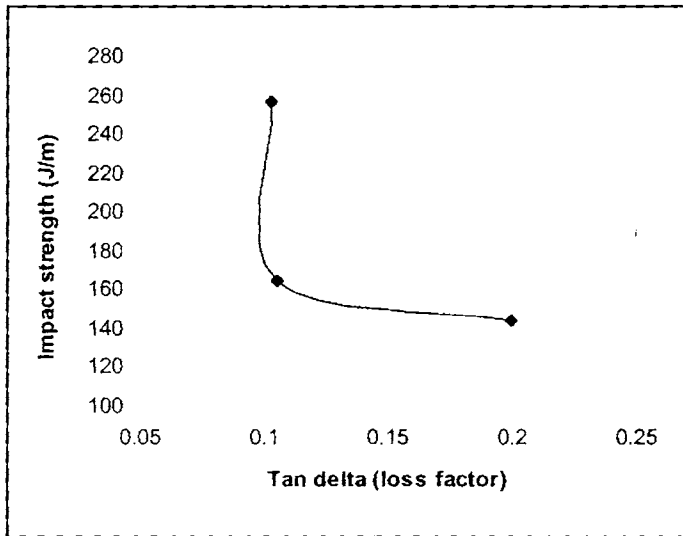
Figure 5a.21 The variation of the impact strength as a function of the total loss tangent peak values for PP- nano ZnO composites
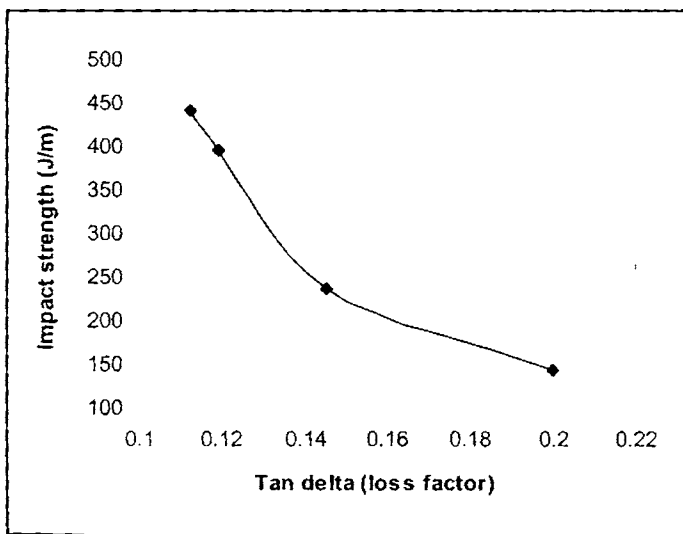
Figure 5a.22 The variation of the impact strength as a function of the total loss tangent peak values for PP- commercial ZnO composites

5a.3.5 Melt rheology

The rheological behaviour of PP-ZnO nanocomposites is studied at three different temperatures 170, 180 & 190 °C. Effect of shear stress, filler loading and temperature on rheological behaviour is investigated.

5a.3.5.1 Effect of shear stress on shear viscosity

Figure 5a.23 present the shear viscosity vs. shear stress curves of PP- ZnO nanocomposites at 180 °C with increasing ZnO concentration from 0.0-3.0 wt%. We also examined the flow behaviour of PP nanocomposites filled with 1.0 % commercial ZnO. As shear stress increases, the viscosity of PP-ZnO composites decreases in all cases, indicating the pseudoplastic flow behaviour. At zero shear, the molecules are randomly oriented and highly entangled and therefore exhibit high viscosity. Under the application of shearing force, the polymer chains orient, resulting in the reduction of shear viscosity and thus exhibit shear-thinning (pseudoplastic behaviour).[50,51] It is just this pseudoplasticity that makes the nanocomposites to be easily melt-processed. Effect of temperature on shear viscosity of PP nanocomposites filled with 1.0 % nano ZnO is given in figure 5a.24. With a rise of temperature from 180 to 190 °C the value of shear viscosity decreases, especially at relatively lower apparent shear stress. The melt viscosity increases when the temperature decreases to 170 °C.
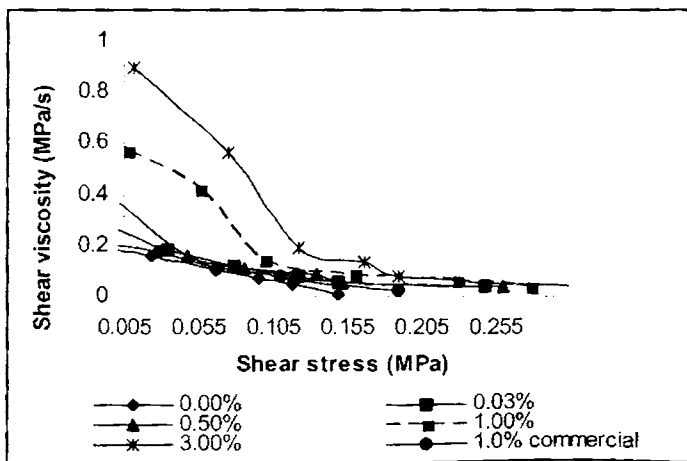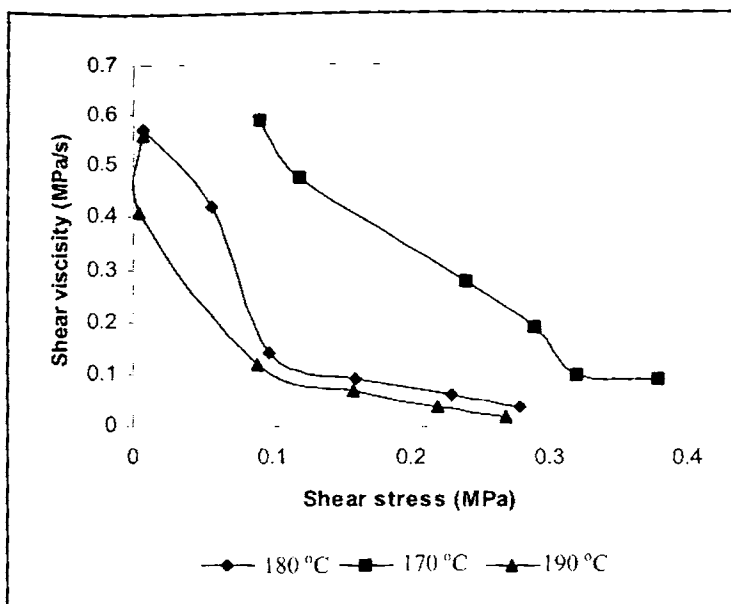

**Figure 5a.23** Effect of shear stress on shear viscosity of PP- ZnO nanocomposites

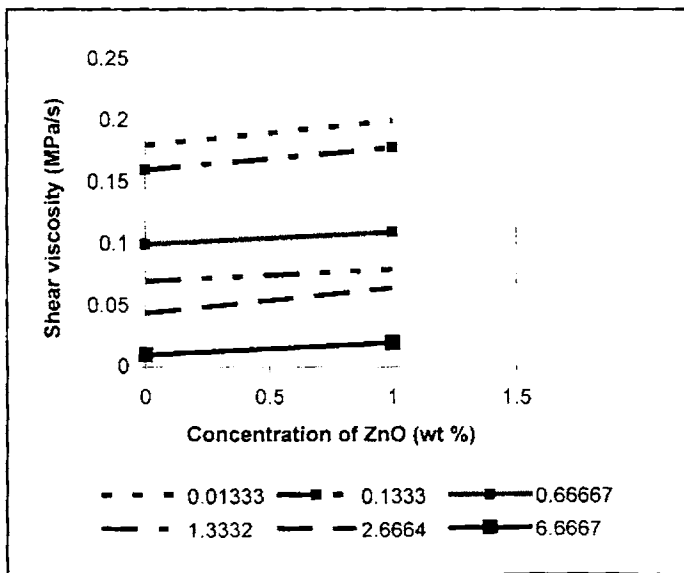**Figure 5a.24** Effect of temperature on shear stress vs. shear viscosity plots

5a.3.5.2 Effect of filler loading

Since entanglements of polymer chains and arrangement of ZnO are not permanent and altered by flow and relaxation processes, any disturbance of this steady state, such as shear, will disrupt the structure of the polymer matrix. Figure 5a.25 shows the variation of shear viscosity with increasing concentration of nano ZnO from 0.0-3.0 wt% at six different shear rates. It is clear from the figure that shear viscosity increases with nano ZnO addition and this increase is more prominent at low shear rates and low ZnO concentration. Also it can be seen from the figure that shear viscosity decreases substantially with increasing shear rate, but increases monotonically with increasing nano ZnO loading at a given shear rate.[52,53]
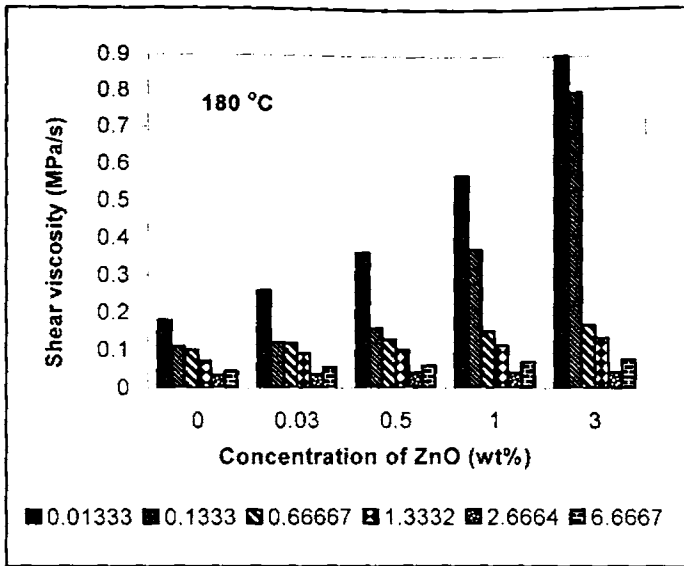
Figure 5a.25 Variation of shear viscosity with concentration of ZnO and shear rates at 180 °C

Figure 5a.26 examines the variation of shear viscosity of PP nanocomposites with concentration of commercial ZnO at six different shear rates. It is clear from the figure that viscosity almost remains constant with ZnO loading.
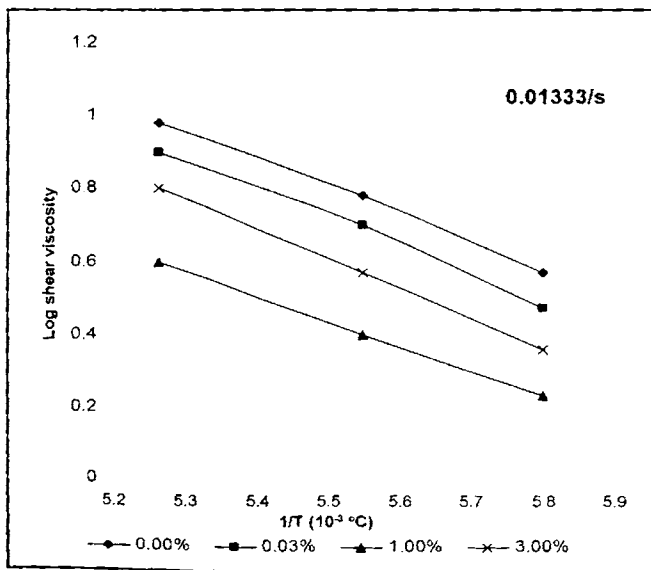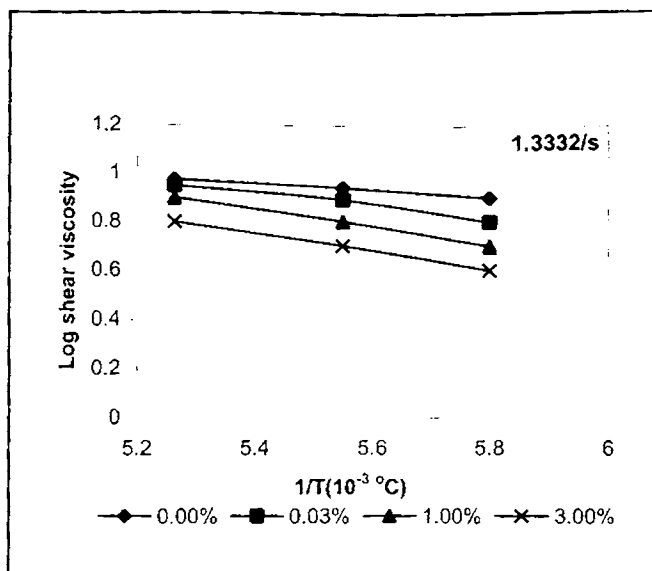

Figure 5a.26 Variation of shear viscosity with concentration of commercial ZnO at six different shear rates at 180 °C

5a.3.5.3 Effect of temperature

Shear viscosities of pure PP and nanocomposite melts decreases with increasing extrusion temperature in the range of 170-190 °C, demonstrating that increasing temperature improves the flow behavior of the polymer melts. However, the effect of temperature on shear viscosity changes with the shear rate. The data indicate that the temperature sensitivity of shear viscosity is higher in lower shear rate region, and drops at higher shear rates. This phenomenon is in agreement to the fact that elevating shear rate always accompanied by a rapid decrease of the entanglement density of macromolecules and the melt viscosity.[54] The Arrhenius plots of PP-nano ZnO composites at two different shear rates is given in figure 5a.27 (a) & (b). A good linear correlation was found in the plot of ln η_a vs. 1/T, which has proved the appropriateness of the Arrhenius–Eyring equation. Values of E_a obtained from the slopes of these plots are given in table 5a.7.

From the table 5a.7 it can be observed that the activation energy of flow of the nanocomposites increases with modification at lower shear rates. But activation energy decreases with modification at higher shear rates.

(b)

Figure 5a.27 (a) & (b) Variation of log viscosity with 1/T for the PP- nano ZnO composites

Table 5a.7 Activation energies of PP- nano ZnO composites at two shear rates

Concentration of ZnO (wt%)	Activation energy (J/mol)	
	0.1333/s	1.3332/s
0.0	0.76187	0.68408
0.03	0.79820	0.67432
1.0	0.81823	0.67167
3.0	0.82367	0.62345

5a.3.5.4 Flow behaviour index (n')

The effects of temperature and concentration of ZnO on the flow behaviour indices of the samples have been studied in detail. The extent of pseudoplasticity or non-Newtonian behaviour of the materials can be understood from n' values. Pseudoplastic materials are characterized by n' below 1. Flow behaviour index values of PP-nano ZnO composites at 180 °C and 190 °C are given in figure 5a.28. It is clear from the figure that n' decreases with increasing concentration of ZnO and also with increasing temperature. This suggests that the system becomes more

pseudoplastic as the ZnO content and temperature increases. A similar trend of decreasing values of n' with an increase in temperature has been reported.[50,55,56]
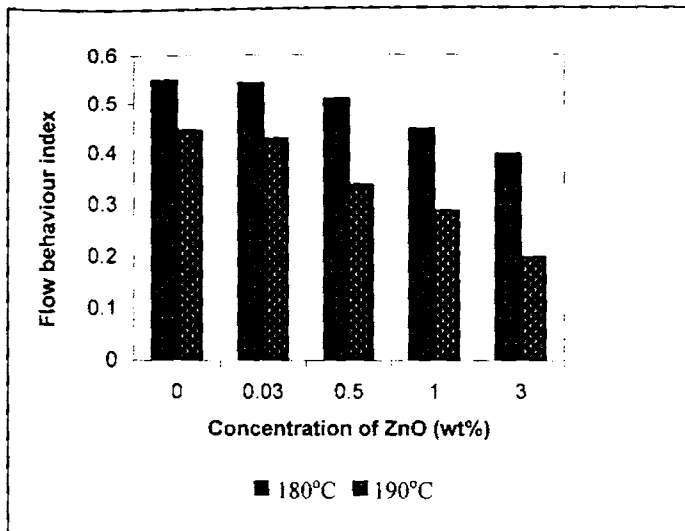

Figure 5a.28 Variation of flow behaviour index with concentration of ZnO
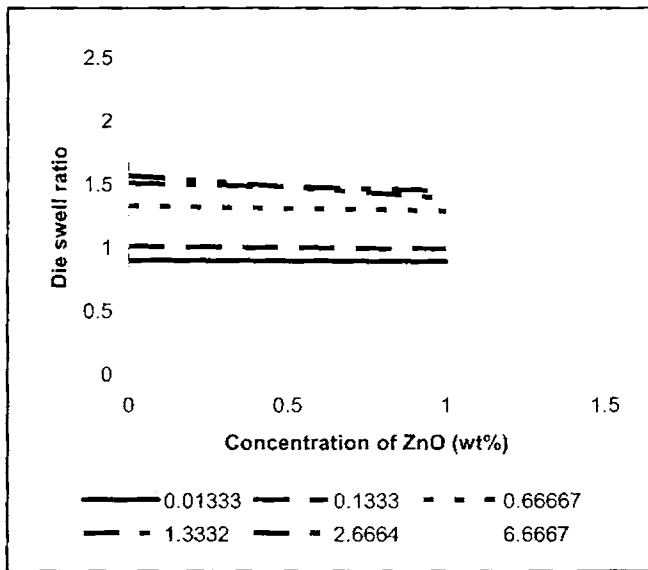
5a.3.5.5 Die swell

Die swell, called Barus effect is an important parameter for characterizing polymer melt elasticity in an extrusion flow and is related to the quality of the end products.

5a.3.5.5.1 Effect of shear rate and concentration of ZnO

Figure 5a.29 shows the plots of the die swell ratio, de/dc for PP and PP-ZnO nanocomposites at 180 °C at six different shear rates. The die swell ratio increases obviously with increasing shear rate at a constant ZnO content. It is noticeable that at a constant shear rate, the die swell ratio decreases slightly with a rise of ZnO content. Figure 5a.30 shows the variation of die swell ratio of PP nanocomposites filled with 1.0 % commercial ZnO at different shear rates. Die swell ratio remains constant with ZnO loading at lower shear rates, but decreases at higher shear rates.
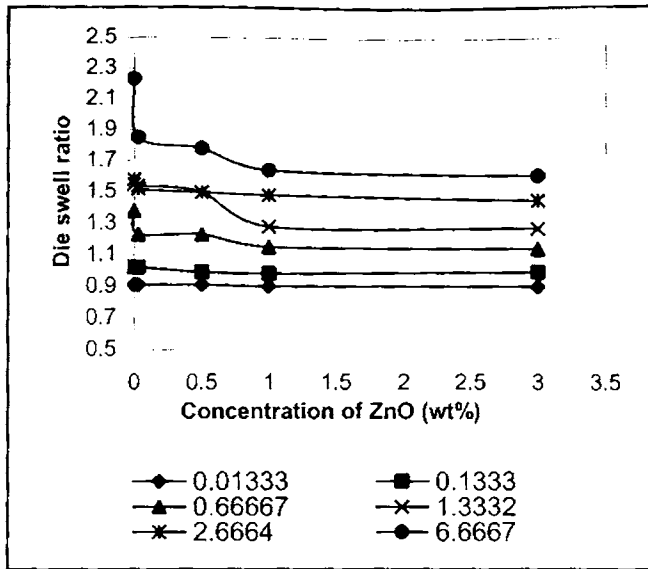
Figure 5a.29 Variation of die swell ratio of PP- nano ZnO composites with concentration of ZnO at different shear rates
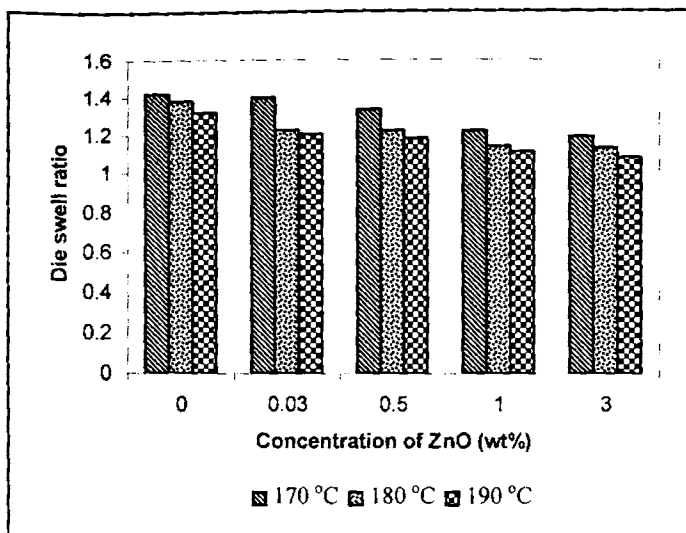

Figure 5a.30 Variation of die swell ratio of PP- commercial ZnO composites with concentration of ZnO at different shear rates

5a.3.5.5.2 Effect of temperature

Variation of die swell ratio of PP-nano ZnO composites at 3 different temperatures is given in figure 5a.31. It is clear from the figure that, die swell
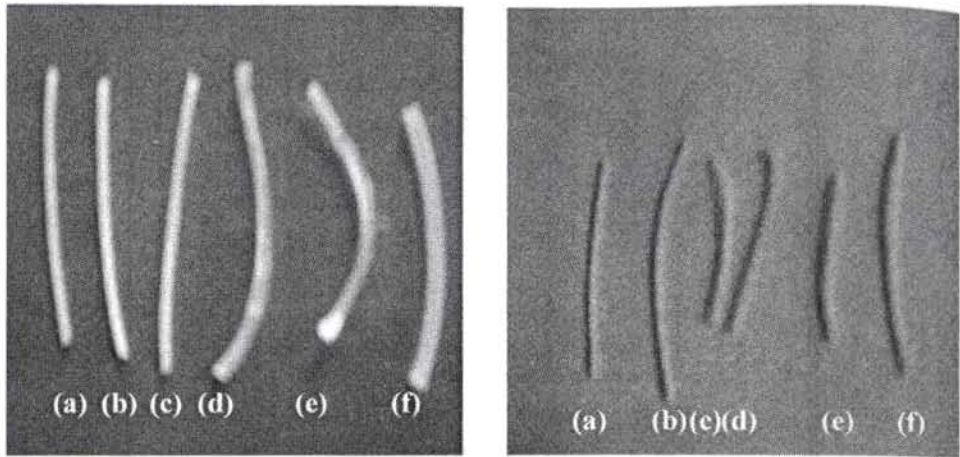
ratio decreases with temperature and concentration of ZnO. At 180 and 190 °C, the change in die swell ratio is negligible.

Figure 5a.31 Variations of die swell ratio of PP- nano ZnO composites with temperature

5a.3.5.6 Extrudate deformation studies

The appearance of the extrudate of neat PP and nanocomposites with 1.0 % ZnO at six different shear rates is shown in figure 5a.32 (a) and (b) respectively. From the figure it is clear that the extrudate distortion tendency increases with the shear rate. At a low shear rate, the extrudate has a smooth surface; however, at a higher shear rate, the surface becomes rougher. The ZnO content of the nanocomposite also plays a major role in determining the surface characteristics. As the ZnO content increases, the surface roughness also increases. Several factors contribute towards surface irregularity. It has been conclusively shown by photographic techniques[57,58] that a fracturing or breaking of the elastically deformed flowing polymer stream occurs at the entrance to the capillary itself at some critical shear stress. Another factor contributing towards extrudate distortion is the successive sticking and slipping of the polymer layer at the wall in the capillary.[59,60] Moreover, there may be an effect at the exit as well. Shear thinning behaviour of the nanocomposites is clearly visible in these photographs.

Figure 5a.32 Extrudate photographs of (a) neat PP and (b) PP- nano ZnO composites filled with 1.0 % nano ZnO at six different shear rates (a) 0.01333/s   (b) 0.1333/s   (c) 0.66667/s (d) 1.3332/s (e) 2.6664/s (f) 6.6667/s

MODIFICATION OF HIGH DENSITY POLYETHYLENE USING NANO ZINC OXIDE

5b.1 Introduction

Recently, organic–inorganic nanocomposites are in the spotlight as a promising class of materials because of their advantages and unique properties synergistically derived from nano-scale structure. These nanocomposites exhibit improved mechanical properties, low thermal expansion coefficient, high barrier properties, flame retardancy, and swelling resistance.[61-65] Further, these benefits can be achieved even at very low concentration in comparison to conventional polymer composites. In recent years, combination of inorganic nanoparticles with polymers has received great interest,[66-71] for the reason that it provides a means of improving strength together with toughness of the polymer matrix, which is almost impossible with conventional filled polymers. The performance of polymer nanocomposites is strongly dependent on the final morphology of the nanoparticles dispersed in the polymer matrix.

High-density polyethylene (HDPE) is considered as a primary material in the materials substitution chain because of availability and recyclability. It is the world's largest volume thermoplastic and finds wide use in packaging, consumer goods, pipes, cable insulation etc. The performance criterion to encourage the application of HDPE requires superior modulus and yield strength in conjunction with high-impact strength. A substantial enhancement in mechanical properties (modulus, yield strength and toughness) of thermoplastic materials can be realized by reinforcement with inorganic minerals including talc[72] mica[73] wollastonite,[74-76] glass bead[77] and calcium carbonate.[49, 78-87]

This study is aimed at producing HDPE nanocomposites with varying ZnO concentration and analyzing them for their crystallization, thermal, mechanical, dynamic mechanical performances and melt rheology.

5b.2 Experimental

A simple melt-compounding route was adopted for the preparation of HDPE-ZnO nanocomposites. The melt compounding was performed using Thermo Haake Rheocord 600 mixing chamber with a volume capacity of 69 cm³ fitted with a roller type rotors operating at 40 rpm for 10 min at 150 °C. Nanocomposites at different concentrations (0.0-3.0 wt%) of ZnO were prepared. In all cases the torque stabilized to a constant value in this mixing time. The crystallization behaviour, thermal stability, morphology, melt rheology, mechanical and dynamic mechanical property of the nanocomposites using commercial and nano ZnO were analyzed according to the details summarized in sections 2.3 of this thesis.

5b.3 Results and discussion
5b.3.1 Differential scanning calorimetry
5b.3.1.1 Non-isothermal

The crystallization behaviour of polymer is a basic problem in polymer physics. Especially, the filler in a polymer will affect the crystallization behaviour of the polymer-based composites very much[88-90] because, the filler may adsorb the polymer molecules and act as crystal nuclei. However, to be relevant to industrial processing, it is desirable to study the crystallization of nanocomposites under non-isothermal conditions. Several authors have reported the crystallization studies on HDPE with nano- filler. Zheng et al.[90] investigated the crystallization behavior of rare earth neodymium-iron-boron (NdFeB) magnetic powder/ high density polyethylene composite. The results showed there was a remarkable heterogeneous nucleation effect of NdFeB on the HDPE matrix. Huang et al.[91] explored HDPE reinforced and toughened by nano-CaCO₃. HDPE can be reinforced and toughened by the adhesion force between nano-CaCO₃ and HDPE matrix even when the surface of nano-CaCO₃ particles is untreated. He et al.[92] prepared HDPE-nano-SiO₂ composites by a new dispersing method, using a vibrational mill to disperse the nano-SiO₂ into HDPE. The composite exhibited excellent abrassive performance.

In this section we compared the crystallization characteristics of HDPE matrix using nano and commercial ZnO. The effect of nano ZnO on the crystallization characteristics of melt compounded HDPE- ZnO nanocomposite samples was analyzed first with non-isothermal DSC experiments. The crystallization temperatures (T_c), the apparent melting temperatures (T_m), the corresponding enthalpies (ΔH_c and ΔH_m) and the degree of supercooling ($\Delta T = T_m - T_c$) are also reported in table 5b.1

**Table 5b.1** DSC-determined thermal characteristics of HDPE- nano ZnO composite samples

Concentration of ZnO (wt%)	T_c (^{o}C)	ΔH_c (J/g)	T_m (^{o}C)	ΔH_m (J/g)	ΔT (^{o}C)
0.0	111.5	147.4	134.5	145.6	23
0.03	116.6	146.4	135.9	144.2	19.3
0.1	118.6	146.4	135.0	145.6	16.4
0.5	125.8	146.2	136.9	146.8	11.1
1.0	127.2	146.9	136.8	145.6	9.6
2.0	131.3	145.6	137.2	145.1	5.9
3.0	132.9	146.0	136.5	147.3	3.6

Figure 5b.1 shows the DSC cooling scans of HDPE- nano ZnO composite samples. During cooling from the melt, the ZnO containing samples show crystallization exotherms earlier than neat HDPE, as also seen from the corresponding T_c values indicated in table 5b.1. It is found that the nanocomposite sample containing nano ZnO at a concentration as low as 0.03 wt% enhances the rate of crystallization in HDPE as the cooling nanocomposites melt crystallizes at a temperature 5 ^{o}C higher as compared to neat HDPE. The T_c values continue to increase with increasing ZnO concentration, further increase in ZnO concentration from 0.03 to 3.0 wt%, the additional T_c increase is about 16 ^{o}C. There is a saturation of the nucleant effect at low ZnO (upto 3.0 wt%) concentrations, resulting in diminishing dependence on the increasing ZnO induced nucleation, possibly because of large surface area and good dispersion

of ZnO. The melting temperature is slightly increased and one possible reason for the increase in the melting temperature is that the processed nanocomposite has a smaller particle size, thus has a larger specific surface and a larger interfacial area, resulting in a stronger interaction between the polymer matrix and the more finely dispersed particles. The stronger interaction constrains the movement of molecular chains, leading to a higher melting point. The enthalpies of HDPE and nanocomposites stay unaffected. The degree of supercooling ($\Delta T = T_m - T_c$) may be a measurement of a polymer's crystallizability: the smaller the ΔT, the higher the overall crystallization rate (figure 5b.2). The ΔT values for the HDPE- nano ZnO were 19-3.6 °C smaller than that of neat HDPE (23 °C). The results indicated that the incorporation of ZnO nanoparticles had little effects on the degree of crystallinity of HDPE. Tjong et al.[93] also observed this behavior in LDPE - ZnO nanocomposites. This was also observed by Osman et al.[94] in HDPE- silicate composites.
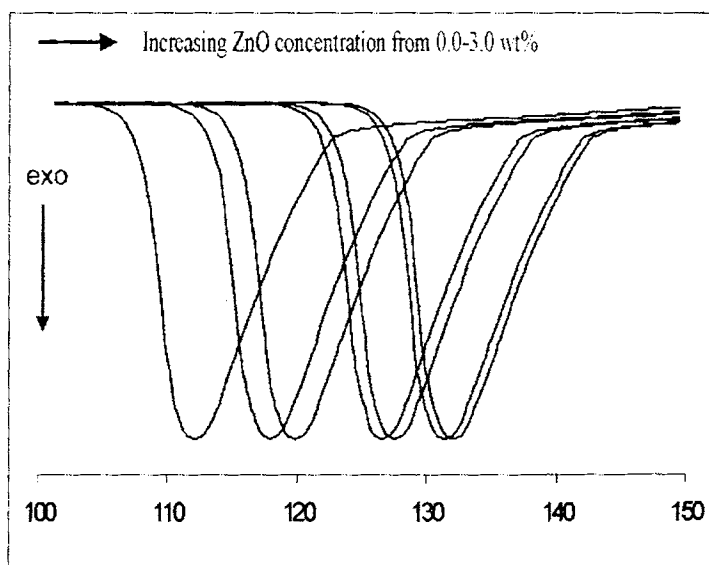

Figure 5b.1 DSC cooling scans (20 °C/min from 200 °C melt) of HDPE nanocomposite samples
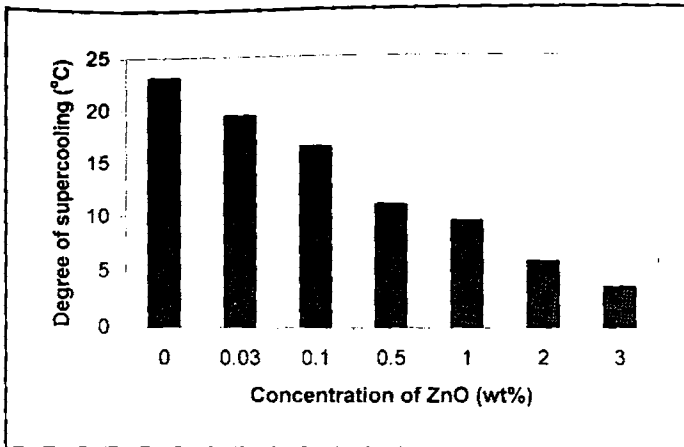
Figure 5b.2 Variation of degree of supercooling with concentration of nano ZnO

On adding commercial ZnO the total increase in crystallization temperature was 1 °C and ΔH_c, ΔH_m, T_c and T_m values remains a constant with ZnO loading. The ΔT values for the HDPE-commercial ZnO composites remains a constant near the neat HDPE value (23 °C). Figure 5b.3 compares the crystallization temperatures of HDPE nanocomposites using commercial and nano ZnO. It can be seen that nano ZnO is a better nucleating agent than commercial ZnO. T_c increase is only about 1 °C on additing 3.0 wt% commercial ZnO, but for nano ZnO addition, the value is about 18 °C. This is because, interactions between the filler surface and the matrix substantially decreases on adding commercial ZnO and the particles do not show to behave as nucleating agents.
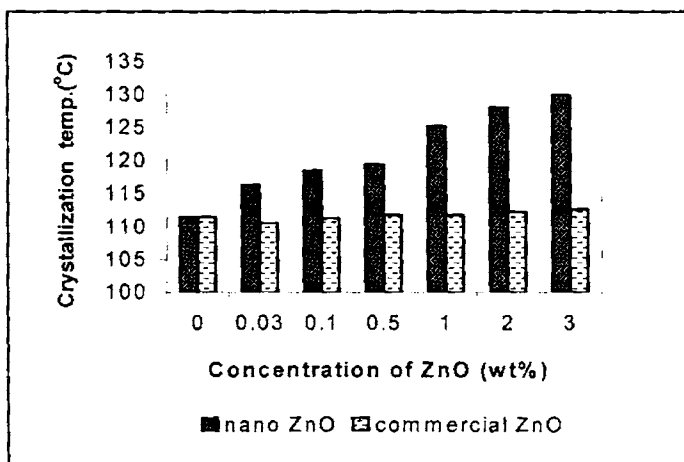

Figure 5b.3 Comparison of crystallization temperatures of HDPE- ZnO nanocomposites using nano and commercial ZnO

The reason for crystallization temperature of HDPE–commercial ZnO composite remaining unaltered may be related to the particle–matrix interaction. The interfacial interaction plays a critical role in the free energy of cluster formation and the rate of nucleation; the weak interaction lowers the rate of nucleation.[95]

5b.3.1.2 Isothermal crystallization characteristics

Figure 5b.4 shows the typical isothermal crystallization curves of the HDPE-nano ZnO composite samples at four temperatures (120 °C, 125 °C, 130 °C and 135°C). The time corresponding to the maximum in the heat flow rate (exotherm) was taken as peak time of crystallization (t $_{peak}$). Such peaks are seen at each of the four isothermal crystallization temperatures for the 0.03 wt% ZnO containing nanocomposite, with the earlier or faster crystallization (smaller t_{peak}) corresponding to lower temperature of isothermal crystallization. For the case of neat HDPE, no exotherm is seen at the highest temperature of 135 °C because; crystallization is very slow and would require longer time than the 4 minutes employed in the DSC program. On the other hand, for the nanocomposite sample with 3.0 wt% ZnO, the rate of crystallization is so fast near the lowest temperature 120 °C that most crystallization occurs already during the cooling scan (60 °C/min) employed to reach those temperature, resulting in absence of exothermic peaks in the heat flow curves at that temperature.
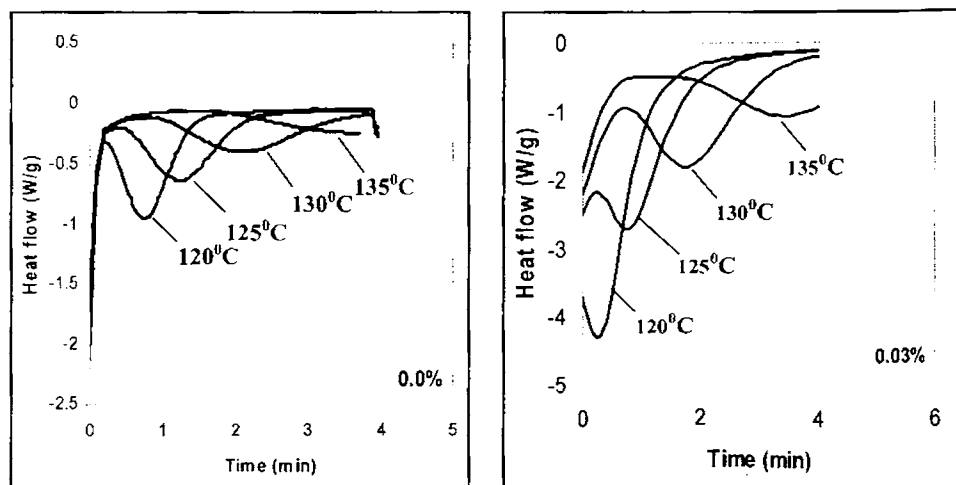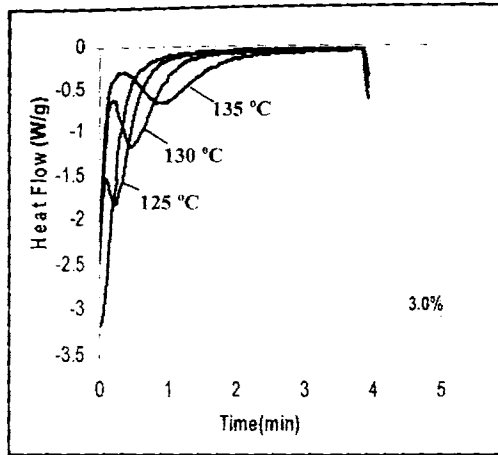
Figure 5b.4 Heat flow during isothermal crystallization of HDPE-nano ZnO composite samples

The peak times of crystallization at each of the temperatures for all the HDPE-ZnO nanocomposite samples are plotted against the isothermal crystallization temperature (figure 5b.5). We notice that due to the presence of ZnO the t_{peak} values for the nanocomposite samples reduced to less than 50 % as compared to neat HDPE at a concentration as low as 0.03 wt%. With the increasing ZnO concentration there is further increase in the crystallization rate (as indicated by the decrease in t_{peak}), demonstrating the role of ZnO in enhancing the rate of crystallization.
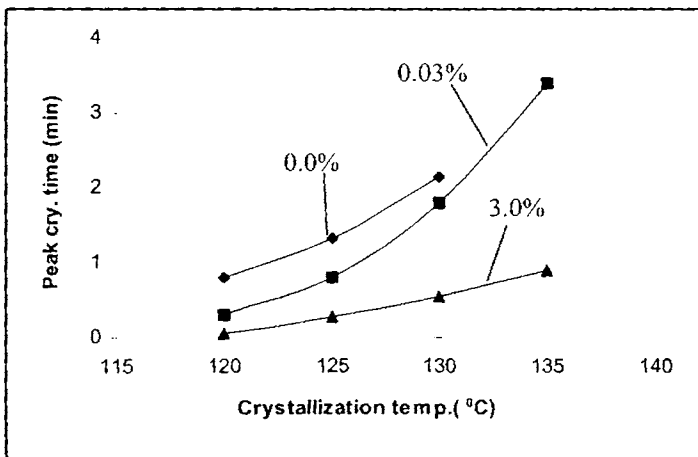
Figure 5b.5 The peak time of crystallization at each of the temperatures for all the HDPE-ZnO nanocomposite samples

5b.3.2 Thermogravimetry

TGA studies shows that inorganic fillers, which are widely used industrially to improve the mechanical properties of polymer materials, have different effects on the thermal oxidation of HDPE. Their addition increases the activation energy of thermal oxidation, and thus, has some stabilization effects. However, once oxidation begins, it will proceed at a much faster rate. At current experimental conditions, HDPE/talc, HDPE/wollastonite, HDPE/diatomite and HDPE/CaCO$_3$ are more stable than HDPE itself before breakage.[96] Thermal stability of HDPE is increased with silicalite-1 content.

The TG and DTG curves of neat HDPE and its nanocomposites using nano ZnO are given in figures 5b.6 & 5b.7 respectively. The temperature of onset of degradation T_i (°C), the temperature at which the rate of decomposition is 10 % [$T_{10\%}$ (°C)], the temperature at which the rate of decomposition is maximum (T_{max} °C), the temperature at which the rate of decomposition is 50 % [$T_{50\%}$ (°C)], the peak degradation rate and the residue at 800 °C are given in table 5b.2. HDPE degrades in a single step. The thermal degradation profiles of HDPE and HDPE-nano ZnO composites exhibit that most of the degradation events occur between 365 and 520 °C. The nanocomposites degrade over a much narrower temperature range than the pure polymer because, the onset point of degradation shifts to higher temperature. The degradation starts at a temperature of 362 °C and the peak rate of degradation is 3.143 %/min at corresponding T_{max} 479.4 °C for HDPE, and in nanocomposites, T_i is 393.4 °C on adding 3.0 wt% of nano ZnO, indicating improved thermal stability of the nanocomposites. The T_{max} temperature also showed an improvement in thermal stability. Residue at 800 °C is only about 0.0307 % for HDPE. Adding 3.0 wt% of ZnO, residue increased to 6.201 % and the peak rate of decomposition decreased from 3.143 to 2.358 %/min. This increase in the thermal stability of the nanocomposites may result from the strong interaction between the nano ZnO and HDPE molecules. On adding commercial ZnO, thermal stability slightly increases (figure 5b.8). The T_{max}

temperature increased from 479.4 °C to 481 °C, on adding 3.0 wt% commercial
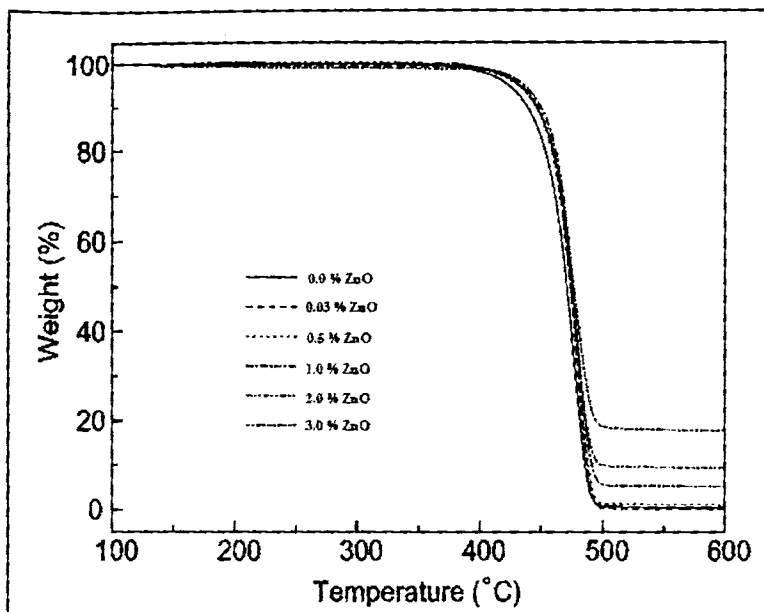ZnO.

Figure 5b.6 Thermogravimetric traces of HDPE – nano ZnO composite samples (lower curves with increasing ZnO concentrations 0.0, 0.03, 1.0, 3.0 wt%).
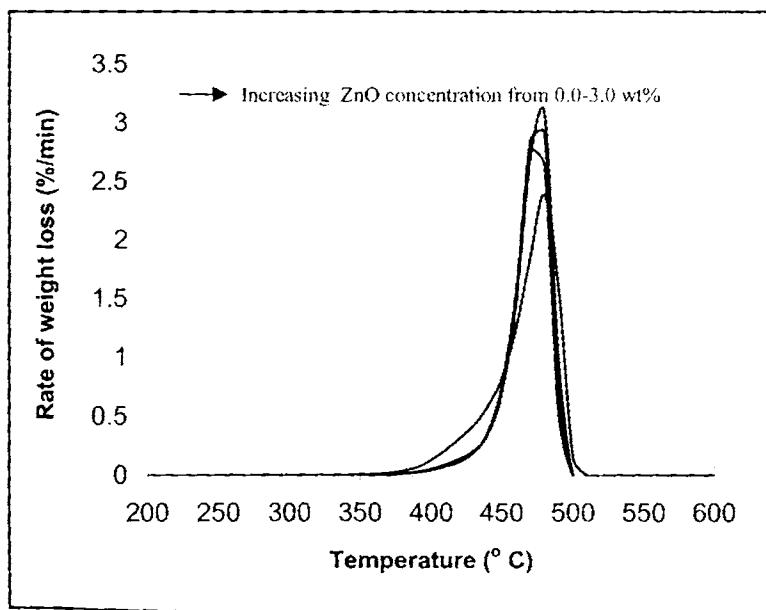

Figure 5b.7 Differential thermogravimetric traces of HDPE- nano ZnO composites

Table 5b.2 Degradation characteristics of HDPE and its nanocomposites

| Concentration of ZnO	T_i (°C)	$T_{10\%}$ (°C)	Residue at 800 °C (%)	Peak rate of decomposition (%/min)	$T_{50\%}$ (°C)	T_{max} (°C)
0	362.6	413.2	0.0307	3.143	471.0	479.4
0.03	369.5	437.1	0.0399	2.996	481.4	485.1
1.0	381.3	440.5	2.340	2.960	481.8	485.7
3.0	393.4	441.0	6.201	2.358	482.6	487.3
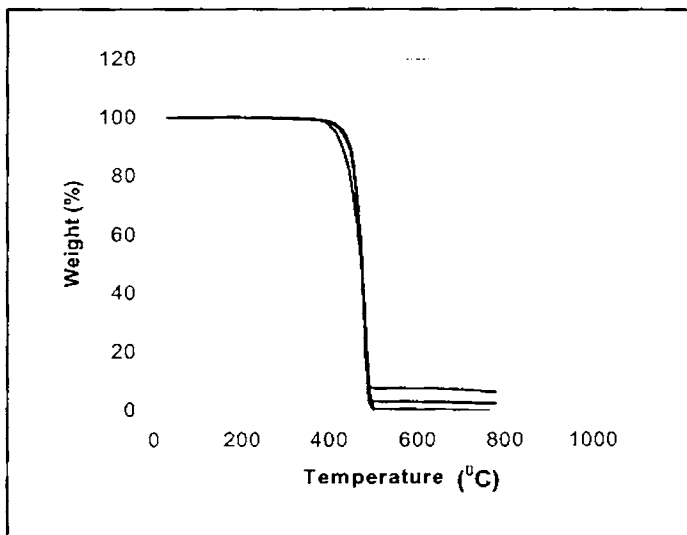
Figure 5b. 8 Thermogravimetric traces of HDPE – commercial ZnO composite samples (lower curves with increasing ZnO concentrations 0.0, 0.03, 1.0, 3.0 wt%)

5b.3.3 Mechanical properties

5b.3.3.1 Torque studies

It has been widely established that the mechanical properties of crystalline polymeric materials strongly depend on processing conditions and techniques used to process the materials. The same polymeric material can be processed into a soft and flexible product or a strong and stiff product under different conditions. The variation of mixing torque with time of mixing at different ZnO loading is shown in figure 5b.9. A mixing time of 10 minutes was fixed since the

torque stabilized to a constant value during this time. The temperature of the mixing chamber was fixed as 150 °C. The stabilization of the torque may be related to the attainment of a stable structure after a good level of mixing. Initially torque increases with the charging of HDPE, but decreases with melting. After homogenization of HDPE, ZnO was added at 2.5 min. There is a little increase in torque on continued mixing with ZnO. After mixing, the torque value is found to be steady. It is clear from the figure that there is no degradation taking place during the mixing stage. Similar trend in torque is observed when commercial ZnO is mixed with HDPE.
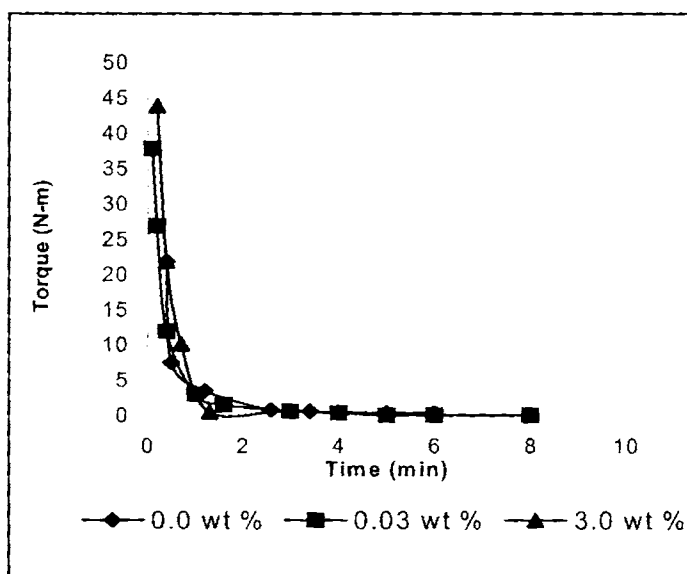
Figure 5b.9 Torque-time graph of HDPE- ZnO nanocomposites

5b.3.3.2 Tensile properties

A polymer consists of long-chain molecules. The atoms constructing the backbones of these chains are held together by covalent bonds. Though covalent bonds are one of the strongest in nature, their strength is not realized in polymers because the molecular chains exist primarily as random coils.[97,98] The response of a polymer to an external force is mainly through the motion of the chain segments of the coils, which dominates the yielding behaviour of the polymer. When a semicrystalline polymer is subjected to an external load, the chain

segments in the crystalline regions slip, causing the lamellae to disintegrate locally and the polymer to yield and neck.[99,100] This gives rise to a low stiffness and strength.

The effects of the nano ZnO on the mechanical properties of HDPE are summarized in table 5b. 3.

Table 5b.3 Tensile properties of HDPE- nano ZnO composites

Concentration of ZnO (wt%)	Tensile strength (MPa)	Tensile modulus (GPa)	Elongation (%)	Shore D hardness	Energy to max (J)	Tensile toughness (J/m)
0.0	22.71	0.366	15.54	65	0.854	406.6
0.03	24.04	0.418	12.40	68	0.983	489.1
0.1	25.59	0.525	11.77	70	1.03	619.0
0.5	26.65	0.597	10.21	72	1.12	664.9
1.0	36.77	0.609	9.65	78	1.36	647.6
2.0	37.81	0.618	8.21	79	1.39	712.8
3.0	39.61	0.627	5.31	80	1.43	713.2

The results in table 5b.3 shows an increase in the tensile modulus and strength of HDPE with an increasing concentration of ZnO content from 0.0 to 3.0 wt%. From 0.0 to 1.0 wt% the change in tensile strength is about 62 % and modulus is about 66 %. But from 1.0 to 3.0 wt% there is only a little increase in tensile strength (about 7 %) and modulus (about 2 %). The tensile strength showed an increment of about 75 % and modulus increased to about 71 % on adding 3.0 wt% of nano ZnO. The Shore D hardness also supports this reinforcement. The elongation to break is found to decrease with the increasing loading of ZnO, indicating that the nanocomposites become somewhat brittle. Energy to max and tensile toughness (energy/ thickness of the sample) values (figure 5b.10) increases by about 67 % and 75 % respectively with 3.0 wt% ZnO loading. Area under the stress-strain curve is directly proportional to the energy absorbed. Since there is an increase in energy absorption some modification has taken place, which is clear from the increase in tensile toughness values. These

results demonstrate that even a small fraction of ZnO provide effective reinforcement to the HDPE matrix. This is due to better interaction between HDPE matrix and ZnO nanoparticles.
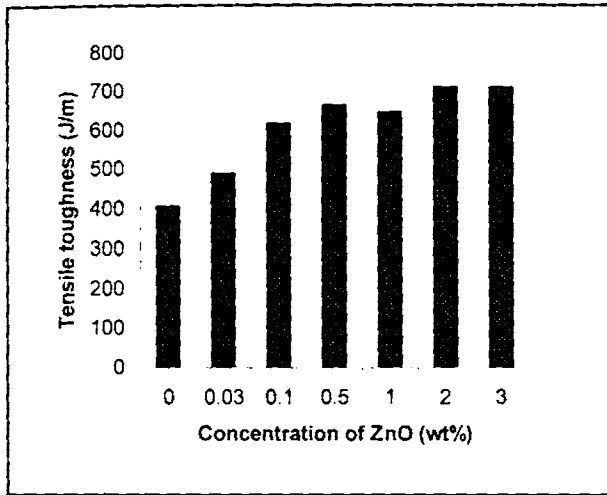

Figure 5b.10 Variation of tensile toughness with concentration of ZnO

Figure 5b.11 and 5b.12 shows a comparison of tensile strength and modulus of HDPE- ZnO composites using nano and commercial ZnO.
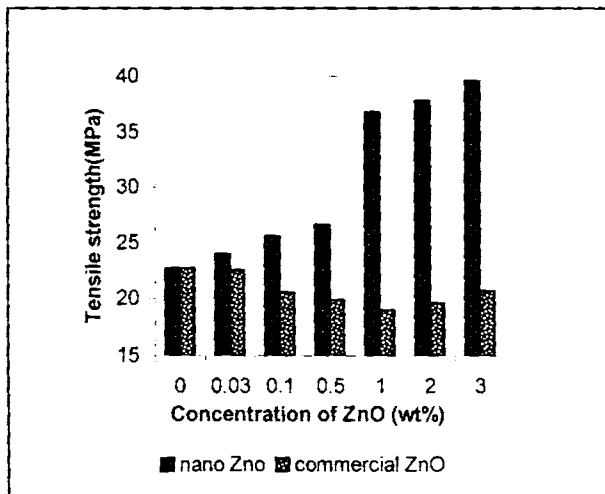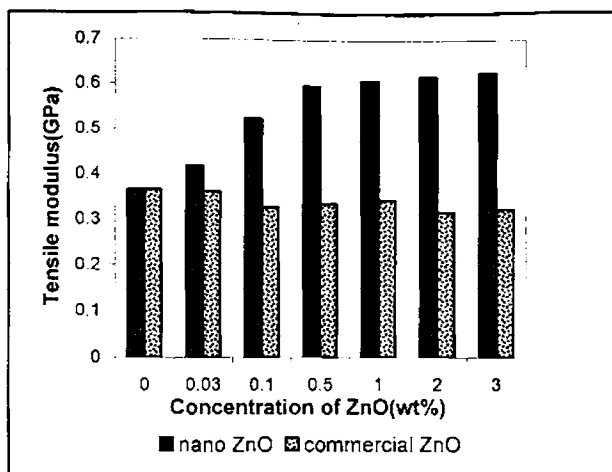

Figure 5b.11 Comparison of tensile strength of HDPE- ZnO nanocomposites

Figure 5b.12 Comparison of tensile modulus of HDPE- ZnO nanocomposites

It is clear from the graph that commercial ZnO loading decreases the strength and modulus of HDPE. Uniform dispersion of commercial ZnO is not attained by melt mixing and aggregates of particles are more in HDPE- commercial ZnO composite than in HDPE- nano ZnO composites. Uniform dispersion is important because, in the case of a matrix with aggregates of particles, the stress field will be concentrated around any aggregates, such that the cracks will propagate and rapidly, causing premature failure. The energy to maximum and tensile toughness values maintains the same value with increasing commercial ZnO concentration. Elongation of the composites also decreases. The tensile properties of HDPE - commercial ZnO composites are summarized in table 5b.4.

Table 5b.4 Tensile properties of HDPE-commercial ZnO composites

Concentration of ZnO (wt%)	Elongation (%)	Shore D hardness	Energy to max (J)	Tensile toughness (J/m)
0.0	15.54	65	0.854	406.6
0.03	15.26	68	0.832	402.3
0.1	12.49	70	0.856	405.8
0.5	10.51	72	0.857	407.3
1.0	10.98	72	0.865	408.1
2.0	11.23	73	0.855	406.9
3.0	11.55	75	0.845	410.3

Stress-strain curves for HDPE and its nanocomposite is shown in figure 5b.13. From the stress-strain curve it is clear that with ZnO loading the elongation (%) decreases, indicating that the composite becomes somewhat brittle compared with neat HDPE. Area under the stress-strain curve increases, which indicate an increase in toughness of composite.
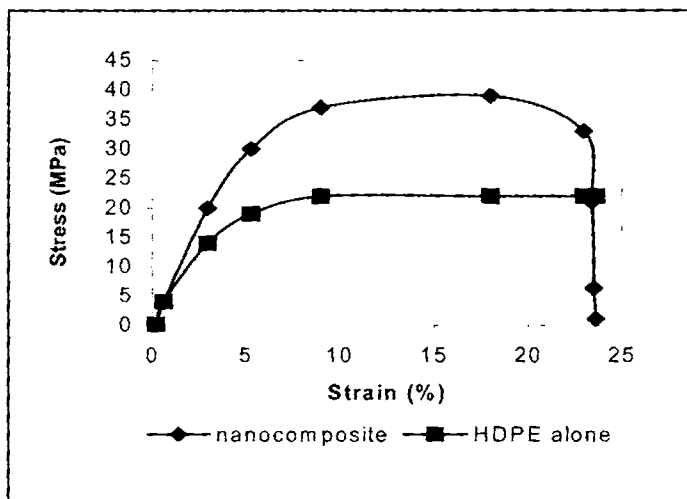

Figure 5b.13 Stress-strain curve for HDPE and its nanocomposites

5b.3.3.3 Morphology of the fractured surfaces

The morphological structure of polymer nanocomposites is important because it ultimately determines many properties of the polymer nanocomposites. The scanning electron micrographs of the fractured surfaces of the tensile test specimens have been studied to acquire an insight into the mechanism of reinforcement. Figure 5b.14 (a) shows the fracture surface for unmodified HDPE. It indicated the necking phenomena of HDPE molecule, because of its ductility. There is no sign of significant plastic deformation. From figure 5b.14 (b) & (c) it is clear that nano ZnO exist as dispersed particles in HDPE matrix and the morphology gets substantially modified. Here we can observe shape transition of ZnO nanoparticles. In nanocomposites, nanoparticle-matrix interactions are expected to determine this shape transition.[101] Due to the dominance of surface states, nanoparticles of a material may exert forces that are different from those exerted by the corresponding bulk material on the surrounding matrix.[102] The shape transition of nanoparticle from

rod to spherical increases the surface area and there is tremendous reinforcement. SEM images are in good agreement with the observed mechanical properties. There is no sign of extensive particle agglomeration as compared to HDPE- commercial ZnO nanocomposite fracture surface shown in figure 5b.15 (d) where we can see large agglomerates and the dispersion is inhomogeneous.


(a)

(b)

(c)

(d)
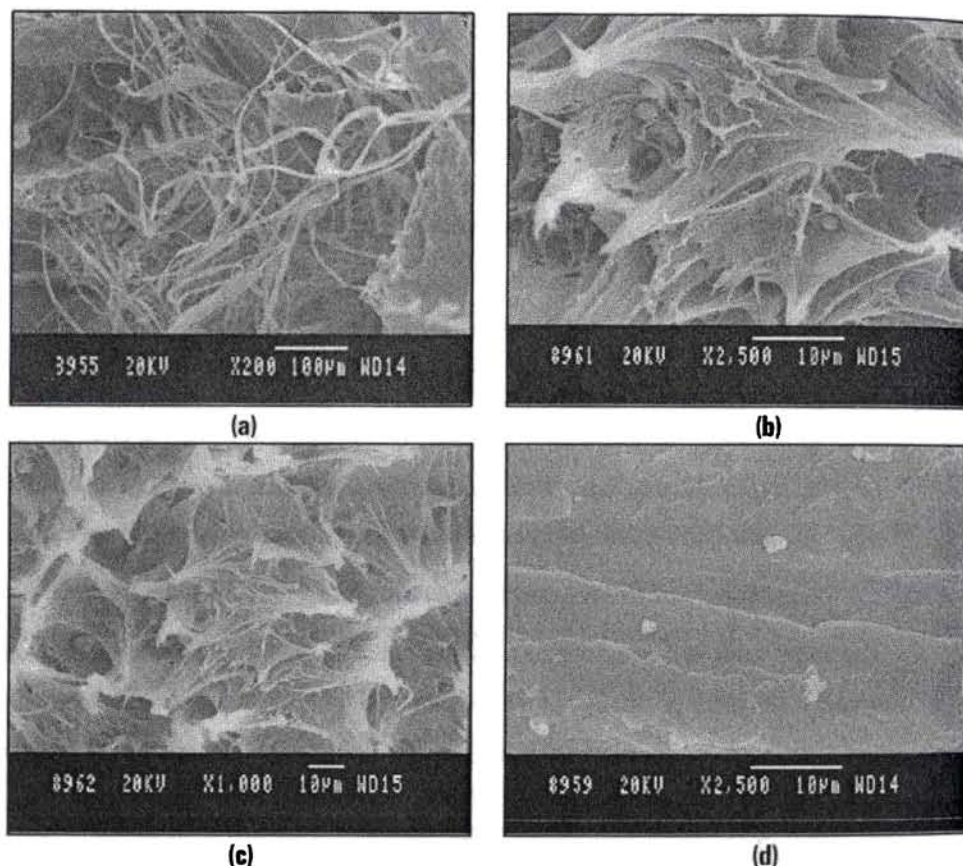
Figure 5b.14 Tensile fracture surface of (a) neat HDPE (b) & (C) HDPE- nano ZnO composite showing nanoparticle shape transition (d) HDPE- commercial ZnO composites

5b.3.3.4 Flexural properties

A comparison of flexural strength and modulus of HDPE-ZnO nanocomposites using nano and commercial ZnO is shown in figure 5b.15 (a) & 5b.15 (b) respectively. With nano ZnO, the flexural modulus as well as the strength of HDPE increases considerably. For example, incorporation of nano ZnO at the level of 3.0 wt%, modulus increases by around 75 % and strength by

around 60 %. With commercial ZnO, the flexural modulus and strength showed an increase of about 15 % and 14 % respectively. The better reinforcement of nano ZnO is due to smaller particle size, high surface area, uniform dispersion and good interfacial interaction with HDPE matrix.
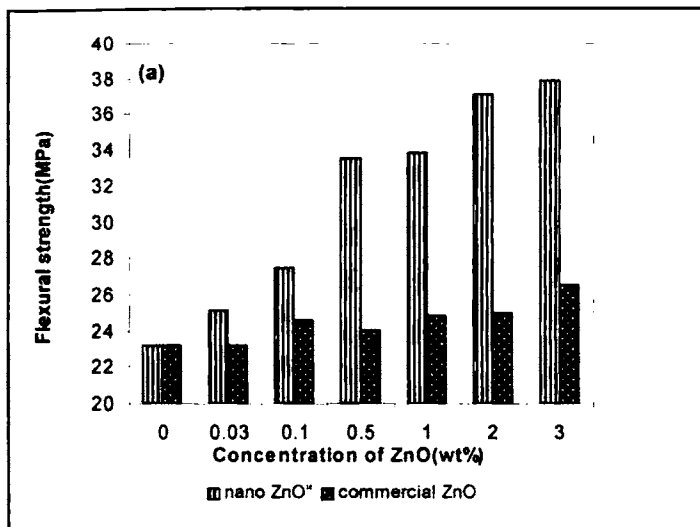
5b.15 (a) comparison of flexural strength of HDPE- ZnO nanocomposites
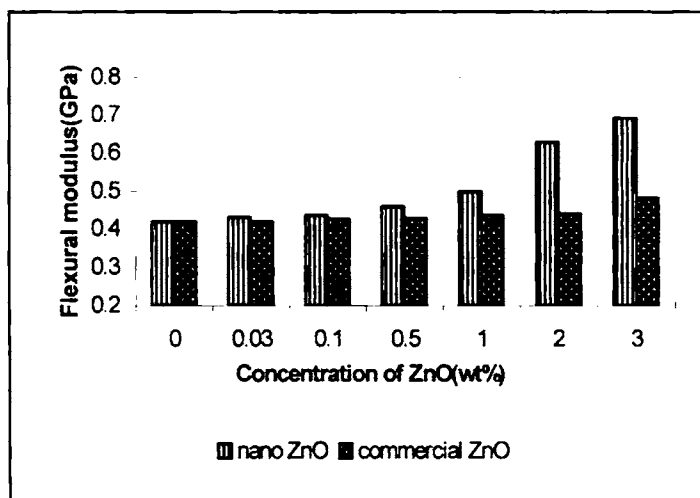
5b.15 (b) comparison of flexural modulus of HDPE- ZnO nanocomposites

5b.3.3.5 Impact strength

The toughness of a material is generally related to the energy dissipating events that occur in the vicinity of a sharp crack. It should be pointed out that the interfacial interaction between fillers and polymer matrix significantly influence the

mechanical properties of particulate filled polymers. Friedrich[103] first emphasized the effect of morphology and provided evidence that semicrystalline polymers consisting of small spherulites are generally tougher than those containing coarse spherulites because larger spherulites have weak boundaries. Ouderni and Philips [104] confirmed Friedrich's conclusion from their study on the effect of crystallinity. It was observed that an increase in crystallinity or spherulite size decreased the toughness. The behaviour of the composite is not a simple function of crystallinity and crystal structure (morphology), but is a complex function of other factors and includes lamellar thickness and interfacial interaction. If the lamellar thickness was increased with percentage of filler, there is reinforcement. The lamellar thickness is an important controlling parameter in the activation of yield, and yield stress in neat semicrystalline polymers is proportional to lamellar thickness. In HDPE- nano ZnO composites there is no change in crystallinity and the reinforcement indicate an increase in lamellar thickness.

Izod impact strength (unnotched) of HDPE- ZnO nanocomposites using nano and commercial ZnO is compared in figure 5b.16. With 3 % commercial ZnO, the impact strength of HDPE increases by about 12 %. But with 3 % nano ZnO, the increase is about 128 %. The increase in impact strength is evidenced by the tensile toughness values shown in figure 5b.10 and from the area of the stress strain curve shown in figure 5b.13. So the toughness of the composite is more improved with nano ZnO addition.
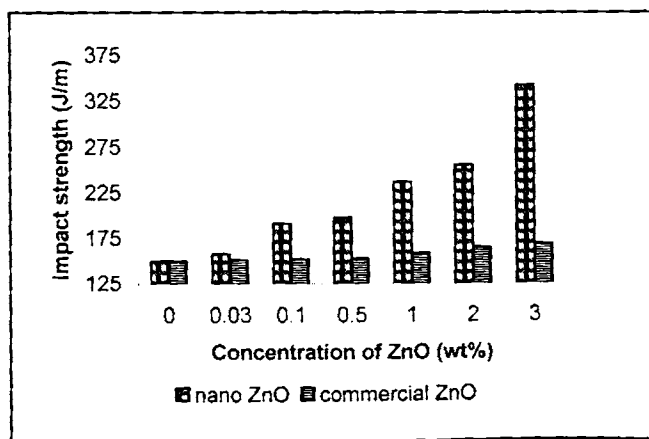

Figure 5b.16 Comparison of impact strength of HDPE- ZnO nanocomposites

5b.3.4 Dynamic mechanical analysis (DMA)

The DMA results for the dynamic storage modulus of the HDPE - ZnO nanocomposite samples as a function of temperature at 1 Hz are shown in figure 5b.17. We were able to examine the variation from room temperature onwards, so unable to determine the glass transition temperatures. A slow decrease in modulii with temperature is observed for the nanocomposites. In the initial stage, storage modulii of the nanocomposite increases substantially with the nano ZnO concentration, showing the stiffening effect of nano ZnO. The storage modulii of the nanocomposite samples increases substantially with the nano ZnO concentration (about 35 % increase with 1 wt% nano ZnO), indicating efficient stress transfer between the HDPE matrix and ZnOs. But with commercial ZnO, the storage modulus decreases i.e., nanocomposite is more soft and flexible. The storage modulus of nanocomposites at 50 $^{\circ}$C & 100 $^{\circ}$C is given in table 5b. 5
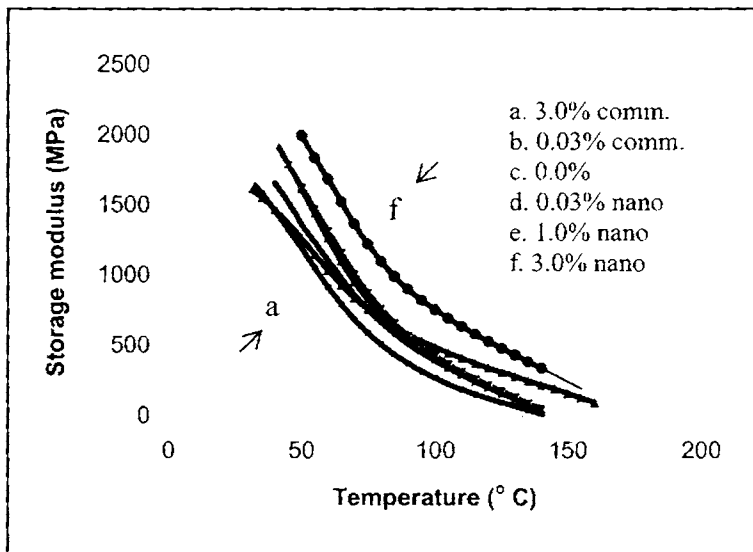

Figure 5b.17 Variation of storage modulus of HDPE- ZnO nanocomposites

Table 5b.5 Storage modulus of HDPE - ZnO nanocomposites at 50 °C & 100 °C

Sample	Storage modulus at 50 °C (MPa)	Storage modulus at 100 °C (MPa)
HDPE alone	1364	400.6
HDPE/0.03 wt% nano ZnO	1627	428.5
HDPE/1.0 wt% nano ZnO	1634	431.2
HDPE/3.0 wt % nano ZnO	1996	757.1
HDPE/0.03 wt% commercial ZnO	1263	365.2
HDPE/3.0 wt% commercial ZnO	1193	270.8

The matrix of the composite can be assumed that consists of two parts. One is the free part, where the state of the macromolecular chains is the same as that in pure HDPE. The other is the interphase. The interphase is formed by the physical or chemical adsorption of the polyethylene molecules and/or trans-crystallization on the filler's surface. The larger the interfacial area and stronger the interaction between the matrix and the fillers, the greater the volume of the interphase. Because the macromolecular chains of the interphase are restricted to the surface of the fillers, the molecular motion is greatly limited. As a result, the storage modulus of the interphase is higher than that of the free part. An increase in the nano ZnO content enlarges the interfacial area and results in an increase volume of interphase. At lower temperatures, motion of ZnO particles at the contact points is possible because of the high modulus of the matrix. This motion contributes significantly to the improvement of the storage modulus of the composites.[105] However, as a result of the aggregation of the ZnO particles, it is considered that the interphase of the composite with ZnO content has been reduced. Therefore, above the transition temperature, the storage modulus of HDPE- commercial ZnO is lower than the rest of the composites.

Figure 5b.18 shows tan δ versus temperature plots for HDPE- ZnO nanocomposites. It is evident from the figure that there is not much difference in the height of the tan δ peak on adding nano ZnO. This indicates that they possess the same order of damping capabilities. It is obtained in many cases that the

improvement of stiffness markedly reduces the ductility. But HDPE-ZnO nanocomposite is prepared with increased stiffness without sacrificing ductility. The height of the damping peak for the nanocomposite decreases with increasing commercial ZnO content because the elastic characteristics of the nanocomposites increase with commercial ZnO content.
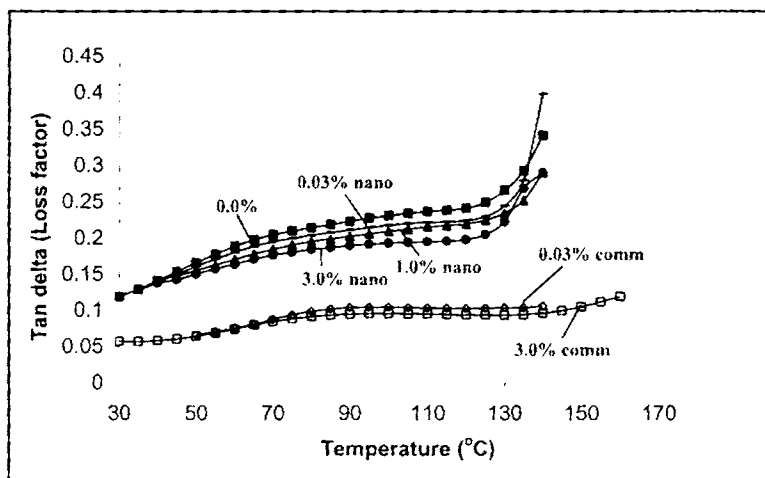

Figure 5b.18 Variation of tan delta of HDPE- ZnO nanocomposites

Loss modulus curves for the HDPE-ZnO composite is given in figure 5b.19. It is clear from the graph that loss modulus increases with nano ZnO modification and decreases with commercial ZnO modification.
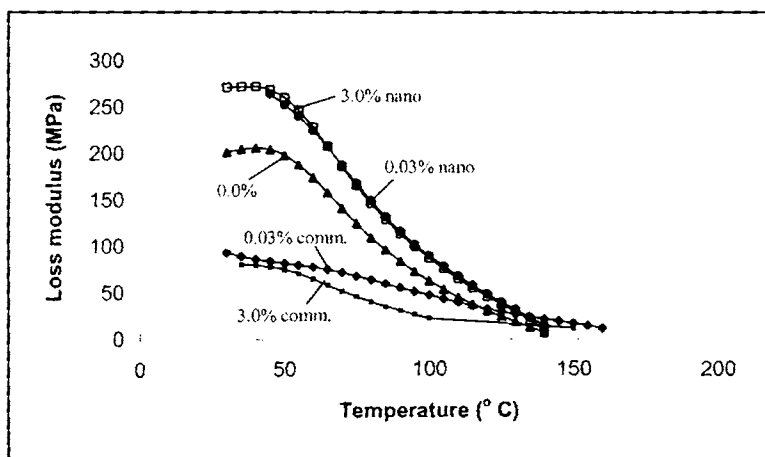

Figure 5b.19 Variation of loss modulus of HDPE- ZnO nanocomposites

Tan δ values of HDPE-ZnO nanocomposite are given in table 5b.6.

Table 5b.6 Tan δ values of HDPE- ZnO nanocomposite

Sample	Loss modulus (MPa)	Tan delta value at 120 °C
HDPE alone	200	0.243
HDPE/0.03 wt% nano ZnO	250	0.205
HDPE/3.0 wt% nano ZnO	252	0.167
HDPE/0.03 wt% commercial ZnO	98	0.092
HDPE/3.0 wt% commercial ZnO	75	0.061

Correlation of impact and dynamical properties in terms of tan δ peak values of the nanocomposites has been done. The variation of the impact strength as a function of the total loss tangent peak values for HDPE- nano ZnO composites and HDPE- commercial ZnO composites is shown in figure 5b.20 (a) & (b) respectively. The curves show a non-linear shape.
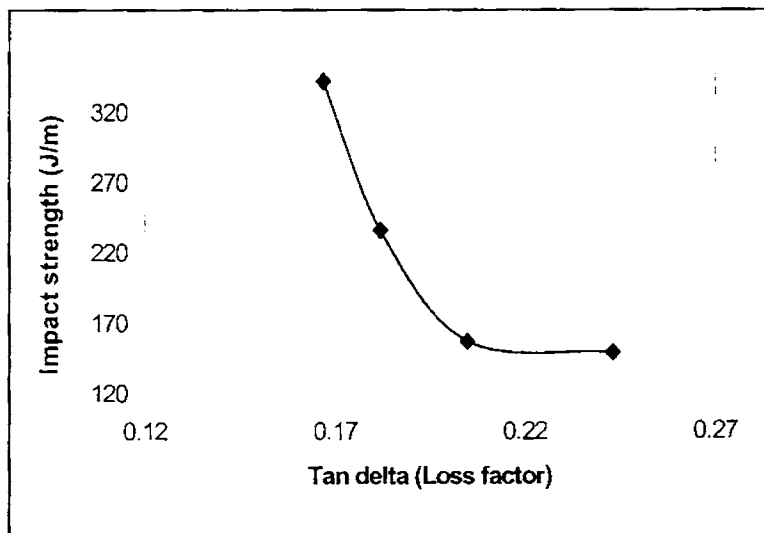
(a)
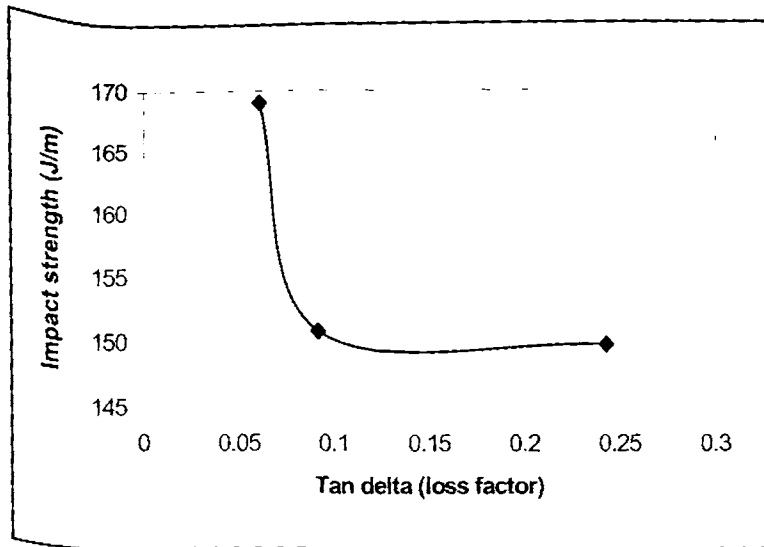
(b)

Figure 5b.20 Variation of the impact strength as a function of the total loss tangent peak for (a) HDPE-nano ZnO composites (b) HDPE-commercial ZnO composites

5b.3.5 Melt rheology

The rheological behaviour of HDPE-ZnO nanocomposites is studied at three different temperatures 140, 150 & 160 °C. Effect of shear stress, filler loading and temperature on rheological behaviour is investigated.

5b.3.5.1 Effect of shear stress on shear viscosity

Figure 5c.21 present the shear viscosity vs. shear stress curves of HDPE-ZnO nanocomposites at 150 °C with an increasing ZnO concentration from 0.0-3.0 wt%. We also examined the flow behaviour of HDPE nanocomposites filled with 1.0 % commercial ZnO. As shear stress increases, the viscosity of HDPE- ZnO composites decreases in all cases, indicating the pseudoplastic flow behaviour. At zero shear, the molecules are randomly oriented and highly entangled and therefore exhibit high viscosity. Under the application of shearing force, the polymer chains orient, resulting in the reduction of shear viscosity and thus exhibit shear thinning (pseudoplastic behaviour). It is just this pseudoplasticity that makes the nanocomposites to be easily melt-processed. Effect of temperature on shear viscosity of HDPE nanocomposites filled with 1.0 % nano ZnO is given in figure 5b.22. With

a rise of temperature from 150 to 160 °C the value of shear viscosity decreases, especially at relatively lower apparent shear stress. The melt viscosity increases when the temperature decreases to 140 °C.
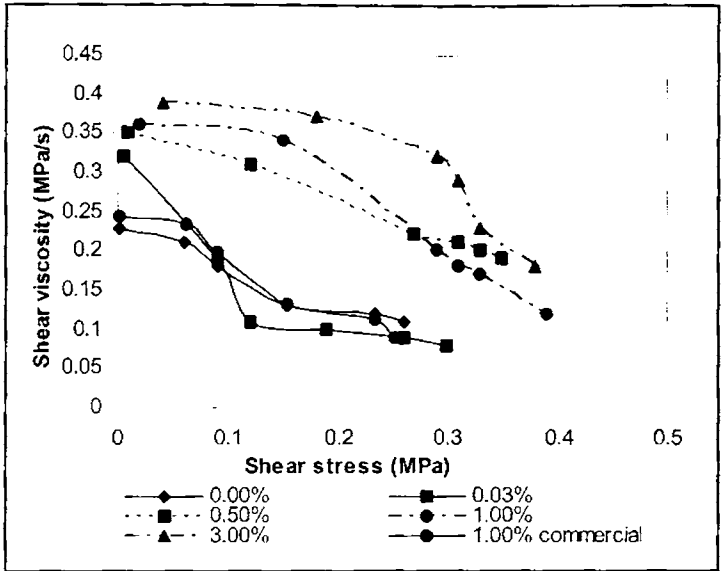

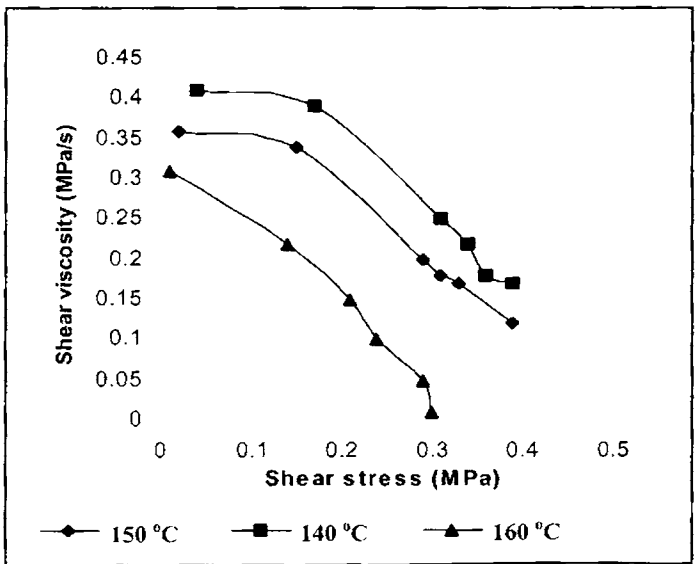**Figure 5b.21** Effect of shear stress on shear viscosity of HDPE- ZnO nanocomposites

Figure 5b.22 Effect of temperature on shear stress vs. shear viscosity

5b.3.5.2 Effect of filler loading

Since entanglements of polymer chains and arrangement of ZnO are not permanent and altered by flow and relaxation processes, any disturbance of this steady state, such as shear, will disrupt the structure of the polymer matrix. Figure 5b.23 shows the variation of shear viscosity with an increasing concentration of nano ZnO from 0.0-3.0 wt% at six different shear rates. It is clear from the figure that shear viscosity increases with nano ZnO addition and this increase is more prominent at low shear rates and low ZnO concentration. Also it can be seen from the figure that shear viscosity decreases substantially with increasing shear rate, but increases monotonically with increasing nano ZnO loading at a given shear rate.
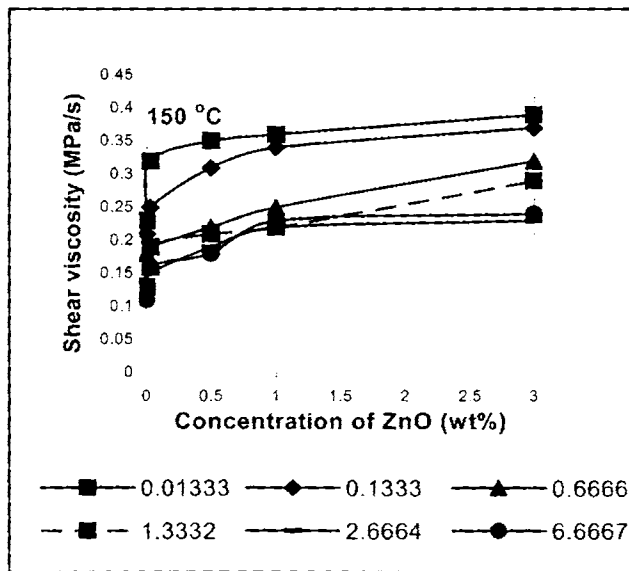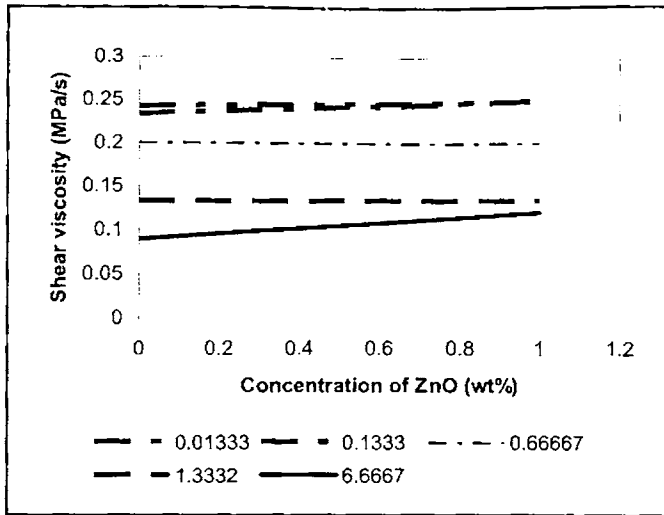

Figure 5b.23 Variation of shear viscosity with concentration of ZnO and shear rates at 150 °C

Figure 5b.24 examines the variation of shear viscosity of HDPE nanocomposites with concentration of commercial ZnO at five different shear rates. It is clear from the figure that viscosity almost remains constant with ZnO loading.
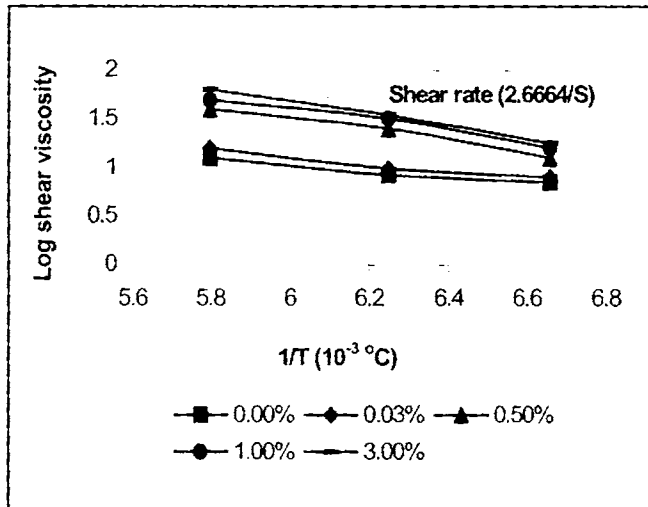
Figure 5b.24 Variation of shear viscosity with concentration of commercial ZnO at five different shear rates at 150 °C

5b.3.5.3 Effect of temperature

Shear viscosities of pure HDPE and nanocomposite melts decreases with increasing extrusion temperature in the range of 140-160 °C, demonstrating that increasing temperature improves the flow behavior of the polymer melts. However, the effect of temperature on shear viscosity changes with the shear rate. The data indicate that the temperature sensitivity of shear viscosity is higher in lower shear rate region, and drops at higher shear rates. This phenomenon is in agreement to the fact that elevating shear rate always accompanied by a rapid decrease of the entanglement density of macromolecules and the melt viscosity.[54] The Arrhenius plots of HDPE- nano ZnO composites at two different shear rates is given in figure 5b.25 (a) & (b). A good linear correlation was found in the plot of ln η_a vs. 1/T, which has proved the appropriateness of the Arrhenius–Eyring equation. Values of E_a obtained from the slopes of these plots are given in table 5b.7. The activation energy of a material provides valuable information on the sensitivity of the material towards the change in temperature. The higher the activation energy, the more temperature sensitive the material will be. Therefore, such information is highly useful in selecting the processing temperature of polymeric materials. From the table 5b.7 it can be observed that the activation energy of flow of the nanocomposites increases with modification at lower and higher shear rates.
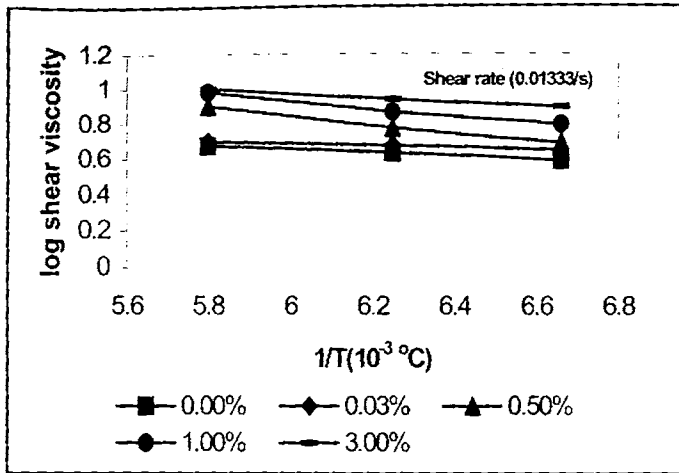
(a)

(b)

**Figure 5b.25** (a) & (b) Variation of log viscosity with 1/T for the HDPE- nano ZnO composites

Table 5b.7 Activation energies of HDPE- nano ZnO composites at two shear rates

Concentration of ZnO (wt%)	Activation energy (J/mol)	
	0.01333/s	**2.6664/s**
0.0	0.0464	0.2924
0.03	0.0871	0.3507
0.5	0.1165	0.5791
1.0	0.2098	0.5673
3.0	0.2331	0.6385

5b.3.5.4 Flow behaviour index (n′)

The effects of temperature and concentration of ZnO on the flow behaviour indices of the samples have been studied in detail. The extent of pseudoplasticity or non-Newtonian behaviour of the materials can be understood from n′ values. Pseudoplastic materials are characterized by n′ below 1. Flow behaviour index values of HDPE- nano ZnO composites at 150 °C and 160 °C are given in figure 5b.26. It is clear from the figure that n′ decreases with increasing concentration of ZnO and temperature. This suggests that the system becomes more pseudoplastic as the ZnO content and temperature increases. A similar trend of decreasing values of n′ with an increase in temperature has been reported.[50,55,56]
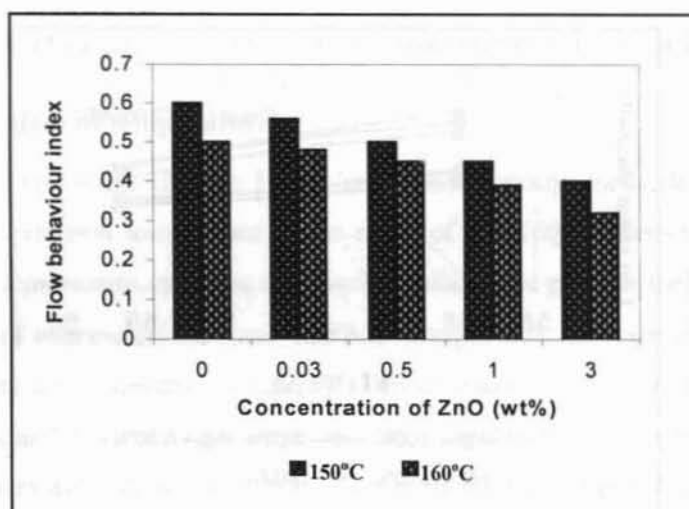
Figure 5b.26 Variation of flow behaviour index of nanocomposites with concentration of ZnO

5b.3.5.5 Die swell

Die swell, called Barus effect is an important parameter for characterizing polymer melt elasticity in an extrusion flow and is related to the quality of the end products.

5b.3.5.5.1 Effect of shear rate and concentration of ZnO

Figure 5b.27 shows the plots of the die swell ratio, de/dc for HDPE and HDPE-ZnO nanocomposites at 150 °C at six different shear rates. The die swell ratio increases obviously with increasing shear rate at a constant ZnO content. It is

noticeable that at a constant shear rate, the die swell ratio decreases slightly with a rise of ZnO content. Figure 5b.28 shows the variation of die swell ratio of HDPE nanocomposites filled with 1.0 % commercial ZnO at different shear rates. Die swell ratio decreases with ZnO loading, which is more at higher shear rates.
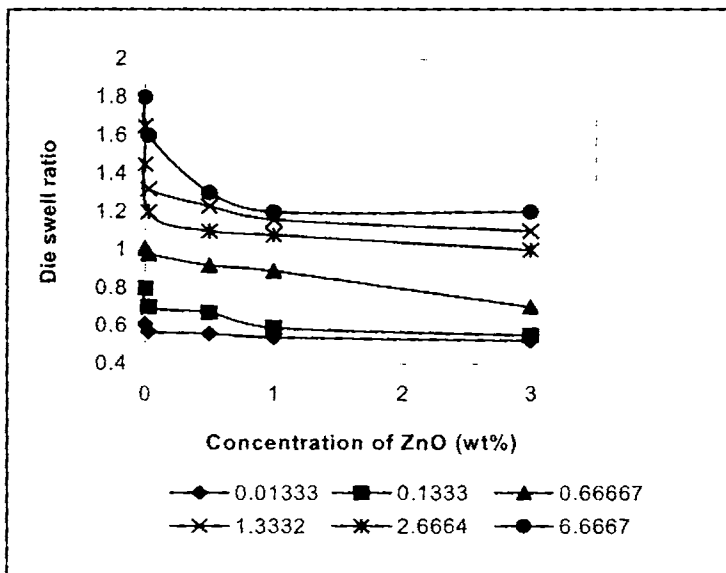

Figure 5b.27 Variation of die swell ratio of HDPE- nano ZnO composites with concentration of ZnO at different shear rates
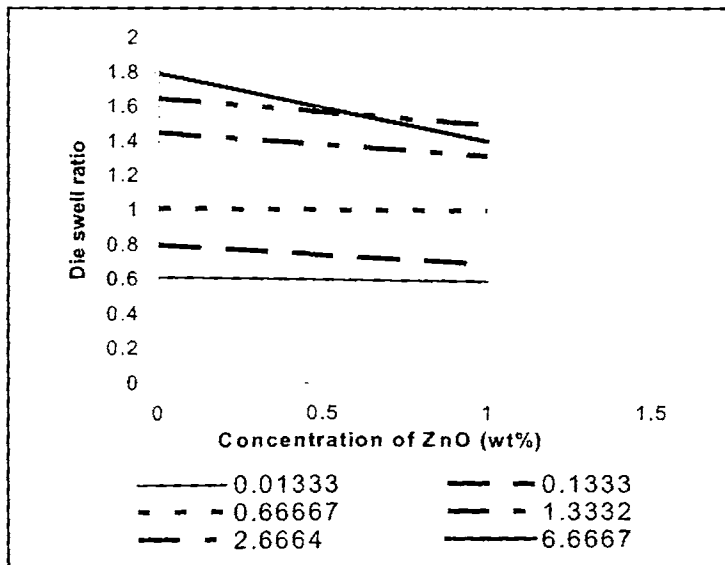

Figure 5b.28 Variation of die swell ratio of HDPE- commercial ZnO composites with concentration of ZnO at different shear rates

5b.3.5.5.2 Effect of temperature

Variation of die swell ratio of HDPE-nano ZnO composites at three different temperatures is given in figure 5b.29. It is clear from the figure that die swell ratio decreases with temperature and concentration of ZnO.
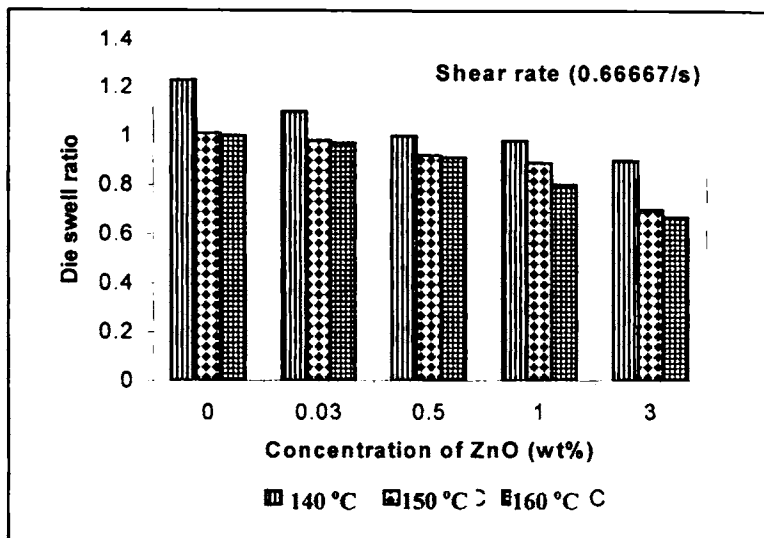
Figure 5b.29 Variations of die swell ratio of HDPE- nano ZnO composites with temperature

5b.3.5.6 Extrudate deformation studies

The appearance of the extrudate of neat HDPE and composites with 1.0 % nano ZnO at six different shear rates is shown in figure 5b.30 (a) and (b) respectively. From the figure it is clear that the extrudate distortion tendency increases with the shear rate. At a low shear rate, the extrudate has a smooth surface; however, at a higher shear rate, the surface becomes rougher. The ZnO content of the nanocomposite also plays a major role in determining the surface characteristics. As the ZnO content increases, the surface roughness also increases. Several factors contribute towards surface irregularity. It has been conclusively shown by photographic techniques[57,58] that a fracturing or breaking of the elastically deformed flowing polymer stream occurs at the entrance to the capillary itself at some critical shear stress. Another factor contributing towards extrudate distortion is the successive sticking and slipping of the polymer layer

at the wall in the capillary.[59,60] Moreover, there may be an effect at the exit as well. Shear thinning behaviour of the nanocomposites is clearly visible in these photographs.

Figure 5b.30 Extrudate photographs of (a) neat HDPE (left) and (b) HDPE- nano ZnO composites filled with 1.0 % ZnO (right) at six different shear rates (a) 0.01333/s (b) 0.1333/s (c) 0.66667/s (d) 1.3332/s (e) 2.6664/s (f) 6.6667/s

Part C

MODIFICATION OF POLYSTYRENE USING NANO ZINC OXIDE

5c.1 Introduction

The development of organic–inorganic nanocomposites with improved properties has attracted much interest in past few years. Organic–inorganic nanocomposites materials have been regarded as new generation of high performance materials since they combine the advantages of the inorganic materials (rigidity, high stability) and the organic polymers (flexibility, dielectric, ductility and processibility).[106-110] Polystyrene (PS) is a hard, rigid, transparent thermoplastic commodity polymer that is used in a number of commercial products because of its versatile properties like low cost, good mouldability, low moisture absorption, good dimensional stability, good electrical insulation, colourability etc. In 2001, PS was counted among the quantitatively most important thermoplastics and continues to be ranked in fourth place after polyethylene, polypropylene, and poly (vinyl chloride).[111-113] The main applications include packaging, extruded sheets, and consumer electronics. Improved mechanical properties with weight reduction, decreased vapour permeability, and low oxygen diffusion are the main development areas for packaging (foamed and foils packaging). Reduced flammability in the area of electronics is also required. Improvement in these properties can be achieved with the nanocomposite approach. There are a number of studies in which PS was used as nanocomposite matrix. Most of these investigations concerned organoclays.[114-120] However, metals,[121,122] metal sulfides (CdS),[123] a metal oxide,[124] nanotubes,[125] SiO_2[126] and graphite [127] are also mentioned. The common conclusion that can be drawn from these studies is that the polymer matrix is significantly affected by the presence of nanofillers. Nevertheless, depending on the particle dimensions, shape and chemical structure, different properties will arise.

In this study PS is mixed with both nano ZnO and commercial ZnO and compared properties like crystallization, thermal stability, mechanical, dynamic mechanical and melt rheology.

5c.2 Experimental

A simple melt-compounding route was adopted for the preparation of PS-ZnO nanocomposites. The melt compounding was performed using Thermo Haake Rheocord 600 mixing chamber with a volume capacity of 69 cm^3 fitted with a roller type rotors operating at 40 rpm for 8 min at 180 °C. Nanocomposites at different concentrations (0.0–3.0 wt%) of ZnO were prepared. In all cases the torque stabilized to a constant value in this mixing time.

5c.3 Results and discussion
5c.3.1 Differential scanning calorimetry

PS is an amorphous polymer. Differential scanning calorimetry (DSC) analysis of PS- nano ZnO composites were carried out. It is of interest to point out that no crystalline melting endothermic peaks were observed in the DSC curves of PS-ZnO composites, and only a glass transition was identified for these composites with 0.03–3 wt% ZnO composition. The reported heat capacity curves are given in figure 5c.1. All DSC thermograms display single glass transition temperatures in the experimental temperature range. It should be pointed out that the single glass transitions erroneously indicate that the hybrids are homogeneous and the observed glass transition is attributed to polystyrene matrices. It can be seen that the glass transition temperature of the nanocomposite is slightly shifted towards a higher temperature. It is seen that addition of 3.0 wt % nano ZnO shifts T_g of PS towards a higher value by 5 °C. This indicates that there is a strong interaction between the polymer matrix and ZnO particle at the interface, and due to this, mobility of the polymer segments near the interface become suppressed. The interaction between the ZnO nanoparticles and the chains of PS becomes so intensively strengthened that the main-chain motion of the polymer is greatly restricted.[128-130]
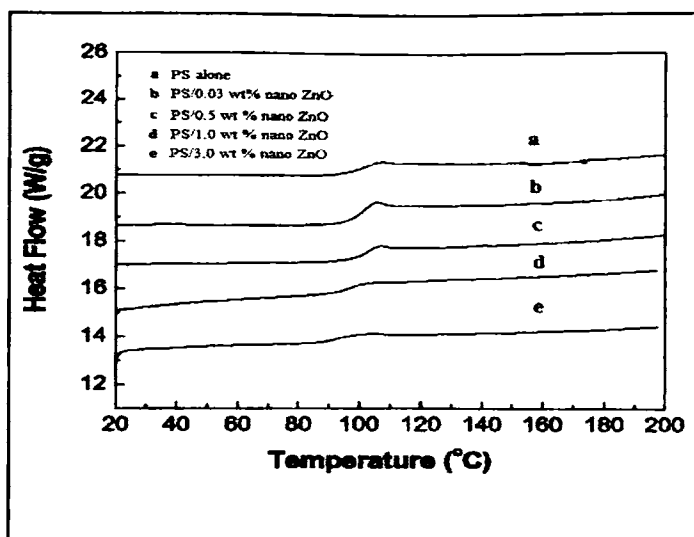
Figure 5c.1 DSC curves for PS- nano ZnO composites

It should be noted that the glass transition is not a true phase transition, since the derivative of the heat capacity can be a continuous function of temperature. The slope of the heat capacity curve represents, in fact, a spectrum of glass transition temperatures, which originate from different segmental motions. On the other hand, broadening of the glass transition region can be noticed after incorporation of the ZnO nanoparticles. This implies that segmental motions in the matrix must be somehow altered, probably due to a change in the packing density of the polymer chains in the vicinity of the filler particles. At the same time, with respect to pure PS, no change in the segmental distribution, i.e., the glass transition region, was observed. On adding 1.0 wt% commercial ZnO, T_g value decreases to 102 °C from 105 °C of pure PS. It is clear that the system is more compatable with nano ZnO. Similar DSC results were obtained when spherical ZnO and ZnO whisker were used in PS matrix.[49] The glass transition temperature of nanocomposites increased by 8 °C on adding ZnO. But they mixed 5-30 wt% of ZnO filler.
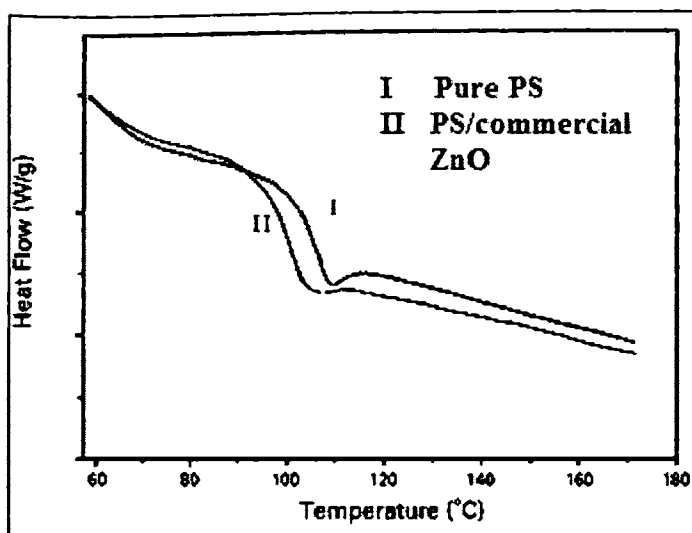
Figure 5c.2 DSC curves for PS- commercial ZnO composites

5c.3.2 Thermogravimetry

Thermal decomposition of polystyrene starts with the formation of free radicals at weak bonds (usually peroxidegroups and/or chain ends).[131] This initial step is followed by chain transfer reactions of the primary free radicals, which propagate until the whole matrix is affected. It is obvious that restricted motion of the chain segments, due to the presence of nano filler, can prevent chain transfer reactions leading to an enhanced thermal stability of the material.

The TGA and DTG thermograms of the pure PS and the PS- ZnO nanocomposites are presented in figure 5c.3 & 5c.4 respectively. Evidently the decomposition onset temperatures of PS-ZnO nanocomposites shift towards higher temperature compared to that of the pure PS, indicating an enhancement in thermal stability of PS. A possible reason for the shifting of onset temperature is that ZnO is an inorganic material with high thermal stability and great heat-resistance, which can prevent heat from transmitting quickly and thus limit the continuous decomposition of the nanocomposites.
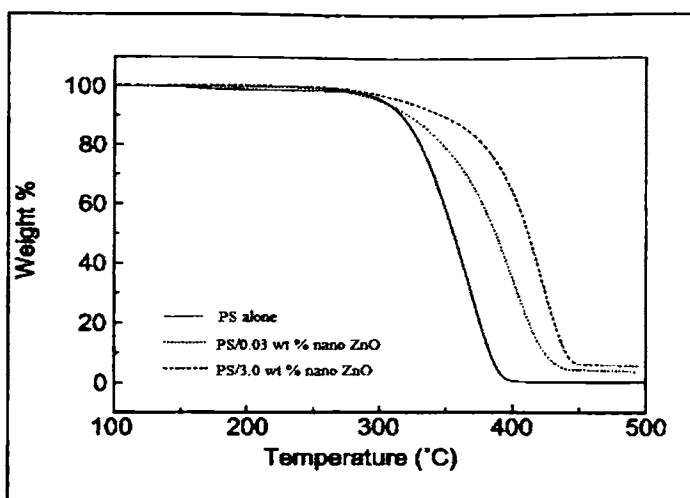
Figure 5c.3 TGA traces for PS- nano ZnO composites
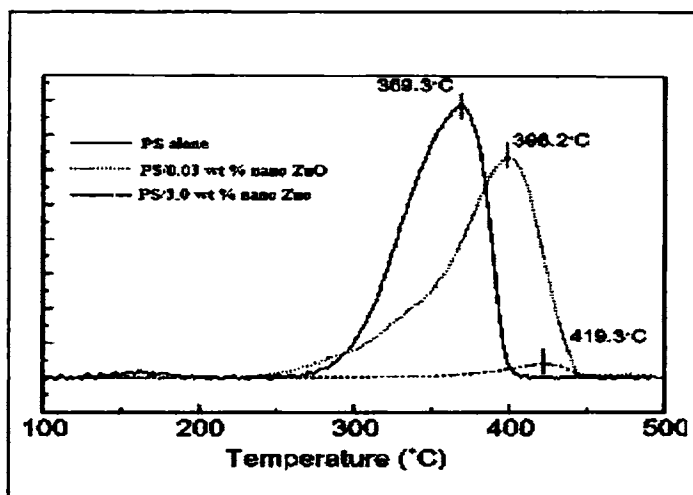
Figure 5c.4 DTG traces for PS- commercial ZnO composites

The temperature of onset of degradation T_i ($^\circ$C), the temperature at which the rate of decomposition is 10 % [$T_{10\%}$ ($^\circ$C)], the temperature at which the rate of decomposition is maximum (T_{max}) ($^\circ$C), the temperature at which the rate of decomposition is 50 % [$T_{50\%}$ ($^\circ$C)], the peak degradation rate and the residue at 800 $^\circ$C are given in table 5c.1. PS degrades in a single step. The degradation starts at a temperature of 232 $^\circ$C and the peak rate of degradation is 2.713 %/min at corresponding (T_{max}) 369 $^\circ$C and in nanocomposites, T_i is 251 $^\circ$C on adding 3.0 wt% nano ZnO, indicating improved thermal stability of the nanocomposites.

The T_{max} temperature also showed an improvement in thermal stability. Residue at 800 °C is 1.253 % for PS. On adding 3.0 wt% ZnO, residue increased to 1.934% and the peak rate of decomposition decreased from 2.713 to 1.456 %/min. This increase in the thermal stability of the nanocomposites may result from the strong interaction between the nano ZnO and PS molecules. But on adding commercial ZnO, themal stability of PC remains unaffected (figure 5c.5). Since nano ZnO has a higher specific surface area (for the same addition amount) than that of commercial ZnO, and so the former has a greater contact surface with polystyrene, thus increasing the thermal stability of the nanocomposite.
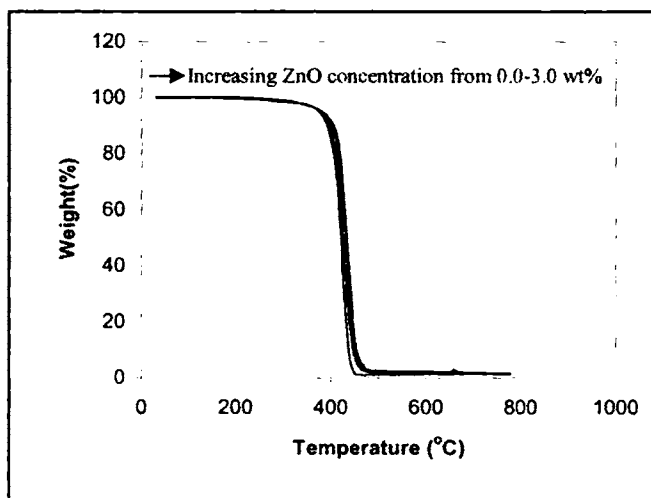
Figure 5c.5 TGA traces for PS- commercial ZnO nanocomposites (lower curves with increasing concentration of ZnO)

Table 5c.1 Degradation characteristics of PS-ZnO nanocomposites

Concentration of ZnO	T_i (°C)	$T_{10\%}$ (°C)	Residue at 800 °C (%)	Peak rate of decomposition (%/min)	$T_{50\%}$ (°C)	T_{max} (°C)
0	232	281	1.253	2.713	356	369
0.03	234	297	1.467	2.398	387	398
3.0	251	312	1.934	1.456	403	419

Increase in thermal degradation temperature of PS- ZnO nanocomposites was also reported by Chen-Chi et al.[47] There is an increase of 35 °C on adding 3.0 wt% ZnO.

5c.3.3 Mechanical properties
5c.3.3.1 Torque studies

The variation of mixing torque with time of mixing at different ZnO loading is shown in figure 5c.6. A mixing time of 8 min was fixed since the torque stabilized to a constant value during this time. The temperature of the mixing chamber was fixed as 180 °C. The stabilization of the torque may be related to the attainment of a stable structure after a good level of mixing. The initial torque values of PS are high because of its high melt viscosity. Initially torque increased with the charging of PS, but decreased with melting. After homogenization of PS, ZnO was added at 2 min. There is a little increase in torque on continued mixing with ZnO. After mixing, the torque value is found to be steady. It is clear from figure that there is no degradation taking place during the mixing stage. Similar trend in torque is observed when commercial ZnO is mixed with PS.
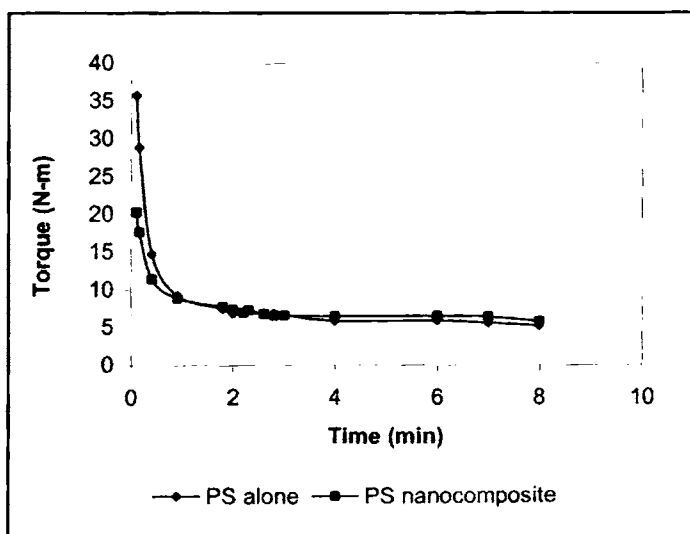

Figure 5c.6 Torque-time curves of PS- ZnO nanocomposites

5c.3.3.2 Tensile properties

As one of the most widely used commodity plastic materials, PS has been modified to enhance mechanical properties in different ways. Tensile properties of PS-nano ZnO composites are summarized in table 5c.2. The simultaneous increase in tensile strength can obviously be attributed to a more efficient stress transfer mechanism between two components of hybrid composites. These phenomena might be a distinctive feature of nanocomposites.

The effects of the nano ZnO on the mechanical properties are summarized in table 5c.2.

Table 5c.2 Tensile properties of PS-nano ZnO composites

Concentration of ZnO (wt%)	Tensile strength (MPa)	Tensile modulus (GPa)	Elongation (%)	Shore D hardness	Energy to max (J)	Tensile toughness (J/m)
0.0	29.5	2.094	6.98	51	0.4532	238.5
0.03	32.8	2.098	6.31	55	0.5612	272.4
0.1	34.1	2.132	6.70	57	0.8954	389.4
0.5	35.6	2.181	6.36	59	0.9234	419.7
1.0	37.0	2.189	6.12	62	1.231	557.0
2.0	38.2	2.196	5.68	67	1.367	666.8
3.0	39.1	2.199	5.05	69	1.642	713.9

The results in table 5c.2 showed an increase in the tensile modulus and strength of PS with an increasing concentration of nano ZnO content from 0.0 to 3.0 wt%. From 0.0 to 1.0 wt% the change in tensile strength is about 25 % and modulus is about 5 %. But from 1.0 to 3.0 wt% the increase in tensile strength is only about 6 % and modulus is almost constant. So, for effective reinforcement only less than 1 % ZnO is necessary. The Shore D hardness also supports the reinforcement. The elongation to break is found to decrease with an increasing loading of ZnO. Energy to maximum and tensile toughness (energy/ thickness of the sample) values (figure 5c.7) increases to 260 % and 199 % respectively with

3.0 wt % filler loading. These results demonstrate that even a small fraction of ZnO provide effective reinforcement to the PS matrix. This is due to better interaction between the PS matrix and ZnO nanoparticles. As aspect ratio of ZnO is high, it has a large surface area available for adhesion between the polymer molecules and ZnO particles. This facilitates better load transfer to the reinforcing phase and contributes to the improved strength and modulus. On adding commercial ZnO, tensile strength remains constant and modulus of PS slightly increased. Energy to maximum and tensile toughness of PS-commercial ZnO nanocomposites showed slight improvement (table 5c.3). But this improvement is negligible when compared with the reinforcement produced by nano ZnO. With 3.0 wt% commercial ZnO the improvement in modulus, energy and tensile toughness is about 1 %, 4 % and 5 % respectively.

So nanocomposites prepared from nano ZnO can attain superior performance over commercial ZnO. This high reinforcement implies a strong interaction between the matrix and nano ZnO interface that can be attributed to the nanoscale and uniform dispersion of the ZnO in the PS matrix.

Figure 5c.7 Variation of tensile toughness with concentration of ZnO
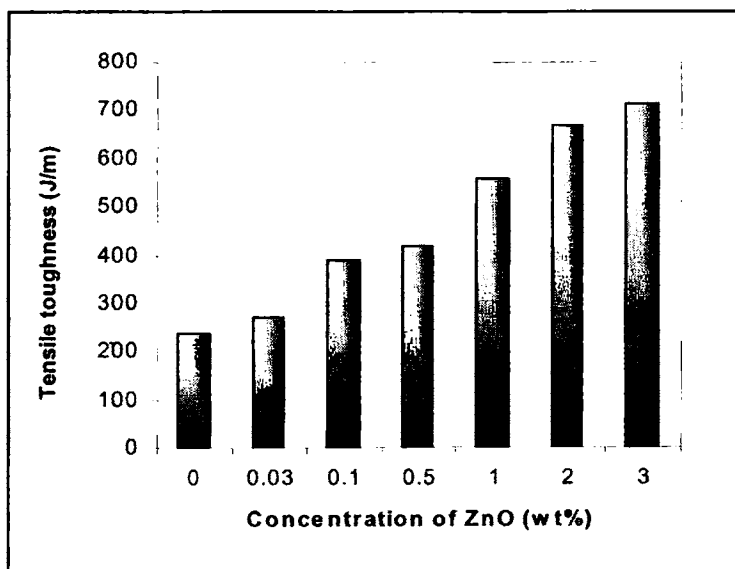
Table 5c.3 Tensile properties of PS-commercial ZnO composites

Concentration of ZnO (wt%)	Tensile strength (MPa)	Tensile modulus (GPa)	Elongation (%)	Shore D hardness	Energy to max (J)	Tensile toughness (J/m)
0.0	29.50	2.094	5.21	51	0.4532	238.5
0.03	29.50	2.094	5.15	55	0.4533	245.1
0.1	29.56	2.098	5.13	57	0.4534	240.3
0.5	29.54	2.098	5.12	57	0.4556	244.1
1.0	29.53	2.103	5.09	68	0.4623	246.9
2.0	29.57	2.116	5.04	61	0.4641	247.1
3.0	29.51	2.119	5.05	61	0.4712	248.9

Stress-strain curves for PS and its nanocomposite is shown in figure 5c.8. Area under the stress-strain curve increases due to energy absorption. So it is clear that modification has taken place in PS matrix with ZnO loading.
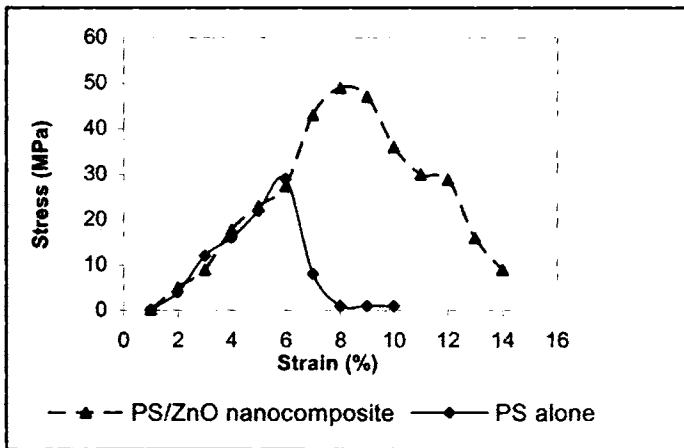
Figure 5c.8 Stress-strain curve for PS and its nanocomposites

5c.3.3.3 Morphology of the fractured surfaces

The morphological structure of polymer nanocomposites is important because it ultimately determines many properties of the polymer nanocomposites. The scanning electron micrographs of the fractured surfaces of the tensile test specimens have been studied to acquire an insight into the mechanism of reinforcement. Figure 5c.9 (a) shows the fracture surface for unmodified PS. The fracture surface is relatively smooth and even, showing a

brittle fracture feature without any sign of significant plastic deformation. From figure 5c.9 (b) it is clear that nano ZnO exist as dispersed particles and the morphology gets substantially modified. SEM images are in good agreement with the observed mechanical properties, which is due to shear yielding. Figure shows that, in different project positions of the matrices of PS-ZnO nanocomposites, nanoscale ZnO particles are homogeneously dispersed in the PS matrices. Nano ZnO leading to stress whitening is prevalent in this figure, indicating localized plastic deformation.

In PS-ZnO nanocomposites shear yielding is the reinforcement mechanism. There is complete stress transfer from the PS matrix to nano rod having high aspect ratio. There is no sign of extensive particle agglomeration as compared to PS-commercial ZnO nanocomposite fracture surface shown in figure 5c.9 (c), where we can see large agglomerates and the dispersion is inhomogeneous.

(a)

(b)

(c)
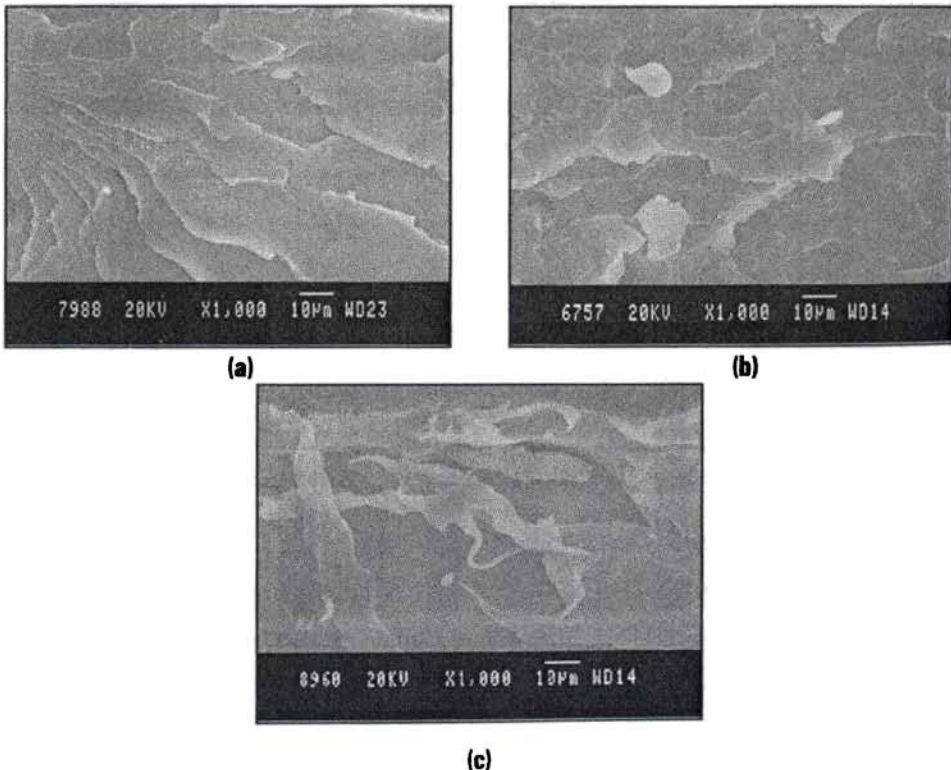
Figure 5c.9 Tensile fractured surfaces of (a) neat PS (b) PS-nano ZnO composites and (c) PS-commercial ZnO composites

5c.3.3.4 Flexural properties

A comparison of flexural strength and modulus of PS-ZnO nanocomposites using nano and commercial ZnO is shown in figure 5c.10 (a) & (b) respectively. With nano ZnO, the flexural modulus as well as the strength of PS increases considerably. For example, incorporation of nano ZnO at the level of 3.0 wt% modulus increases by around 12 % and strength by around 35 %. With commercial ZnO, the flexural modulus and strength remains a constant. Nano ZnO has a unique structure, and so it is easily inserted into the matrix, increasing the contact area between the ZnO and matrix. Moreover, from the perspective of reinforcement of composite, nano ZnO will increase the flexural strength and flexural modulus than commercial ZnO, because it has a higher aspect ratio. Chen et al.[47] also reported an improvement in flexural strength and modulus of PS matrix by ZnO particles.
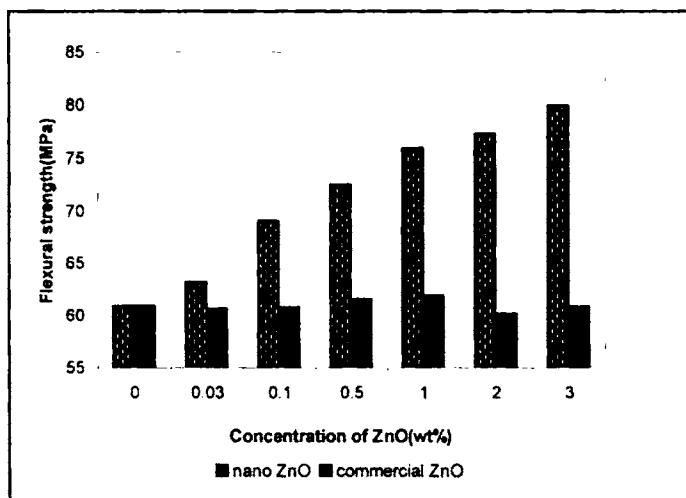
(a)
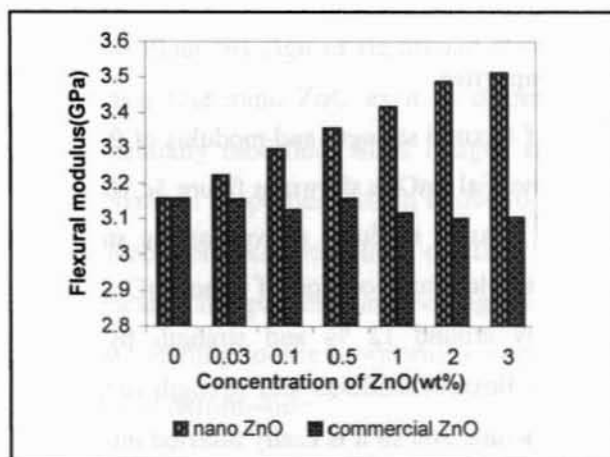
(b)

Figure 5c.10 Comparison of (a) flexural strength (b) flexural modulus of PS- ZnO nanocomposites

5c.3.3.5 Impact strength

Unnotched Izod impact strength of PS- ZnO nanocomposites using nano and commercial ZnO is compared in figure 5c.11. With commercial ZnO, the impact strength improvement is about 9 %, but with nano ZnO, the increase is about 160 % on adding 3 wt% of ZnO. The increase in impact strength is evidenced by the tensile toughness values given in figure 5c.7 and from the area of the stress strain curve given in fgure 5c.8. So the toughness of the nanocomposite improved with nano ZnO addition.
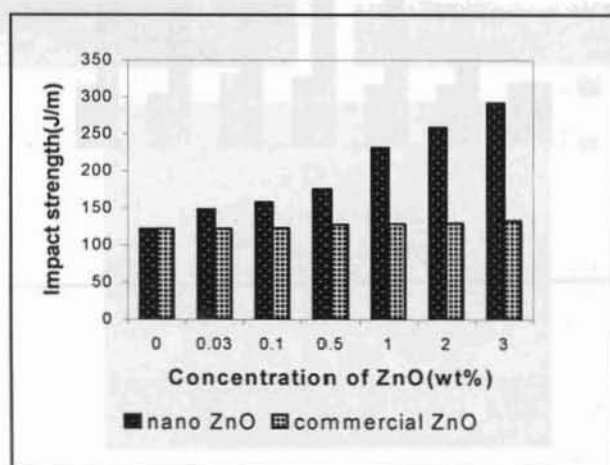

Figure 5c.11 Comparison of impact strength of PS- ZnO nanocomposites using nano and commercial ZnO

This variation in unnotched impact strength can be attributed to two things. First, when small amount of nano ZnO is added there is seldom agglomerated particle in the matrix. As Nakagawa showed,[132] the presence of fine particles dispersed within the matrix make plastic deformation easier. So, during the fracture of a composite in which the nanoparticle is well dispersed, the stress will have to be bigger to start the microcrack on a nanoparticle, and the impact energy will largely be absorbed by the exhibited plastic deformation, which occurs more easily around the nanoparticles. Hence, the good nano-ZnO dispersion resulting from no agglomeration led to a better impact strength of the nanocomposites. However, when commercial ZnO is introduced into the PS matrix, the nanoparticles do not retain their uniform dispersion, it is dispersed in the form of large agglomerates in the PS matrix, and these will become the site of stress concentration and act to initiate microcracks.[133] So, a large aggregate is a weak point that lowers the stress required for the composite to fracture and thus the impact strength of nanocomposites would be decreased or sometimes remains constant.

5c.3.4 Dynamic mechanical analysis (DMA)

The DMA results for the dynamic storage modulus of the PS-ZnO nanocomposite samples as a function of temperature at 1 Hz are shown in figure 5c.12. Following a slow decrease of the modulii with temperature in the glassy state, a rapid decrease in modulii is observed corresponding to the glass-rubber transition at about 105 °C. The storage modulii of the nanocomposite samples below glass transition increases substantially with the nano ZnO concentration (about 20 % increase with 1 wt% and about 40 % increase with 3 wt% nano ZnOs) due to the stiffening effect of ZnO, and indicating efficient stress transfer between the PS matrix and ZnOs. But with commercial ZnO, the storage modulus decreases, (about 20 % with 1wt% ZnO). The storage modulus of nanocomposites at 35 °C, 50 °C & 100 °C is given in table 5c.4.
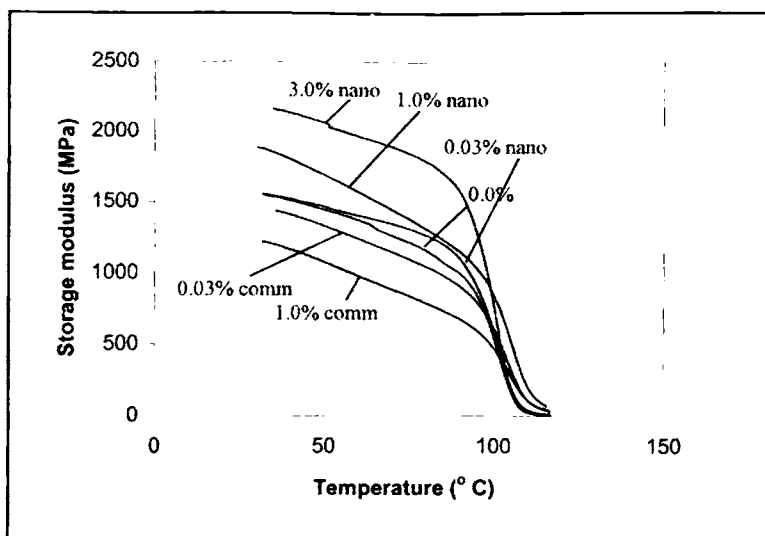
Figure 5c.12 Storage modulus of PS- ZnO nanocomposites

Table 5c.4 Storage modulus of PS- ZnO nanocomposites at 35 °C, 50 °C & 100 °C

Sample	Storage modulus at 35 °C (MPa)	Storage modulus at 50 °C (MPa)	Storage modulus at 100 °C (MPa)
PS alone	1545	1456	407
PS/0.03 wt% nano ZnO	1551	1466	529
PS/1.0 Wt%nano ZnO	1845	1695	854
PS/3.0 wt% nano ZnO	2154	2063	589
PS/0.03 wt% commercial ZnO	1430	1329	541
PS/1.0 wt% commercial ZnO	1211	1080	476

The DMA results for the loss modulus of the PS-ZnO nanocomposite samples as a function of temperature at 1 Hz are shown in figure 5c.13. Modifying with ZnO, loss modulus value decreases. This decrease in loss modulus value is more observed for PS-nano ZnO composites than that of PS-commercial ZnO composites.
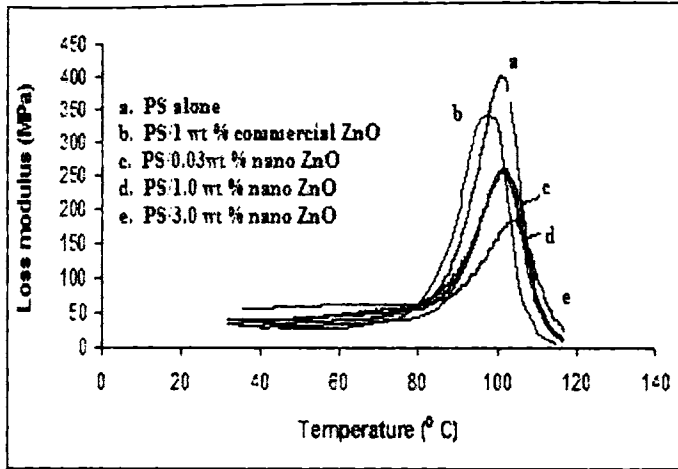
Figure 5c.13 loss modulus of PS- ZnO nanocomposites

Figure 5c.14 shows tan δ versus temperature plots for PS-ZnO nanocomposites. From the tan delta peak it is clear that some compatibility is achieved as a result of mixing PS with nano ZnO which is evident from peak broadening. PS-ZnO nanocomposite is prepared with increasing stiffness. From the tan δ peak it is clear that with nano ZnO, only a slight increase in glass transition temperature is observed, but it decreases by around 5 °C with commercial ZnO loading. T_g, loss modulus and tan δ values of PS-ZnO nanocomposite are given in table 5c.5.
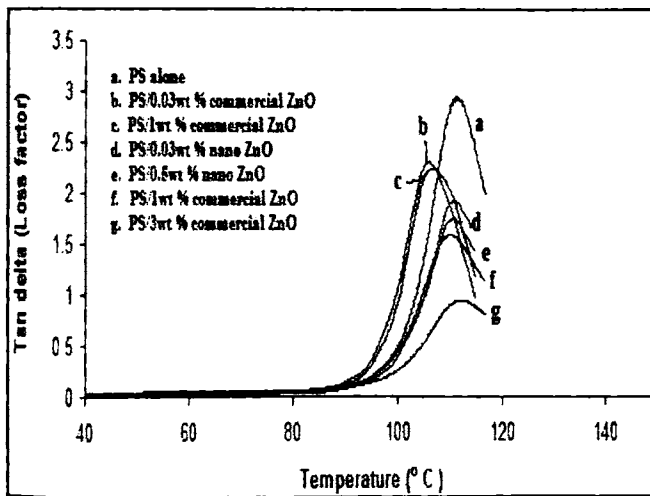
Figure 5c.14 Effect of ZnO concentration on the tan δ of PS-ZnO nanocomposite samples

Table 5c.5 T_g, loss modulus and tan δ values of PS- ZnO nanocomposite samples

| Sample	Loss modulus (MPa)	T_g °C (from tan δ peak)	Peak values of tan δ at T_g
PS alone	388	110.1	2.93
PS/0.03 wt% nano ZnO	252	110.2	1.86
PS/1 wt% nano ZnO	231	110.5	1.74
PS/3 wt% nano ZnO	173	110.1	0.94
PS/0.03 wt% commercial ZnO	340	105.8	2.27
PS/ 1.0 wt % commercial ZnO	355	105.2	2.16

We note the modulus, $E^* = (\text{loss modulus }^2 + \text{storage modulus }^2)^{1/2}$ for the neat PS is numerically consistent with the tensile modulus reported by the Dow Chemical Co. PS chains are severely entangled and the function of nanoparticles as physical anchorage points is relatively insignificant. The mobility of molecular chain segments is largely determined by entangling conditions. Therefore, T_g of PS does not have a clear variation by introduction of the nano ZnO particles. The T_g of PS-nano ZnO composites slightly increases with ZnO content, because ZnO nanorods having larger aspect ratio can restrict the segmental motion of PS molecules and reduce the free volume of polymer chain folding. But in the case of commercial ZnO nanocomposites due to the coarse nature of ZnO, T_g value decreases. So we can conclude that nano ZnO serves as a nano-filler leading to the increase in T_g and storage modulus; on the other hand, commercial ZnO is a plasticizer leading to the decrease in T_g and modulus.[134-135]

Correlation of impact and dynamical properties in terms of tan δ peak values of the nanocomposites has been done. The variation of the impact strength as a function of the total loss tangent peak values for PS- nano ZnO composites and PS- commercial ZnO composites is shown in figure 5c.15 (a) & (b) respectively. The curves show a non-linear shape.
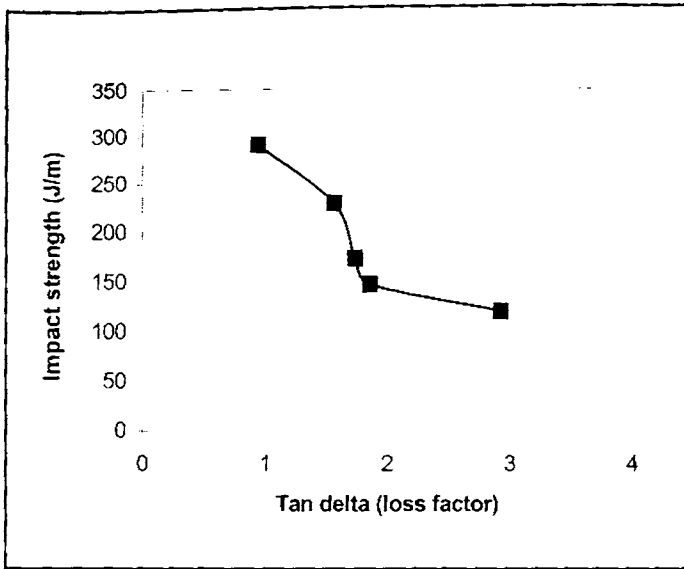
(a)
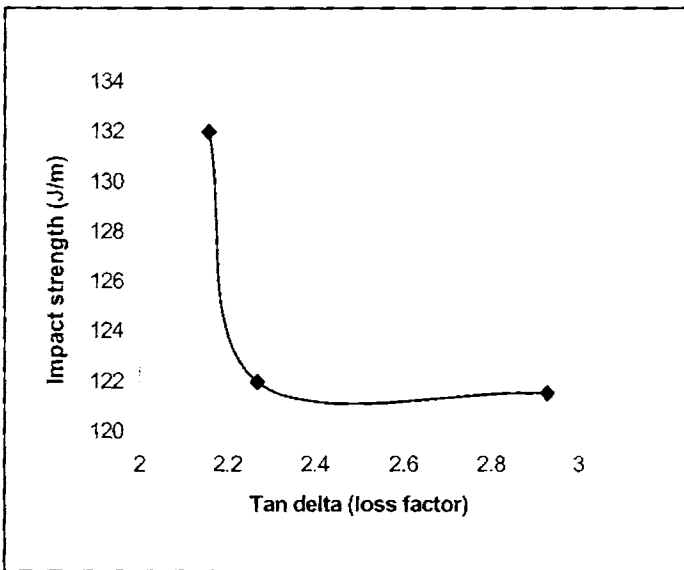
(b)

Figure 5c.15 Variation of the impact strength of PS- ZnO nanocomposites as a function of the total loss tangent peak on using (a) nano ZnO (b) commercial ZnO

5c.3.5 Melt rheology

The rheological behaviour of PS- ZnO nanocomposites is studied at three different temperatures 170, 180 & 190 °C. Effect of shear stress, filler loading and temperature on rheological behaviour is investigated.

5c.3.5.1 Effect of shear stress on shear viscosity

Figure 5c.16 present the shear viscosity vs. shear stress curves of PS-ZnO nanocomposites at 180 °C with an increasing ZnO concentration from 0.0-3.0 wt%. We also examined the flow behaviour of PS nanocomposites filled with 1.0% commercial ZnO. As shear stress increases, the viscosity of PS-ZnO composites decreases in all cases, indicating the pseudoplastic flow behaviour. At zero shear, the molecules are randomly oriented and highly entangled and therefore exhibit high viscosity. Under the application of shearing force, the polymer chains orient, resulting in the reduction of shear viscosity and thus exhibit shear thinning (pseudoplastic behaviour). It is just this pseudoplasticity that makes the nanocomposites to be easily melt-processed. Effect of temperature on shear viscosity of PS nanocomposites filled with 1.0 % nano ZnO is given in figure 5c.17. With a rise of temperature from 180 to 190 °C the value of shear viscosity decreases, especially at relatively lower apparent shear stress. The melt viscosity increases when the temperature decreases to 170 °C.
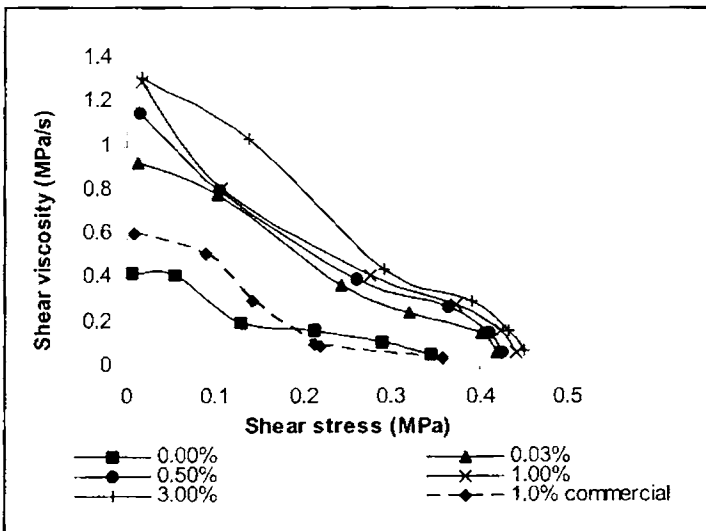
Figure 5c.16 Effect of shear stress on shear viscosity of PS- ZnO nanocomposites
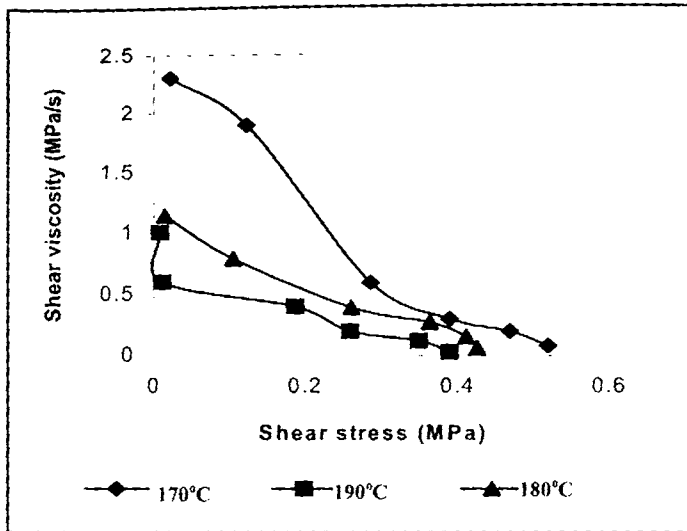
Figure 5c.17 Effect of temperature on shear stress vs. shear viscosity

5c.3.5.2 Effect of filler loading

Since entanglements of polymer chains and arrangement of ZnO are not permanent and altered by flow and relaxation processes, any disturbance of this steady state, such as shear, will disrupt the structure of the polymer matrix. Figure 5c.18 shows the variation of shear viscosity with increasing concentration of nano ZnO from 0.0-3.0 wt% at six different shear rates. It is clear from the figure that shear viscosity increases with nano ZnO addition and this increase is more prominent at low shear rates and low ZnO concentration. At higher shear rate shear viscosity maintains the same value with increasing concentration of ZnO. Also it can be seen from the figure that shear viscosity decreases substantially with increasing shear rate, but increases monotonically with increasing nano ZnO loading at a given shear rate.
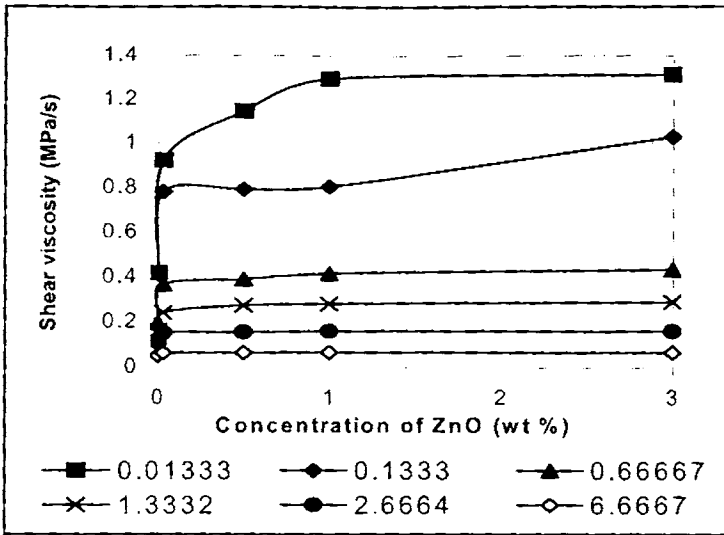
Figure 5c.18 Variation of shear viscosity with concentration of ZnO and shear rates at 180 °C

Figure 5c.19 examines the variation of shear viscosity of PS nanocomposites with concentration of commercial ZnO at six different shear rates. At lower shear rates shear viscosity increases with concentration of ZnO. But at higher shear rates shear viscosity almost remains constant.
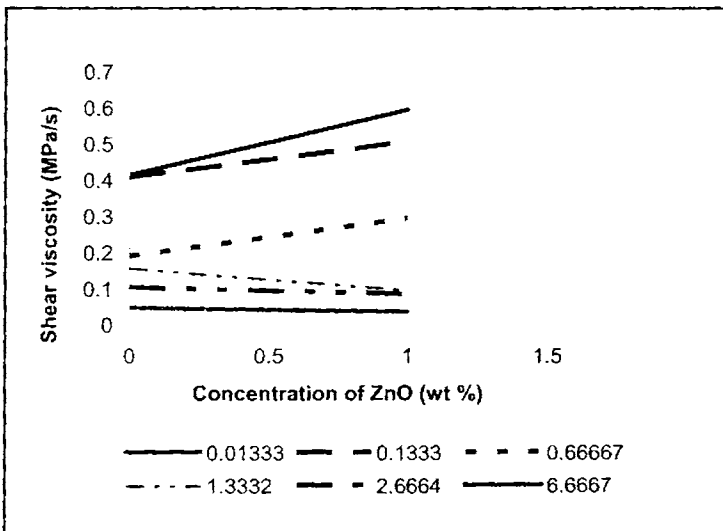
Figure 5c.19 Variation of shear viscosity with concentration of commercial ZnO at six different shear rates at 180 °C

5c.3.5.3 Effect of temperature

Shear viscosities of pure PS and nanocomposite melts decreases with increasing extrusion temperature in the range of 170-190 °C, demonstrating that increasing temperature improves the flow behaviour of the polymer melts. However, the effect of temperature on shear viscosity changes with the shear rate. The data indicate that the temperature sensitivity of shear viscosity is higher in lower shear rate region, and drops at higher shear rates. This phenomenon is in agreement to the fact that elevating shear rate always accompanied by a rapid decrease of the entanglement density of macromolecules and the melt viscosity. The Arrhenius plot of PS-nano ZnO composites at two different shear rates is given in figure 5c.20 (a) & (b). A good linear correlation was found in the plot of ln η_a vs. 1/T, which has proved the appropriateness of the Arrhenius–Eyring equation. Values of E_a obtained from the slopes of these plots are given in table 5c.7. The activation energy of a material provides valuable information on the sensitivity of the material towards the change in temperature. The higher the activation energy, the more temperature sensitive the material will be. Therefore, such information is highly useful in selecting the processing temperature of polymeric materials.

From the table 5c.7 it can be observed that the activation energy of flow of the nanocomposites decreases with modification at lower shear rates. But activation energy increases with modification at higher shear rates.
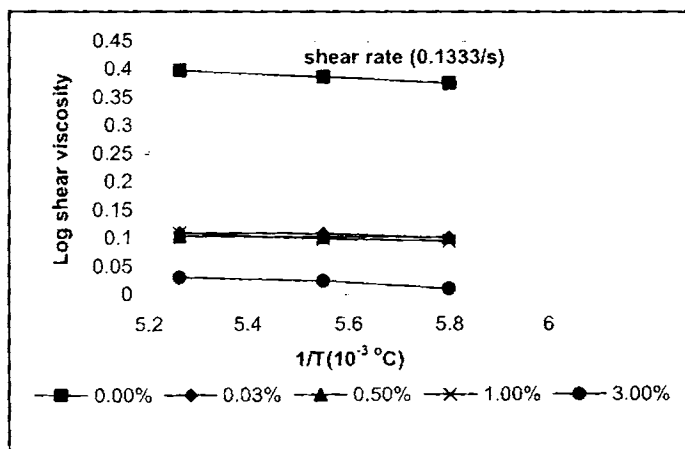
(a)
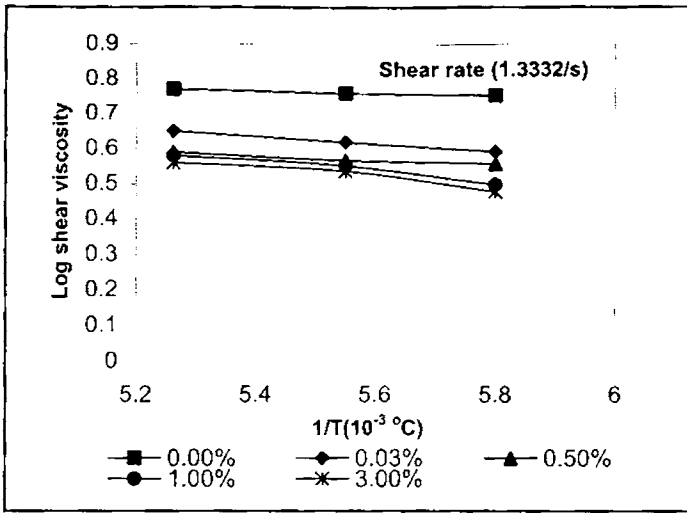
(b)

Figure 5c.20 (a) & (b) Variation of log viscosity with 1/T for the PS- nano ZnO composites

Table 5c.7 Activation energies of PS- nano ZnO composites at two shear rates

Concentration of ZnO (wt%)	Activation energy (J/mol)	
	0.1333/s	1.3332/s
0.0	0.0409	0.0294
0.03	0.0162	0.0563
0.5	0.0055	0.1054
1.0	0.0281	0.1476
3.0	0.0368	0.1472

5c.3.5.4 Flow behaviour index (n′)

The effects of temperature and concentration of ZnO on the flow behaviour indices of the samples have been studied in detail. The extent of pseudoplasticity or non-Newtonian behaviour of the materials can be understood from n′ values. Pseudoplastic materials are characterized by n′ below 1. Flow behaviour index values of PS- nano ZnO composites at 180 °C and 190 °C are given in figure 5c.21. It is clear from the figure that n′ decreases with increasing concentration of ZnO and temperature. This suggests that the system becomes more pseudoplastic as the ZnO content and temperature increases.
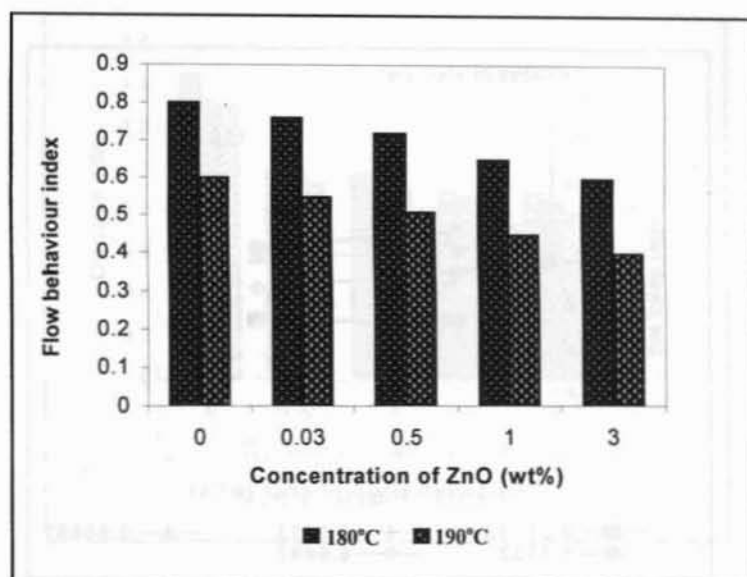
Figure 5c.21 Variation of flow behaviour index of PS nanocomposites with concentration of ZnO

5c.3.5.5 Die swell

Die swell, called Barus effect is an important parameter for characterizing polymer melt elasticity in an extrusion flow and is related to the quality of the end products.

5c.3.5.5.1 Effect of shear rate and concentration of ZnO

Figure 5c.22 shows the plots of the die swell ratio, de/dc for PS and PS-ZnO nanocomposites at 180 °C at five different shear rates. The die swell ratio increases obviously with increasing shear rate at a constant ZnO content. It is noticeable that at a constant shear rate, the die swell ratio decreases slightly with a rise of ZnO content. Figure 5c.23 shows the variation of die swell ratio of PS nanocomposites filled with 1.0 % commercial ZnO at different shear rates. Die swell ratio decreases with ZnO loading and increases with shear rates.
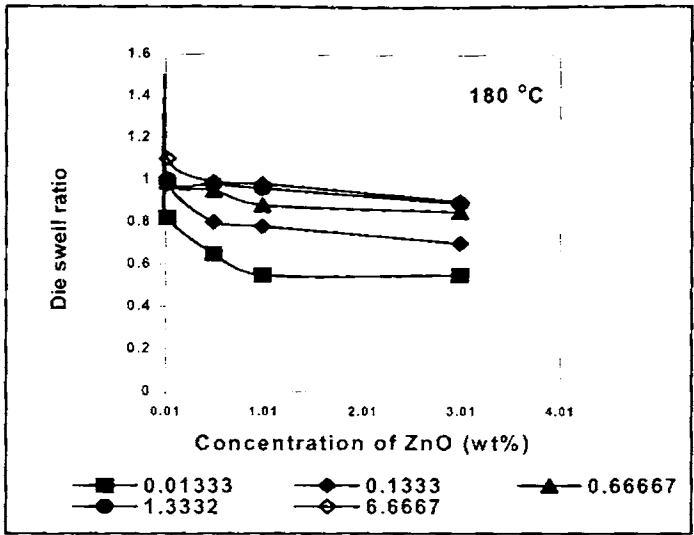
Figure 5c.22 Variation of die swell ratio of PS- nano ZnO composites with concentration of ZnO at different shear rates
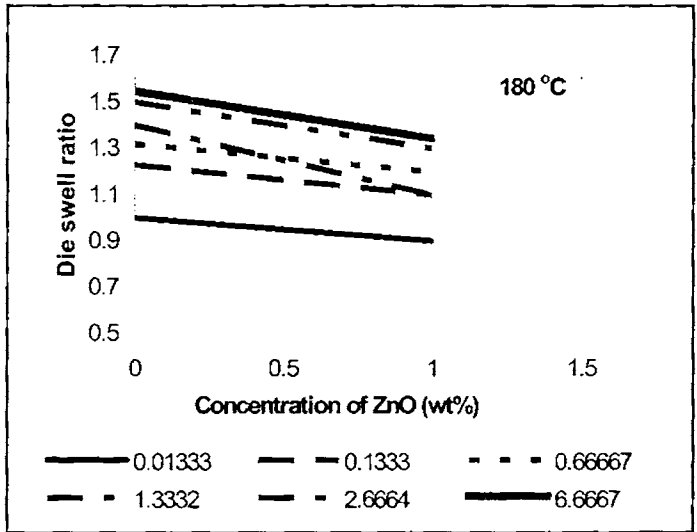
Figure 5c.23 Variation of die swell ratio of PS- commercial ZnO composites with concentration of ZnO at different shear rates

5c.3.5.5.2 Effect of temperature

Variation of die swell ratio of PS- nano ZnO composites at 3 different temperatures is given in figure 5c.24. It is clear from the figure that die swell ratio decreases with temperature and concentration of ZnO.
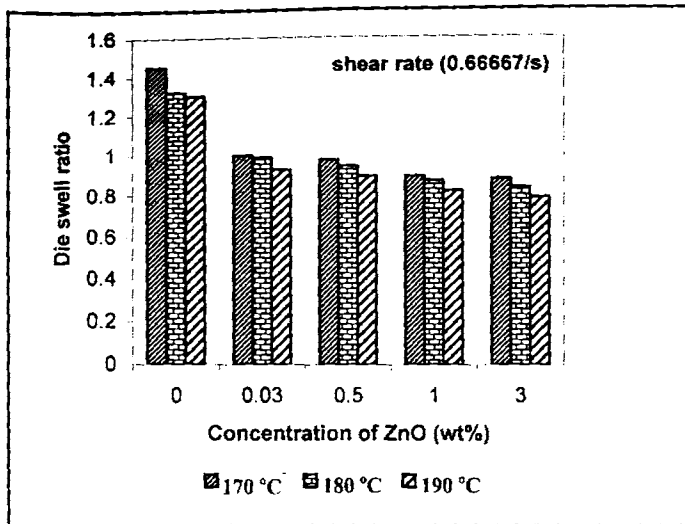
Figure 5c.24 Variations of die swell ratio of PS- nano ZnO composites with temperature

5c.3.5.6 Extrudate deformation studies

The appearance of the extrudate of neat PS and nanocomposites with 1.0 % ZnO at six different shear rates is shown in figure 5c.25 (a) and (b) respectively. From the figure it is clear that the extrudate distortion tendency increases with the shear rate. At a low shear rate, the extrudate has a smooth surface; however, at a higher shear rate, the surface becomes rougher. The ZnO content of the nanocomposite also plays a major role in determining the surface characteristics. As the ZnO content increases, the surface roughness also increases. Several factors contribute towards surface irregularity. It has been conclusively shown by photographic techniques that a fracturing or breaking of the elastically deformed flowing polymer stream occurs at the entrance to the capillary itself at some critical shear stress. Another factor contributing towards extrudate distortion is the successive sticking and slipping of the polymer layer at the wall in the capillary. Moreover, there may be an effect at the exit as well. Shear thinning behaviour of the nanocomposites is clearly visible in these photographs.
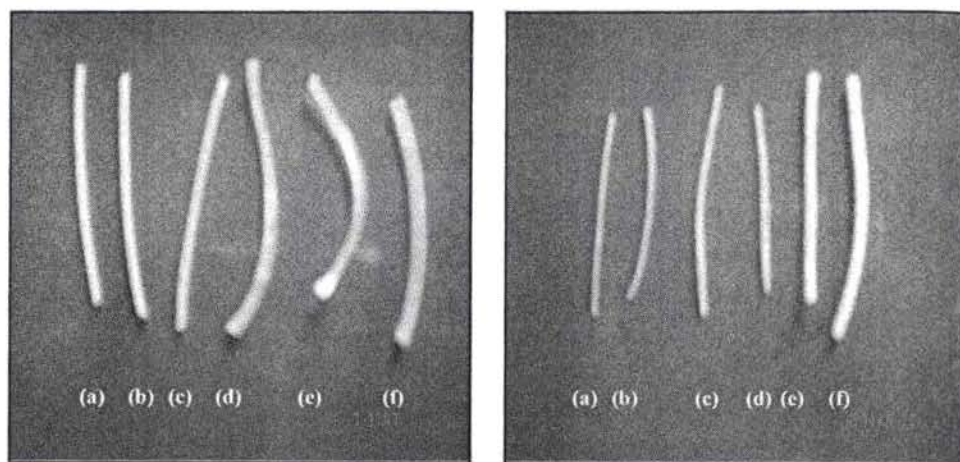
Figure 5c.25 Extrudate photographs of (a) neat PS (left) and (b) PS- nano ZnO composites filled with 1% ZnO (right) at six different shear rates (a) 0.01333/s (b) 0.1333/s (c) 0.66667/s (d)1.3332/s (e) 2.6664/s (f) 6.6667/s

5c.4 Conclusions

The study showed that nano ZnO is a good modifier for commodity thermoplastics like PP, HDPE and PS. Nanocomposites have been prepared through a simple melt compounding route. Melt compounded nano ZnOs have been shown to act as effective nucleating agents for PP and HDPE crystallization. The nano ZnOs at a concentration as low as 300 ppm enhanced the crystallization temperature during melt cooling by 5 °C in PP matrix and 6 °C in HDPE matrix, and reduced melt's isothermal crystallization time by more than 50 % in PP matrix and HDPE matrix. No crystalline melting endothermic peaks were observed in the DSC curves of PS- ZnO composites. A comparison of the nucleation ability of nano ZnO with commercial ZnO also revealed that nano ZnOs are potentially very attractive candidate as nucleating agents. Thermogravimetric analysis showed improved thermal stability for nano ZnO composites than their counterparts. The improved mechanical properties (tensile, flexural and impact) of the nano ZnO composites revealed that a small concentration of nano ZnO could substantially reinforce all the three matrices. Scanning electron microscope studies revealed that the reinforcement mechanism of nano ZnO is shear yielding in PP and PS matrix and in HDPE

matrix, mechanism is shape transition of ZnO nanoparticle from rod to spherical. The dynamic mechanical analysis indicated an improvement in storage and loss modulus of nano ZnO composites than commercial ZnO composites. The rheological characteristics revealed that shear viscosity of the nano ZnO composites increased with concentration of nano ZnO and decreased with increasing shear stress. Melt flow index value and die swell ratio decreased with nano ZnO concentration indicating pseudoplastic behaviour of the flow. Activation energies of the PP nanocomposites increased with modification at lower shear rates. In HDPE nanocomposites, activation energy increased at both lower and higher shear rates, whereas in PS nanocomposites it increased at higher shear rates. Apparently, nano ZnO is a good modifier compared to commercial ZnO for commodity thermoplastics.

5c.5 References

1. Stamhuis JE. Polym Compos 1984, 5, 202.
2. Hadal RS, Misra RDK. Mater Sci Eng A 2004, 374, 374.
3. Radhakrisnan S, Saujanya C. J Mater Sci 1998, 33, 1069.
4. Rong MZ, Zhang MQ, Zheng YX, Zeng HM, Friedrich K. Polymer 2001, 42, 3001.
5. Wu CL, Zhang MQ, Rong MZ, Friedrich K. Compos Sci Technol 2002, 62, 1327.
6. Tabitiang A, Venables R. Eur Polym J 2000, 36, 137.
7. Wah CA, Choong L, Neon GS. Ibid 2000, 36, 789.
8. Premphet K, Horanot P. Polymer 2000, 41, 9283.
9. Bartczakz A, Argon S, Cohen RE, Weinberg M. Polymer 1999, 40, 2347.
10. Liang JZ, LI RKY. J Appl Polym Sci 2000, 77, 409.
11. Mitsuishi K, Kodama S, Kawasaki H. Polym Engng Sci 1985, 25, 1069.
12. Wei GX, Sue HJ. J Mat Sci 2000, 35, 555.
13. Jangar J, Dibenedetto AT. Polym Engng Sci 1993, 33, 559.
14. Demjen Z, Pukanszky B, Jozsef N. Composites Part A 1998, 29, 323.
15. Rothon R, in "Particulate-Filled Polymer Composites" (Wiley, New York, NY, 1995).
16. Sergey Lapshin, Isayev AI. J of Vinyl and Additive Technology 2006, 12(2), 78.
17. Sumita M, Shizuma T, Miyasaka K, Ishikawa K. J Macromol 1983, B22, 601.
18. Sumita M, Tsukurmo T, Miyasaka K, Ishikawa K. J Mater Sci 1983, 18, 1758.
19. Fujiyama M, Wakinino T. J Appl Polym Sci 1991, 42, 2749.
20. Alexander M, Dubois P. Mater Sci Eng 2000, 28, 1.
21. Kato M, Usuki A, Okada A. J Appl Polym Sci 1997, 66, 1781.

22. Oya A, Kurokawa Y. J Mater Sci 2000, 35, 1045.

23. Galgali G, Ramesh C, Lele A. Macromolecules 2001, 34, 852.

24. Kawasumi M, Hasegawa N, Kato M, Usuki A, Okada A. Macromolecules 1997, 30, 6333.

25. Chan CM, Wu J, Li JX, Cheung YK. Polymer 2002, 43, 2981.

26. Fu Q, Wang GH, Shen JS. J Appl Polym Sci 1993, 49, 673.

27. Yuan Q, Jiang W, Zhang HX, Yin JH, An LJ, Li RKY. J Polym Sci Part B: Polym Phys 2001, 38, 1855.

28. Liang JZ, Li RKY. Polymer 1999, 40, 3191.

29. Yuan Q, Jiang W, An LJ, Li RKY. Polym Adv Technol 2004, 15, 409.

30. Liang JZ, Li RKY. Polym Compos 1998, 19, 698.

31. Zuiderduin WCJ, Westzaan C, Hue'tink J, Gaymans RJ. Polymer 2003, 44, 261.

32. Jianguo Tang, Yao Wanga, Haiyan Liua, Laurence A Belfioreb. Polymer 2004, 45, 2081.

33. Maiti P, Nam PH, Okamoto M, Kotaka T, Hasegawa N, Usuki A. Polym Eng Sci 2002, 42, 1864.

34. Leelapompisit W, Ton-That MN, Perrin-Sarazin F, Cole KC, Denault J, Simard B. J Polym Sci Part B: Polym Phys 2005, 43, 2445.

35. Xu WB, Ge ML, He PS. J Polym Sci Part B: Polym Phys 2002, 40, 408.

36. Avella M, Cosco S, Di Lorenzo ML, Di Pace E, Errico ME. J Therm Anal Calorim 2005, 80, 131.

37. Marco C, Gomez MA, Ellis G, Arribas JM. J Appl Polym Sci 2002, 84(9), 1669.

38. Hongxia Zhao, Robert KY Li. Polymer 2006, 47, 3207.

39. Dobreva A, Gutzow I. J Non-Cryst Solids 1993, 162, 1.

40. Wang S, Hu Y, Song L, Wang Z, Chen Z, Fan W. Polym Degrad Stab 2002, 77, 423.

41. Chaganti Srinivasa Reddy, Chapal Kumar Das. J of Appl Polym Sci 2006, 102, 2117.

42. Sangeetha Hambir, Neelima Bulakh, Jog JP. Polymer Engineering and Science 2002, 42(9), 1800.

43. Hasegawa N, Okamoto H, Kato M, Usuki A. J Appl Polym Sci 2000, 78, 1918.

44. Gilman JW. Appl Clay Sci 1999, 15, 31.

45. Yong Tang, Yuan Hu, Rui Zhang, Zhengzhou Wang, Zhou Gui, Zuyao Chen, Weicheng Fan. Macromol Mater Eng 2004, 289, 191.

46. Pravin Kodgire, Rajendra Kalgaonkar, Sangeeta Hambir, Neelima Bulakh, Jog JP. J of Appli Polym Sci 2001, 81, 1786.

47. Chen-Chi Ma M, Yi-Jie Chen, Hsu-Chiang Kuan. J of Appl Polym Sci 2006, 100, 508.

48. Thio YS, Argon AS, Cohen RE, Weinberg M. Polymer 2002, 43, 3661.

49. Deshmane C, Yuan Q, Perkins RS, Misra RDK. Mat Sci and Eng A 2007, 458, 150.

50. Asaletha R, Groeninckx G, Kumaran MG, Sabu Thomas. J of Appl Polym Sci 1998, 69, 2673.

51. Oommen Z, Thomas S, Premalatha CK, Kuriakose B. Polymer 1997, 38, 5611.

52. Kim TH, Jang LW, Lee DC, Choi HJ, Jhon MS. Macromol Rapid Commun 2002, 23, 191.

53. Kim TH, Lim ST, Lee CH, Choi HJ, Jhon MS. J Appl Polym Sci 2003, 87, 2106.

54. Li SC, Jarvela PK, Jarvela PA. J Appl Polym Sci 1999, 71, 1641.

55. Thomas S, Kuriakose B, Gupta BR, De SK. Plast Rubber Process Appl 1986, 6, 85.

56. Saini DR, Shenoy AV. J Macromol Sci Phys 1983, B22, 437.

57. Tordella JP. J Appl Phys 1956, 27, 454.

58. Bagley EB, Birks AM. J Appl Phys 1960, 31, 556.

59. Tordella JP. J Appl Polym Sci 1963, 7, 215.

60. Benbow JJ, Lamb P. SPE Trans 1963, 3, 7.

61. Bartczak Z, Argon AS, Cohen RE, Weinberg M. Polymer 1999, 40, 2347.

62. Ke Y, Long C, Qi Z. J Appl Polym Sci 1999, 71, 1139-46.

63. Yano K, Usuki A, Okada A. J Polym Sci Part A: Polym Chem 1997, 35, 2289.

64. Pawlak A, Zinck P, Galeski A, Gerard JF. Macromol Symp 2001, 169, 197.

65. Rong JF, Jing ZH, Li HQ, Sheng M. Macromol Rapid Commun 2001, 22, 329.

66. Messersmith PB, Giannelis EP. Chemistry of Materials 1994, 6, 1719.

67. Cai H, Yan FY, Xue QJ, Liu WM. Polymer Testing 2003, 22, 875.

68. Vaia RA, Jandt KD, Kramer EJ, Giannelis EP. Macromolecules 1995, 28, 8080.

69. Uksuki A, Tukigase A, Kato M. Polymer 2002, 43, 2185.

70. Jimenez G, Ogata N, Kawai H, Ogihara T. J of Appl Polym Sci 1997, 64, 2211.

71. Morgan AB, Jeffrey WG. J of Appl Polym Sci 2003, 87, 1329.

72. Yang R, Liu Y, Yu J, Wang K. Polym Degdn and Stability 2006, 91(8), 1651.

73. Trotigon JP, Verdu J, Boissard RDe, Vallios ADe. In: Sedlaucek B, editor. Polymer composites: proceedings of prague IUPAC microsymposium on macromolecules. Berlin: De Grugter; 1985. p. 191.

74. Dasari A, Sarang S, Misra RDK. Mater Sci Eng A 2004, 368, 191.

75. Dasari A, Rohrmann J, Misra RDK. Mater Sci Eng A 2004, 364, 357.

76. Dasari A, Misra RDK. Acta Mater 2004, 52, 1683.

77. Yuan Q, Jiang W, Zhang HZ, Yin JH, An LJ, Li RKY. J Polym Sci Part B: Polym Phys 2001, 39, 1855.

78. Sahebian S, Zebarjad SM, Saijadi SA, Sherafal Z, Lazzeri A. J of Appl Polym Sci 2007, 104 (6), 3688.

79. Haworth B, Raymond CL, Sutherland I. Polym Eng Sci 2001, 41, 1345.

80. Albano C, Gonzalez J, Ichazo M, Rosales C, Urbina de Navarro C, Parra C. Compos Struct 2000, 49, 48.

81. Wang Y, Wang JJ. Polym Eng Sci 1999, 39, 190.

82. Gonzalez J, Albano C, Ichazo M, Diaz B. Eur Polym J 2002, 38, 2465.

83. Price GJ, Ansari DM. Polym Int 2004, 53, 430.

84. Vollenberg PHTh, Heikens D. J Mater Sci 1990, 25, 3089.

85. Misra RDK, Nerlikar P, Bertrand K, Murphy D. Mater Sci Eng A 2005, 384, 284.

86. Tanniru M, Misra RDK, Bertrand K, Murphy D. Mater Sci Eng A 2005, 404, 208.

87. Tanniru M, Misra RDK. Mater Sci Eng A 2005, 405, 178.

88. Xu WB, Ge ML, He PS. J Polym Sci Part B: Polym Phys Ed 2002, 40, 408.

89. Idem. J Appl Polym Sci 2001, 82, 2281.

90. Zheng QA, Peng M, YI XS. Materials Letters 1999, 40, 91.

91. Xu YP, Huang R, Cai BH, Fan W. China Plastics 1998, 12(6), 30 (in Chinese).

92. He PS, Zhao AC. Plastics 2001, 30(1), 39 (in Chinese).

93. Tjong Sc, Liang GD, Bao SP. J of Appl Polym Sci 2006, 102, 1436.

94. Maged Osman A, Joärg Rupp EP, Ulrich Suter W. Polymer 2005, 46, 8202.

95. Tanniru M, Yuan Q, Misra RDK. Polymer 2006, 47, 2133.

96. Rui Yang, Ying Liu, Jian Yu, Kunhua Wang. Polymer Degradation and Stability 2006, 91, 1651.

97. Tashiro K. Prog Polym Sci 1993, 18, 377.

98. Flory PJ, Yoon DY. Nature 1978, 272, 226.

99. Li JX, Cheung WL. Polymer 1998, 39, 6935.

100. Li JX, Cheung WL, Chan CM. Polymer 1999, 39, 6935.

101. Sudeshna Chattopadhyay, Alokmay Dutta. Synthetic Metals 2005, 155, 365.

102. Cantele G, Ninno D, Iadonisi G. J Phy Condens Matter 2000, 12, 9019

103. Friedrich K. Adv Polym Sci 1983, 52/53, 225.

104. Ouderni M, Philips PJ. J Eng Appl Sci 1996, 2, 2312.

105. Lee BL, Nielsen LE. J Polym Sci Phys Ed 1977, 15, 683.

106. Lichtenhan JD, Otonari YA, Carr MJ. Macromolecules 1995, 28, 8435.

107. Lee A, Lichtenhan JD. J Appl Polym Sci 1999, 73, 1993.

108. Haddad TS, Lichtenhan JD. Macromolecules 1996, 29, 7302.

109. Romo-Uribe A, Mather PT, Haddad TS, Lichtenhan JD. J Polym Sci Part B: Polym Phys 1998, 36, 1857.

110. Li GZ, Wang L, Toghiani H, Daulton TL, Pittman Jr CU. Polymer 2002, 43, 4167.

111. Xiao Yan Song, Hai Ping Geng, Qi Fang Li. Polymer 2006, 47, 3049.

112. Gilman JW, Jakson CL, Morgan AB, Harris RH, Manias E, Giannelis EP, Wuthenow M, Hilton D, Philips SH. Chem Mater 2000, 12, 1866.

113. Zhu J, Morgan AB, Lamelas FJ, Wilkie CA. Chem Mater 2001, 13, 3774.

114. Giannelis EP, Krishnamoorti R, Manias E. Adv Polym Sci 1999, 138, 108.

115. Hoffmann B, Dietrich C, Thomann R, Friedrich C, Mülhaupt R. Macromol Rapid Commun 2000, 21, 57.

116. Xaoan F, Qutubuddin S. Mater Lett 2000, 42, 12.

117. Okamoto M, Morita S, Taguchi H, Kim YH, Kotaka T, Tateyama H. Polym Commun 2000, 41, 3887.

118. Noh MW, Lee DC. Polym Bull 1999, 42, 619.

119. Olson BG, Peng ZL, McGervey JD, Jamieson AM, Manias E, Giannels EP. Mater Sci Forum 2007, 336, 255.

120. Wizel S, Margel S, Gedanken A. Polym Int 2000, 49, 445.

121. Kumar Vijaya R, Koltypin Yu, Palchik O, Gedanken A. J Appl Polym Sci 2002, 86, 160.

122. Ăjinović DS, ăponjić ZVS, Cvjetianinć N, Marinović-Cincović M, Nedeljković JM. Chem Phys Lett 2000, 329, 168.

123. Yu SH, Yoshimura M, Moreno JMC, Fujiwara T, Fujino T, Teranishi R. Langmuir 2001, 17, 1700.

124. Djoković V, Nedeljković JM. Macromol Rapid Commun 2000, 21, 994.

125. Liao K, Li S. Appl Phys Lett 2001, 79, 42.

126. Hsiue GH, Kuo WJ, Huanh YP, Jeng RJ. Polymer 2000, 41, 2813.

127. Xiao M, Sun L, Liu J, Li Y, Gong K. Polymer 2002, 43, 2245.

128. Sreekumari Nair P, Radhakrishnan T, Revaprasadu N, Van Sittert CGCE, Djoković V, Luyt AS. Mater Lett 2004, 58, 361.

129. Mbhele ZH, Salemane MG, Van Sittert CGCE, Nedeljković M, Djoković V, Luyt AS. Chem Mater 2003, 15, 5019.

130. Kuljanin J, Vućković M, ćomor MI, Bibić N, Djoković V, Nedeljković M. Euro Polym J 2002, 38, 1659.

131. Marcilla A, Beltran M. Polym Degrad Stab 1995, 50, 117.

132. Nakagawa H, Sano H. Polym Prep (Am Chem Soc, Div Polym Chem) 1992, 26, 249.

133. Mareri P, Bastide S, Binda N, Crespy A. Compos Sci Technol 1998, 58, 74.

134. McNally T, Murphy WR, Lew C, Turner R, Brennan G. Polymer 2003, 44, 2761.

135. Xie W, Hwu JM, Jiang GJ, Buthelezi TM, Pan WP. Polym Eng Sci 2003, 43(1), 214.

SUMMARY AND CONCLUSION

Abstract

The major findings of the study are summarized in this chapter.

Nanocomposites are multiphase materials where at least one of the constituent phases has one dimension less than 100 nm. The promise of nanocomposites lies in their multifunctionality and the possibility of realizing unique combinations of properties unachievable with traditional materials forever. The challenges in reaching this promise are tremendous. They include control over the distribution in size and dispersion of the nanosize constituents, tailoring and understanding the role of interfaces between structurally or chemically dissimilar phases on bulk properties. Large scale and controlled processing of many nanomaterials is yet to be realised.

In the present investigation, ZnO in nanoparticle size was prepared by matrix mediated process. This nano ZnO was used to modify the processability and mechanical properties of thermoplastics. Three engineering thermoplastics, viz. polyethylene terephthalate (PET), polyamide 6 (PA 6) and polycarbonate (PC) and three commodity plastics, viz. polypropylene (PP), high density polyethylene (HDPE) and polystyrene (PS) were selected for the study. The processability and properties were compared with those containing commercial ZnO.

Nano ZnO was prepared from $ZnCl_2$ and NaOH in chitosan medium by in situ deposition technique. Transmission electron microscopy and scanning electron microscopy revealed that mode of preparation has a specific role in the size and shape of zinc oxide particles. The particle size is smaller than that of commercial ZnO and is rod shaped with a large aspect ratio. Further the particles are found to be of high purity by thermogravimetric analysis and differential scanning calorimetry. ZnO nanoparticles have a very strong photoluminescence (PL) band at ultraviolet wavelength range. This method has many advantages, such as simplicity, low cost, high input, high purity, high yield and little pollution in addition to its fineness.

As the next part of the study, nanocomposites of PET, PA 6 and PC were prepared with varying concentration of ZnO (0.0-3.0 wt%) and the crystallization, mechanical, dynamic mechanical and rheological properties of the composites were evaluated. Nanocomposites were prepared by the melt-compounding route in

a torque rheometer. Nano ZnO was found to be an effective nucleating agent for the PET and PA 6 crystallization. The nano ZnOs at a concentration as low as 300 ppm enhanced the crystallization temperature during melt cooling by 32 °C in PET and 10 °C in PA 6 polymer, and reduced melt's isothermal crystallization time by more than 50 % in PET and 20 % in PA 6 matrix. No crystalline melting endothermic peaks were observed in the DSC curves of PC- ZnO composites. A comparison of the nucleation ability of nano ZnO with commercial ZnO revealed that nano ZnOs are made superior nucleating agents. Nano ZnO composites also show improved thermal stability than their counterparts.

On incorporating 1.0 % nano ZnO into PET, tensile strength and modulus improved by 15 % and 13 % respectively. Incorporation of nano ZnO at the level of 3.0 wt%, flexural modulus increased by around 286 %, flexural strength by around 20 % and impact strength by around 160 %. The improvement in mechanical properties for PA 6 nanocomposites was even more significant. There was about 38 % increase in both tensile strength and modulus. Flexural modulus increased by five times the value of pure PA 6, while flexural strength increased by around 17 % and impact strength by around 53 % on adding 3.0 wt% of nano ZnO. The tensile strength increased by about 15 % and modulus by about 9 % and flexural modulus and strength increased by 5 % on adding 3.0 wt% of nano ZnO to PC. Impact strength of PC was found to decrease with nano ZnO addition. The reinforcement by nano ZnO is far superior to the reinforcement produced by commercial ZnO in all the three matrices.

The dynamic mechanical analysis indicated an improvement in storage and loss modulus of nano ZnO composites than commercial ZnO composites. The rheological characteristics revealed that shear viscosity of the nano ZnO composites increased with concentration of nano ZnO and decreased with increasing shear stress. Melt flow index value and die swell ratio decreased with nano ZnO concentration indicating pseudoplastic behaviour. Activation energies of the nanocomposites increased with modification at lower shear rates.

Apparently, nano ZnO is a good modifier compared to commercial ZnO for engineering thermoplastics.

In the last part of the work, commodity thermoplastics based nanocomposites were prepared with nano ZnO. Nano ZnO was found to be an effective nucleating agent for PP and HDPE crystallization. The nano ZnOs at a concentration as low as 300 ppm enhanced the crystallization temperature during melt cooling by 5 °C in PP matrix and 6 °C in HDPE matrix, and reduced melt's isothermal crystallization time by more than 50 % in PP matrix and HDPE matrix. No crystalline melting endothermic peaks were observed in the DSC curves of PS-ZnO composites. A comparison of the nucleation ability of nano ZnO with commercial ZnO revealed that nano ZnOs are efficient nucleating agents for commodity plastics also. Thermogravimetric analysis showed improved thermal stability for nano ZnO composites than their counterparts.

Reinforcement of commodity thermoplastics by ZnO nanoparticles was significant compared to commercial ZnO. It revealed that a small concentration of nano ZnO could considerably reinforce polymers. For example, ZnO at a level of 0.03 wt% increased the tensile strength of PP and HDPE by about 5 % and modulus by over 10 %. In PS nanocomposites the improvement in tensile strength and modulus was about 25 % and 5 % respectively on adding 1.0 wt% nano ZnO. The flexural strength and modulus of PP nanocomposites improved by about 18 % and 7 % respectively and in HDPE nanocomposites, flexural strength and modulus was increased by about 8 % and 1 % respectively at a level of 0.03 wt% ZnO. In PS nanocomposites, flexural strength and modulus increased by 5 % and 3 % respectively at a level of 0.03 wt% ZnO. There was about 65 %, 5 % and 21 % increase in impact strength of PP, HDPE and PS nanocomposites respectively at a level of 0.03 wt% nano ZnO.

The dynamic mechanical analysis indicated an improvement in storage and loss modulus of nano ZnO composites than commercial ZnO composites. The rheological characteristics revealed that shear viscosity of the nano ZnO composites increased with concentration of nano ZnO, but decreased with

increasing shear stress. Melt flow index value and die swell ratio decreased with nano ZnO concentration indicating pseudoplastic behaviour of the flow. Activation energies of the PP nanocomposites increased with modification at lower shear rates. In HDPE nanocomposites, activation energy increased at both lower and higher shear rates, whereas in PS nanocomposites it increased at higher shear rates. So, nano ZnO is a good modifier compared to commercial ZnO for commodity thermoplastics.

To conclude, nano zinc oxide particles prepared by in situ deposition technique in chitosan solution is a promising material for modification of engineering as well as commodity plastics.

Publications

1. "Zinc oxide induced crystallization of polypropylene", Aswathy K.V, Rani Joseph: *Journal of Applied Polymer Science 2007* (Accepted for publication).

2. "Crystallization and thermal behaviour of polyethylene terephthalate-ZnO nanocomposites", Aswathy K.V, Rani Joseph: *Polymer 2007* (Accepted for publication).

3. "Crystallization and mechanical properties of PA 6-ZnO anocomposites", Aswathy K.V, Rani Joseph: *European Polymer Journal 2007* (Communicated).

4. Mechanical and rheological properties of PS/ZnO nanocomposites", Aswathy K.V, Rani Joseph: *International Journal of Polymeric Materials 2007* (Communicated).

5. "ZnO reinforced polypropylene nanocomposite by melt-compounding", Aswathy K.V, Rani Joseph: *Progress in Rubber, Plastics and Recycling Technology 2007* (Communicated).

6. Crystallization and mechanical properties of HDPE-ZnO nanocomposites", Aswathy K.V, Rani Joseph: *Journal of Elastomers and Plastics 2007* (Communicated).

7. "Dynamic mechanical and rheological properties of PET-ZnO nanocomposites", Aswathy K.V, Rani Joseph: *Macromolecules 2007* (Communicated).

8. "Characterization of PC-ZnO nanocomposites", Aswathy K.V, Rani Joseph: *Journal of Applied Polymer Science 2007* (Communicated).

9. "Morphology and rheological properties of PA 6- ZnO nanocomposites", Aswathy K.V, Rani Joseph: *Polymer* (to be communicated).

10. "Dynamic mechanical behaviour of ZnO reinforced HDPE", Aswathy K.V, Rani Joseph: *International Journal of Polymeric Materials 2007* (to be communicated).

Conference Papers

1. "ZnO-reinforced polypropylene: crystallization and mechanical properties", Aswathy K.V, Rani Joseph: *18th Kerala Science Congress, Jan 29-31, 2006, CESS, Thiruvananthapuram, India.*

2. "Polyethylene terephthalate-active ZnO nanocomposites: thermal and mechanical properties", Aswathy K.V, Rani Joseph: *National Conference on Frontiers in Polymer Science and Technology- POLYMER 2006, Feb 10-12, 2006, Indian Association for the Cultivation of Science, Jadavpur, Kolkata, India.*

3. "Polyamide 6-active ZnO nanocomposites: crystallization and Mechanical properties", Aswathy K.V, Rani Joseph: *17th Annual General Meeting of Materials Research Society of India- AGM-MRSI, Feb 13-15, 2006, University of Lucknow, India.*

4. "Zinc oxide induced crystallization of High Density Polyethylene", Aswathy K.V, Rani Joseph: *International Conference- Asia Rub Tech Expo '06, Nov 23-25, 2006, Cochin, India.*

5. "Zinc Oxide Reinforced High Density Polyethylene", Aswathy K.V, Rani Joseph: *9th National Conference, MACRO-2006, Polymers for advanced Technologies, Dec 17-20, National Chemical Laboratory, Pune, India.*

6. "Morphology and Mechanical Properties of Polystyrene/Zinc Oxide Nanocomposites", Aswathy K.V, Rani Joseph: *National Seminar - Frontiers in Organic Chemistry, Jan 11-12, 2007, Department of Chemistry, University of Calicut, Kerala, India.*

7. "Crystallization and dynamic mechanical properties of polyethylene terephthalate- Zinc oxide nanocomposites", Aswathy K.V, Rani Joseph: *19th Kerala Science Congress, Jan 29- 31, 2007, Kannur, India.*

List of abbreviations and symbols

ASTM	American standards and testing methods manual
CNTs	Carbon nanotubes
CVD	Chemical vapour deposition
DMA	Dynamic mechanical analysis
DSC	Differential scanning calorimetry
DTG	Differential thermogravimety
EB	Elongation at break
EDX	Energy dispersive X-ray spectrometer
FTIR	Fourier transform infrared
HDPE	High density polyethylene
HDT	Heat distortion temperature
ICP-AES	Inductively coupled plasma -Atomic emission spectrometer
MOD	Metal organic decomposition
PA 6	Polyamide 6
PAN	Polyacrylonitrile
PBT	Polybutylene terephthalate
PC	Polycarbonate
PET	Polyethylene terephthalate
PMMA	Polymethyl methacrylate
PNCs	Polymer nanocomposites
PP	Polypropylene
PS	Polystyrene
SEM	Scanning electron microscope
TEM	Transmission electron microscopy
TGA	Thermo gravimetric analysis
TP	Thermoplastics
TS	Thermosets
UTM	Universal testing machine
XRD	X-ray Diffraction

$\dot{\gamma}_w$	Shear strain
%	Percentage
λ	Wave length
τ_w	Shear stress
atm	Atmosphere
d_c	Diameter of the capillary
d_e	Diameter of the extrudate
e.g.	Example
E_a	Activation energy
GPa	Giga pascal

J	Joules
m	Meter
min	Minutes
mol	Mole
MPa	Mega Pascal
n'	Flow behaviour index
NaOH	Sodium hydroxide
nm	Nanometer
T	Time
$T_{10\%}$	Temperature at 10% decomposition
$T_{50\%}$	Temperature at 50% decomposition
tan δ	Loss factor
T_c	Crystallization temperature
Temp.	Temperature
T_g	Glass transition temperature
T_i	Temperature of onset of degradation
T_m	Melting temperature
T_{max}	Peak temperature
$Zn(OH)_2$	Zinc hydroxide
$ZnCl_2$	Zinc chloride
ZnO	Zinc oxide
ΔH_c	Enthalpy of crystallization
ΔH_m	Enthalpy of melting
ΔT	Degree of supercooling

CURRICULUM VITAE

ASWATHY K.V.
Kallamparambil House,
Edappally P.O,
Padivattom,
Ernakulam Dist,
Pin.682024.

aswathy_ramesh@yahoo.com
aswathyramesh@hotmail.com

Personnel Details

Date of birth	:	01-06-1978
Religion and Caste	:	Hindu, Nair
Marital status	:	Married
Nationality	:	Indian

Academic Profile

Exam Passed	Year of passing/Institution	Class/ Division	Subject studied
M.Sc	2000 (S.H.College, Thevera)	Second Rank	Chemistry Pure
B.Sc	1998 (S.H.College, Thevera)	Third Rank	Chemistry Main Maths /Phy (Sub)
Pre-Degree	1995 (S.H.College, Thevera)	Distinction	Chemistry, Biology, Physics, Maths
S.S.L.C.	1993 (State Board of Public Examinations	Distinction	State Syllabus

Topic of Research   :   Polymer Nanocomposites

Research experience   :   Five years research experience in the field of Polymer Nanocomposites